UCLouvain

Faculté des bioingénieurs

Rainfall and land use control Si cycling in wet tropical Andosols

Thèse soutenue en vue de l'obtention du grade de docteur en sciences agronomiques et ingénierie biologique par

Charles Vander Linden

Composition du Jury

Pr. Bruno Delvaux (UCLouvain/ELIe) – *Promoteur*
Pr. Sophie Opfergelt (UCLouvain/ELIe – *Promoteur*
Pr. Marnik Vanclooster (UCLouvain/ELIe) – *Président*
Pr. Xavier Draye (UCLouvain/ELIa)
Dr. Hugues Titeux (UCLouvain/ELIe) – *Secrétaire*
Pr. Jean-Dominique Meunier (CNRS/CEREGE)
Pr. Jean-Thomas Cornelis (ULiège/BIOSE)

Louvain-la-Neuve

Septembre 2019

Remerciements

Mon premier orteil dans l'unité SOLS fût un mail à Brieuc Hardy en août 2014 pour lui demander si par hasard il n'avait pas un mémoire à me proposer. J'étais quelque peu en retard pour le choix de ce dernier car, comme à mon habitude, j'avais beaucoup de mal à me décider. Gardant un bon souvenir des cours et TPs de sciences du sol, je décide finalement d'envoyer ce fameux mail. C'est alors, par la négative, que Brieuc me répond… Cependant, il m'oriente alors vers un mémoire ayant pour objet la mise en place d'un vignoble didactique à la ferme de Marbaix. Une ou deux réunions plus tard je me retrouve finalement dans le bureau de Monsieur Bruno Delvaux qui transmet tel un virus virulent sa passion pour le terroir et le vin à quiconque ose aborder le sujet. J'avais alors non-plus un orteil mais bien les deux pieds dans l'unité SOLS. Après la réalisation d'un mémoire passionnant sur le terroir, Bruno me propose de me lancer dans une aventure d'une autre envergure, la thèse.

Avec Clémence on avait l'idée de passer une année ou deux aux Antilles à la suite de nos études. J'en avais touché un mot à Bruno pour son énorme carnet d'adresses et ses expériences en Martinique et Guadeloupe. A la fin de mon mémoire, Bruno me demande donc si, par hasard, je ne serais pas intéressé par l'idée de faire une thèse, et pourquoi pas en Guadeloupe. Les sols sableux du Château Marbaix, les porte-greffes et les cépages sont alors remplacés par les sols volcaniques, les champs de banane, les champs de canne et la forêt tropicale en Guadeloupe. Et une aventure passionnante commence.

C'est donc avant tout Bruno Delvaux que je souhaiterais remercier. Bruno, je te remercie d'avoir ouvert ta porte à un jeune étudiant il y a maintenant bientôt 5 ans et de l'avoir toujours (littéralement) laissée ouverte. Tu m'as transmis ta passion pour le vin, le sol, les plantes, le rhum, j'en passe, et je t'en remercie. Tu m'as également appris énormément de choses, ce qui a une valeur inestimable pour moi. Finalement, tu as pu me donner une confiance que je n'avais pas en complimentant toujours ce que j'ai pu faire. Je pense qu'il y a peu de promoteurs qui font cela avec leurs étudiants. C'est pourtant ce qui m'a permis d'arriver au bout de ce travail et qui, j'en suis sûr, m'aidera beaucoup dans le futur.

C'est ensuite à Sophie Opfergelt que je voudrais adresser un merci particulier. Sophie, tu as immédiatement accepté de te lancer dans l'aventure de ma thèse il y a quatre ans et tu as pu y apporter une dimension supplémentaire en y ajoutant toute la partie dédiée au traçage du Si. Tu étais également toujours disponible et prête à m'aider quand j'en ai eu besoin. Un grand merci pour cela.

Si je suis l'histoire dans son ordre chronologique, c'est ensuite Aurélien que j'aimerais remercier. En effet, cette aventure a forcément commencé par l'épreuve du FRIA. Une épreuve qui fût un peu moins douloureuse grâce au duo que nous avons formé pour la préparer. Ensuite, durant toute la période de la thèse, tu fus une oreille toujours ouverte pour m'écouter.

Une fois le FRIA obtenu, Hugues Titeux et Frédéric Laurent m'ont directement aidé pour la conception de lysimètres efficaces, bon marchés, compactes et légers. Ensuite, j'ai pu discuter avec Xavier Draye pour établir une méthode d'échantillonnage des plantes.

En parallèle, mon départ imminent pour la Guadeloupe s'organise et sans l'aide de Françoise pour toutes les démarches administratives cela aurait été sans aucun doute beaucoup plus compliqué.

Arrive ensuite le jour de quitter la Belgique pour débarquer en Guadeloupe. Après deux semaines pour trouver un logement et s'installer, je débarque au CIRAD où je suis accueilli par Philippe Cattan, que je remercie pour cela. J'ai ensuite eu le plaisir de travailler au sein du CIRAD auprès d'Irina Comte, Marc Dorel et Vincent Bonnal dont la porte était toujours ouverte lorsque j'avais l'une ou l'autre question. A force de toquer à la porte d'Irina, une amitié s'est peu à peu établie jusqu'à ce que je mange presque tous les midis chez elle et Guilhem. Aujourd'hui je suis tellement heureux de pouvoir vous compter, Irina et Guilhem, dans mes amis proches. Vous apportez tellement aux gens qui ont la chance de croiser votre chemin.

Germain m'a également beaucoup aidé durant mon séjour au CIRAD. Il a été mon principal contact avec les agriculteurs et m'a aidé de nombreuses fois sur le terrain.

J'ai également pu croiser de nombreux stagiaires avec qui j'ai pu tisser des liens en des temps record ! Je pense particulièrement à Clément, Marion, Magali, Marine, Lou.

Ensuite, j'ai eu la chance d'obtenir de l'aide de chercheurs et techniciens d'autres centres de recherches. A l'INRA, Patrick Andrieux, Lise Ponchant, Thierry et Jean-Baptiste m'ont énormément aidé pour l'échantillonnage des crues. Au BRGM, Jean-Baptiste Charlier m'a patiemment expliqué le fonctionnement hydrologique des bassins versants étudiés et m'a permis d'échantillonner de nombreuses sources et eaux souterraines.

Après dix-neuf mois en Guadeloupe et la collecte de centaines d'échantillons, il était temps pour moi de rentrer en Belgique pour assommer Anne et Claudine d'analyses. Je voudrais donc adresser un merci particulier à vous deux pour les milliers d'analyses réalisées et pour les nombreux conseils. Sans vous cette thèse n'aurait tout simplement pas été possible.

En rentrant de Guadeloupe, c'est finalement l'occasion pour moi d'apprendre à mieux connaître mes fabuleux collègues du labo SOLS. Merci à Zimin, Mathilde, Inga, Noa, Marlon, Michelle, François, Aubry, Benoît, Arthur, Carlos, Gabriella, Catherine, Elisabeth, Clayria, Fidèle, et également Yolanda, Rawaa et Marie-Liesse.

J'ai également eu la chance d'encadrer des mémorants exceptionnels que j'aimerais remercier. Pierre, Alexis, Maxime et Alexandre votre enthousiasme m'a apporté énormément et a donné du sens à mon travail.

Je voudrais également remercier les membres de mon jury de thèse, Hugues Titeux, Jean-Thomas Cornelis, Jean-Dominique Meunier et Xavier Draye pour leurs commentaires et conseils. Ceux-ci ont nettement amélioré ma thèse.

Finalement, j'aimerais terminer par Clémence. Sans toi cette thèse n'aurait tout simplement jamais commencé. Quand bien même elle aurait commencé, je n'aurais pu la terminer.

Abstract

Plants take up silicon (Si) from soil solution, and form biogenic silica bodies (phytoliths) that return to soil with plant debris. In soils, phytoliths readily dissolve, and thus contribute to the reservoir of plant available Si. The soil-plant cycle of Si depends on soil type, plant species, climate and land use.

We show that the control of soil weathering stage on the soil-plant Si cycle in the tropics depends on land use. In rice croplands, an increase in weathering leads to a decrease in annual plant Si uptakes. The opposite trend is observed for tropical forests. This difference is linked to contrasting rooting systems and subsequent biological pumping, which is much deeper in forest than in cropland.

We further study the Si soil-plant cycle under forest and intensive cropping of banana and sugarcane on strongly desilicated Andosols in the humid tropical conditions of Basse-Terre, Guadeloupe. Here, we first set up a new protocol to estimate the pool of phytoliths in soil. Then, we show that mean annual rainfall (MAR) and land use control the fluxes of Si in these soil-plant systems. The increase in MAR increases the leaching of Si, decreases the amount of plant available Si, and enhances phytolith dissolution. Converting forest into banana and sugarcane cropland promotes the “mobility” of Si in the soil-plant system. Indeed, relatively to a neighboring forest, the annual Si plant uptake and return to soil is ~4 and ~10 times larger in banana and sugarcane, respectively. Moreover, the return of inedible plant parts to soil limits Si exports by crop harvesting, and built up an important soil phytolith pool that controls ~70-95% of the dissolved Si pool. This highlights how much the management of the inedible plant parts is important in cultivated ecosystems.

Résumé

Les plantes prélèvent le silicium dans la solution du sol et forment des particules siliceuses amorphes (phytolithes) qui retournent au sol avec les débris végétaux. Dans les sols, les phytolithes se dissolvent aisément et alimentent le réservoir du silicium disponible pour les plantes. Le cycle sol-plante du silicium dépend du type de sol, de l'espèce végétale, du climat et de l'usage des sols.

Nous montrons que le cycle sol-plante du silicium en régions tropicales dépend du degré d'altération et de l'usage des sols. En riziculture, l'augmentation de l'altération entraîne une diminution du stock de silicium biodisponible. La tendance inverse est observée en forêt tropicale. Cette différence est due aux enracinements contrastés et au prélèvement biologique qu'ils conditionnent : l'enracinement est beaucoup plus profond en forêt que sous culture.

Ensuite, nous avons étudié le cycle sol-plante du silicium sous forêt et sous culture de bananier et canne à sucre, sur des Andosols fortement désilicifiés en conditions tropicales humides (Guadeloupe). Nous avons d'abord mis au point un protocole analytique pour estimer le stock de phytolithes dans le sol. Ensuite, nous montrons que les précipitations annuelles moyennes et l'utilisation des terres contrôlent les flux de silicium. L'augmentation des précipitations annuelles moyennes accroît le lessivage du silicium diminuant la quantité de silicium biodisponible. Elle favorise aussi la dissolution des phytolithes. Convertir la forêt en bananeraie et canne à sucre favorise la "mobilité" du silicium dans le système sol-plante. En effet, par rapport à la forêt, le prélèvement annuel du silicium par la végétation et son retour au sol est ~4 fois supérieur sous banane et ~10 fois supérieur sous canne à sucre. En outre, le retour au sol des résidus de culture réduit les exportations de silicium par la récolte. Ce retour au sol alimente le réservoir de phytolithes lequel contrôle ~70-95% du stock de silicium dissous. Ces résultats montrent à quel point la gestion des résidus de culture est importante.

List of abbreviations

ANOVA – ANalysis Of VAriance
ASi – Amorphous Silicon
asl – above sea level
BS – Base Saturation
BSi – Biogenic Silicon
CEC – Cation Exchange Capacity
dbh – diameter at breast height
DCB – Dithionite-Citrate-Bicarbonate
dr – dissolution rate
DSi – Dissolved Silicon
EG – Ethylene Glycol
ET - EvapoTranspiration
GDVC – Grande Découverte Volcanic Complex
ICP-AES – Inductively Coupled Plasma-Atomic Emission Spectroscopy
ICP-MS – Inductively Coupled Plasma-Mass Spectroscopy
ISi – Inorganic Silicon
LSi – Lithogenic Silicon
MAR – Mean Annual Rainfall
OC – Organic carbon
OMA – Organo-mineral associations
PhSi – Phytogenic Silicon
PSi – Pedogenic Silicon
Q-I – Quantity-Intensity
SEB – Sum of Exchangeable Bases
SOC – Soil Organic Carbon
SOM – Soil Organic Matter
SRO – Short Range-Ordered
TGA – ThermoGravimetric Analysis
TRB – Total Reserve in Bases
XRD – X-Ray Diffraction

Table of content

General background

General introduction

Silicon (Si) is the second mass abundant element of the Earth's crust (28.8% wt) after oxygen (Wedepohl, 1995). It early appears in soil and plant sciences because of its omnipresence in the pedosphere and biosphere (Sommer et al. 2006). In soils, total Si content ranges from 5 to 470 g kg^{-1} depending on soil mineralogy (McKeague and Cline, 1963). In shoot plant tissues, the mean Si concentration ranges between 1 and 100 g Si kg^{-1} and may exceed that of major nutrients (Hodson et al., 2005).

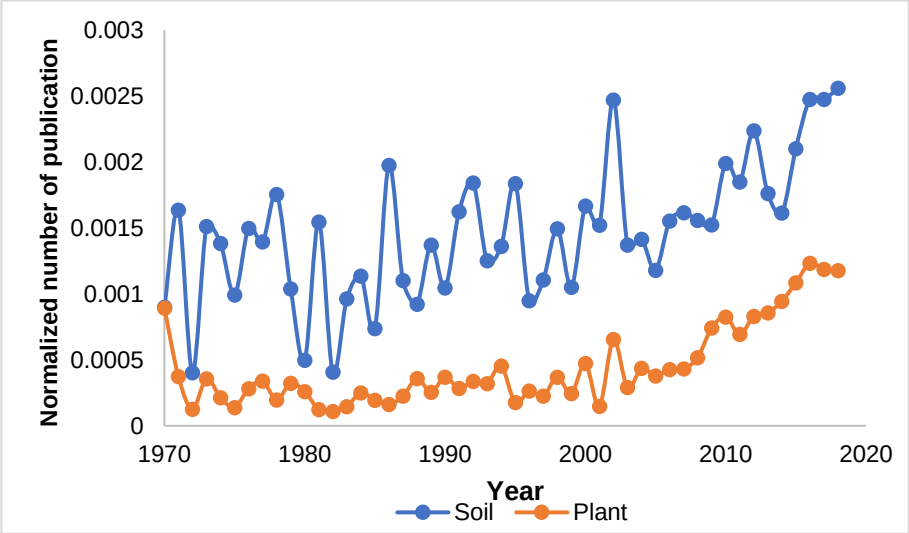

Figure GB-1: Normalized number of silicon (Si)-related publications in the soil (orange line) and plant (blue line) sciences from 1970 to 2018 (based on Scopus search with the words 'silicon' or 'silicate' or 'silicic' in the title, and the word 'soil' in the title, abstract or keywords for the soil sciences, and the word 'plant' in the title, abstract or keywords for the plant sciences). Normalization is done by dividing the number of publications by the number of publications containing the word 'soil' in the title, abstract or keywords for soil sciences and containing the word 'plant' in the title, abstract or keywords for plant sciences.

Figure GB-1 illustrates the recent and increasing interest of the scientific community to *silicon soil and plant sciences* that contributes to the understanding of the global cycle of silicon. The Si cycle plays a number of ecological roles related to eminent global problematics and provision of ecosystem services. One of the most cited is the link between the Si and carbon (C) cycles. On continents, the weathering of silicate minerals may

consume carbon dioxide (CO_2) and release dissolved Si (DSi). Part of DSi may be exported to watersheds and reach marine ecosystems where it is taken up by diatoms (photosynthetic phytoplankton), hence impacting the oceanic capacity to fix C.

In 1983, the pioneer study by Bartoli highlighted the importance of the biological Si cycle in controlling the mobility of Si in the soil-plant system of temperate forest ecosystems. The biological Si cycle encompasses the Si absorption by plant roots, the precipitation of amorphous silica bodies in plant, called phytoliths, the return of phytoliths to soil through litterfall, and phytolith dissolution in soil. Further, Lucas et al. (1993), Cornu et al. (1995, 1998), Alexandre et al. (1994, 1997), Meunier et al. (1999) followed the path traced by Bartoli et al. (1983), and demonstrated the major impact of plants on the biogeochemical cycle of Si in various ecosystems.

In 2005, Derry et al. showed that plants strongly control the Si fluxes toward rivers. This study confirmed that plants play a central role in controlling the Si cycle. As initiated by Bartoli (1983) and Lucas et al. (1993), this major breakthrough combined with new knowledge about the soil-plant cycle of silicon led to the first studies considering the impact of land use changes on the Si cycle (Clymans et al., 2011; Guntzer et al., 2012; Jennerjahn et al., 2006; Keller et al., 2012; Struyf et al., 2010; Vandevenne et al., 2011). Indeed, this question appeared crucial given the numerous beneficial effects of Si on plant growth and development (Coskun et al. 2019 for a review), and the coupling of the Si and C cycles (a.o. Smetacek, 1999; Tréguer and Pondaven, 2000).

In 2010, Struyf et al. compared Si fluxes at base flow in 51 small watersheds with long agricultural history (> 1000 years) and different land use types. They observed that when agricultural surfaces increase, the fluxes of DSi and particulate biogenic Si (BSi) decrease. In contrast, Conley et al. (2008) had shown earlier that DSi fluxes to watersheds increased just after deforestation. From these observations, Struyf et al. (2010) proposed a conceptual model predicting the modifications of Si fluxes toward rivers once land use switches from developing to climax forest, and eventually to a cultivated ecosystem (Figure GB-2). In a developing forest, small amounts of DSi are released from the soil PhSi pool compared with the amount that is

annually incorporated in the vegetation and in the soil PhSi pool (Meunier et al., 2010). The major part of the DSi from mineral weathering is introduced in the biocycling of Si before it is eventually released into rivers. In the climax forest, the biological Si feedback loop is intense and the export fluxes of Si are controlled by the dissolution of soil phytoliths (a.o. Farmer et al., 2005; Sommer et al., 2013). After deforestation, the amount of DSi exported to rivers strongly increases as the large PhSi pool accumulated in the forest soil dissolves (Conley et al., 2008; Williams et al., 2007). In croplands, the harvest exports of PhSi from the soil-plant system lead to a depletion of the PhSi pool in soil (Barão et al., 2014; Clymans et al., 2015b; Guntzer et al., 2012; Keller et al., 2012; Vandevenne et al., 2011, 2015). Moreover, soil erosion increases. The PhSi pool, predominant in topsoil, can be exported within PhSi particles if soil erosion occurs (Clymans et al., 2015b). According to Struyf et al. (2010) (Figure GB-2), deforestation leads to the exhaustion of the soil PhSi pool and Si fluxes are maximal. However, once the cultivated ecosystem has reached the climax stage, the PhSi pool in soil remains constant whereas Si

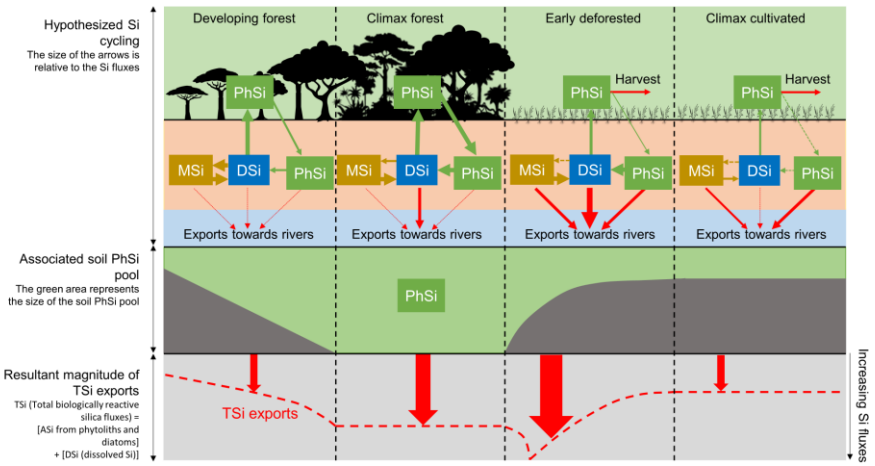

Figure GB-2: Conceptual model by Struyf et al. (2010) describing the changes in Si cycling with long-term soil disturbance, and illustrating (i) hypothesized Si cycling along the sequence developing forest / climax forest / early deforested area / cropland, (ii) associated soil PhSi stock, and (iii) the resultant magnitude of TSi export. PhSi (phytogenic Si); DSi (dissolved Si); MSi (mineral Si: including pedogenic Si and lithogenic Si) ; TSi (total biologically reactive Si fluxes), PhSi+DSi. Adapted from Struyf et al. (2010).

fluxes are lower than under forest (see also Barão et al., 2014 and Vandevenne et al., 2015).

This model did not consider, however, all the possible impacts of the agricultural land use on the Si cycle. , In particular, the possible impact of liming was not taken into account while soil pH greatly influences the dissolution of soil Si pools (Fraysse et al., 2009, 2006; van Breemen et al., 1983), and the Si bioavailablity (Li et al., 2019; Meunier et al., 2018). The impact of Si fertilizers was not explored neither despite it can greatly increase the pool of bioavailable Si (a.o. Ayres, 1966; Haynes and Zhou, 2018; Mantovani et al., 2016).

Moreover, the influence of soil type and climate was not considered in this model. In particular, the soil weathering stage and buffering capacity could both importantly influence the impact of deforestation on the Si cycle (Cornelis and Delvaux, 2016; Li et al., 2019), while rainfall could affect the bioavailable and biogenic Si pools (Quigley et al., 2017).

Finally, the impact of agricultural land use on the Si cycle has been mostly studied under temperate conditions (e.g. Barão et al., 2014; Guntzer et al., 2012; Keller et al., 2012; Struyf et al., 2010; Vandevenne et al., 2011) or for rice crops (a.o. Desplanques et al., 2006; Klotzbücher et al., 2018; Seyfferth et al., 2013; Wickramasinghe and Rowell, 2006; Yang and Zhang, 2018). It is still poorly known, however, in tropical croplands. In particular, the impact of banana crop on the Si cycle is poorly known (Henriet et al., 2008a; Opfergelt et al., 2010) despite it is a Si-accumulating plant (Henriet et al., 2006; Hodson et al., 2005). Though sugarcane takes up large amounts of Si (70-700 kg ha^{-1} yr^{-1}) (Anderson, 1991; Crusciol et al., 2018; Keeping, 2017; Matichenkov and Calvert, 2002; Meena et al., 2014; Ross et al., 1974), the impact of its cultivation on soil Si pools is poorly known. Moreover, sugarcane (1) and banana (15) rank in the top 15 of the most widely grown crops (FAO, 2018). Eventually, the inedible parts of these plants are generally restituted to soil, unlike maize, rice, wheat, or barley crops. Therefore, the impact of these two crops on the cycle of Si could be very different from that of other crops. The present PhD thesis focuses on the study of the Si cycle in banana, sugarcane, and forest in a tropical volcanic watershed in Guadeloupe.

Objective of the thesis

In the volcanic island of Basse-Terre, Guadeloupe, soils are intensively used for sugarcane and banana cropping. Mean Annual Rainfall (MAR) ranges from 850 to above 7000 mm. Soil age varies from 2.77 Ma to less than 1,000 years. As a result, contrasted soil types occur in this island on short distances (Vitric Andosols, perhydrated, Aluandic Andosols, Cambisols, Nitisols, Ferralsols, Vertisols…). The Basse-Terre Island thus offers a great opportunity to study the biogeochemical Si cycle under various land uses, soil and climate conditions. For a better understanding of the terrestrial Si cycle, such studies of Si pools and fluxes in natural and cultivated environments under various climate and soil conditions are crucial.

The general objective of this thesis is to identify the parameters that govern the silicon cycle in the humid tropics. This objective will be achieved by answering the following questions (**Q**):

Q1. What is the impact of MAR on the plant availability of Si in perhydrated, gibbsitic Andosols?

Q2. What are the respective impacts of soil weathering stage and land use on the soil-plant Si cycle in the humid tropics?

Q3. How does the conversion from forest to cropland impact the soil-plant cycle of Si? How critical is the management of inedible plant parts?

Q4. How does land use impact the dissolved Si fluxes to volcanic watersheds?

To investigate these questions, we have conducted field experiments along a topo-climosequence on the eastern flank of 'La Soufrière' volcano on the Basse-Terre Island, Guadeloupe (**Q1**). We have realized a literature review (**Q2**), and then carried out field experiments under banana, sugarcane, and forest (**Q3**). We further traced Si from soil solution to rivers (**Q4**).

Outline of the thesis

Figure GB-3 gives an overview of the thesis outline. The thesis is divided into two parts.

General Introduction. It presents briefly the general problematics and defines the objectives of the thesis without giving a comprehensive state of the art. We have chosen this configuration to avoid redundancies with the respective introductions of the different chapters as well as in a specific review chapter (*Chapter 4* see below) that introduces Part II that is devoted to land use impacts. In addition, the particularity of the soils studied requires a prior understanding of the determinants of silicon bioavailability as well as a prior adaptation of extraction procedures.

Part I: Environmental framework. Part I provides an overview of the environmental framework of the study, and focuses on the peculiarities of the soil cover as well as on the bioavailability of Si. *Chapter 1* gives the environmental characteristics of the Guadeloupe archipelago, the Basse-Terre Island, and the two studied watersheds. *Chapter 2* is aimed at quantifying the impact of increasing mean annual precipitations on the bioavailability of Si along a topo-climosequence in Guadeloupe (**Q1**). *Part I.Chapter 2* raises the need to improve the procedure for chemical quantification of phytoliths in these peculiar soils. Therefore, *Chapter 3* is a methodological chapter in which we compare different methods to improve the chemical quantification of soil phytoliths in Andosols.

Part II: Impact of land use on the soil-plant cycle of silicon. Part II focuses on the impact of land use on the Si cycle. It encompasses four chapters (4-7). *Chapter 4* is a review addressing the impact of both soil weathering stage and land use on the soil-plant Si cycle under humid tropics (**Q2**). *Chapter 5* is devoted to the quantification of the Si pools and fluxes under banana and sugarcane (**Q3**). *Chapter 6* reports the results on the quantification of the Si pools and fluxes in a tropical rainforest. Si pools and fluxes of the forest are further compared to that of neighboring banana to assess the impact of the conversion of forest into cropland on the Si soil-plant cycle (**Q3**). *Part II.Chapter 7* discusses the respective contribution of soil solution, runoff and groundwater to river water in base flow and flood flow. The possible impact of the agricultural land use on the dissolved Si fluxes in rivers is further discussed (**Q4**).

General Discussion. It concludes the PhD thesis, and discusses future perspectives.

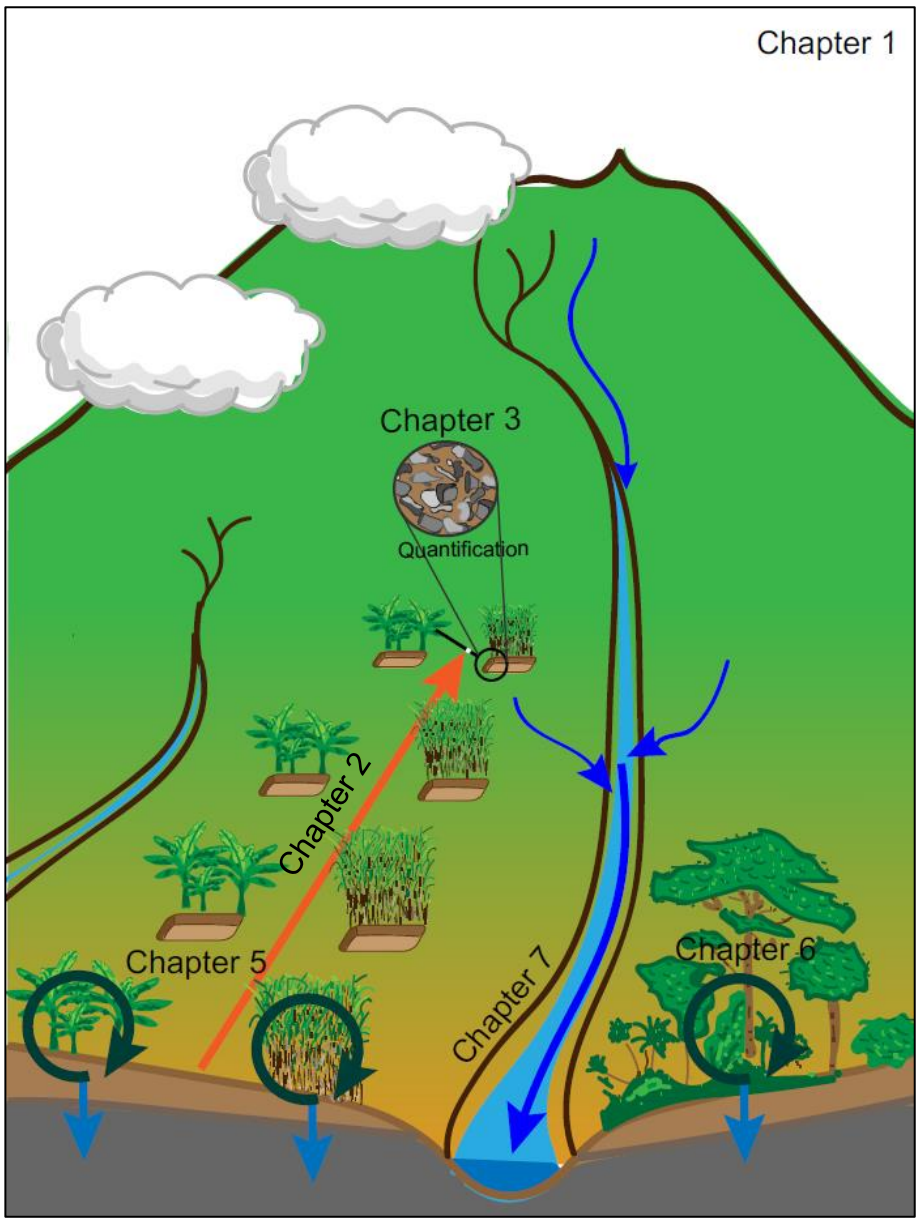

Figure GB-3: Schematic representation of the thesis outline.

Chapters 2 to 7 are presented in a succession of articles. This presentation has the advantage that each chapter can be easily read and understood

independently. Nevertheless, I apologize for the discomfort that the redundancies among chapters may provide to people who would afford a complete and continuous reading.

Part I. Environmental framework

Chapter 1 Environmental conditions

1.1 The Guadeloupe archipelago

Guadeloupe is an archipelago located in the lesser West Indies volcanic arc (61°W, 16°N) (Figure 1-1) generated by the subduction of the oceanic Atlantic plate beneath the Caribbean plate. The archipelago is composed of two main islands separated by the narrow channel *La rivière salée*: The volcanic island of Basse-Terre (848 km², culminating at 1467 m) and the calcareous island of Grande-Terre (590 km², culminating at 150 m). The other islands called "the dependences" are Marie-Galante, Les Saintes, La Désirade and Petite Terre (Figure 1-1). The Guadeloupe archipelago offers, on a small surface (1.709 km²), a wide diversity of landscapes because of its geological and climatic characteristics (Morell and Jérémie, 1994). The different islands of the archipelago have developed from distinct volcanic arcs and their associated carbonate platforms (Komorowski et al., 2005). The island of La Désirade bears witness to the oldest volcanic arc of Upper Jurassic age (145 Ma) (Bouysse et al., 1990; Komorowski et al., 2005; Westercamp and Tazieff, 1980) overlain by volcanic materials belonging to an old Oligocene volcanic arc (Westercamp and Tazieff, 1980). The islands of Petite-Terre, Marie-Galante and Grande-Terre are composed of calcareous reef of Pleistocene age (Komorowski et al., 2005). Finally, the islands of Basse-Terre and Les Saintes result from the most recent arc activity that was initiated during Pliocene and that is still active (Maury et al., 1990; Samper et al., 2007; Wadge, 1986). The climate is tropical humid and the rain-bearing winds that blow from east to west cause many micro-climate and very important variations of rainfall over very short distances (Colmet-Daage and Lagache, 1965; Morell and Jérémie, 1994). At some places, the mean annual rainfall (MAR) amounts to 850 mm with a pronounced and long dry season, and to 8000 mm with no dry season at the summit of the volcanic island (Colmet-Daage and Lagache, 1965; Morell and Jérémie, 1994; Plaisir et al., 2003). These varying geological and climate conditions over very short distances have led to diverse landscapes, and offer an excellent scientific framework to study the impact of geology, climate and land use on soil processes.

Figure 1-1: Location of the Guadeloupe archipelago and of the islands composing the archipelago.

1.2 General settings of the island of Basse-Terre

1.2.1 Geology

The volcanic activity of the island of Basse-Terre has migrated from north where the oldest volcanic massifs are found to south where *La Soufrière* volcanic massif recently developed (Figure 1-2a, Samper et al., 2007). The ages of the geological formations have recently been updated (Samper et al., 2007). The volcanic activity initiated in the north in the Basal Complex at 2.79 Ma and lasted about 110 kyr. After a 900 kyr dormancy period, the Septentrional Chain settled along a NNW-SSE axis between about 1.81 and 1.15 Ma. The Axial Chain started to settle after a dormancy period of about 100 kyr between about 1023 and 435 ka. The Mont Caraïbes Massif was established during the same period. The Grande Découverte Volcanic Complex (GDVC) started to settle at about 200 ka (Carlut et al., 2000; Komorowski et al., 2005; Samper et al., 2007). The last magmatic eruption of the GDVC occurred in 1440 AD and the last eruptions were phreatic eruptions in 1976-77 (Komorowski et al., 2005). The GDVC settlement can be divided into three main phases. The Grande Découverte phase that started 200 ka ago corresponds to a series of effusive eruptions producing andesitic lava flows interrupted by explosive caldera-forming eruptions (Komorowski et al., 2005). Then the Carmichaël phase that took place from about 42,000 to 11,500 yrs BP during which succession of lava flows and domes, and several explosive pyroclastic phases occurred in the Grande Découverte caldera to reconstruct the Carmichaël composite volcano (Dagain, 1981; Komorowski

et al., 2005). Finally, the *Soufrière* phase began 8,500 yrs BP into the Amic crater and corresponds to a succession of lava dome eruptions and long periods of phreatic activity (Komorowski et al., 2005). The last magmatic eruption took place about 1440 AD and shaped *La Soufrière* volcano as it is known today.

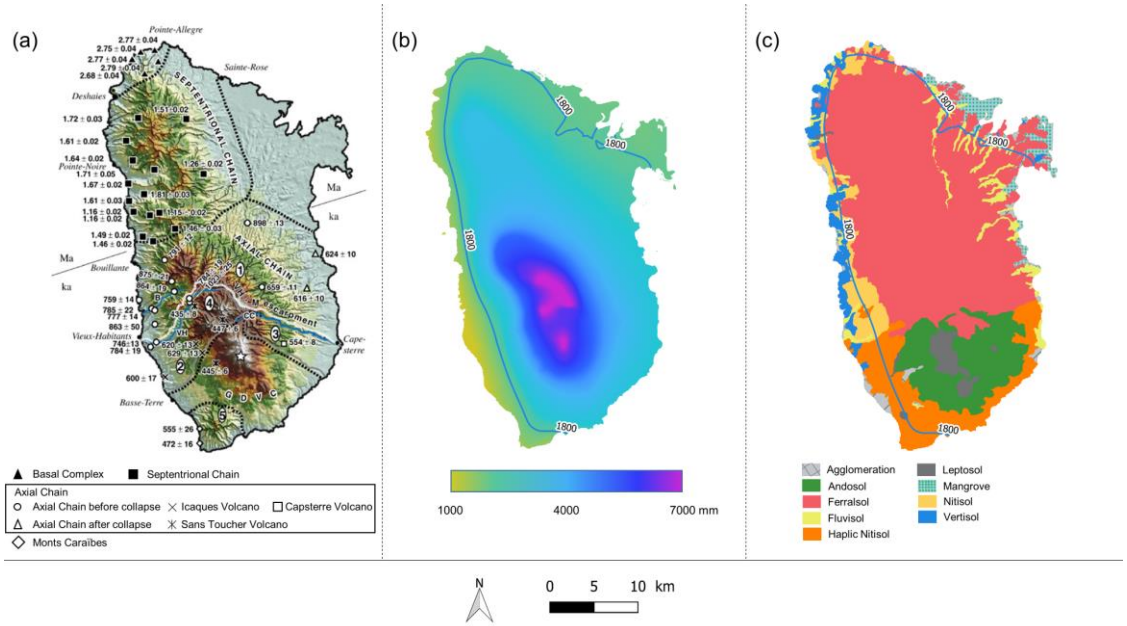

Figure 1-2: (a) Basse-Terre Island shaded digital elevation model with limits of Basal Complex, Septentrional Chain and Axial Chain massifs (dotted lines) (From Samper et al. (2007)). Ages of geological materials as measured by Samper et al. (2007) are given within each massif. (b) Map of the mean annual rainfall on the Basse-Terre Island. (c) Simplified pedological map of the Basse-Terre Island modified from (Colmet-Daage and Lagache, 1969). The 1800 mm isohyet, that corresponds to the threshold where MAR minus potential evapotranspiration becomes negative, is superimposed on the MAR and soil maps.

1.2.2 Climate

The Basse-Terre Island has a wet tropical climate (Colmet-Daage and Lagache, 1965) with a mean annual temperature of 23°C and a mean annual humidity of 75%. Temperatures are quiet stable during the year (± 3°C) whereas the seasons are defined by different rainfall patterns. The dry season from January to June and the wet rainy season from July to December, characterized by the appearance of tropical waves and cyclones (about 60% of the annual precipitation occurs during this season, MétéoFrance data). The trade winds blowing from east to west are very humid. The orographic interception of the moisture carried by these winds generates an orographic lift promoting the formation of clouds and rainfalls on windward slopes and dry and cloudless air on the leeward slopes (Figure 1-2b). Consequently, on the east coast, the MAR evolves from 2500 mm at the sea level to 7000 mm at 1467 m above sea level (asl) and, on the west coast, the MAR evolves from 1000 mm at the sea level to 7000 mm at 1467 m asl (Figure 1-2b) (Chaperon et al., 1985). As the mountains are smaller in the north of the Basse-Terre Island, the Foehn effect is less pronounced and pluviometry is globally lower.

1.2.3 Pedology

On the island of Basse-Terre, soils developed from andesitic ash deposits of Pliocene to Holocene age. These deposits are mostly of andesitic composition with plagioclase, pyroxene and ferromagnesian volcanic glasses as the main weatherable minerals (Dagain, 1981; Ndayiragije, 1996; Ndayiragije and Delvaux, 2003). The distribution of the soils of Basse-Terre is linked (1) to the age of the volcanic deposits and (2) to the climate (Colmet-Daage and Lagache, 1965; Henriet et al., 2008a; Ndayiragije, 1996). The ancient volcanic formations (0.5 Ma to 2.79 Ma) are located in the two third north of the island and the recent ones (< 0.2 Ma) in the south (Samper et al., 2007). In the south, the soils of the western flank of the *La Soufrière* volcano derive from debris flows from 11,500 and 3,100 years BP eruptions while the soils of the east flank derive from older lava flows and lapilli deposits (30,000-18,000 years BP) (Beauducel, 2005). As rainfall depends on altitude and on the exposure to the trade wind, three main climo-toposequences are observed (Figure 1-2c; Colmet-Daage and Lagache, 1969).

(1) **In the north** of the island, soils are old and MAR raises with altitude. The climo-toposequence is: Ferralsol in altitude (humid conditions) and Vertisol at sea level but only on the western side where conditions are dry enough. The mineralogy evolves from (i) the combination of Fe oxides and kaolinite to (ii) smectite (Colmet-Daage and Lagache, 1969; Ndayiragije, 1996; Ndayiragije and Delvaux, 2004, 2003). The formation of Fe oxides and kaolinite in Ferralsol testifies the intense leaching of base cations and Si where MAR is above evapotranspiration (at about 1800 mm of MAR) that led to the relative accumulation of Fe and Al, and the depletion of Si (Chadwick et al., 2003). In contrast, on the western coast at low altitude, MAR is below evapotranspiration (MAR < 1800 mm). Base cations and Si were relatively little leached and smectite, a Si-rich secondary mineral, neoformed (Figure 1-2). (2) **In the south-eastern part** of the island, soils are younger than in the north. MAR is high at sea level (2500 mm) and raises with altitude. The climo-toposequence is: perhydrated Andosol - Andosol (humid conditions) - Nitisol at sea level (humid conditions with a short dry season). The mineralogy evolves from (i) the combination of allophane, gibbsite, kaolinite and hydroxyl-Al interlayered 2:1 minerals to (ii) allophane, to (iii) a combination of halloysite and Fe oxides (Colmet-Daage and Lagache, 1969; Ndayiragije, 1996; Ndayiragije and Delvaux, 2004, 2003). In altitude, kaolinite and gibbsite formed because of strong desilication. However, this contrasts with the presence of 2:1 clay minerals. Ndayiragije and Delvaux (2003) attributed the presence of 2:1 minerals to their inheritance from the parent ash, and not from pedogenic processes. Al interlayering occurred in these 2:1 minerals during soil formation and provided an anti-gibbsitic effect (Ndayiragije and Delvaux, 2003). (3) **In the south-western part** of the island, soils are the youngest and MAR is low at sea level (1000 mm), and raises with altitude. The climo-toposequence is: Vitric Andosol - Cambisol. The mineralogy evolves from (i) ash to (ii) allophane, and to (iii) the combination of halloysite and smectite (Colmet-Daage and Lagache, 1965; Henriet et al., 2008a; Ndayiragije, 1996; Ndayiragije and Delvaux, 2003, 2004; Opfergelt et al., 2012b, 2012a).

1.2.4 Soil occupation and agriculture

The agricultural surfaces cover 33% of the Guadeloupe (Morell and Jérémie, 1994). Sugarcane and banana are the two main crops produced in Guadeloupe, with 29% and 13% of the agricultural area occupied by these

croplands respectively (Morell and Jérémie, 1994). On the island of Basse-Terre, agriculture is not evenly distributed. Commonly, banana plantations are cultivated in the south on steep slopes and sugarcane is cultivated in the north on plains (Rad et al., 2011). However, sugarcane plantations are also present in the south of the island on shallow areas. In altitude, well preserved tropical rainforests dominate (Rousteau, 1996; Rousteau et al., 1994).

1.3 The Pérou River and Pères River catchments

1.3.1 Location

The Pérou River and Pères River catchments are located on the eastern flank of the volcano *La Soufrière* in the south east of Basse-Terre Island in the municipality of Capesterre-Belle-Eau (Figure 1-3a).

1.3.2 Climate

MAR increases from 2500 mm at sea level to 4700 mm at the summit of the Pères River catchment (474 m asl) and to 7000 mm at the summit of the Pérou River catchment (1386 m asl) (Figure 1-3b, c, d).

1.3.3 Geology

From a geological point of view, four main kinds of formations are observed on these catchments (Figure 1-3b) (Charlier et al., 2015) from the oldest to the youngest: (1) The massive andesitic lavas of the Capesterre Mountain, mostly located to the right of the Pérou River that originate from the volcanism of the axial chain (between 1023 and 435 ka). (2) The debris flows that have filled a paleo valley that settled from the Pérou River to the right bank of the Saint Denis River (< 0.5 Ma). (3) Pyroclastic deposits and pyroclastic surge from two different origins. The first located at the Féfé catchment (from the GDVC < 0.2 Ma) and the second that flows from the "Petites Mamelles" andesitic dome (< 0.5 Ma). (4) The superficial formations (alluvium) in the edge or in the bed of the river. All these volcanic materials, were more recently (30,000 to 18,000 years BP) covered by successive pumice lapilli volcanic deposits that lead to the superposition of several Andosols (Beauducel, 2005; Charlier et al., 2008).

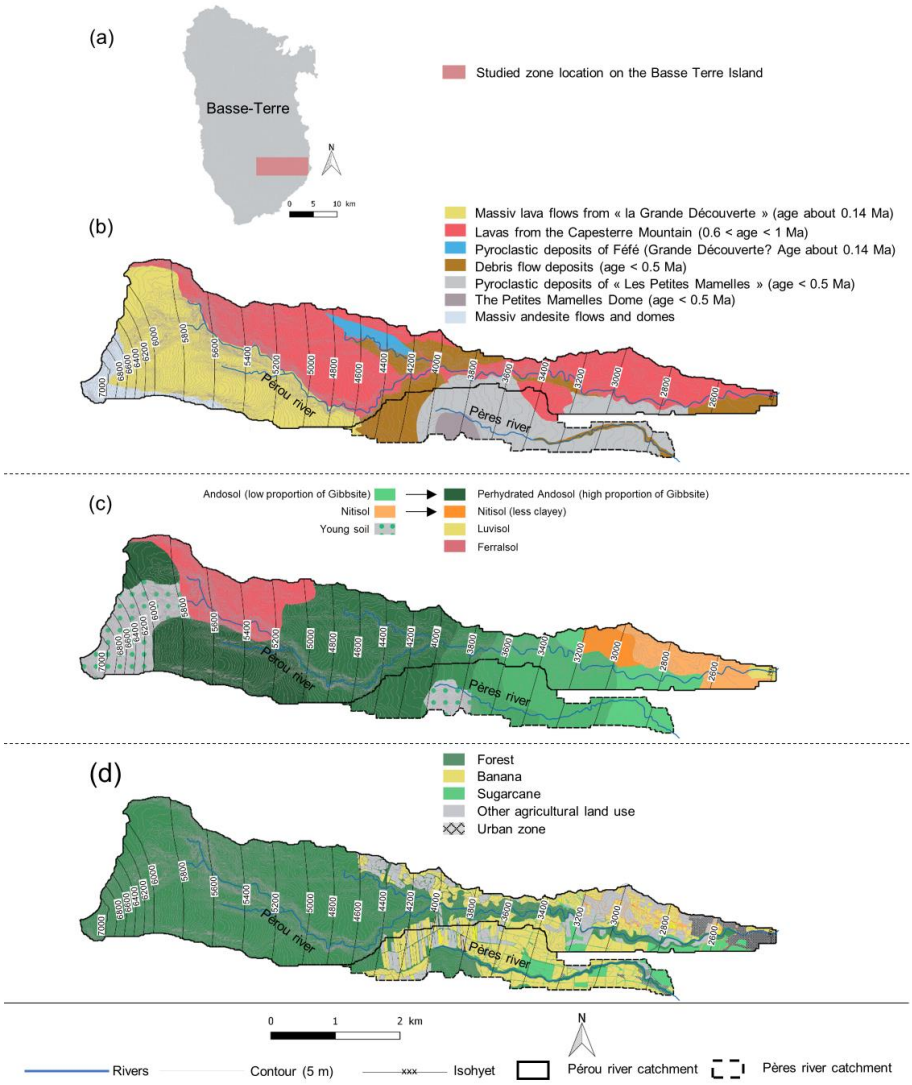

Figure 1-3: (a) Localization of the studied zone. (b) Geological map of the studied watersheds (Charlier et al., 2015). (c) Simplified pedological map of the studied watersheds modified from (Colmet-Daage and Lagache, 1969). (d) Map of the main land use of the studied watersheds (updated in 2017). Altitudinal contours and mean annual rainfall isohyets are superposed on the (b-c-d) maps.

1.3.4 Pedology

The soils of these catchments developed in a topo-climo-litho-chrono-sequence very comparable to that studied by Henriet et al. (2008a), Opfergelt et al. (2012a, 2012b). From sea level to altitude, soils evolve from Nitisol to Andosol to perhydrated Andosol and even to Ferralsol on a small part of the Pérou River catchment (Figure 1-3c) (Colmet-Daage and Lagache, 1965). Low altitude Nitisol and high altitude Ferralsol probably have an older origin than Andosols. At high altitude where soils are exposed to abundant rainfalls (> 4000 mm), perhydrated Andosols developed with the combination of allophane/gibbsite as dominant secondary minerals and very high organic matter content (Colmet-Daage and Lagache, 1965). Beneath 4000 mm of MAR, Andosols developed with allophane as the dominant secondary mineral. Finally, Nitisols developed in the lowest part of the catchments with halloysite/Fe oxides as the dominant secondary minerals.

1.3.5 Soil occupation and agriculture

The soil occupation of the two catchments has been updated in 2017 by field observations (Figure 1-3d). The Pères River catchment has a surface of 300 ha. The cultivated surface and forests cover 56.7% and 17.4% of the total surface respectively. The intensive banana production and the intensive sugarcane production represent 60.1% and 11.4% of the cultivated areas respectively. The major part of the forest is present in altitude above 400 m asl the rest being concentrated along the river. The Pérou River catchment has a surface of 1234 ha. The cultivated surface and forests cover 18.8% and 75.3% of the total surface respectively. The intensive banana production and the intensive sugarcane production represent 38.8% and 9.9% of the cultivated areas respectively.

Chapter 2 Evolution of the silicon bio-availability in volcanic soils along a climo-toposequence in Guadeloupe[1]

Abstract

The amount of water available to leach solutes from soil is one of the major features determining mineral weathering, secondary mineral synthesis and soil properties. It affects the fate of dissolved silicon (Si), which may follow four routes: leaching, mineral synthesis, adsorption, uptake by plants to form phytoliths. Here, we quantify the reservoirs of bioavailable Si and phytolithic Si in wet tropical Andosols along a topoclimosequence where mean annual rainfall (MAR) increases from 2650 to 4400 mm with increasing altitude (65-375m above sea level) in the volcanic island of Basse-Terre, Guadeloupe. We assessed bioavailable Si through $CaCl_2$ extraction in soil, and by foliar analysis in banana plants. We evaluated the pool of phytolithic Si through Na_2CO_3 extraction and heavy liquid separation. The Na_2CO_3 extraction was performed on both the bulk soil and oxalate–treated soil (ox- Na_2CO_3) cleared of its amorphous aluminosilicates. The Andosols have reached an advanced weathering stage. Their secondary products included (Al, Fe)-humus complexes, ferrihydrite, gibbsite and aluminous allophanic substances. The contents of organic C, metal-humus, ferrihydrite and gibbsite increased in wettest conditions (>3000mm) whereas allophane content concomitantly decreased. Si leaf content varied little (3.8–5.3 g kg^{-1}), but slightly decreased with increasing MAR. Bioavailable Si content in soil decreased from 63 to 12 mg kg^{-1} with increasing MAR (r = -0.92), and was strongly correlated (r = +0.95) to that of phytolithic Si as assessed after ox-Na_2CO_3 extraction. The Si/Al ratio of the ox-Na_2CO_3 extract regularly decreased from 1.06 to 0.37 with increasing MAR, hence corroborating strongest desilication in wettest conditions. In these highly leached, gibbsitic Andosols, rainfall is thus the major driver of plant Si availability.

[1] Manuscript in preparation for submission in an international peer-reviewed journal.

2.1 Introduction

In soils experiencing net acidification (van Breemen et al., 1983), weatherable primary silicates inherited from parent materials dissolve and release monosilicic acid ($H_4SiO_4^0$), aluminum (Al), iron (Fe) and other aqueous solutes. The solutes may recombine to synthesize pedogenic secondary silicates, or precipitate as oxides, a.o. Al and Fe (Garrels and Christ, 1965). Through its impact on solute concentration and fate, rainfall, in particular the amount of water available to leach solutes from soil, is one of the major features determining mineral weathering, secondary mineral synthesis and soil properties (Garrels and Christ, 1965; Rai and Kittrick, 1989). For instance, in volcanic soils derived from basalt, the water regime strongly imprints soil processes and mineral composition, and fixes steep thresholds that define soil properties, buffering capacity and their biogeochemical behavior (Chadwick et al., 2003). The fate of silicon (Si) is crucial, given its role in mineral synthesis (Churchman and Lowe, 2012). Once released, aqueous $H_4SiO_4^0$ may take four routes: (i) leaching and export to watersheds (Conley, 2002); (ii) synthesis of clay minerals (Garrels and Christ, 1965) and/or amorphous silica (Drees et al., 1989); (iii) adsorption on Fe and Al oxides (Beckwith and Reeve, 1963; Jones and Handreck, 1963; McKeague and Cline, 1963); (iv) uptake by plant roots (Jones and Handreck, 1965). Abundant precipitation and intense leaching enhance mineral weathering and export of solutes to watersheds. Secondary minerals synthesized from dilute solutions include aluminosilicates with low Si/Al ratio, and Al and Fe oxides. In perhumid volcanic ash soils, typical compositions encompass allophane, imogolite, gibbsite and ferrihydrite as well as (Al, Fe)-humus complexes if soil organic matter (SOM) accumulates (Colmet-Daage and Lagache, 1965; Huang et al., 2002; Jongmans et al., 1994; Ndayiragije and Delvaux, 2003; Nieuwenhuyse and Van Breemen, 1997; Nizeyimana et al., 1997; Parfitt et al., 1983; Parfitt and Wilson, 1985). Apart from mineral synthesis, aqueous $H_4SiO_4^0$ can also be retrieved from soil solution through adsorption on oxide surfaces and root uptake. Plants absorb $H_4SiO_4^0$ and form amorphous silica bodies ($SiO_2.nH_2O$, opal A) called phytoliths (Jones and Handreck, 1965; Piperno, 1988; Raven, 1983; Sangster and Hodson, 1986). Silicon returns to soil through phytolith deposition within plant debris. In soil, phytoliths readily dissolve at common pH values of soil solution (Fraysse et al., 2009) and contribute to supply the pool of dissolved Si (DSi) (Derry et al., 2005). The Si uptake by roots, phytolith formation in plant and dissolution in soil

providing bioavailable Si for plant uptake defines a biological Si feedback loop, which governs the terrestrial biogeochemical cycle of Si (e.g. Alexandre et al., 1997; Bartoli, 1983; Henriet et al., 2008a; Lucas et al., 1993; Meunier et al., 1999). Because of mineral depletion, this loop may be particularly active in highly weathered, desilicated soils (Cornelis and Delvaux, 2016). This biological effect keeps Si from being leached, and accounts for the stability of kaolinite in the surface horizons of gibbsitic ferrallitic soils (Lucas et al., 1993). Following Chadwick et al. (2003), at mean annual rainfall (MAR) above 1400 mm, soil buffering capacity has been totally exhausted in basalt-derived soils from Hawaii. Yet the biological cycling of Si may alleviate natural soil desilication, and "buffer" the release of plant available Si to some extent. An increase in Si uptake by plants from 22 to 67 kg ha^{-1} yr^{-1} with increasing MAR from 340 to 1110 mm has been reported in grasslands from the Great Plains (Blecker et al., 2006). In Serengeti savanna ecosystems under MAR ranging from 600 to 900 mm, Quigley et al. (2017) identified soil pH, sand content and, to a lesser extent, rainfall as drivers controlling dissolved Si and soil phytogenic Si pools. In humid tropical forests under MAR ranging from 1600 to 3200 mm, Schaller et al. (2018) identified soil weathering stage and pH as drivers of plant available Si, but not rainfall.

Yet, to the best of our knowledge, the impact of rainfall on Si bioavailability in the humid tropics is still unknown. Here, we quantify the reservoirs of bioavailable Si and phytolithic Si in perhumid volcanic ash soils along a topoclimosequence where MAR increases from 2650 to 4400 mm with increasing altitude (65-375m above sea level (asl)) in the volcanic island of Basse-Terre, Guadeloupe.

2.2 Environmental framework

The studied zone is located on the Pères river catchment on the east flank of *La Soufrière* volcano in the south east of the Basse-Terre Island in Guadeloupe (16°N, 61°W) (Figure 2-1a). The trade winds blowing from east to west are very humid. The orographic interception of the moisture carried by these winds generates an orographic lift promoting the formation of clouds and rainfalls on windward slopes. Consequently, on the studied catchment, the MAR evolves from 2650 mm at 65 m asl to 4400 mm at the top of the catchment (400 m asl) (Figure 2-1b). The soils are thus distributed along a topoclimosequence. They formed from pyroclastic andesitic deposits

of pumice lapilli type from 30,000 to 18,000 years BP (Figure 2-2) (Charlier et al., 2011; Colmet-Daage and Lagache, 1965; Crabit et al., 2016; Dagain, 1981) with plagioclase, pyroxene and volcanic glass as dominant weatherable minerals (Dagain, 1981; Ndayiragije, 1996). At MAR > 4000 mm, perhydrated Andosols contain (Al, Fe)-humus, allophane and gibbsite as dominant secondary products (Figure 2-1b). In particular, the abundance of large particles of gibbsite, developing as pseudomorphs of plagioclase and pyroxene, reflects a strong desilication of the soil (Ndayiragije and Delvaux, 2003). At MAR < 4000 mm, allophane is the dominant clay mineral, while C and gibbsite contents slightly decrease (Colmet-Daage and Lagache, 1969). Halloysite and Fe oxide are abundant in the Nitisols that developed in the lowest parts of the catchment. All soils are strongly microaggregated (Dorel et al., 2000). Croplands and forests cover 56.7% and 17.4% of the total surface, respectively. Intensive banana and sugarcane cropping represent, respectively, 60.1% and 11.4% of croplands. The catchment is probably intensively cultivated since the late seventeenth century AD (Doumenge, 1985).

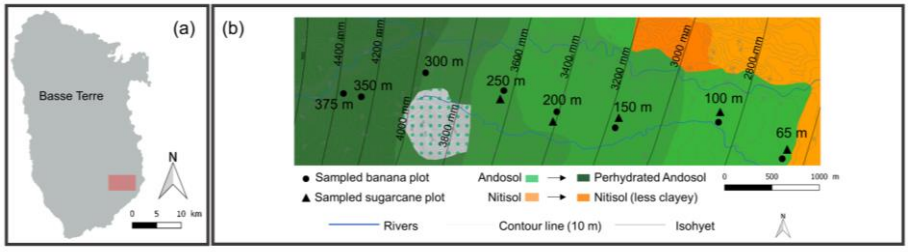

Figure 2-1: (a) Location of the studied soil topoclimosequence, Basse-Terre Island, Guadeloupe. (b) Location of sampling sites on the soil map figured out with isohyets (MAR black lines): banana (●), sugarcane (▲).

2.3 *Materials and methods*

2.3.1 General sampling scheme

Eight banana (*Musa acuminata*, Cavendish, group AAA, desert banana) and five sugarcane (*Saccharum officinarum*) cultivated plots were selected along

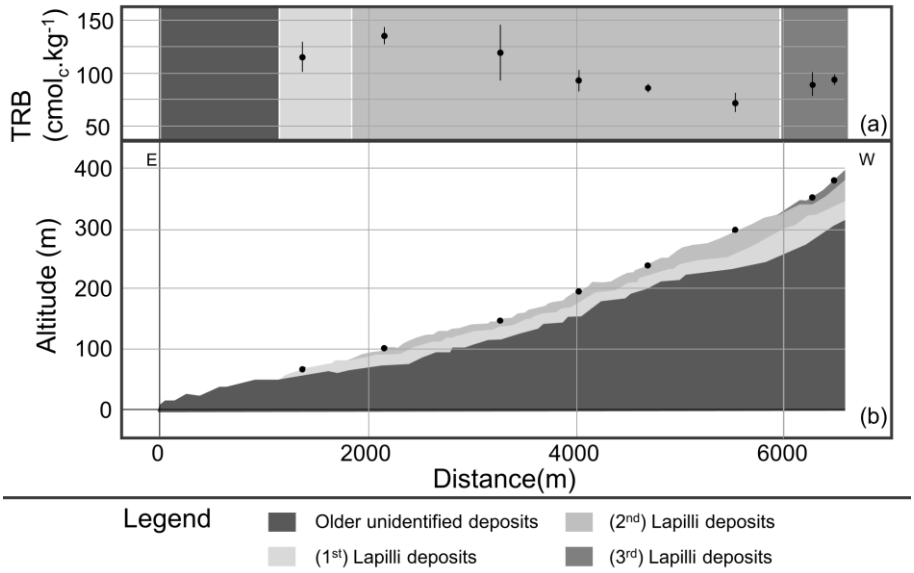

Figure 2-2: (a) Evolution of TRB along the soil topoclimosequence; (b) schematic geological profile. Depth of the deposits are not scaled but enlarged to improve visualization.

a climo-toposequence at 65, 100, 150, 200, 250, 300, 350, 375 m asl, and 65, 100, 150, 200, 250 m asl, respectively (Figure 2-1). On each banana plot (except at 375 m), 18 plants were randomly selected at flowering stage. For each plant, we sampled the external part of the lamina at the center (100 mm width) of the antepenultimate leaf (leaf III) following the international standard set up for banana foliar diagnosis (Martin-Prével, 1980). Afterwards, three groups of 6 leaves were randomly constituted and mixed to obtain three composite samples for each site. Sugarcane leaves could not be sampled because the field study took place just after harvesting. In each plot, nine topsoil samples (00-20 cm) were collected randomly, and combined into 3 composite samples. Six undisturbed moist topsoil samples were collected at field capacity using Kopecky cylinders to measure the bulk density.

2.3.2 Basic soil analyses

Soil texture was determined by quantitative recovery of clay, silt and sand fractions after sonication and dispersion with Na^+ saturated resins without any previous oxidation of SOM (Rouiller et al., 1972). pH was measured in H_2O using 5 g : 25 ml suspensions. Phosphate retention was measured

according to Blakemore (1983). Dark oxalate-extractable (o), dithionite-citrate-bicarbonate (DCB) extractable (d) and pyrophosphate-extractable (p) contents of Si, Al and Fe were determined in the respective extracts by inductively coupled plasma-atomic emission spectrometry (ICP–AES) following the methods compiled in Dahlgren (1994). Total C and N contents were determined by high temperature dry combustion using a Vario EL Cube elemental analyzer. Crystalline soil minerals were identified by X-ray diffraction (XRD) on powder soil samples using Cu$K\alpha$ radiation in a Bruker Advance diffractometer. Total elemental contents were determined on soil samples by ICP-AES after fusion in Li-metaborate and Li-tetraborate at 1000°C (Chao and Sanzolone, 1992). The contents of major alkaline and alkaline-earth cations were summed up to compute the Total Reserve in Bases (TRB) (Herbillon 1986).

2.3.3 Thermogravimetric analyses

Thermogravimetric analysis (TGA) was used to determine the content of gibbsite in the Mg^{2+}-saturated clay fraction (5-10 mg) (Ndayiragije and Delvaux, 2003). TGA was carried out with a Mettler Toledo TGA/SDTA 851e in a flowing nitrogen atmosphere (50 ml min^{-1}) from 30°C to 1000°C with a heating rate of 10°C min^{-1}, using gibbsite from Alcoa® Company <https://www.alcoa.com> for calibration purposes. The thermal events were interpreted by plotting the derivatives of the TGA curves.

2.3.4 Specific Si extractions

$CaCl_2$. $CaCl_2$-extractable Si content ($CaCl_2$-Si) is considered to assess the bioavailable Si pool in soils (Haysom and Chapman, 1975; Sauer et al., 2006). We carried out a 6 h to 64 days kinetic extraction using a solid:liquid ratio 5 g:50 mL (0.01 M $CaCl_2$) in 100 mL polyethylene cups shaken at 25 °C following the procedure of Li et al. (2019). The Si concentration in the $CaCl_2$ extract (diluted 10 times and neutralized by 50 µl of a 15 M HNO_3 solution) was measured by ICP-AES.

Na_2CO_3. Na_2CO_3-extractable Si content was determined to assess phytolithic Si (PhSi) in soils (DeMaster, 1981; Koning et al., 2002; Sauer et al., 2006). We carried out a kinetical extraction (DeMaster, 1981). Forty milligrams of soil sample (f<2mm) were mixed with 40 ml of 0.1 M Na_2CO_3 at 85°C during 7h. One milliliter of solution was collected after 15, 60, 120, 180, 240, 300, and 360 min, diluted with 9 ml of deionized water and acidified with 50 µl of

Suprapur HNO_3. Si, Al, Fe, and Mg concentrations were measured at each time by ICP-AES. According to DeMaster (1981), the intercept of the linear part of the time release of Si estimates the amorphous Si (ASi) pool. Na_2CO_3 kinetical extractions were performed on soil samples respectively untreated and pretreated using dark oxalate extraction (Blakemore, 1981), immediately followed by a rinsing using $CaCl_2$ 0.01 M (Sauer et al., 2006) to remove residual DSi. Dark oxalate buffered at pH3 dissolves organo-mineral associations (OMA), short range ordered (SRO) pedogenic silicates (PSi) (allophane and imogolite), adsorbed forms of Si, and Fe oxide (ferrihydrite) (Parfitt and Childs, 1988; Wada, 1989, 1977), and possibly poorly crystalline Al hydroxide (Huang et al., 2002). The dark oxalate pretreatment was carried out to bring the ASi pool as close as possible to the PhSi pool. The ASi content of untreated soil is named Na_2CO_3-Si whereas the PhSi content of oxalate-treated soil is ox-Na_2CO_3-Si.

Heavy liquid separation. This physical extraction was carried out on one composite sample for each plot. Following Henriet et al. (2008b), the silt fraction was recovered after sonication and dispersion with Na^+ saturated resins without any previous oxidation of SOM (Rouiller et al., 1972), then treated with H_2O_2 and DCB. An additional dispersion using Na^+-saturated resins (Rouiller et al., 1972) was carried out overnight to discard any clay contamination. The silt fraction was then divided into light and heavy components , through a series of heavy liquid separations, using a Na polytungstate solution with a density of 2.3 g cm^{-3} (adapted from Kelly, 1990). Each silt fraction was mixed with 20 ml of Na polytungstate and centrifuged at 4000 rpm for 10 min. After centrifugation, the supernatant containing floating particles was carefully removed with a pipette and collected on a Teflon filter (2 µm). The operation was repeated until the supernatant was clear. The filter was then rinsed with 1 M HCl and washed with deionized water. The light fraction was submitted to a XRD analysis, and to a total analysis by fusion in Li-metaborate and Li-tetraborate at 1000°C. Extracted Si, Al, Fe, and Mg contents were determined by ICP-AES. XRD data were further used to quantify the components of the light fraction using the SIROQUANT © quantitative XRD software (version 2.5). In fact, we did not count the phytolithic particles on microscope images because of the substantial occurrence of other minerals in the light fractions. We further calculated the content of phytolithic Si from that of PhSi particles as

estimated after XRD quantification, in order to compare it with the Si concentration measured in $CaCl_2$ and Na_2CO_3 extracts. A pytholith mean water content of 10% was assumed (equivalent to 0.37 moles of H_2O for 2 moles of SiO_2) (Alexandre et al., 1997; Meunier et al., 2014). The PhSi content as assessed by XRD after heavy liquid (*hl*) separation is named XRD-*hl*PhSi.

2.3.5 Foliar analysis

Leaf samples were thoroughly washed with 70% ethanol in order to remove eolian pollution. They were dried at 70°C for four days and then grinded. Mineral analysis was carried out after calcination at 450°C for 1 day and fusion in Li-metaborate + Li-tetraborate at 1,000°C (Chao and Sanzolone, 1992), followed by the pellet dissolution in 15% HNO_3. Nutrient and Si concentrations were measured by ICP-AES.

2.3.6 Hypotheses and statistical analyses

All statistical analyses were conducted with the R programing language (version 3.4.4). First, differences of means were tested with a t-test with the pairwise.t.test function. Next, we explored linear relationship among soil Si pools ($CaCl_2$-Si, Na_2CO_3-Si, ox-Na_2CO_3-Si, total Si, XRD-*hl*PhSi) and the three hypothesized possible influencing paramaters: MAR, TRB (reflecting soil weathering stage), and pH. To do this, we used the *lm* function of the R programing language (Equation 1).

$$Si_{pool} \sim a + bMAR + cTRB + dpH \quad (Eq\ 1)$$

2.4 Results

2.4.1 Soil properties and constituents

At a given altitude, soil properties in banana (BA) and sugarcane (SC) plots were similar (Tables 2-S1 and 2-S2). Therefore, we considered the whole data set as based on six repetitions per altitude level. As inferred from Table 2-1, our results are in perfect line with previous soil survey data (Colmet-Daage and Lagache, 1969) and mineralogical characterization (Ndayiragije and Delvaux, 2003). Soil texture is clay loam to clay. With increasing altitude, bulk density decreases from 0.8 to 0.5 g cm^{-3} while C content increases from 42 to 97 g kg^{-1}. Given the values of the Si/(Al+Fe) ratio (1.0-0.8) and Fe_d/Fe_t (0.52-0.47), all soils have reached an advanced stage of mineral weathering and desilication, in particular above 150 m asl where TRB is below 100 $cmol_c$ kg^{-}

[1]. Considering that soil weathering stage is advanced and comparable all along the toposequence, rainfall is likely the most important factor controlling soil formation. Oxalate extractable Fe content (Fe_o), which refers to SRO Fe oxide and Fe-humus, represents 23 to 29% of free iron below 300 m asl, and 39 to 49% above that level, in relation to the large C content (78-97 g kg^{-1}). Strong desilication is confirmed by large gibbsite contents as measured by TGA (31-113 g kg^{-1}).

XRD data (Figure 2-S1) point to the occurrence of gibbsite, halloysite, and 2:1:1 phyllosilicate (>350 m asl) as previously identified (Ndayiragije and Delvaux, 2003). Remarkably, the intensity of the 002 XRD reflection at 0.485 nm typical for gibbsite increases with increasing altitude, similarly to gibbsite content as measured by TGA (Table 2-1).

Table 2-1: Selected soil properties: particle size analysis, bulk density, Total Reserve in Bases (TRB), Si/(Al+Fe), Fe_d/Fe_t and Fe_o/Fe_d atomic ratios, contents of organic C and allophane, $Si_o/(Al_o-Al_p)$ atomic ratio. The average values are computed from individual values as determined on six composite samples collected in banana (3) and sugarcane (3) plots at 65, 100, 150, 200, and 250 m, but on three composite samples in banana plots at 300, 350, and 375 m. Different lowercase letters express significant differences at $p<0.05$ level for TRB, Si/(Al+Fe), Fe_d/Fe_t, Fe_o/Fe_d, C, allophane content and $Si_o/(Al_o-Al_p)$. Differences were tested with a t-test with the pairwise.t.test function of the R programming language.

Alitude	**Particle size analysis (%)**			**Bulk density**	**TRB**	**Si/(Al+Fe)[a]**	**Fe_d/Fe_t**	**Fe_o/Fe_d**	**C**	**Allophane[b]**	**$Si_o/(Al_o-Al_p)$[c]**	**Gibbsite**	**P ret**
m	**Clay**	**Silt**	**Sand**	**g cm^{-3}**	**$cmol_c$ kg^{-1}**				**g kg^{-1}**	**g kg^{-1}**		**g kg^{-1}**	**%**
65	39.2	48.0	12.8	0.82	114 abc	1.01 a	0.52 a	0.27 ab	42.3 a	95 ab	0.61 a	31.0	96
100	48.7	32.5	18.8	0.78	134 a	0.90 b	0.49 a	0.27 ab	49.9 ab	161 c	0.55 a	72.7	97
150	40.6	36.5	22.9	0.74	118 ab	0.80 cd	0.50 a	0.27 ab	55.0 b	122 a	0.65 a	101.1	98
200	30.2	46.4	23.4	0.73	92 cd	0.79 cd	0.51 a	0.29 a	54.6 b	104 ab	0.62 a	112.9	96
250	18.4	45.9	35.7	0.70	85 d	0.79 c	0.53 a	0.23 b	48.8 ab	73 b	0.65 a	101.8	96
300	37.1	41.0	21.9	0.73	71 d	0.78 cd	0.53 a	0.27 ab	51.6 ab	95 ab	0.54 a	112.7	96
350	34.1	47.6	18.3	0.57	88 bcd	0.87 bcd	0.48 a	0.39 ac	78.2 c	85 b	0.61 a	103.6	96
375	35.5	38.2	26.3	0.51	93 bcd	0.91 bcd	0.47 a	0.49 d	97.0 d	80 b	0.52 a	101.9	97

[a] computed from total elemental contents Si_t, Al_t and Fe_t (Table 2-S1)

[b] Allophanic substances; estimated according to Parfitt and Wilson (1985), using Si_o, Al_o and Al_p contents (Table 2-S1).

[c] computed from Si_o, Al_o and Al_p contents (Table 2-S1).

2.4.2 XRD and total analyses of the *hl*PhSi particles

XRD data performed on *hl*PhSi particles reveals the occurrence of cristobalite, tridymite, and gibbsite particles (Figure 2-S2), which could not be separated from phytoliths because of their respective densities of 2.32-2.36, 2.25-2.28 g cm^{-3}, and 2.34 g cm^{-3} (Huang et al., 2002; Monger and Kelly, 2002), very close to that of phytoliths (~2.3 g cm^{-3}).

Loss on ignition of *hl*PhSi particles ranged between 3.7 and 15.1% irrespective of altitude (Table 2-2). The ranges of SiO_2 and Al_2O_3 concentrations were, respectively 70.3 – 92.2%, and 3.3 – 15% (Table 2-2). The Si/Al ratio of *hl*PhSi particles amounted to 30 at 375 m asl, but ranged between 5 and 13 in BA plots, and between 9 and 15 in SC plots. The concentrations of other oxides were below 1%. The elemental composition of *hl*PhSi particles did not show any trend in relation to altitude.

The quantification of phytoliths, tridymite, cristobalite, and gibbsite with SIROQUANT software shows that the percentage of phytoliths in heavy liquid extracts varies widely from one sample to another (Table 2-3). It ranges from 12.7 to 63.8% in BA plots samples and from 10 to 76.2% in SC plots samples.

Table 2-2: Elemental composition and ignition loss (on phytoliths dried overnight at 105°C) of the particles extracted by heavy liquid separation for each plot at each altitude (BA: banana; SC: sugarcane).

Altitude	Land use	Al_2O_3	CaO	Fe_2O_3	K_2O	MgO	Na_2O	SiO_2	TiO_2	Ignition loss	Si:Al
m						%					atomic ratio
65	BA	9.52	0.19	0.58	0.13	0.12	0.28	78.72	0.18	10.29	8.99
65	SC	6.27	0.14	0.51	0.13	0.09	0.35	86.63	0.18	5.70	15.03
100	BA	15.04	0.14	0.88	0.13	0.14	0.35	69.49	0.23	13.59	5.02
100	SC	11.57	0.15	0.74	0.13	0.10	0.34	76.53	0.21	10.22	7.19
150	BA	12.68	0.16	1.03	0.18	0.13	0.20	70.32	0.19	15.10	6.03
150	SC	7.24	0.11	0.58	0.13	0.08	0.19	82.57	0.15	8.95	12.40
200	BA	10.84	0.14	0.95	0.11	0.09	0.35	70.67	0.19	16.66	7.09
200	SC	6.67	0.14	0.66	0.10	0.06	0.10	81.84	0.14	10.28	13.34
250	BA	6.49	0.20	0.70	0.15	0.12	0.15	81.32	0.14	10.74	13.6
250	SC	9.47	0.14	0.89	0.19	0.12	0.25	79.99	0.20	8.76	9.19
300	BA	7.84	0.14	0.66	0.04	0.12	0.20	83.82	0.16	7.02	11.63
350	BA	12.71	0.35	0.69	0.15	0.13	0.20	74.65	0.15	10.96	6.39
375	BA	3.29	0.21	0.28	0.10	0.06	0.09	92.24	0.09	3.65	30.50

Table 2-3: Portion of each component of the particles extracted by heavy liquid separation for each plot at each altitude (BA: banana; SC: sugarcane) as estimated with the SIROQUANT © quantitative XRD software (version 2.5).

Alitude	**Land use**	**Total (*hl* particles[1])**	**Phytolith**		**Cristobalite**		**Tridymite**		**Gibbsite**	
m		**g kg^{-1}**	**%**	**g kg^{-1}**	**%**	**g kg^{-1}**	**%**	**g kg^{-1}**	**%**	**g kg^{-1}**
65	BA	47.59	12.7	6.04	31.4	14.94	52.1	24.79	3.8	1.81
65	SC	60.63	10.0	6.06	51.8	31.41	36.5	22.13	1.7	0.91
100	BA	66.6	38.5	25.64	29.7	19.78	25.2	16.78	6.7	4.13
100	SC	60.69	27.9	16.93	37.8	22.94	28.9	17.54	5.3	2.79
150	BA	61.69	24.7	15.24	24.3	14.99	43.3	26.71	7.8	4.63
150	SC	46.39	38.0	17.63	15.5	7.19	40.8	18.93	5.6	2.51
200	BA	51.71	43.3	22.39	12.2	6.31	37.0	19.13	7.4	3.67
200	SC	46.62	76.2	35.52	2.4	1.12	18.9	8.81	2.4	1.07
250	BA	40.07	65.6	26.29	3.7	1.48	28.8	11.54	1.9	0.76
250	SC	50.97	36.1	18.40	12.4	6.32	46.0	23.45	5.5	2.80
300	BA	71.3	38.0	27.09	12.4	8.84	45.2	32.23	4.4	3.14
350	BA	91.2	51.6	47.06	9.6	8.76	23.9	21.80	14.9	13.59
375	BA	83.78	63.8	53.45	3.8	3.18	29.0	24.30	3.4	2.85

[1]hl particles are the extracted particles with the heavy liquid extraction method.

2.4.3 Si pools in soils and leaf Si content

As for soil properties, Si concentrations in soil were similar at a given altitude between neighboring BA and SC plots (Table 2-S3). We thus considered the whole data set as based on six repetitions per altitude level. The Na_2CO_3-Si content ranged between 10.3 to 12.6 g kg^{-1} irrespective of altitude. The XRD-*hl*PhSi content increases with altitude from 2.54 to 22.45 g kg^{-1}. In contrast, Si_t, $CaCl_2$-Si and ox-Na_2CO_3-Si contents significantly decreased with increasing altitude (Table 2-4): Si_t from 179 to 142 g kg^{-1}, $CaCl_2$-Si from 66 to 14 mg kg^{-1}, and ox-Na_2CO_3-Si from 7.7 to 2.0 g kg^{-1}. The banana leaf Si content ranged between 3.81 and 5.30 g kg^{-1}, regardless of altitude. Except at the lowest altitude level (65m), XRD-*hl*PhSi is invariably higher than ox-Na_2CO_3-Si: from 1.5 times at 100m to 11 times higher at 375m.

Table 2-4: Average concentrations in soil of total Si (Si_t), bioavailable Si ($CaCl_2$-Si), Na_2CO_3-Si, ox-Na_2CO_3-Si, and physically extracted PhSi, and Si concentration in banana leaf III. The average values are computed from individual values as determined on six composite samples collected in banana (3) and sugarcane (3) plots at 65, 100, 150, 200, and 250 m asl, but on three composite samples in banana plots at 300, 350, and 375 m asl. Different lowercase letters express significant differences at $p<0.05$ level for Si_t, $CaCl_2$-Si, Na_2CO_3-Si, ox-Na_2CO_3-Si, banana leaf Si content. Differences were tested with a t-test with the pairwise.t.test function of the R programming language.

Altitude	**Si_t**	**$CaCl_2$-Si**	**Na_2CO_3-Si**	**ox-Na_2CO_3-Si**	**XRD-*hl*PhSi** [1]	**Leaf Si concentration (banana)**
m	**g kg^{-1}**	**mg kg^{-1}**	**g kg^{-1}**	**g kg^{-1}**	**g kg^{-1}**	**g kg^{-1}**
65	179.3 a	65.5 a	11.2 a	7.68 a	2.54	4.49 ab
100	162.3 b	73.9 a	12.6 a	5.86 ab	8.94	5.30 a
150	148.0 c	31.3 bc	11.7 a	4.34 bc	6.90	4.77 ab
200	147.2 c	30.8 b	11.0 a	4.07 bc	12.16	4.03 b
250	148.6 c	31.1 b	11.5 a	4.30 bc	9.38	3.81 b
300	145.9 c	24.4 bc	10.4 a	3.37 bc	11.38	4.31 ab
350	145.6 c	21.1 bc	10.1 a	2.64 c	19.76	4.44 ab
375	141.5 c	14.0 c	11.4 a	2.04 c	22.45	nd[2]

[1] XRD-*hl*PhSi: phytolithic Si as assessed by XRD analysis after heavy liquid separation.

[2] nd refers to no data.

2.5 Discussion

2.5.1 Methodological considerations

The heavy liquid separation extracted phytoliths, but also tridymite, cristobalite, and gibbsite (Figure 2-S2). These silica minerals have a specific gravity (g cm^{-3}) (2.2–2.3) close to that of phytolith (2.3) unlike quartz (2.53–2.65) (Huang et al., 2002; Monger and Kelly, 2002). Quantitative assessment from XRD data showed that phytolith content in heavy liquid extracts ranged from 10 to 76.2%. The heavy liquid separation allows to quantify the phytolith pool if the physical extraction is followed by particles counting or by the XRD assessment presented above in section 2.3.4.

Na_2CO_3–Si values as deduced from the *DeMaster* procedure (DeMaster, 1981) were as high as 10.0-14.2 g kg^{-1} (Table 2-S3), because of the release of structural Si from the alkaline dissolution of allophanic constituents (Wada, 1989). Probably, minor quantities of adsorbed Si could have been released from secondary oxides (Jones and Handreck, 1963), particularly SRO Fe oxide (Delstanche et al., 2009) and allophanic substances (Harsh et al., 2002; Wada, 1989). After the dark oxalate extraction of SRO aluminosilicates (Wada, 1989), SRO Fe and Al oxides (Bigham et al., 2002; Huang et al., 2002), and possibly adsorbed Si if any (Jones and Handreck, 1963), ox-Na_2CO_3–Si markedly decreased to 2.0-7.9 g kg^{-1} (Table 2-S3). However, Al content in the Na_2CO_3 extract after dark oxalate pretreatment was very high (5.2-8.5 g kg^{-1}, Table 2-S3). We thus tentatively attribute ox-Na_2CO_3–Si to phytolithic silicon, and ox-Na_2CO_3–Al to SRO Al oxide and/or microcrystalline gibbsite (Huang et al., 2002), as further discussed in next sections.

2.5.2 The gibbsitic Andosols are strongly desilicated

Andic properties. The sodium fluoride field test (Fieldes and Perrot, 1966) gave a rapid, strong and positive response indicating the occurrence of

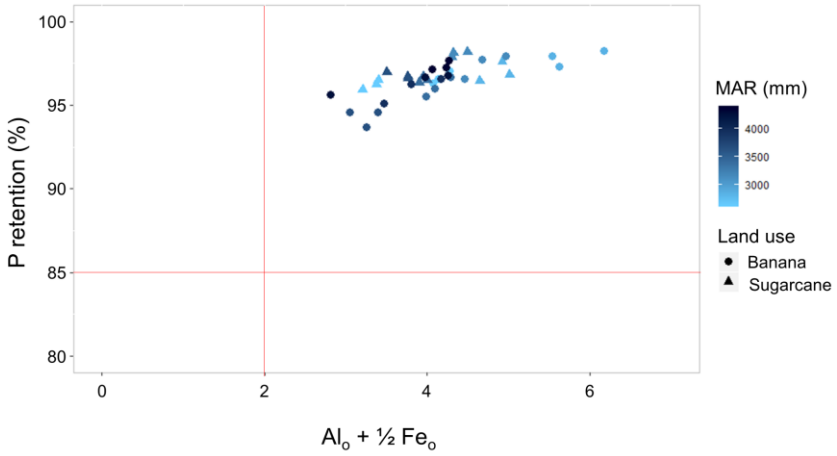

Figure 2-3: Plot of P retention against Al_o + ½ Fe_o ratio. The color of each point reveals the MAR level. Red lines show the lower limits of each parameter for Andic properties.

allophane and/or organo-aluminum complexes in both topsoil and subsoil whatever the altitude. Analytical data illustrate the strong expression of andic properties in all studied soils. The values of bulk density ≤ 0.82 (Table 2-1), phosphate retention ≥ 96% and [Al_o + ½Fe_o] ≥ 2% (Figure 2-3) fulfill the diagnostic criteria that are required for andic properties (IUSS, 2014) regardless of rainfall and altitude.

Soil weathering stage and secondary products. The studied Andosols have reached an advanced weathering stage. Strong desilication is revealed by particularly low soil Si/(Al+Fe) atomic ratios (1.01-0.78), large gibbsite contents (31-113 g kg^{-1}), low TRB (134-71 $cmol_c$ kg^{-1}), in particular at MAR >3000 mm (TRB = 93-71 $cmol_c$ kg^{-1}) as well as relatively high contents of allophanic substances (80-161 g kg^{-1}), Al-humus components (Al_p: 6.7-12.3 g kg^{-1}), and ferrihydrite (Fe_o: 10.9-18.4 g kg^{-1}). Allophanic substances have a low Si/Al atomic ratio (0.51-0.65), which denotes their aluminous composition close to that of imogolite (Si/Al=0.5). Imogolite, however, was not identified in the clay fractions in contrast to its occurrence in weathered soil horizons developed from recent (≈ 500 yr old) andesitic ash on the western flank of

the volcano at 1000 m asl and MAR ≥ 4500 mm (Jongmans et al., 1994). Abundant gibbsite is a major indicator of strong desilication. Actually, gibbsite occurs in soils of any age whenever Si is in low supply, hence under strong leaching (Churchman and Lowe, 2012). Where there is a gradation in the extent of leaching, often because an altitude change, gibbsite occurs in the most heavily leached soils whereas 1:1 phyllosilicates are dominant secondary minerals where there is a lesser degree of leaching (Churchman and Lowe, 2012; Herbillon et al., 1981; Huang et al., 2002; Nieuwenhuyse and Van Breemen, 1997; Norfleet et al., 1993). In the wettest sites of the studied catchment, the complexation of Al by organic matter may have exerted anti-allophanic and/or anti-gibbsitic effects (Churchman and Lowe, 2012; Ndayiragije and Delvaux, 2003; Shoji et al., 1993). Given the absence of imogolite, the aluminous composition of dark oxalate extracts may tentatively be linked to the occurrence of Al-rich allophane (proto-imogolite allophane: Churchman and Lowe, 2012; Farmer and Lumsdon, 2001; Harsh et al., 2002), and a continuum Al-humus complex – SRO Al oxide – gibbsite, as earlier proposed by Huang et al. (2002). SRO Al oxide might encompass *proto-gibbsite* (Alary et al., 2013) or *poorly crystalline Al hydroxide* (Huang et al., 2002) the content of which was 5–10 g kg^{-1} in Brazilian ferrallitic soils as assessed by dark oxalate extraction at pH 3 (Huang et al., 2002). Here, we could not quantify the content of proto-gibbsite because of the presence of allophanic substances of unknown Si/Al ratio.

2.5.3 Climatic controls on mineral neoformation and base saturation

Mineral synthesis. The climatic controls on mineral synthesis thus resulted in the formation of Al-rich allophane, proto-gibbsite, gibbsite and Fe oxide whereas the relative importance of (Al, Fe)-humus complexes increased at wettest sites. The most significant expressions of these climatic controls are the strong desilication and the increase in gibbsite content (101-113 g kg^{-1}) at MAR > 3000 mm, concomitantly to the abrupt decrease in TRB from 134-114 to 93-71 $cmol_c$ kg^{-1}.

Base saturation and buffering capacity. Soil ion exchange properties are controlled by a combination of weathering, leaching intensity and soil constitution (Chadwick et al., 2003). At MAR > 3000 mm, despite the abundant precipitation, the sum of exchangeable bases (16.9–3.8 $cmol_c$ kg^{-}

[1]), base saturation (36-7%) and pH (6.5-5.1) show well-defined trends along the rainfall gradient (Figure 2-4) as observed earlier (Chadwick et al., 2003; Henriet et al., 2008a). Average base saturation is invariably below 36% and is lowest (7-22%) in the wettest sites where the sum of exchangeable bases is particularly low (4-10 $cmol_c\ kg^{-1}$). The loss of buffering capacity at high rainfall directly resulted from mineral weathering and the removal of base cations, and it led to a steep decline in effective cation exchange capacity and base saturation, despite the soils under banana cultivation are fertilized and limed. Actually, N and K fertilizer management in these perhydrated Andosols under intensive banana cropping is particularly acute, as it requires frequent applications of small fertilizer doses to reduce nutrient losses through leaching (Godefroy and Dormoy, 1984; Ndayiragije and Delvaux, 2004). Besides, it should be noted that the only case of phosphorus deficiency in intensive banana plantations worldwide was reported in these perhydrated Andosols, due to P fixation on Al oxide surfaces (Lacoeuilhe and Godefroy, 1971). Though the soil buffering capacity has been exhausted for base cations, the release of plant available Si might have been "buffered" to some extent through the biological cycling of Si, which may alleviate natural soil desilication (Lucas et al., 1993), and possibly to Si adsorption on oxide surfaces (Jones & Handreck, 1963).

Soil weathering stage. TRB (Herbillon, 1986) and the degree of individualization of free iron (Fe_d/Fe_t ratio) can be used to estimate soil weathering stage (Brahy et al., 2000; Delfosse et al., 2005; Delvaux et al., 1989; Henriet et al., 2008a). In the studied climosequence, TRB did not decrease linearly with increasing rainfall, whereas Fe_d/Fe_t varied little regardless of rainfall. From Table 2-1 and Figure 2-2, we may tentatively attribute the variation in TRB to three pyroclast deposits of different ages, from the oldest to the youngest: (i) at 65 m asl, (ii) 100-300 m asl, (iii) 350-375 m asl (Figure 2-2). In the second deposit (100-300 m asl), TRB progressively decreased from 134 to 71 $cmol_c\ kg^{-1}$ (Table 2-1) with increasing MAR. This environmental framework gives the opportunity to infer about the respective impacts of rainfall and soil weathering stage on the pools of plant

available Si and phytoliths in soil.To do this we did linear models using the *lm* function of the R programing language (see Equation 2-1).

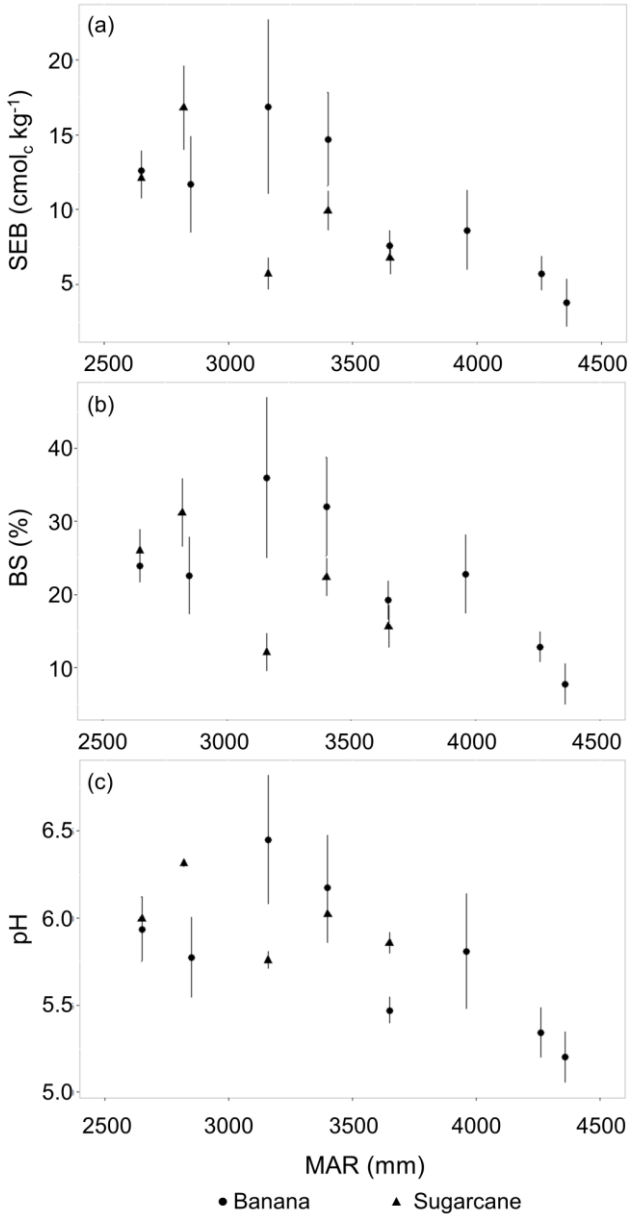

Figure 2-4: Sum of exchangeable bases (SEB) (a), base saturation (BS) (b), and soil pH (c), as plotted against mean annual rainfall (MAR). Error bars represent standard deviations.

2.5.4 Rainfall strongly impacts the pools of plant available Si and phytoliths

Results of the linear models are shown in Table 2-S4. They show that MAR was the only parameter that significantly explained the different Si pools ($CaCl_2$-Si p<0.001, Na_2CO_3-Si p<0.05, ox-Na_2CO_3-Si p<0.001, XRD-*hl*PhSi p<0.003, and total Si p<0.001). In contrast, TRB and soil pH did not explain the differences in Si pools (p>0.05). From these observations, we plotted Si_t, $CaCl_2$-Si, Na_2CO_3-Si, ox-Na_2CO_3-Si, XRD-*hl*PhSi contents in soils and leaf Si content against MAR (Figure 2-5). The correlation was particularly strong with the first five variables (r = 0.81-0.93). XRD-*hl*PhSi content increased with increasing MAR. In contrast, Si_t, $CaCl_2$-Si, Na_2CO_3-Si and ox-Na_2CO_3-Si and leaf Si contents decreased with increasing MAR (Figure 2-5 a, b, c, d). Rainfall was thus the main factor that affected the contents of total Si, plant available Si, phytolithic Si, and leaf Si, though to a much lesser extent. Actually, the narrow range of leaf Si content (3.8-5.3 g kg^{-1}, Table 2-4) was close to that measured by Henriet et al. (2008a) (1.8-3.9 g kg^{-1}) for bananas cropped on soils covering a range of TRB from 36 to 131 $cmol_c$ kg^{-1}, which compares to that measured here (71–134 $cmol_c$ kg^{-1}). Besides leaf Si concentration in banana leaf may increase with the decrease of plant biomass with increasing MAR (Dorel et al., 2000), making Si mineralomass a better plant indicator of Si availability in soil. Rainfall directly controls the leaching intensity and the loss of elements (Chadwick et al., 2003), and was thus here the main parameter that controlled the availability of Si for plants.

A surprising point is that rainfall has an opposite impact on the ox-Na_2CO_3-Si and XRD-*hl*PhSi pools (Figure 2-5d, e). These pools are thus inversely correlated (r = -0.88, p = 0.004; Figure 2-6). Both the ox-Na_2CO_3-Si and XRD-*hl*PhSi pools were associated to phytoliths (section 2.5.1). We propose that, in the studied soils, ox-Na_2CO_3-Si and XRD-*hl*PhSi contents do not represent the same phytolith pool.

2.5.5 Quantification of different phytolith pools

Phytoliths with different dissolution rates can coexist in soil: fresh phytoliths quickly dissolve whereas aged ones dissolve slowly (Alexandre et al., 2011, 1997; Meunier et al., 2014). Actually, phytoliths in soil are considered in our

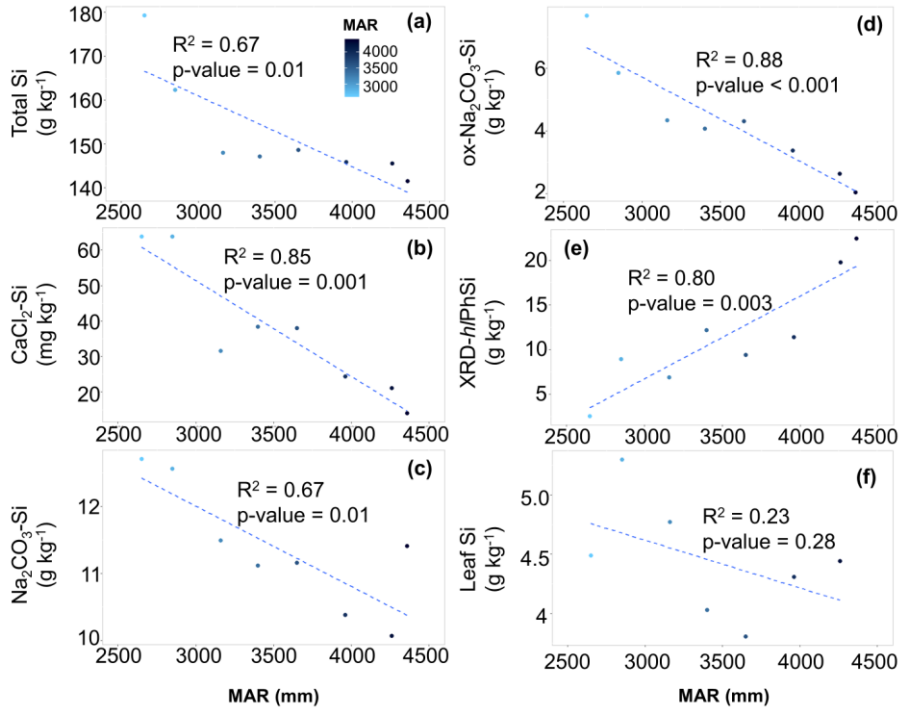

Figure 2-5: Contents of total Si –Sit– (a), $CaCl_2$-Si (b), Na_2CO_3-Si (c), ox-Na_2CO_3-Si (d), XRD-*hl*PhSi (e) concentrations in soils; leaf Si concentration (banana, leaf III) (f), as plotted against mean annual rainfall MAR with associated R^2 and p values. The color of each point reveals the MAR level.

scientific community as a major contributor to DSi because of their high dissolution rate (a.o. Alexandre et al., 2011; Bartoli, 1983; Farmer et al., 2005; Lucas et al., 1993; Sommer et al., 2013), whereas they are used in other disciplines as microfossils to reconstruct paleoenvironments because of their stability over millennia (a.o. Barboni et al., 1999;

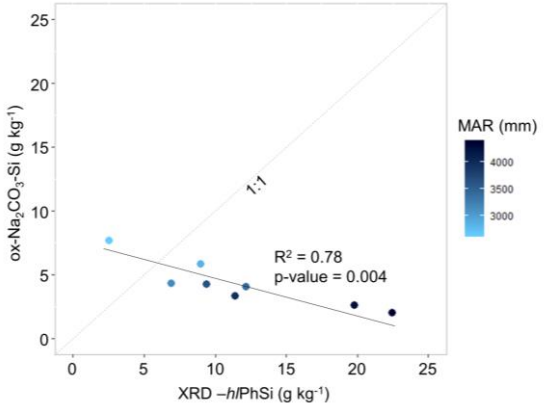

Figure 2-6: Plot of the XRD-*hl*PhSi concentration against ox-Na_2CO_3-Si concentration in soils. The intensity of the blue color for each point reveals the MAR level.

Cabanes et al., 2011; Kealhofer and Penny, 1998; Neumann et al., 2012; Rashid et al., 2019).

In this study, the ox-Na_2CO_3-Si and XRD-*hl*PhSi pools are inversely correlated to each other (Figure 2-6). As assessed by Meunier et al. (2014) the chemical extraction using ox-Na_2CO_3-Si likely quantifies fresh phytoliths that dissolve quickly. In contrast, the physical extraction using heavy liquid separation (XRD-*hl*PhSi) would quantify the whole phytolith pool though it may dissolve some phytolithic particles during the alkaline DCB pretreatment.

In this line, we propose that, with increasing MAR, the pool of fresh phytoliths (ox-Na_2CO_3-Si) decreases while that of aged ones (XRD-*hl*PhSi) increases. The ratio [XRD-*hl*PhSi]/[ox-Na_2CO_3-Si] indeed increases from 0.33 to 11.0 with increasing MAR (Figure 2-7). As discussed here above (section 2.5.4), rainfall directly controls the leaching intensity and the loss of elements (Chadwick et al., 2003). On one hand, following the *Le Chatelier* principle, rainfall would increase the dissolution rate of fresh phytoliths. On the other hand, higher rainfall is associated with higher contents of secondary oxide and organic matter (section 2.5.3), which positively influence soil aggregation (Dorel et al., 2000). Soil aggregates may entrap phytoliths and protect them from dissolution (Li, 2019). Soil components such as SOM, OMA, ferrihydrite, Al hydroxide and allophanic substances all promote soil microaggregation (Bigham et al., 2002; Deng and Dixon, 2002; Harsh et al., 2002; Huang et al., 2002). The role of SRO Fe and Al oxides in soil microaggregation is further enhanced by their large surface area and reactivity (Bigham et al., 2002; Huang et al., 2002). Since the contents of soil organic matter, Al oxide, SRO Fe oxide

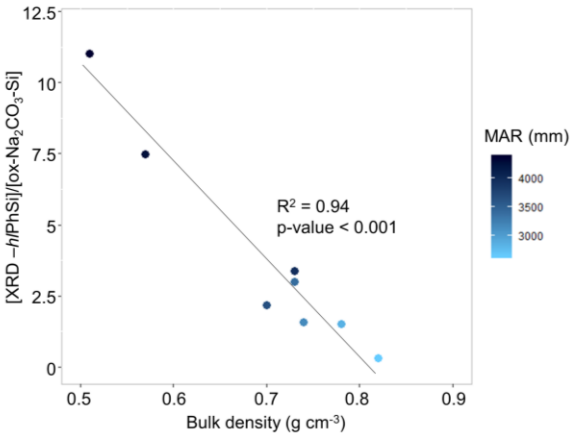

Figure 2-7: Plot of the XRD-hlPhSi/ox-Na2CO3-Si ratio against the soil bulk density. The bulk density is used as an indicator of the soil micro-aggregation process. The intensity of the blue color for each point reveals the MAR level.

increased with increasing MAR (Table 2-1), soil microaggregation probably increased with increasing MAR. This hypothesis is supported by the decrease in bulk density with increasing MAR (Table 2-1). The very strong inverse correlation between the ratio [XRD-*hl*PhSi]/[ox-Na_2CO_3-Si] and bulk density (r = -0.97) (Figure 2-7) supports that the increasing dominance of aged phytoliths with increasing MAR could be linked to phytoliths entrapement since bulk density is an indicator of soil aggregation. Thus, following Li (2019) and as suggested by the Figure 2-7, we further hypothesize that soil micro-aggregation processes are intimately linked to phytolith stabilization processes. Within this view, phytoliths could be physically or chemically entrapped into micro-aggregates that protect them from dissolution. In the studied Andosols, the reactive phytolith surfaces (Bartoli, 1985; Fraysse et al., 2009) could possibly interact with SRO (Fe, Al) oxides, allophanic substances, SOM (Bartoli, 1985) in the overall process of soil microaggregation. These soil constituents may indeed promote the chemical or physical stabilisation of phytoliths as their respective contents increases with increasing rainfall. This model might therefore explain the observed results.

2.5.6 Phytolith controls on plant available Si

From Figure 2-8, $CaCl_2$–Si is positively and strongly correlated with ox-Na_2CO_3–Si (r = 0.95), but negatively correlated to XRD-*hl*PhSi (r = -0.57). The strong positive correlation between $CaCl_2$–Si and ox-Na_2CO_3–Si suggests that plant available Si was controlled by the pool of fresh phytoliths in soil that could quickly dissolve. The values of pH and H_4SiO_4 concentration in $CaCl_2$–Si extracts support that amorphous silica bodies controlled dissolved Si (Table 2-S6). The controls of phytolith were governed by MAR since the lowest values of $CaCl_2$–Si

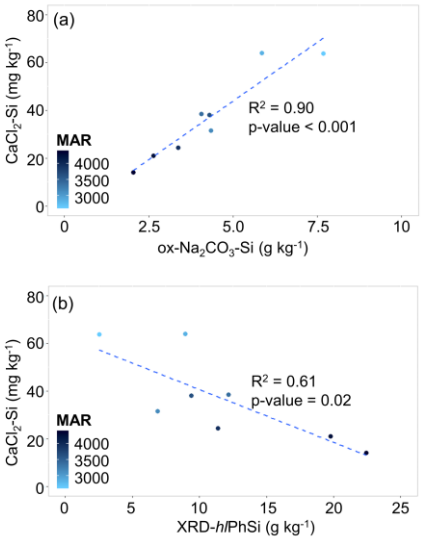

Figure 2-8: Plot of $CaCl_2$-Si content against the contents of (a) ox-Na_2CO_3-Si and (b) XRD-*hl*PhSi. The intensity of the blue color for each point reveals the MAR level.

and ox-Na_2CO_3–Si were both measured in the wettest sites (Figure 2-8a). Furthermore, our coupled experimental data ($CaCl_2$–Si, ox-Na_2CO_3–Si) reasonably compared to the literature data reported in Figure 2-9 as well as to the range of coupled values [$CaCl_2$–Si, Na_2CO_3–Si] recently reported for humid tropical forests in Panama (see Figure 1a in Schaller et al., 2018). In this latter study, within a MAR gradient from 1600 to 3200 mm, the ranges of $CaCl_2$–Si and Na_2CO_3–Si values were indeed 1–40 mg kg^{-1} and 1–7 g kg^{-1}, respectively (Schaller et al., 2018). Thus, as discussed above, the climatic controls on mineral synthesis in the studied Andosols led to advanced

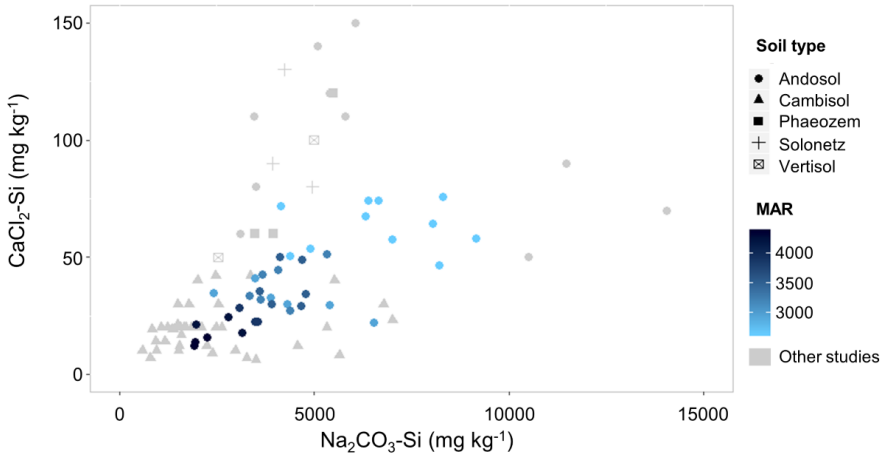

Figure 2-9: Plot of $CaCl_2$-Si content against contents of Na_2CO_3-Si in different soil-plant systems. Light grey symbols are literature data for various soil types in temperate forests (Clymans et al., 2011; Cornelis et al., 2011), and tropical savannas (Quigley et al., 2017). Blue points are from this study and are ox-Na_2CO_3-Si values to discard the SRO PSi contribution. The intensity of the blue color for each point reveals the MAR level.

desilication (Chadwick et al., 2003) and resulted in the formation of Fe oxide, aluminous allophane, gibbsite and possibly proto-gibbsite. Furthermore, they resulted in the exhaustion of the buffering capacity with respect to ion exchange properties as previously reported (Chadwick et al., 2003), but also to plant available Si, likely because of the rapid dissolution of fresh phytoliths in strongly desilicated soil environments.

Aluminous character of ox-Na_2CO_3 extracts. In the ox-Na_2CO_3 extract, the [ox-Na_2CO_3–Si/ox-Na_2CO_3–Al] atomic ratio was ≤ 1.0, actually close to 1.0 in the least humid sites (Figure 2-10a). Furthermore, the Si/Al ratio of the ox-Na_2CO_3 extract sharply decreased from 1.0 to 0.5 with increasing MAR below 3000 mm, but remained constant at ~ 0.48 at MAR > 3000 mm (Figure 2-10b). Since gibbsite content increased while that of allophane decreased at MAR > 3000 mm, we attribute the ox-Na_2CO_3–Al content to (i) phytolith Al, and (ii) gibbsite and possibly proto-gibbsite (Alary et al., 2013; Huang et al., 2002). We can only speculate on how much proto-gibbsite or poorly crystalline Al hydroxide occurred in the studied perhydrated Andosols because there are no unambiguous methods for its identification and quantification (Huang et al., 2002). We can argue that various environmental factors might have promoted the formation of a series of Al-rich secondary products encompassing Al-humus, proto-gibbsite or poorly crystalline Al hydroxide (Huang et al., 2002), gibbsite and aluminous allophane of proto-imogolite type (Churchman and Lowe,

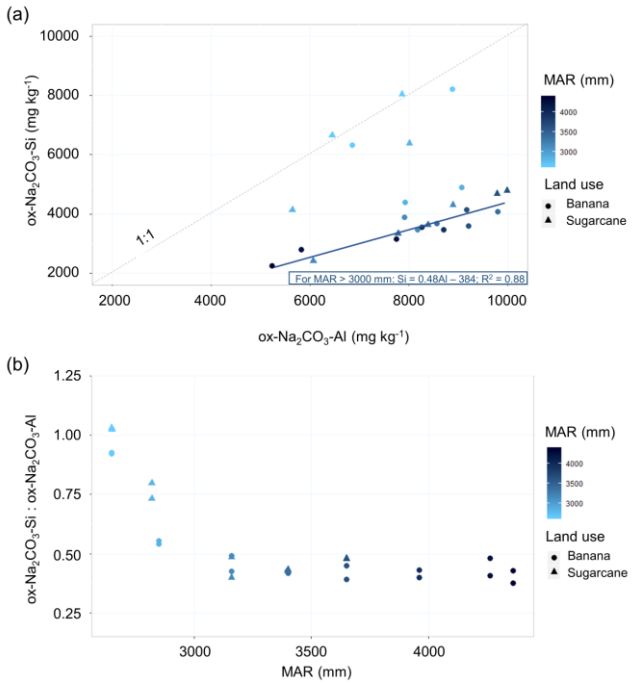

Figure 2-10: (a) Plot of the ox-Na_2CO_3-Si concentration against ox-Na_2CO_3-Al concentration in soils. Si and Al concentrations in the Na_2CO_3 extracts were derived using the technique of DeMaster (1981) on soils samples after allophane dissolution by dark oxalate (ox). (b) Plot of the evolution of the ox-Na_2CO_3–Si:Al ratio with increasing MAR. The intensity of the blue color for each point reveals the MAR level.

2012; Harsh et al., 2002), added to Al-rich phytoliths. These environmental factors include a.o. (i) the rapid weathering of volcanic glass, (ii) the great intensity of leaching linked to high MAR and large porosity of ash material, (iii) the strong desilication, (iv) the accumulation of organic substances that can hamper the crystallization of gibbsite (Huang et al., 2002). On the other hand, the slow kinetics of macrocrystalline gibbsite formation enhance the precipitation of poorly crystalline and microcrystalline Al hydroxide at aqueous H_4SiO_4 of 10^{-4} mol l^{-1} where gibbsite should be stable (Harsh et al., 2002).

2.5.7 Critical assessment of the PhSi quantification methods

As illustrated in Figure 2-6, our experimental data show significant differences in Si concentration between chemical extraction by alkaline dissolution (ox-Na_2CO_3-Si: 2-7.6 g kg^{-1}) and physical separation by heavy liquid (XRD-*hl*PhSi: 2.5-22.4 6 g kg^{-1}). As discussed above, the particular constitution of the studied soils may explain such discrepancies, which are particularly acute at the highest altitude levels.

The DeMaster technique using alkaline dissolution. The first point deals with the dissolution of phytoliths in Na_2CO_3 whereas the second one concerns the selectivity of Na_2CO_3 for phytoliths in an assemblage including phytoliths, SRO lithogenic silicate (LSi) and PSi minerals. First, Na_2CO_3 extractant mainly dissolves fresh phytoliths while it is less selective for aged phytoliths that poorly dissolve in Na_2CO_3 (Meunier et al., 2014). As discussed earlier (section 2.5.5), we hypothesize that weathering, mostly governed by MAR, has promoted the ageing of phytoliths in soil, and probably their relatively high Al content (Figure 2-10; Bartoli; 1985) as well their interactions with organic and mineral constituents in soil in the overall process of soil aggregation. Second, the Na_2CO_3 extraction dissolves SRO PSi minerals (Kamatani and Oku, 2000), and amorphous LSi components (Clymans et al., 2015a). Besides, it dissolves wollastonite, a crystalline silicate (Li et al., 2019). Thus, the *DeMaster* technique (DeMaster, 1981) does not discriminate phytolith from SRO PSi and LSi minerals. Barão et al. (2014), Clymans et al. (2015), Kamatani and Oku (2000), and Koning et al. (2002) developed alternative techniques to discriminate PhSi from LSi and PSi SRO minerals based on the monitoring of the Si/Al atomic ratio during the kinetical alkaline extraction. Gibbsite, however, may dissolve in alkaline reagents (Huang et al., 2002), making the use of the Si/Al ratio very hazardous, as shown in this study. The procedure

developed by Clymans et al. (2015) is also based on the use of the Si/Al to discriminate phytolithic Si from volcanic glass through a kinetical alkaline extraction, but the presence of gibbsite makes this technique unusable. Here, the pre-treatment of soil samples with dark oxalate buffered at pH 3 removed allophanic Si, i.e. Si from SRO PSi minerals. Given the advanced soil weathering stage in the studied Andosols, the pool of amorphous LSi minerals (volcanic glass) was considered as being exhausted. Much better than Na_2CO_3-Si, ox-Na_2CO_3-Si thus represented the PhSi pool since the dark oxalate pretreatment removed SRO PSi minerals with little effect, if any, on phytolith dissolution at pH 3 (Fraysse et al., 2009).

Heavy liquid separation. As far as the extraction of phytoliths by heavy liquid separation is concerned, the presence of cristobalite, tridymite, and gibbsite prevents an accurate assessment from being made for the phytolith content in soil. Here, we propose a quantification of inorganic components occurring in the light fraction using SIROQUANTsoftware. By doing this way we could evaluate the respective contents of phytolith, critobalite, tridymite and gibbsite and distinguish fresh from aged phytoliths.

2.6 Conclusion

The perhydrated Andosols under study have reached an advanced weathering stage. The climatic controls on mineral synthesis have resulted in the formation of Fe oxide, Al-rich allophane, gibbsite and possibly proto-gibbsite or poorly crystalline Al hydroxide. This mineralogical assemblage denotes intense leaching and strong desilication. In addition, the contents of SOM and (Al, Fe)-humus increased at wettest sites. These climatic controls generate an abrupt threshold in soil properties at MAR ≥ 3000 mm. They have also led to (i) the exhaustion of the soil buffering capacity, (ii) the decrease in plant available Si and fresh phytolith content. Thus, within a thin gradient of soil weathering degrees, the increase in MAR has resulted in the strong decrease in all Si pools in soil: PSi minerals, fresh PhSi reservoir and plant available Si. However, within the same gradient, an increasing amount of phytoliths was entrapped in soil aggregates.

We conclude that rainfall is the major, if not exclusive, driver of plant Si availability in the highly leached, gibbsitic Andosols from Basse-Terre, Guadeloupe.

We further conclude that research is required to improve the procedures quantifying phytolith content in soil and to investigate possible phytolith entrapment in soil microaggregates.

Chapter 3 Phytolith quantification through alkaline extraction in gibbsitic Andosols[2]

Abstract

Quantifying the phytolith pool in soil is a prerequisite to assess the biological control of Si fluxes from the soil-plant system to watersheds. It is routinely carried out through the *DeMaster* procedure using the Na_2CO_3 kinetic extraction at 85°C for 6h, stipulating that the dissolution of amorphous silica is fast while that of crystalline minerals is slow and linear. Volcanic ash soils that exhibit andic properties usually contain short-range-ordered (SRO) minerals such as allophane, imogolite and poorly crystalline Fe and Al oxides. Here, we quantified the phytolith pool in perhydrated Andosols rich in gibbsite through the kinetical Na_2CO_3 extraction of Si. Prior to this extraction, we tested three pretreatments, separately: (1) no pretreatment, (2) dark oxalate, (3) sequentially hydrogen peroxide (H_2O_2), dithionite-citrate-bicarbonate (DCB), and dark oxalate. For comparison purpose, the same procedures were applied to phytolithic-biochar:basalt mixtures and phytolithic-biochar:basalt:gibbsite mixtures. Our results show that Na_2CO_3 readily and quickly dissolves phytoliths, but also weatherable primary minerals, SRO alumino-silicates as well as Al-bearing constituents such as Al-humus, poorly crystalline Al oxide and gibbsite. Unlike dark oxalate at pH 3, DCB at pH~9 may dissolve phytoliths. We thus recommend to use the kinetical Na_2CO_3 extraction, but preceded by dark oxalate dissolution of SRO minerals to quantify phytoliths in soil.

[2] Manuscript in preparation for submission in an international peer-reviewed journal.

3.1 Introduction

Silicon (Si) has a crucial role in several biogeochemical processes, notably in regulating atmospheric CO_2 and buffering soil acidification through mineral weathering, and as a nutrient for terrestrial and marine biota. Plants exert a biological control on both the terrestrial Si cycling and Si export flux to watersheds (Derry et al., 2005), making the global Si cycle strongly dependent on the soil-plant cycle of Si (Carey and Fulweiler, 2012; Conley, 2002). The weathering of silicate minerals releases dissolved Si (DSi), which is taken up by plant roots, transferred to transpiration termini, and precipitates in plant tissues as amorphous silica bodies called phytoliths (PhSi) (Jones and Handreck, 1965; Piperno, 1988; Sangster and Hodson, 1986). PhSi is recycled through the return of plant debris to soil (Smithson, 1956) where phytoliths form an important reservoir of plant available Si (Drees et al., 1989). PhSi bodies indeed readily dissolve at common values of soil solution pH (Fraysse et al., 2009), and feed the DSi reservoir, especially in highly weathered, desilicated soils (Alexandre et al., 1997; Cornelis and Delvaux, 2016; Lucas et al., 1993; Meunier et al., 1999). Quantifying the PhSi pool in soil is thus a prerequisite to assess the biological control of Si fluxes from the soil-plant system to rivers and oceans.

Soil phytoliths are chemically extracted with alkaline reagents (Saccone et al., 2007; Sauer et al., 2006). They are assumed to dissolve quickly in Na_2CO_3 0.1 M at 85°C while crystalline silicates dissolve slowly and linearly. Plotted against time, the release of DSi in Na_2CO_3 presents two steps: a quick release followed by a slow and linear one, allowing to quantify the PhSi pool at the Y-intercept of the linear release (Figure 1 in DeMaster, 1981). However, the *DeMaster* technique partly dissolves wollastonite, a crystalline silicate mineral (Li et al., 2019), and may dissolve short range-ordered (SRO) minerals (Huang et al., 2002; Kamatani and Oku, 2000; Wada, 1989). The use of Si/Al atomic ratio of alkaline extracts was proposed to discriminate PhSi from SRO minerals, attributing $Si/Al \geq 5$ to PhSi and $2 \geq Si/Al \geq 0.5$ to SRO and crystalline minerals in soil (Barão et al., 2014; Clymans et al., 2015a; Kamatani and Oku, 2000; Koning et al., 2002). Yet inorganic amorphous silica minerals may dissolve in alkaline extracts (Drees et al., 1989). Although used in various environments (Barão et al., 2014; DeMaster, 1981; Guntzer et al., 2012; Saccone et al., 2007; Sauer et al., 2006), the interpretation of Na_2CO_3 extracts to quantify the PhSi pool remains hazardous in a number of soils. For example, some ash derived Andosols contain volcanic glass, allophanic substances, Al-

humus, poorly crystalline Al oxide and gibbsite, which dissolve in alkaline solutions (Clymans et al., 2015a; Jackson, 1956; Kamatani and Oku, 2000; Pereira et al., 2009; Taboadela, 1953; Wada, 1977). Actually, the following values of the atomic Si/Al ratio of the Na_2CO_3-extract from soils best refer to the following respective silicates (Li, 2019):

1) **Si:Al ≥ 5** to PhSi (phytoliths), but also to some SRO silicates either lithogenic (e.g. volcanic glass) or pedogenic (e.g. allophane, non-biogenic amorphous silica), as well as crystalline silicates such as a.o. wollastonite and fine-sized Si oxides (quartz, tridymite, cristobalite);
2) **5 ≥ Si:Al ≥ 1** to LSi (e.g. plagioclase, Mg-chlorite, biotite), 2:1:1, 2:1 and 1:1 PSi clay minerals (e.g. illite, vermiculite, smectite, kaolinite);
3) **Si:Al < 1** to some SRO PSi silicates (imogolite), $H_4SiO_4^0$ adsorbed onto oxide surfaces.

The use of the Si/Al atomic ratio is thus not unequivocal because several soil components are soluble in alkaline solutions.

Moreover, Andosols are strongly aggregated (Totsche et al., 2018), and phytoliths may be entrapped into soil clusters protecting them from dissolution (Li, 2019). The protocol for the physical extraction of phytoliths provides for the prior destruction of soil aggregates (Kelly, 1990) whereas the chemical alkaline extraction does not.

Here, we attempt to quantify the PhSi pool in Andosol samples through the kinetical extraction of Si using 0.1 M Na_2CO_3 at 85°C for 6h. Prior to this extraction, we test three methods, separately: (1) no pretreatment, (2) dark oxalate pretreatment, (3) sequential H_2O_2, dithionite-citrate-bicarbonate (DCB), and dark oxalate pretreatments. The pretreatments in methods (2) and (3) are routinely used to extract soil components that are majorly involved in soil aggregation such as SRO secondary silicates and Al, Fe oxides, soil organic matter (SOM) and organo-mineral associations (OMA). For comparison purpose, we apply the same procedures to phytolithic-biochar:basalt and phytolithic-biochar:gibbsite:basalt mixtures.

3.2 Materials

3.2.1 Soil samples

The Andosols are distributed along a climo-toposequence on the Eastern flank of the volcano *La Soufrière* (1467 m above sea level (asl)) exposed to rain-bearing winds (Colmet-Daage and Lagache, 1965). They derived from pyroclastic andesitic ash containing plagioclase, pyroxene, and volcanic glass as the main primary minerals (Boudon et al., 1987; Dagain, 1981; Komorowski et al., 2005; Ndayiragije, 1996). Seventeen plots were selected under forest (FO), banana (BA) and sugarcane (SC) crops from 65 m to 390 m asl on the Pères River catchment. Mean annual rainfall (MAR) evolves from 2650 mm at 65 m to 4400 mm at the top of the catchment. At MAR >4000 mm, the perhydrated Andosols contain Al-humus, gibbsite, allophane and kaolinite as dominant secondary minerals (Colmet-Daage and Lagache, 1969; Ndayiragije and Delvaux, 2003). In particular, the abundance of large particles of gibbsite, developing as pseudomorphs of plagioclase and pyroxene, reflects a strong soil desilication (Ndayiragije and Delvaux, 2003). At MAR < 4000 mm, allophane is the dominant secondary mineral, while C content slightly and progressively decreases with decreasing altitude (Colmet-Daage and Lagache, 1969). The soils are strongly microaggregated (Dorel et al., 2000). We sampled topsoils (ts) (00-20cm) in 14 plots (BA, SC, FO) out of the 17 plots at all altitude levels (65-390 m). In addition, we sampled the genetic soil horizons in three pedons (pd), two in cultivated plots (BA, SC) and one under forest (FO). ts sampling involved collecting of 9 ts samples per plot, combined randomly into 3 composite samples. pd sampling involved the prior description of three soil pedons, respectively under banana (170 m asl), sugarcane (180 m asl) and forest (390 m asl), and the sampling of 15 soil horizons in total. The total of ts and pd samples thus amounts to 14*3 ts + 15 pd = 57 samples. The soil samples were moderately air-dried during 16 h and sieved at 2 mm. The analyses were carried out on the fine earth fraction (< 2 mm).

3.2.2 biochar:basalt mixtures

Biochar was produced from rice straws (Li et al., 2019). Rice plants were grown in the Yoshida nutrient solution (Yoshida, 1981) enriched with aqueous $H_4SiO_4^0$ at the concentration of 40 mg L^{-1}. The biochar was produced through a slow pyrolysis procedure as described by Ronsse et al. (2013),

passed through a 0.154 mm sieve prior to experimental use. PhSi content in biochar amounted to 51.3 g kg^{-1} (Li et al., 2019). *Basalt* was obtained from DCM Inc.Co. www.dcm-info.com as a powder of fresh natural basaltic lava (Eifel, Germany) crushed and sieved at 83 µm. The basalt was rich in weatherable lithogenic Si (LSi) minerals as it contained augite, olivine, leucite, nepheline, plagioclase, mica and some oxides as well as weathered glasses (Figure 3-S1). Five *mixtures of biochar:basalt* were prepared in the following weight proportions : 0:100, 25:75, 50:50, 75:25, and 100:0. The mixtures were carefully and thoroughly mixed.

3.2.3 biochar:basalt:gibbsite mixtures

Gibbsite was obtained from Alcoa® Company <https://www.alcoa.com>. Four mixtures of biochar:basalt:gibbsite were prepared in the following weight proportions: 47.5:47.5:5, 45:45:10, 42.5:42.5:15, 40:40:20. The mixtures were carefully and thoroughly mixed.

3.3 Methods

3.3.1 Soil analyses

Soil texture was determined by quantitative recovery of clay, silt and sand fractions after sonication and dispersion with Na^+ saturated resins without any previous oxidation of SOM (Rouiller et al., 1972). Dark oxalate-extractable (o), DCB extractable (d) and pyrophosphate-extractable (p) contents of Si, Al and Fe were determined in the respective extracts by inductively coupled plasma-atomic emission spectrometry (ICP–AES) following the methods compiled in Dahlgren (1994). Total C and N contents were determined by high temperature dry combustion using a Vario EL Cube elemental analyzer. Crystalline minerals were identified by X-ray diffraction (XRD) on powder soil and basalt samples as well as on clay fractions using Cu$K\alpha$ radiation in a Bruker Advance diffractometer. Prior to XRD, the clays were saturated with either K^+ or Mg^{2+} after batch equilibration with 1 M KCl and 0.5 M $MgCl_2$, respectively. XRD was performed at room temperature (20 °C), after formamide intercalation (Churchman et al., 1984), overnight ethylene–glycol saturation (EG) (8 d) at room temperature, as well as after heating at 110, 300 and 550 °C (4 h), using Cu$K\alpha$ radiation in a Bruker Advance diffractometer. Total elemental contents were determined on soil and basalt samples by ICP-AES after fusion in Li-metaborate and Li-

tetraborate at 1000°C (Chao and Sanzolone, 1992). The contents of major alkaline and alkaline-earth cations were summed up to compute the Total Reserve in Bases (TRB) (Herbillon 1986).

3.3.2 Chemical quantification of PhSi

Na_2CO_3-extractable Si content was determined to assess PhSi in soils (DeMaster, 1981; Koning et al., 2002; Saccone et al., 2007). The *DeMaster (dm)* procedure was applied after kinetical Na_2CO_3-extraction of Si (DeMaster, 1981). Forty milligrams of soil sample (f<2mm) were mixed with 40 ml of 0.1 M Na_2CO_3 at 85°C during 7h. One milliliter of solution was collected after 15, 60, 120, 180, 240, 300, 360, and 420 min, diluted with 9 ml of deionized water and acidified with 50 µl of Suprapur HNO_3 (Figure 3-1a). Si, Al, Fe, and Mg concentrations were measured at each time by ICP-AES. The intercept of the linear part of the kinetics release of Si estimates the PhSi pool, named *dm*Na_2CO_3-Si (DeMaster, 1981 - Figure 3-1b). The experimental data were used to compute the dissolution rate (*dr*) using the following equation (1):

$$dr_t = \frac{Si_t - Si_{t-1}}{T_t - T_{t-1}} \qquad Eq(1)$$

where dr_t was the dissolution rate (g min^{-1} kg^{-1}) at time t; Si_t, the Si concentration at time t; T_t the duration of extraction at time t.

Following DeMaster (1981), the *dr* from 120 min of extraction was attributed to crystalline minerals (Figure 3-1c). The *dr* of crystalline minerals was extrapolated to the whole extraction with a linear regression on *dr* from 120 to 420 min. The *dr* of PhSi particles was then estimated at each time by subtracting the *dr* of crystalline minerals from total *dr*. At each time increment, the product of the mean dr_t of PhSi particles by ($T_t - T_{t-1}$) was the amount of extracted PhSi during that time increment (Figure 3-1d). The PhSi content estimated from the *dr* procedure, named *dr*Na_2CO_3-Si could then be calculated by considering the whole extraction time. If the dissolution rate of crystalline minerals was really linear from 120 min of extraction the *dm*Na_2CO_3-Si concentration would be equal to the *dr*Na_2CO_3-Si concentration. However, we believe that the dissolution rate of crystalline minerals, instead of being linear, decreased slightly during extraction as solute concentrations gradually approached chemical equilibrium. The *dr*

procedure would therefore allow to take into account the evolution of the dissolution rate and to improve the estimation of the PhSi quantification. Prior to the Na_2CO_3 extraction, the soil samples were pretreated following three methods, separately: (1) no pretreatment, (2) dark oxalate extraction, (3) successive H_2O_2, DCB, and dark oxalate. Dark oxalate and DCB extractions were carried out following Blakemore et al. (1981) and Mehra and Jackson (1960), respectively. The oxidation of SOM was performed by adding 15 ml H_2O_2 6% to 750 mg soil at 60°C, and renewing H_2O_2 until reaction ceased. After the respective pretreatments 2 and 3, but prior to the Na_2CO_3 kinetical extraction, the methods 2 and 3 integrated a rinsing of the pretreated soil samples with $CaCl_2$ 0.01 M following Sauer et al. (2006) to remove residual

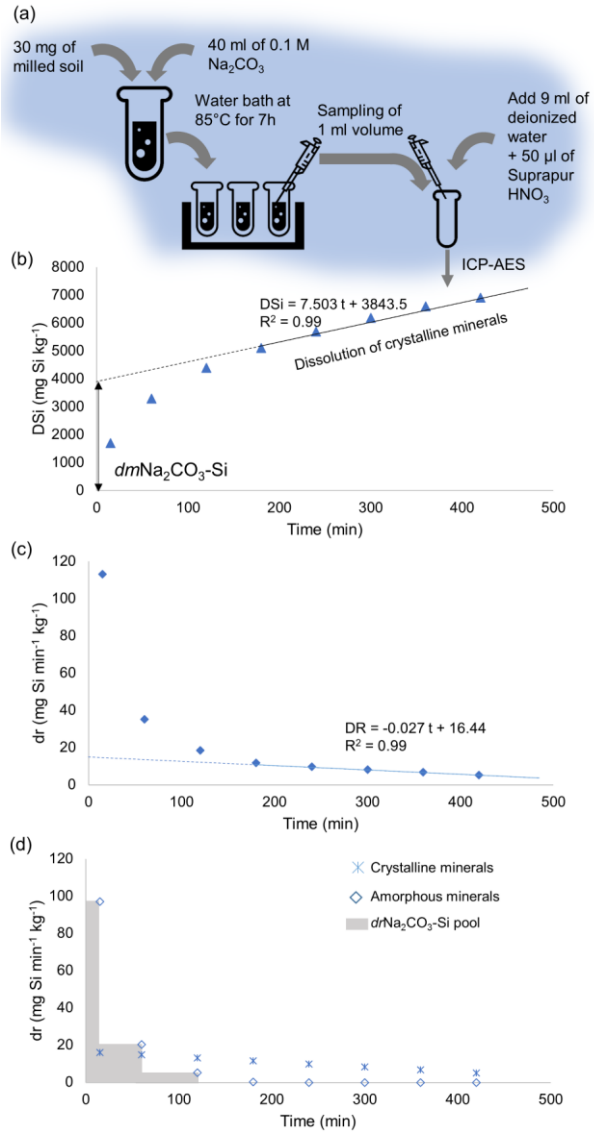

Figure 3-1: (a) Experimental scheme of the extraction kinetics of Si in Na_2CO_3 0.1M at 85°C. (b) Quantification of amorphous Si (ASi) by the intercept value on Y-axis (DeMaster 1981) (*dm*Na_2CO_3-Si). (c) Plot of the dissolution rate (*dr*) against extraction time, the linear part being attributed to crystalline minerals. (d) Deduced ASi pool (*dr*Na_2CO_3-Si).

dissolved Si. Figure 3-2 schematizes the effect of the pretreatments on soil components. Dark oxalate buffered at pH3 dissolves OMA, SRO pedogenic silicates (PSi) (allophanic substances) and Fe oxide (ferrihydrite) (Parfitt and Childs, 1988), and possibly poorly crystalline Al hydroxide (Huang et al., 2002). DCB buffered at pH~9 extracts free iron, i.e Fe-humus complexes, SRO and crystalline Fe oxides (Schwertmann and Taylor, 1989). DCB might dissolve PhSi particles at pH~9 (Fraysse et al., 2006).

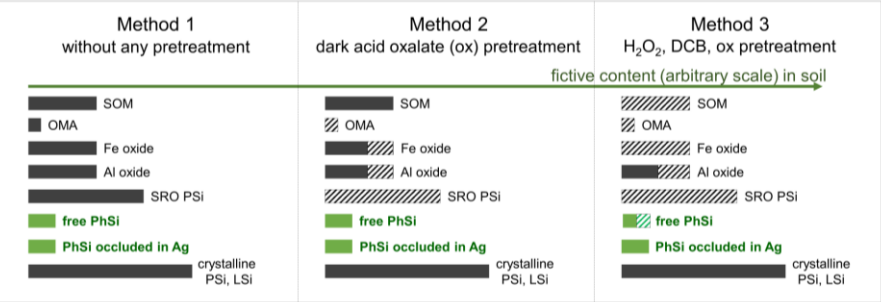

Figure 3-2: Sketch out of hypothetical soil compositions prior to the Na_2CO_3 extraction, but after the pretreatments for methods 1, 2 and 3. Hatched parts refer to the dissolved, targeted soil components (PhSi is not targeted, as well as crystalline PSi and LSi). SOM: soil organic matter. OMA: organo-mineral associations. SRO: short range-ordered minerals. PSi: pedogenic silicates. LSi: lithogenic silicates.
PhSi: phytogenic silica (note that DCB is buffered at pH~9).

In practice, executing the complete procedure involving the methods 1, 2, 3 was heavy and time consuming. Therefore, we carried it out only for two samples: tsBA350 and tsFO396. However, we compared the two procedures, i.e. *DeMaster (dm)* and *dissolution rate (dr)*, on all ts and pd samples (i.e. 57 samples), but only applying method 2 where Na_2CO_3 extraction was done after dark oxalate pretreatment.

3.3.3 Chemical modeling with PHREEQC

The PHREEQC 3.4.0-12927 software was used to model the equilibria that were established between the solid and liquid phases after 15 min of extraction in the alkaline solution. General solution characteristics were pH 11.2, pe 4, temperature 85°C. Individual element input were given from ICP-AES measurements after 15 min of extraction for Al^{3+}, Ca^{2+}, Mg^{2+}, and H_4SiO_4. Na^+ and CO_3^{2-} concentrations were 0.2 M and 0.1 M.

3.4 Results and discussion

3.4.1 Basic soil properties

The soils have attained an advanced stage of weathering, in particular at altitude levels above 150 m asl, as inferred from TRB values below 100 $cmol_c$ kg^{-1} and the relative importance of free iron (Fe_d), which accounted for about 50% of total iron (Fe_t) (Table 3-1). The advanced weathering stage was further confirmed by the very low $Si_t/(Al_t+Fe_t)$ atomic ratio that ranged from 0.75 to 1.01 in ts samples, and from 0.38 to 0.96 in pd samples. These features support that these gibbsite-rich Andosols (Colmet-Daage and Lagache, 1969) were strongly desilicated (Ndayiragije and Delvaux, 2003). They had relatively high clay contents: 37-51% below 150m asl and 24-37% above 150m asl in ts samples, 34-65% in pd horizons. Total Si content (Si_t) ranged from 128.7 to 181.1 g kg^{-1} in ts samples, and decrease with increasing altitude. In pd samples, Si_t ranges from 108.0 g kg^{-1} to 166.8 g kg^{-1}.

Soil properties (Table 3-1) were in perfect line with previous data from soil mapping and characterization of the Guadeloupean perhydrated Andosols (Colmet-Daage and Lagache, 1969; Ndayiragije and Delvaux, 2003). The carbon content of topsoils increased with increasing altitude from 43 to 97 g kg^{-1} in BA and SC croplands, and up to 155 g kg^{-1} in the forest area. The content of organic C (OC) regularly decreased at depth in each pedon (pd), from A to BC horizon. Oxalate extractable Fe (Fe_o) represented between 25 and 31% of free iron in topsoils (ts) below 300 m asl. Above 300 m, this proportion abruptly increased (42-54%) in relation to the large C content (78-155 g kg^{-1}). The low $Si_o/(Al_o-Al_p)$ ratio (0.52-0.72 in ts and 0.19-0.70 in pd horizons), denotes the aluminous character of allophanic substances and/or the occurrence of poorly crystalline Al hydroxide (Harsh et al., 2002; Huang et al., 2002). Thus OC, OMA, allophane, ferrihydrite, gibbsite and possibly poorly crystalline Al hydroxide likely dominate the secondary products in this weathering sequence. These soil constituents greatly favor soil microaggregation processes, and thus the development of a large microporosity (Colmet-Daage and Lagache, 1969; Dorel et al., 2000).

3.4.2 PhSi pools estimated from DeMaster (*dm*) and dissolution rate (*dr*)

Following method 2, the Na_2CO_3 extraction was performed on ts and pd soil samples cleared of their amorphous aluminosilicates after dark oxalate pretreatment at pH3. *dm*Na_2CO_3-Si and *dr*Na_2CO_3-Si represented the PhSi pool as determined through the *DeMaster* and *dissolution rate* procedures, respectively (Table 3-2, Figure 3-3). The ranges of *dm*Na_2CO_3-Si and *dr*Na_2CO_3-Si contents (g kg^{-1}) were 1.1-7.9 and 0.9-5.6, respectively, whereas the ones of *dm*Na_2CO_3-Al and *dr*Na_2CO_3-Al (g kg^{-1}) were 5.2-12.2 and 4.2-11.8, respectively. Four main points could be deduced from Table 3-2 and Figure 3-3: (i) ts and pd soil samples largely differed in Na_2CO_3-Si and Na_2CO_3-Al, (ii) Na_2CO_3 dissolved Al-bearing minerals, possibly gibbsite and poorly crystalline Al hydroxide (Huang et al., 2002), (iii) *dm*Na_2CO_3-Si and *dr*Na_2CO_3-Si were positively correlated with each other (r=0.95), but *dr*Na_2CO_3-Si was below *dm*Na_2CO_3-Si, (iv) both *dm* and *dr*Na_2CO_3-Si decreased with increasing altitude and thus MAR. Besides, after 120 min of Na_2CO_3 extraction, *dr* systematically decreased with increasing time (Figure 3-4), which infers that the dissolution of crystalline minerals was not linear in the studied samples. We hypothesize that equilibrium was not reached and/or Si bearing minerals could precipitate during the extraction.

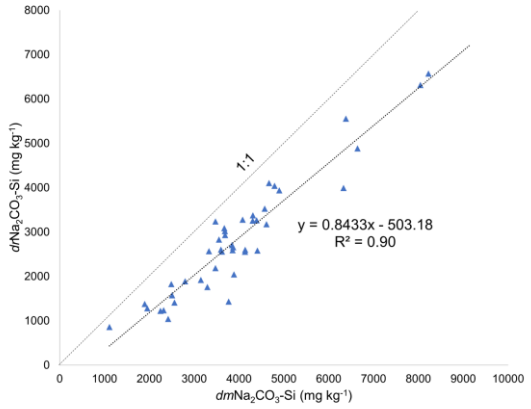

Figure 3-3: Plot of *dr*Na_2CO_3-Si as deduced from the dissolution rate (*dr*) method against *dm*Na_2CO_3-Si as deduced from the DeMaster (*dr*) technique (DeMaster, 1981) for the quantification of the PhSi pool.

Table 3-1: Selected soil properties: particle size analysis, Total Reserve in Bases (TRB), Si/(Al+Fe), Fe_d/Fe_t and Fe_o/Fe_d atomic ratios, contents of organic C and allophanic substances, $Si_o/(Al_o-Al_p)$ ratio (standard deviations in brackets). ts are topsoil samples collected in banana plots (tsBA), sugarcane plots (tsSC), and forest plot (tsFO) at various altitude levels (from 65 to 390 m asl). pd are samples collected in soil horizons from pedons pdBA, pdSC and pdFO.

	Particle size analysis (%)			**TRB**	**$Si_t/(Al_t+Fe_t)$[a]**	**Fe_d/Fe_t**	**Fe_o/Fe_d**	**C**	**Allophanic substances[b]**	**$Si_o/(Al_o-Al_p)$[c]**
	Clay	**Silt**	**Sand**	**$cmol_c\ kg^{-1}$**				**$g\ kg^{-1}$**	**$g\ kg^{-1}$**	
tsBA 65	41.4	46.6	12.0	110 (19)	1.01 (0.03)	0.54 (0.02)	0.24 (0.02)	43.3 (1.6)	110 (1)	0.57 (0.05)
tsSC 65	37.1	49.5	13.4	118 (10)	1.02 (0.02)	0.51 (0.01)	0.28 (0.03)	41.4 (3.8)	70 (4)	0.64 (0.01)
tsBA 100	45.7	34.9	19.4	136 (2)	0.83 (0.02)	0.46 (0.03)	0.27 (0.01)	49.8 (0.6)	170 (10)	0.55 (0.02)
tsSC 100	51.6	30.0	18.4	137 (11)	0.98 (0.03)	0.52 (0.03)	0.26 (0.02)	50.0 (1.2)	10 (7)	0.55 (0.02)
tsBA 150	40.1	34.3	25.6	134 (29)	0.80 (0.04)	0.49 (0.06)	0.24 (0.02)	45.9 (8.3)	140 (4)	0.58 (0.01)
tsSC 150	41.2	38.6	20.2	102 (4)	0.79 (0.06)	0.51 (0.01)	0.30 (0.02)	64.2 (3.8)	100 (4)	0.72 (0.03)
tsBA 200	24.2	50.7	25.1	98 (6)	0.77 (0.02)	0.51 (0.01)	0.27 (0.02)	47.6 (2.3)	110 (2)	0.64 (0.04)
tsSC 200	36.2	42.2	21.6	85 (8)	0.82 (0.02)	0.52 (0.01)	0.31 (0.01)	61.6 (2.0)	90 (1)	0.60 (0.02)
tsBA 250	37.0	47.3	15.7	86 (5)	0.82 (0.04)	0.53 (0.00)	0.22 (0.01)	50.1 (3.8)	65 (8)	0.69 (0.18)
tsSC 250	34.5	44.5	21.	83 (3)	0.76 (0.01)	0.54 (0.01)	0.24 (0.02)	47.5 (2.5)	80 (9)	0.59 (0.02)
tsBA 300	37.1	41.0	21.9	71 (9)	0.78 (0.06)	0.53 (0.01)	0.27 (0.02)	51.6 (2.2)	95 (13)	0.54 (0.01)
tsBA 350	34.1	47.6	18.3	88 (11)	0.87 (0.07)	0.48 (0.02)	0.39 (0.05)	78.2 (1.6)	85 (5)	0.61 (0.15)
tsBA 375	35.5	38.2	26.3	93 (5)	0.91 (0.06)	0.47 (0.03)	0.49 (0.01)	97.0 (10.3)	80 (6)	0.52 (0.03)
tsFO 396	34.0	44.9	21.1	85 (14)	0.94 (0.04)	0.41 (0.02)	0.54 (0.05)	155 (23.0)	30 (3)	0.68 (0.15)
pdBA 173 Ap	48.0	20.8	31.2	89	0.83	0.50	0.39	60.1	137	0.62
pdBA 173 AB	38.4	22.8	38.8	86	0.77	0.50	0.39	43.9	158	0.60
pdBA 173 Bw	54.8	13.9	31.3	98	0.61	0.45	0.42	25.2	236	0.53
pdBA 173 BC	38.9	18.1	43.0	161	0.70	0.43	0.43	9.4	347	0.63
pdSC 180 Ap	51.8	28.0	20.2	73	0.87	0.58	0.34	80.6	105	0.70

pdSC 180 AB	56.4	16.2	27.4	74	0.84	0.52	0.38	49.5	124	0.68
pdSC 180 Bw1	56.2	21.2	22.6	79	0.86	0.50	0.36	36.8	147	0.64
pdSC 180 Bw2			28.4	98	0.84	0.47	0.31	22.2	207	0.63
pdSC 180 BC	60.8	15.4	23.8	121	0.86	0.40	0.30	10.8	268	0.64
pdFO 396 Ah1	35.9	46.2	17.9	172	0.79	0.60	0.52	167	18.5	0.37
pdFO 396 Ah2	44.7	31.5	23.8	102	0.95	0.60	0.49	112	25.9	0.49
pdFO 396 AB	56.0	26.0	18.0	118	0.77	0.52	0.56	62.7	49.2	0.42
pdFO 396 Bw1	65.0	20.0	15.0	68	0.96	0.61	0.58	43.4	240	0.19
pdFO 396 Bw2	50.5	22.6	26.9	99	0.92	0.55	0.51	25.0	353	0.26
pdFO 396 BC	34.0	22.0	37.0	115	0.39	0.24	0.30	6.1	187	0.41

[a] computed from total elemental contents Si_t, Al_t and Fe_t (Table 3-S1)

[b] estimated according to Parfitt and Wilson (1985), using Si_o, Al_o and Alp contents (Table 3-S1).

[c] computed from Si_o, Al_o and Al_p contents (Table 3-S1).

Table 3-2: *dm* and *dr* Na_2CO_3-Si and Na_2CO_3-Al contents of ts and pd samples pretreated with dark oxalate (Method 2) as deduced from the DeMaster (*dm*) and dissolution rate (*dr*) procedures, respectively.

		Method 2: pretreatment with dark oxalate			
	Plot name and altitude (m)	***dm* procedure**		***dr* procedure**	
		***dm*Na_2CO_3-Si (mg kg^{-1})**	***dm*Na_2CO_3-Al (mg kg^{-1})**	***dr*Na_2CO_3-Si (mg kg^{-1})**	***dr*Na_2CO_3-Al (mg kg^{-1})**
Top soil samples	tsBA 65	7277.2 (1336.8)	7873.2 (1429.5)	5282.2 (1824.3)	6859.0 (1640)
	tsSC 65	7946.3 (1257.7)	7157.4 (997.5)	5600.7 (1010.3)	6457.0 (768)
	tsBA 100	5433.8 (1386.9)	8500.5 (808.6)	3602.0 (479.2)	7222 (477)
	tsSC 100	6277.3 (2091.1)	6826.6 (1675.2)	4077.6 (2089.0)	5972 (1702)
	tsBA 150	4630.0 (1658.2)	8051.0 (186.7)	2641.0 (843.5)	6753.5 (2173)
	tsSC 150	4044.7 (1513.5)	7483.4 (1998.1)	2207.9 (1652.1)	5540.5 (2827)
	tsBA 200	4356.5 (858.1)	9183.2 (874.8)	3182.9 (135.2)	9055 (559)
	tsSC 200	3777.7 (544.8)	8087.2 (427.4)	2653.0 (5.063)	7798.5 (437.5)
	tsBA 250	4143.3 (551.2)	9193.7 (28.85)	2578.9 (32.00)	7927 (599)
	tsSC 250	4459.9 (473.1)	9888.5 (143.5)	4072.0 (42.65)	10551 (430)
	tsBA 300	3372.6 (246.4)	8487.0 (317.0)	2509.3 (454.7)	6758.3 (613)
	tsBA 350	2636.3 (608.6)	6792.2 (1358.4)	1903.0 (21.20)	6007.7 (418.6)
	tsBA 375	2344.8 (343.1)	5222.6 (20.65)	2642.4 (331.1)	4642.6 (17.98)
	tsFO 396	3465.5 (530.8)	5940.8 (460.0)	1635.7 (346.0)	5782.9 (1860)
Pedon samples	pdBA 173 Ap	4411.2	7673.5	2581	5793.1
	pdBA 173 AB	3843.5	8250.5	2707	7694.2
	pdBA 173 Bw	2490.4	9343.8	1828	9040.1
	pdBA 173 BC	4304.2	8244.3	3255	7243.6
	pdSC 180 Ap	3858.2	5840.3	2589	4240.3
	pdSC 180 AB	3871.3	8141.8	2657	5973.1
	pdSC 180 Bw1	4574.1	9179.2	3528	8290.9
	pdSC 180 Bw2	3689.6	7020.8	2934	6157.8
	pdSC 180 BC	3682.5	7129.2	3020	7061.4
	pdFO 396 Ah1	3768.5	6769.9	1431	5712.8
	pdFO 396 Ah2	3294.0	8463.3	1759	6746.2
	pdFO 396 AB	2559.5	8557.2	1409	7381.4
	pdFO 396 Bw1	1894.6	9702.2	1379	9402.8
	pdFO 396 Bw2	1110.7	12189	857.4	11760.8
	pdFO 396 BC	4610.3	9611.7	3174.5	8414.9

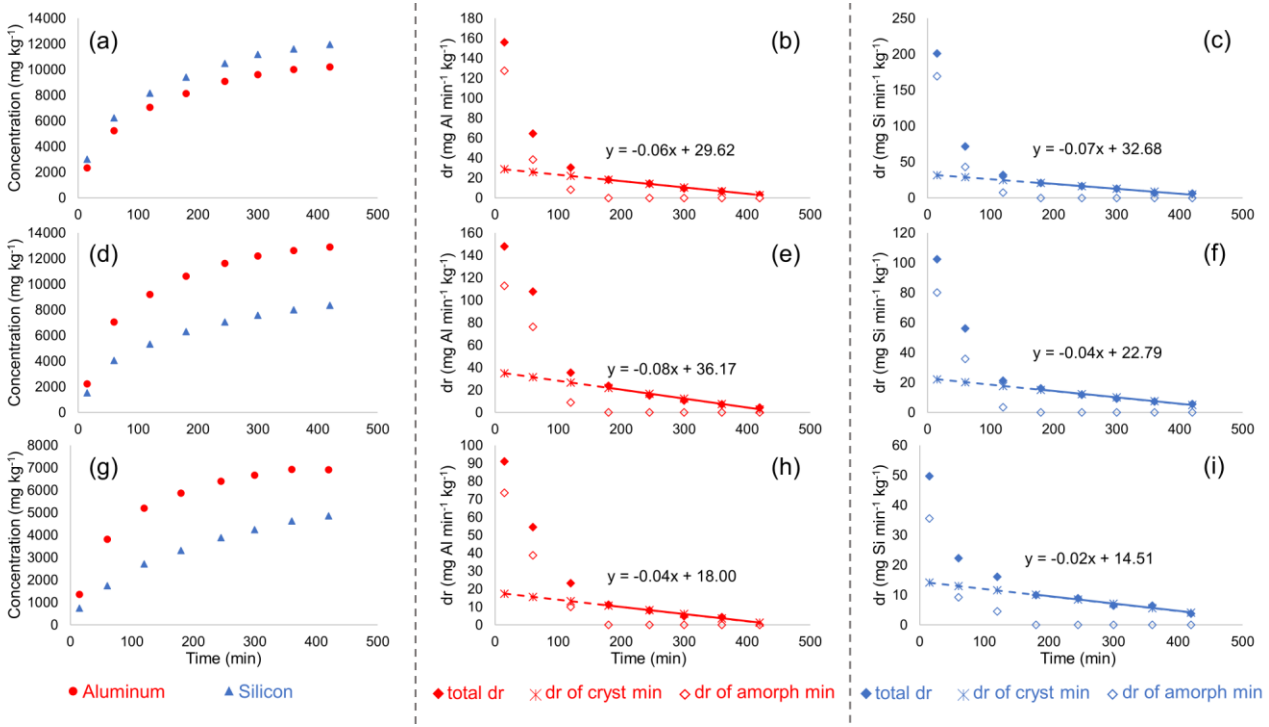

Figure 3-4: Time evolution of: (a, d, g) Si (▲), Al (●) concentrations in Na_2CO_3, (b, e, h) dissolution rate of total, crystalline, and amorphous Al-bearing phases, and (c, f, i) dissolution rate of total, crystalline, and amorphous Si-bearing phases for tsBA-65 (a, b, c), tsBA-250 (d, e, f), and tsBA-375 (g, h, i) pretreated with dark oxalate.

3.4.3 Primary weatherable Si minerals may contribute to Na_2CO_3-Si

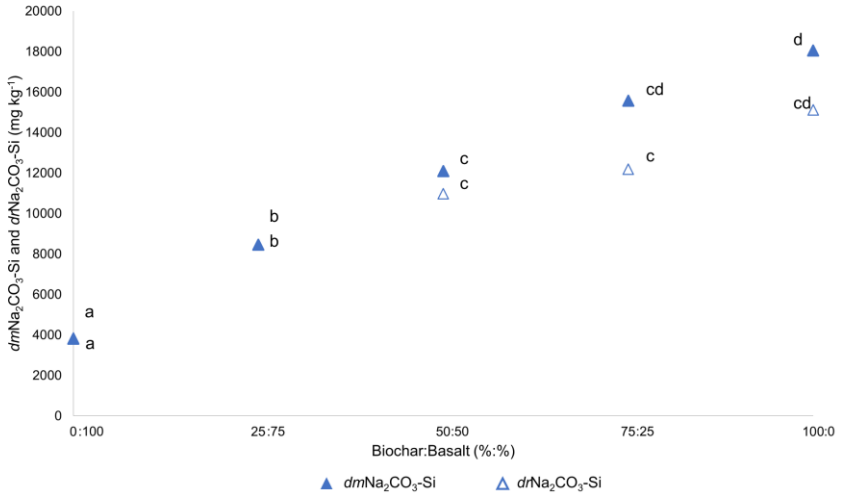

Figure 3-5: *dr*Na_2CO_3-Si concentration deduced from the dissolution rate method (△) and *dm*Na_2CO_3-Si deduced from the *DeMaster* technique (▲) for samples having different biochar:basalt proportions. Lowercase letters indicate a significant difference at $p < 0.05$ level. The difference was tested with a t-test with the pairwise.t.test function of the R programming language.

Both the *dm*Na_2CO_3-Si and *dr*Na_2CO_3-Si contents increased with dosed additions of biochar within biochar:basalt mixtures (Figure 3-5). *dm*Na_2CO_3-Si was significantly above *dr*Na_2CO_3-Si in biochar:basalt mixtures 50:50, 75:25, and 100:0. The biochar had a total Si concentration (Si_t) of 51.3 g kg^{-1}. We could therefore assess that *dm*Na_2CO_3-Si represented 66, 47, 41, and 35% of biochar-Si_t for the 25, 50, 75, 100% biochar mixtures respectively. *dr*Na_2CO_3-Si represented 66, 43, 32, and 30% of biochar-Si_t for the 25, 50, 75, 100% biochar mixtures respectively. Two points could be deduced: (i) primary weatherable minerals released Si, accounted for in the *dm*Na_2CO_3-Si and *dr*Na_2CO_3-Si pools, (ii) the higher the total quantity of biochar-Si_t, the lower the proportion of phytoliths extracted by Na_2CO_3.

3.4.4 Does precipitation occur during the alkaline extraction?

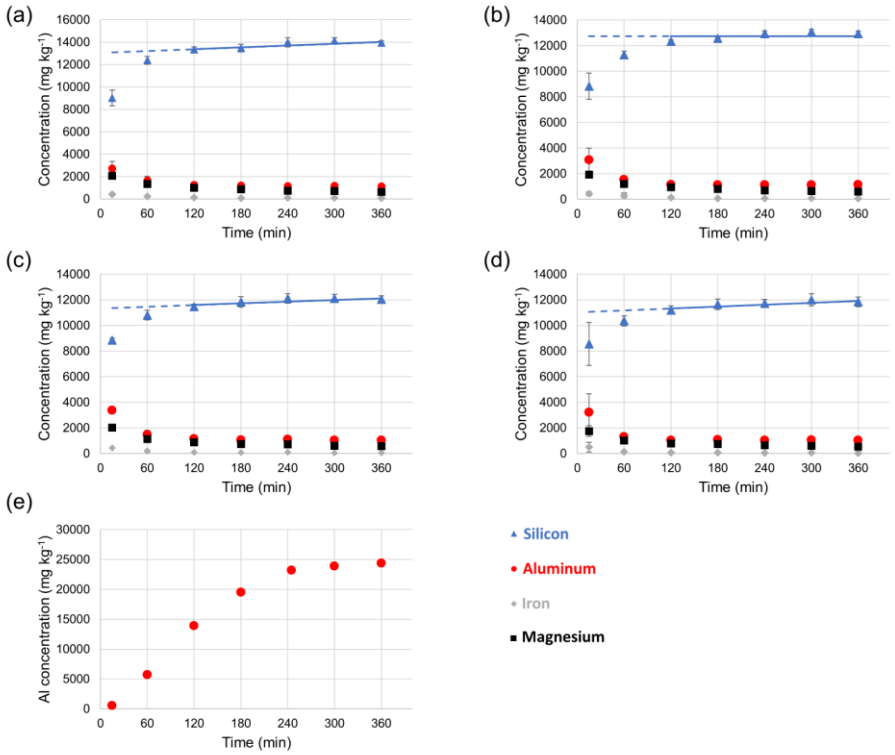

Figure 3-6: Extraction kinetics of Si (▲), Al (●), Fe (♦), and Mg (■) in Na_2CO_3 0.1 M for the different biochar:basalt:gibbsite mixtures (%): (a) 47.5:47.5:5; (b) 45:45:10; (c) 42.5:42.5:15; (d) 40:40:20; and (e) gibbsite.

Figure 3-6 shows the kinetical Na_2CO_3 extractions performed for the different biochar:basalt:gibbsite mixtures (a-d) and gibbsite (e). For the mixtures (Figure 3-6a-d), Si concentration in Na_2CO_3 abruptly increased up to 1.2-1.4 g kg^{-1} after 120 min, then stabilized between 120 and 300 min, before slightly decreasing beyond 300 min (Figure 3-6a, b, c, d). In contrast, Al, Fe, Mg concentrations in Na_2CO_3 were highest at 15 min, and then decreased steadily beyond that time. For gibbsite (Figure 3-6e), Al concentration sharply increased up to 24 g kg^{-1} after 240 min, and then stabilized. Both the *dm*Na_2CO_3-Si and *dr*Na_2CO_3-Si decreased with increasing gibbsite content in the biochar:basalt:gibbsite mixtures (Figure 3-7). *dm*Na_2CO_3-Si and *dr*Na_2CO_3-Si represented 52-54% and 43-46% of biochar-Si_t respectively, whatever the proportion of gibbsite. We thus point that (i) the decrease in Na_2CO_3-Si with increasing gibbsite content was due to the decrease in

biochar supply, and (ii) *dm*Na_2CO_3-Si was invariably above *dr*Na_2CO_3-Si. Given that Al, Fe, Mg concentrations decreased with increasing extraction time (Figure 3-6a-d), we hypothesize that minerals have formed during the extraction. In contrast, this hypothesis is not valid for single gibbsite, biochar and basalt samples. Using appropriate entering conditions within PHREEQC 3.4.0-12927, chlorite ($Mg_5Al_2Si_3O_{10}(OH)_8$) and goethite (FeOOH) could have started to precipitate after 15 min, which could be in line with the decrease in Al, Fe, Mg concentrations in Na_2CO_3 beyond that time. Unlike that, Na_2CO_3-Si did not decrease before 300 min. Our results thus suggest that Na_2CO_3 extraction data of single components cannot simply be added to each other once these components are mixed.

3.4.5 Allophane and Al hydroxide partly dissolve in Na_2CO_3

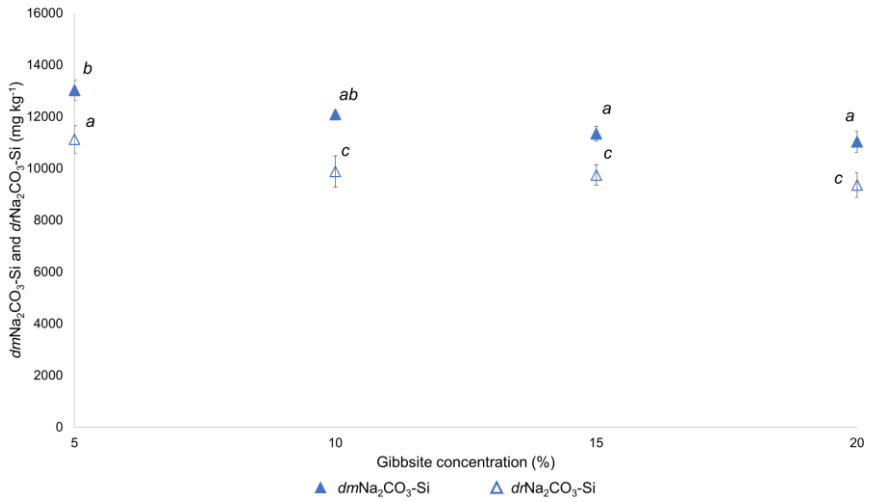

Figure 3-7: *dr*Na_2CO_3-Si (Δ) and *dm*Na_2CO_3-Si (▲) concentrations as plotted against gibbsite content (5, 10, 15, 20%) in the various biochar:basalt:gibbsite mixtures (47.5:47.5:5, 45:45:10, 42.5:42.5:15, 40:40:20). Lowercase letters indicate a significant difference at $p < 0.05$ level. The difference was tested with a t-test with the pairwise.t.test function of the R programming language.

Methods 1, 2 and 3 were applied to samples tsBA350 and tsFO396 (see the DCB and oxalate extraction data in Table 3-S2). The *dm*Na_2CO_3-Si and -Al values are shown in Table 3-3 while Si, Al, Fe, Mg concentrations in Na_2CO_3 as plotted against extraction time are illustrated in Figure 3-8. Fe and Mg concentrations are negligible, whatever the method used. At each extraction

time and for each method, Si concentration is systematically below Al concentration, the *dm*Na_2CO_3-Si/*dm*Na_2CO_3-Al atomic ratio being invariably below 0.50, denoting a prominently aluminous character of the Na_2CO_3 extract whatever the method. From method 1 to 3, *dm*Na_2CO_3-Si decreased in tsBA350 from 5.0 to 1.4 g kg^{-1}, whereas *dm*Na_2CO_3-Al decreased from 18.2 to 5.7 g kg^{-1}.

In tsFO396, *dm*Na_2CO_3-Si varied little between methods 1 and 2 (3.3, 3.5 g

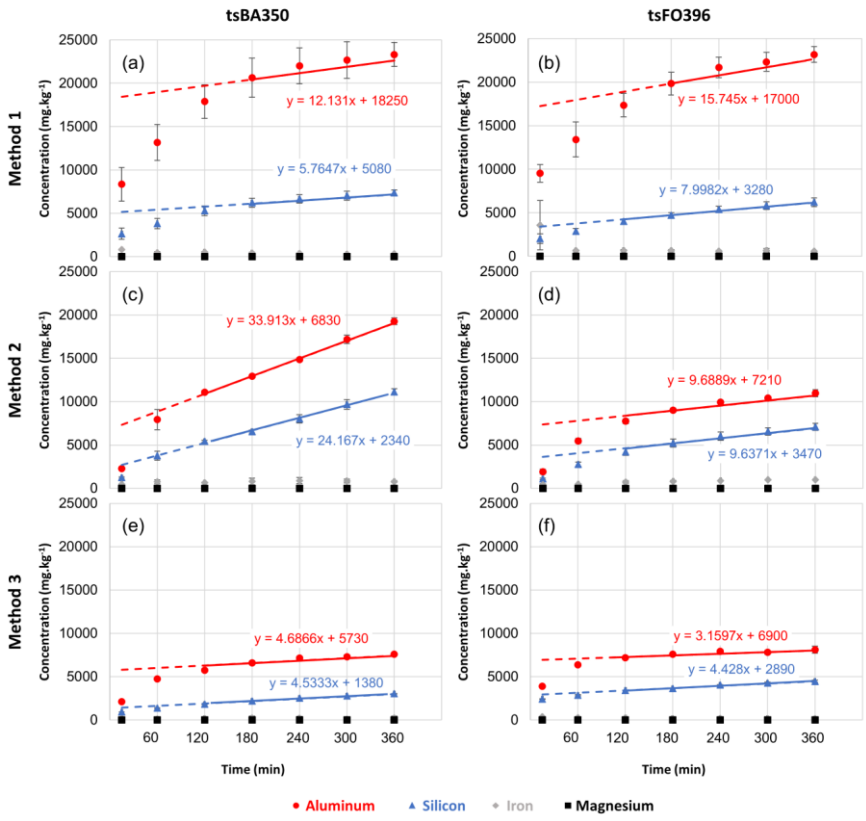

Figure 3-8: Plots of the concentrations of Si (▲), Al (●), Fe (♦), and Mg (■) in Na_2CO_3 against extraction time for sample tsBA350 (a,c,e) and sample tsFO390 (b,d,f) for method 1 (a,b), 2 (c,d), and 3 (e,f).

kg^{-1}), and slightly decreased after method 3 (2.9 g kg^{-1}). In contrast, *dm*Na_2CO_3-Al strongly decreased from method 1 (17 g kg^{-1}) to 2 and 3 (7.2-6.9 g kg^{-1}) for tsFO396. Gibbsite and SRO PSi minerals (allophanic constituents) partly dissolve in Na_2CO_3 (Jackson, 1956; Huang et al., 2002; Kamatani and Oku, 2000; Wada, 1977, 1989). SRO PSi minerals selectively

dissolve in dark oxalate buffered at pH3 (Dahlgren, 1994; Parfitt and Childs, 1988), but not gibbsite (McKeague and Day, 1966). Thus, here, apart from (Fe, Al)-humus, ferrihydrite and allophanic substances, dark oxalate most likely extracted poorly crystalline Al hydroxide (Huang et al., 2002). Following Wada and Greenland (1970), we hypothesize the occurrence of poorly crystalline Al hydroxide that could dissolve in both dark oxalate and Na_2CO_3. The increase in the *dm*Na_2CO_3-Si/*dm*Na_2CO_3-Al atomic ratio from method 1 to 2 supports our hypothesis in tsFO396, particularly rich in SOM (Table 3-1). We propose that strong desilication and high SOM content have promoted the formation of a continuum humus-Al – poorly crystalline Al hydroxide – gibbsite (Huang et al., 2002). In this continuum, organic matter has likely impeded the crystallization of Al hydroxide (Huang et al., 2002), and the formation of allophanic substances through anti-gibbsitic and anti-allophanic effects (Churchman and Lowe, 2012; Ndayiragije and Delvaux, 2003; Shoji et al., 1993). The allophane content in tsFO396 was indeed 2.8 times lower than in tsBA350 whereas SOM content in tsFO396 was twice as high as in tsBA350.

Table 3-3: Contents of Na_2CO_3-extractable Si and Al as deduced from the DeMaster technique (DeMaster, 1981) and respective values of the Na_2CO_3-Si/Na_2CO_3-Al atomic ratio following the three methods: (1) no pretreatment, (2) dark oxalate pretreatment, (3) H_2O_2 + DCB + dark oxalate pretreatment for samples tsBA350 and tsFO396. Italic lowercase letters indicate if the difference between the different methods and samples is significant (at $p < 0.05$ level) for Na_2CO_3-Si, Na_2CO_3-Al, and Na_2CO_3-Si/Na_2CO_3-Al atomic ratio. Difference was tested with a t-test with the pairwise.t.test function of the R programming language.

Topsoil (ts) Sample	**Method**	***dm*Na_2CO_3-Si**	***dm*Na_2CO_3-Al**	**Na_2CO_3-Si/Na_2CO_3-Al atomic ratio**
		mg kg^{-1}	**mg kg^{-1}**	
tsBA350	1	5080 *a*	18250 *a*	0.27 *a*
	2	2340 *bd*	6830 *b*	0.33 *a*
	3	1380 *d*	5730 *b*	0.23 *b*
tsFO396	1	3280 *bc*	17000 *a*	0.18 *c*
	2	3470 *c*	7210 *b*	0.46 *d*
	3	2890 *bcd*	6900 *b*	0.40 *d*

3.4.6 Does H_2O_2–DCB give added value?

From Table 3-3, both *dm*Na_2CO_3-Si and *dm*Na_2CO_3-Al did not differ between methods 2 and 3.

Thus, the removal of SOM (H_2O_2) and free iron (DCB) did not significantly modify *dm*Na_2CO_3-Si and *dm*Na_2CO_3-Al, but could slightly decrease them. We hypothesize that a part of the *dm*Na_2CO_3-Si pool could dissolve in DCB because of the relatively high temperature (75°C) and alkalinity (pH~9) that enhance phytolith dissolution (Fraysse et al., 2009, 2006). The slight decrease in *dm*Na_2CO_3-Al from method 2 to 3 could indicate that a small part of Al hydroxides could dissolve in DCB. The decrease in the *dm*Na_2CO_3-Si/*dm*Na_2CO_3-Al atomic ratio from method 2 to 3 indicates a relative concentration of alkaline extractable Al-bearing phases after H_2O_2 and DCB, suggesting a possible dissolution of phytoliths during DCB extraction at pH~9. The abrupt decrease in the Si/Al atomic ratio of the Na_2CO_3 extract from method 3 at early steps of alkaline extraction supports the hypothesis of a rapid phytolith dissolution (Figure 3-9). Considering residual minerals after pretreatments in methods 2 and 3 (Figure 3-2), phytoliths and poorly crystalline Al hydroxide might have been the two main contributors of Si and Al released at early alkaline extraction steps for both the methods 2 and 3. From our data, we thus point that (i) phytolith content was largest after method 2; (ii) phytoliths readily dissolve within the first 15 min of Na_2CO_3 extraction; (iii) the proportion of phytoliths that dissolved after 15 min was larger in method 3 than 2, which is likely due to the relatively lower phytolith pool for method 3 samples than for method 2 samples.

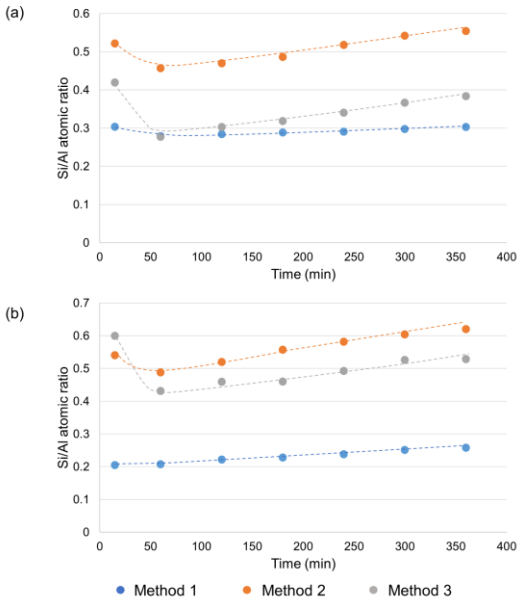

Figure 3-9: Plot of the Si/Al atomic ratio in Na_2CO_3 0.1 M extracts against time for tsB350 (a) and tsF390 (b) for method 1 (●), 2 (●), and 3 (●).

3.4.7 Silicate precipitation during Na_2CO_3 extraction did not occur

Both the low Si/Al atomic ratio and the negligible concentrations of Fe and Mg in Na_2CO_3 (Figure 3-8), suggest a very low reserve in weatherable SRO LSi minerals (volcanic glass) that could dissolve in Na_2CO_3, which is in perfect line to the advanced weathering stage of the studied soils. Besides, even after the removal of SRO aluminosilicates, part of poorly crystalline Al hydroxide, and Al-humus (methods 2 and 3), a substantial Na_2CO_3–Al pool is still extracted (Table 3-3), and attributed here to gibbsite (Figure 3-6e) and poorly crystalline Al oxide (Jackson, 1956; Wada, 1977) that were not removed by pretreatments. Unlike for biochar:basalt:gibbsite mixtures, dissolved Na_2CO_3–Al did not precipitate, likely because LSi minerals are almost exhausted in the studied soils, limiting the release of Mg and further precipitation of silicates during the extraction.

3.5 Conclusion

The perhydrated Andosols studied here are strongly weathered and desilicated. Their secondary products are SOM, (Fe, Al)-humus, allophane, ferrihydrite, gibbsite and possibly poorly crystalline gibbsite, denoting a prominently aluminous character of secondary minerals. We first showed that the release of Si from crystalline phases in Na_2CO_3 could be non-linear, which is not considered in the *DeMaster* procedure. We therefore proposed a *dissolution rate* procedure that could address the possible non-continuous dissolution of crystalline minerals in Na_2CO_3. We have further shown on synthetic mixtures of phytolithic biochar, fresh basalt and gibbsite that Na_2CO_3 dissolved primary weatherable silicate minerals and gibbsite and that secondary products could precipitate during alkaline extractions.

In the studied Andosols, the phytolith quantification through alkaline extraction might be hazardous because the soil contained SRO silicate minerals that dissolve partly in Na_2CO_3. Furthermore, the use of Si/Al atomic ratio was also hazardous. Indeed, attributing unequivocally Na_2CO_3 extractable Si to specific silica phases is hampered for at least two reasons. Firstly, gibbsite and possibly poorly crystalline Al hydroxide, which occur in the studied soils, dissolved in Na_2CO_3. Secondly, secondary silicate phases may precipitate during alkaline extraction. We thus recommend to quantify phytoliths in soils using the Na_2CO_3 kinetic extraction after removal of SRO silicate minerals by dark oxalate buffered at pH3.

Part II. Land use impact on the Si cycle

Chapter 4 The weathering stage of tropical soils affects the soil-plant cycle of silicon, but depending on land use

Abstract

Plants take up silicon (Si) from soil solution, and form biogenic silica bodies (phytoliths) that return to soil with plant debris. Since phytolith dissolution releases plant available Si, the soil-plant Si cycle tremendously influences the global Si cycle. Si plant uptake ranges from 0.7 to 1470 kg ha^{-1} yr^{-1} among different terrestrial ecosystems depending on soil properties and processes, climate, plant species, and management practices. The humid tropics shelter a huge variety of soils. Many of them are strongly weathered and desilicated, and exhausted in plant nutrients. Nevertheless, these soils support evergreen forests with the greatest biodiversity and biomass because of an intense pumping of nutrients. This pumping involves non-essential Si, and further governs the soil-plant Si cycle, which is perturbed after converting forest area into cropland. Here, we used literature data quantifying the Si soil-plant cycle in natural forest areas and croplands established on soils that differ in weathering stage. We particularly focused on comparing forest to Si-accumulating rice crop. We show that the impact of soil weathering stage on the soil-plant Si cycle markedly differs depending on land use in the tropics. In slightly or moderately weathered soils, cultivated plants take up Si in larger amounts than forest trees do, likely because the former are stimulated to pump nutrients and dissolve Si from less soluble lithogenic and pedogenic silicates. With increasing soil weathering and desilication, Si plant uptake increases in natural forest ecosystems while it decreases in cultivated ecosystems. Four factors may explain this discrepancy: (i) since they are more soluble than lithogenic and pedogenic silicates, phytoliths make the pool of plant available Si; (ii) forest litter, which is densely exploited by roots, is a place of intense mineral pumping; (iii) deep rooting of forest trees enhances pumping too; (iv) crop harvesting exports Si out of cultivated ecosystems.

Charles Vander Linden and Bruno Delvaux, Published in Geoderma

Converting forest into cropland in the tropics: what impact for silicon? ©Frans Lanting /Lanting.com

4.1 Introduction

Silicon (Si) is the second mass abundant element in the Earth's crust (28.8% wt) after oxygen (Wedepohl, 1995). In soils, total Si content ranges from 5 to 470 g kg^{-1} depending on soil mineralogy (McKeague and Cline, 1963) whereas the content of plant available Si varies from $3x10^{-3}$ to $4.5x10^{-1}$ g Si kg^{-1} (Liang et al., 2015). In shoot plant tissues, the mean Si concentration ranges between 1 and 100 g Si kg^{-1} and may exceed that of major nutrients (Hodson et al., 2005).

Despite the huge silicate mineral reserve in the Earth's crust, only a small portion of Si is mobile within the biogeochemical cycle of Si (Conley, 2002; Sommer et al., 2006). This cycle plays numerous ecological roles related to eminent global problematics and provision of ecosystem services, as illustrated through three examples. The global Si cycle is linked to the carbon (C) cycle (a.o. Goudie and Viles, 2012; Street-Perrott and Barker, 2008; Tréguer and Pondaven, 2000; Tréguer et al., 2018). In terrestrial ecosystems, mineral weathering consumes carbonic acid from dissolved carbon dioxide (CO_2) and releases monosilicic acid ($H_4SiO_4^0$ or dissolved silicon - DSi) and other solutes. Once DSi is transferred to watersheds and reaches marine ecosystems, it acts as a major nutrient for diatoms, and thus impacts the capacity of oceans to fix C (a.o. Ragueneau et al., 2006; Tréguer and Pondaven, 2000; Tréguer et al., 2018). In coastal areas, the ratio of Si to nitrogen (N) and phosphorus (P) in continental waters is a crucial factor in eutrophication (Cloern, 2001; Schelske and Stoermer, 1971). Eventually, Si is beneficial in protecting plants against biotic and abiotic stresses (see Coskun et al. 2019 for a review).

In a pioneer work, Bartoli (1983) reported the crucial role of plants in the biogeochemical cycle of Si and related soil weathering processes in temperate deciduous forests. He demonstrated that the biological cycling of Si controlled Si release from mineral weathering. Further studies confirmed the importance of the biological pumping in controlling the biogeochemical Si cycle (Alexandre et al., 1997; Derry et al., 2005; Lucas et al., 1993; Meunier et al., 1999). Compiling literature data, Cornelis and Delvaux (2016) proposed that plant impact depended on soil weathering stage in natural ecosystems, highlighting an increased biological Si feedback loop with increasing weathering stage.

The conversion of forest areas into croplands alters the biogeochemical cycle of Si (a.o. Clymans et al., 2011; Guntzer et al., 2012; Keller et al., 2012; Struyf et al., 2010; Vandevenne et al., 2011). Actually, this transition results in the exhaustion of the soil phytolith pool (Barão et al., 2014; Guntzer et al., 2012; Struyf et al., 2010; Vandevenne et al., 2015). It also decreases the plant available Si pool (Klotzbücher et al., 2015; Savant et al., 1996; Struyf et al., 2010), and the Si fluxes to watersheds (Struyf et al., 2010), thus affecting the ecological functions of Si. Thus, in croplands, the biological Si feedback loop would decrease with increasing soil weathering stage. Indeed, in tropical banana and rice croplands, plant accumulation of Si decreases with increasing soil weathering stage (Henriet et al., 2008a, 2008b; Klotzbücher et al., 2015a; Tavakkoli et al., 2011). In natural ecosystems, on the contrary, the biological feedback loop of Si increases with increasing degree of alteration (Cornelis and Delvaux, 2016).

Here we test the idea that land use may affect the relationship between plant Si accumulation and soil weathering stage in the tropics. We use published data collected in humid tropical regions worldwide. We particularly focus on comparing forest to Si-accumulating rice crop. We first recall that the soil-plant cycle of Si is constrained by the dissolution of weatherable minerals in slightly to moderately weathered soils (section 4.2) and by that of phytoliths in highly weathered soils (section 4.3). Next, we focus more specifically on the control of the Si soil-plant cycle in natural ecosystems (section 4.4) and then in croplands (section 4.5). Finally, we discuss the impact of soil weathering stage and land use on the soil-plant cycle of Si.

Our methodological approach is based on the use of published data and their statistical processing. In particular, we have identified Si uptake data, as well as climate and soil types in tropical regions. The soils have been categorized according to their weathering stage, identifiable via the mineral reserve or taxon. We performed descriptive statistics, mainly using the ggplot function of the R programming language. We then discuss the data based heavily on well-known mechanisms and soil processes.

4.2 Mineral dissolution controls the Si soil-plant cycle in slightly to moderately weathered soils

As illustrated in Figure 4-1, the continental cycle of Si is mainly based on the Si soil-plant cycle where the original source of Si is the reserve of primary weatherable lithogenic silicates (LSi) (Alexandre et al., 1997; Henriet et al.,

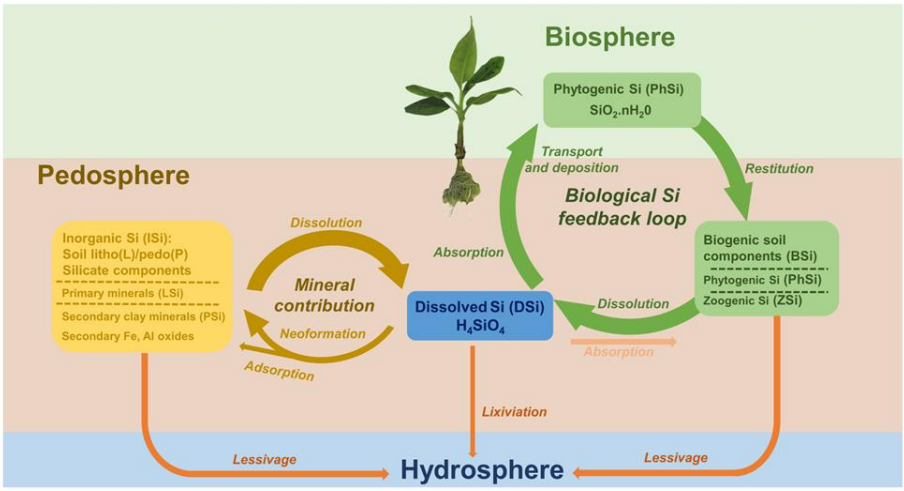

Figure 4-1: Dissolved Si (DSi) originates from the inorganic Si and biogenic Si pools. DSi it can follow four routes: (i) leaching and export to watersheds; (ii) PSi synthesis through the formation of clay minerals and/or amorphous silica; (iii) adsorption on Fe and Al oxides; (iv) uptake by plant roots. Adapted from Cornelis and Delvaux (2016).

2008b; McKeague and Cline, 1963). In soils undergoing net acidification (van Breemen et al., 1983), LSi dissolution releases aqueous $H_4SiO_4^0$ (dissolved Si: DSi), aluminum (Al), iron (Fe) and other solutes. The fate of DSi may take four main routes: (i) leaching and export to watersheds; (ii) synthesis of pedogenic silicates (PSi) through the formation of clay minerals (Garrels and Christ, 1965) and/or amorphous silica (Drees et al., 1989); (iii) adsorption on Fe and Al oxides (Beckwith and Reeve, 1963; Jones and Handreck, 1963; McKeague and Cline, 1963); (iv) uptake by plant roots (Jones and Handreck, 1965).

According to Cornelis and Delvaux, (2016), both the LSi dissolution and PSi neoformation [routes (i) and (ii)] govern the mobility of Si in slightly to moderately weathered soils. At advanced weathering stage, Al and Fe oxides accumulate whereas silica exhaustion vanishes the contribution of LSi and PSi silicates to the pool of plant available Si [route (iv)]. The latter pool is fed

through phytolith dissolution (Lucas et al., 1993), hence creating a biological Si feedback loop, thus inducing a steady state (Alexandre et al., 1997).

4.3 The biological Si feedback controls the Si soil-plant cycle in highly weathered soils

The **biological Si feedback loop** encompasses the processes of plant uptake of Si, phytolith formation in plant tissues, return to soil, and dissolution to feed the plant available Si reservoir (Alexandre et al., 1997).

Briefly, once taken up by plant roots, $H_4SiO_4^0$ is translocated to shoots through the transpiration stream (Mitani and Ma, 2005). At transpiration sites, water evaporation provokes $H_4SiO_4^0$ oversaturation with respect to amorphous Opal A silica ($SiO_2.nH_2O$) named phytolith (PhSi) (Piperno, 1988; Raven, 2001, 1983; Sangster and Hodson, 1986).

Plant species take up Si through: active, passive or rejective mechanisms (Ma et al., 2001, 2006; Ma and Takahashi, 2002), and are classified as Si high-, intermediate-, or non-accumulating plant species, respectively. Thus, plant Si uptake considerably varies from 0.7 to 1470 kg ha^{-1} yr^{-1} (Table 4-1). In temperate forest ecosystems, it ranges from 2 to 44 kg Si yr^{-1} depending on tree species and soil type (Bartoli, 1983; Cornelis et al., 2010; Farmer et al., 2005; Fulweiler and Nixon, 2005; Gérard et al., 2008; Markewitz and Richter, 1998; M. Sommer et al., 2013). In humid tropical forests, Si uptake by trees varies from 7 to 76 kg ha^{-1} yr^{-1} (Alexandre et al., 1997; Lucas, 2001; Lucas et al., 1993; Meunier et al., 2010), and even from 450 to 957 kg ha^{-1} yr^{-1} in the particular case of bamboo forest (Li et al., 2006; Meunier et al., 1999). The Si uptake by grasses ranges from 12 to 67 kg ha^{-1} yr^{-1} in dry and humid temperate grasslands (Blecker et al., 2006; White et al., 2012), and from 98 to 552 kg ha^{-1} yr^{-1} in intertropical savannas (Alexandre et al., 2011; Melzer et al., 2010). In croplands, Si uptake by cultivated plants varies widely from 0.7 to 1470 kg ha^{-1} yr^{-1} depending on plant species and environmental conditions (Desplanques et al., 2006; Guntzer et al., 2012; Klotzbücher et al., 2016; Makabe et al., 2009; Prakash et al., 2011; Ross et al., 1974; Tubana et al., 2016; Vandevenne et al., 2011; Yang and Zhang, 2018).

The global annual production of phytogenic Si by higher plants ranges from 1.7 to 5.6 x 10^{12} kg Si yr^{-1} (Conley, 2002; Laruelle et al., 2009), and rivals with

that of biogenic Si (BSi) production by diatoms in oceans (6.7 x 10^{12} kg Si yr^{-1}) (Treguer et al., 1995).

The quantity of soil PhSi commonly ranges from <1 to 30 g kg^{-1} on a total soil basis (Drees et al., 1989), but is above 50 g kg^{-1} in a number of soils (Clarke, 2003). Actually, it depends on soil type, but also on the type of terrestrial ecosystem, which influences the Si cycling. The largest PhSi amounts are measured in soils of coastal and inland swamps, flood plains, grasslands and forests (Clarke, 2003). In natural climax ecosystems, the annual Si returns from plant to soil matches the annual Si plant uptake, hence reaching steady state (e.g. Alexandre et al., 1997; Sommer et al., 2013). Once climax is not reached, and if net above-ground biomass productivity is above biomass return to soil, PhSi return is generally below plant Si uptake (Meunier et al., 2010). In agricultural ecosystems, crop harvesting reduces the restitution of PhSi to soil (Vandevenne et al., 2011).

PhSi particles readily dissolve at common soil solution pH values (Fraysse et al., 2010, 2009). Their dissolution rate is 1 to 100 order of magnitude higher than that of LSi and PSi minerals, and decreases with increasing acidity (Fraysse et al., 2010, 2009, 2006), as well as increasing salinity (Loucaides et al., 2008). Thus, only a small part of annual PhSi deposition remains undissolved (~ 8% in tropical forests (Alexandre et al., 1997)). Since phytolith dissolution depends also on plant species (Alexandre et al., 1997; Blecker et al., 2006; Li et al., 2014; Wilding and Drees, 1974), the origin of phytoliths influences the contribution of PhSi to the DSi pool at given pH. For example, the proportion of DSi released from phytolith dissolution ranges from ~10-30% in pine forests and forest tundra (Bartoli, 1983; Pokrovsky et al., 2005), but to ~90% in forested Hawaiian watersheds (Derry et al., 2005; Street-Perrott and Barker, 2008).

Table 4-1: Experimental values of Si uptake by plants in forest, grass and cultivated ecosystems.

Ecosystem	Si uptake (kg ha^{-1} yr^{-1})	References	Ecosystem	Si uptake (kg ha^{-1} yr^{-1})	References
Forest ecosystems			**Cultivated ecosystems**		
Tropical forest	7	Meunier et al. (2010)	Triticale	36-44	Vandevenne et al. (2011)
Tropical forest	21	Lucas (2001)	Flax	0.7-0.9	Vandevenne et al. (2011)
Tropical forest	40-50	Lucas (2001)	Barley	15-24	Vandevenne et al. (2011)
Tropical forest	58	Alexandre et al. (1997)	Barley	99	Tubana et al. (2016)
Tropical forest	76	Alexandre et al. (1997)	Maize	112-127	Vandevenne et al. (2011)
Bamboo forest	450-670	Meunier et al. (1999)	Maize	129	Tubana et al. (2016)
Bamboo forest	957	Li et al. (2006)	Oat	19-27	Vandevenne et al. (2011)
Bamboo forest	77-330	Umemura and Takenaka (2014)	Oat	48	Tubana et al. (2016)
Coniferous forest (Black pine)	2.3	Cornelis et al. (2010)	Sorghum	62	Tubana et al. (2016)
Coniferous forest (Douglas fir)	30.6	Cornelis et al. (2010)	Soybean	59	Tubana et al. (2016)
Coniferous forest (Spruce)	43.5	Cornelis et al. (2010)	Sugar beet	3-8	Vandevenne et al. (2011)
Coniferous forest (Fir)	35.7	Farmer et al. (2005)	Sugar beet	1408	Tubana et al. (2016)
Coniferous forest (Pine)	7.9	Farmer et al. (2005)	Wheat	37-113	Vandevenne et al. (2011)
Coniferous forest	8	Bartoli (1983)	Wheat	108	Tubana et al. (2016)
Coniferous forest (Douglas fir)	44.4	Gérard et al. (2008)	Wheat	94	Guntzer et al. (2012)
Mixed forest beech and pine	35	Sommer et al. (2013)	Weath	20	Guntzer et al. (2012)
Mixed forest beech and fir	25.8	Farmer et al. (2005)	Rice	329	Tubana et al. (2016)
Deciduous forest (Beech)	23.3	Cornelis et al. (2010)	Rice	270	Desplanques et al. (2006)
Deciduous forest (Oak)	18.5	Cornelis et al. (2010)	Rice	500	Makabe et al. (2009)
Deciduous forest (Beech)	36.5-46.3	Farmer et al. (2005)	Rice	218	Yang and Zhang (2018)

Deciduous forest	26	Bartoli (1983)
Grass ecosystems		
Temperate grassland	87-215	Melzer et al. (2010)
Temperate grassland	22	Blecker et al. (2006)
Temperate grassland	26	Blecker et al. (2006)
Temperate grassland	55	Blecker et al. (2006)
Temperate grassland	56	Blecker et al. (2006)
Temperate grassland	58	Blecker et al. (2006)
Temperate grassland	59	Blecker et al. (2006)
Temperate grassland	67	Blecker et al. (2006)
Temperate grassland	12	White et al. (2012)
Temperate grassland	18	White et al. (2012)
Temperate grassland	23	White et al. (2012)
Temperate grassland	46	White et al. (2012)
Temperate grassland	48	White et al. (2012)
Tropical savanna	98-552	Melzer et al. (2010)
Tropical savanna	127	Alexandre et al. (2011)
Rice	1470	Klotzbücher et al. (2016)
Rice	1140	Klotzbücher et al. (2016)
Rice	600	Klotzbücher et al. (2016)
Rice	600	Klotzbücher et al. (2016)
Rice	360	Klotzbücher et al. (2016)
Rice	28-390	Klotzbücher et al. (2016)
Rice	370-470	Klotzbücher et al. (2016)
Rice	234	Prakash et al. (2011)
Rice	130	Prakash et al. (2011)
Sugarcane	160	Tubana et al. (2016)
Sugarcane	248	Ross et al. (1974)
Sugarcane	408	Ross et al. (1974)
Sugarcane	379	Samuels (1969)

Figure 4-2 illustrates that the biological Si feedback loop progressively takes over the mineral contribution to Si plant uptake (Table 1 in Cornelis and Delvaux, 2016).

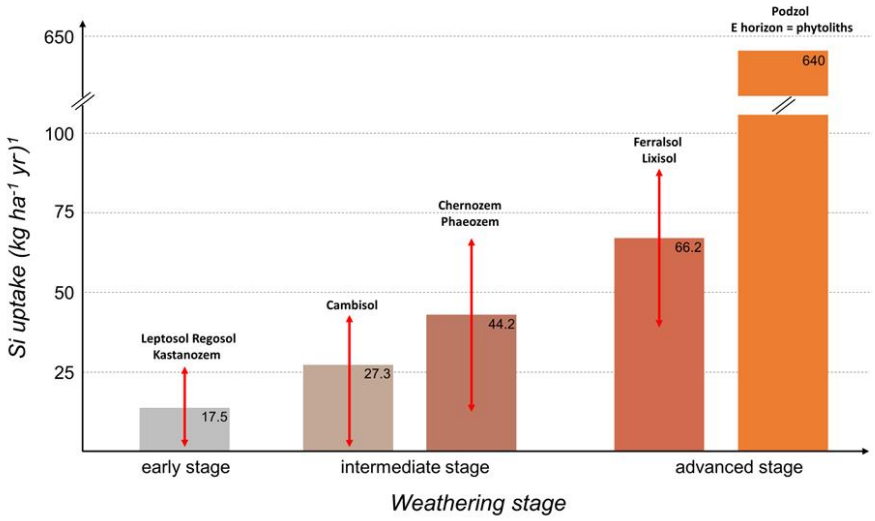

Figure 4-2: Impact of soil weathering stage on plant Si uptake as measured in various natural ecosystems: forest and prairie in Leptosol, Regosol, Kastanozem; forest in Cambisol, prairie in Chernozem and Phaeozem; rainforest and tall savanna in Ferralsol and Lixisol, bamboo forest in Podzol. In each box, the arrow represents the range of values; the figure is the average value of Si uptake as computed from Table 1 in Cornelis & Delvaux (2016).

Based on this model, we redraw the Q-I relationship for natural ecosystems in Figure 4-3b. In slightly weathered soils, LSi/PSi mineral dissolution/neoformation processes control the activity of $H_4SiO_4^0$, and thus govern the Si soil-plant cycle (Figure 4-3b-(1)). LSi depletion leads to the progressive increase in the PhSi pool, which is largest in highly desilicated soils (Figure 4-3b – from (1) to (4)).

Humid tropical regions conditions of temperature and rainfall promote mineral weathering and loss of silica. A number of soils in the humid tropics are highly weathered, since they cover more than 50% of the humid tropical areas (Sanchez, 2019), notably in central Africa. Their mineral assemblage consists of residual unalterable primary minerals, and neoformed secondary minerals typical for desilicated soils such as kaolinite, gibbsite, hematite, and goethite. In the humid tropics, slightly weathered soils mostly occur in areas

affected by recent tectonic faulting and subsequent rock outcropping, and/or volcanic activity (e.g. the African Great Lakes Region, Carribean, Central and South America, Indonesia, Philippines…).

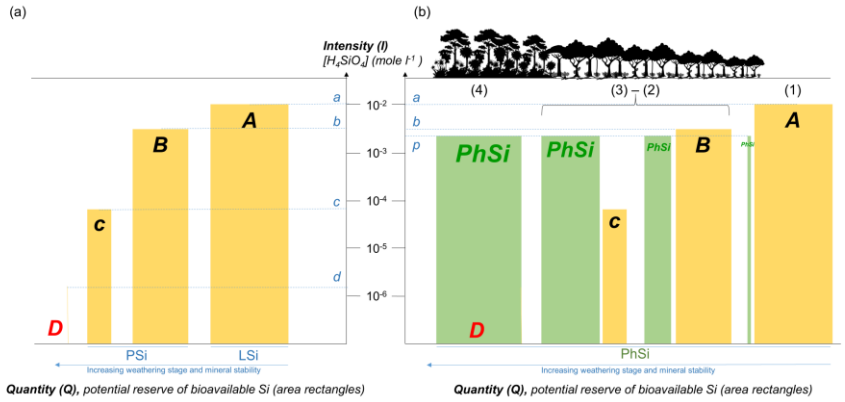

Figure 4-3: **(a)** The Si quantity-intensity (Q-I) relationship exclusively considers the mineral contribution. With increasing weathering, successive LSi (A) and PSi (B, C) dissolution controls the activity of aqueous $H_4SiO_4^0$ at different levels (>10^{-4}M). Upon PSi exhaustion, secondary oxides are devoid of Si (D), hence the activity of aqueous $H_4SiO_4^0$ is very low (<10^{-4}M). **(b)** The Si Q-I relationship considers both the mineral contribution and biological Si feedback loop, the concomitant evolution (1-4) of the ecosystem being schematized. (1) At early stage of weathering, LSi/PSi mineral dissolution/neoformation governs plant Si uptake. Upon gradual development of forest ecosystem (2-3) and intermediate weathering stage, biological pumping and soil PhSi pool increase. At advanced weathering (4), the PhSi pool is largest, while the forest climax stage is reached. The biological Si feedback loop takes over the mineral contribution, and the PhSi pool alleviates natural soil desilication (Lucas et al., 1993). The size of each rectangle represents the related Si stock. Adapted from Cornelis and Delvaux (2016).

Highly weathered soils in the humid tropics are well-known to support the growth and development of the densest forests with the greatest biomass and biodiversity in the world (Beer et al., 2010; Laliberté et al., 2013; Myers, 1988) because mineral fertility is concentrated in forest biomass and litter. Once deforested and used for cropping, these ferrallitic soils are widely recognized as unfertile soils (Sanchez, 2019). In contrast, little weathered soils in the humid tropics are highly fertile and productive, and they can support high yielding crops (Sanchez, 2019). Thus, in the tropics, soils may react differently to the conversion of forest to cropland according to their weathering stage. In particular, the soil-plant Si cycle may differ depending on weathering stage but also on land use.

4.4 The Si soil-plant cycle in humid tropical forests

4.4.1 In forests on slightly weathered soils, mineral dissolution controls the Si soil-plant cycle

In the young volcanic soil of the Marelongue reserve (Réunion Island), the soil-plant Si cycle was not dominated by the biological Si feedback loop because basalt weathering and wood storage of nutrients were still active processes (Meunier et al., 2010) (Table 4-2). The input from dying trunks was not significant in such a young forest unlike older tropical forest (Lucas et al., 1996). The elemental biocycling in the Marelongue reserve depended on plant species for both the litterfall and wood storage (Meunier et al., 2010). The four tree species that contributed mostly to litterfall (70%) represented only 45% of the annual Si biocycling, while one species contributing to 2% of the litterfall represented 13.2% of the annual Si biocycling. In this ecosystem, the leaching output of Si was 15 kg ha^{-1} yr^{-1}, i. e. about twice the restitutions of Si by litterfall. Meunier et al. (2010) explained it by a combination of two factors enhancing weathering: the basaltic nature of the parent-rock rich in weatherable silicates, and the hot and wet conditions. In agreement with Meunier et al (2010), Yang and Zhang (2018) demonstrated that the Si cycle in forests on slightly altered Leptosols and Cambisols was more dependent on the dissolution of LSi minerals than on the recycling of Si by plants (Table 4-2). In these little weathered humid tropical soils, the Si cycle was thus characterized by high LSi dissolution rates that led to large Si outputs by leaching, and a virtually absent biological Si feedback loop.

4.4.2 In forests on highly weathered soils, the biological Si feedback loop controls the soil-plant Si cycle

At advanced stage of weathering in humid tropical conditions, the soil mineralogical assemblage includes residual LSi minerals that resist to weathering (e.g. quartz, muscovite), kaolinite and secondary Al and Fe oxides (e.g. gibbsite, goethite, hematite). Ferralsols, Lixisols, Acrisols, and Podzols are typical highly weathered soils of the humid tropics. Alexandre et al. (1997) and Lucas et al. (1993) showed that the biological Si feedback loop was crucial to maintain the Si “fertility” in the topsoils of Ferralsols. Cornu (1995), Cornu et al. (1998), and Lucas et al. (1993) studied the Si cycle in neighboring forests on a Ferralsol and a Podzol. In both soils (Table 4-2), the biological pumping and subsequent biocycling of Si were crucial since plants

took up Si in deep soil horizons and returned it to the topsoil, where DSi governed clay formation. In the Ferralsol, the availability of Al and Si promoted the formation of kaolinite whereas in the Podzol, the leaching of Al as mobile Al-humus complex led to a relative accumulation of residual quartz. Meunier et al. (1999) measured an exceptional Si uptake in a bamboo forest (*Nastus borbonicus,* high Si-accumulating) that developed on a Podzol overlying a strongly weathered Andosol. The Si biocycling was so active that the bamboo forest recycled huge quantities of phytoliths that accumulate in soil to eventually build up a bleached phytolithic E horizon over a spodic Bhs horizon. In this case, the loop was partial because of soil phytoliths accumulation (Meunier et al. 1999).

4.5 The impact of agricultural land use on the Si soil-plant cycle

Agricultural practices impact the silicon cycle through (i) harvesting plant parts that contain phytoliths (Guntzer et al., 2012; Vandevenne et al., 2011), (ii) changing soil pH (Fraysse et al., 2006; Guntzer et al., 2012; Haynes and Zhou, 2018), (iii) promoting erosion (Clymans et al., 2015b), (iv) using silicate amendments (e.g. Haynes and Zhou, 2018; Ross et al., 1974; Savant et al., 1996, 1999), (v) altering soil aggregates through tillage practices (Li, 2019). Agriculture especially impacts the silicon soil-plant cycle since the five most cultivated crops - sugarcane, maize, rice, wheat, and barley - (ranked by mass produced globally, FAO 2018) are high-Si-accumulating plant species. Carey and Fulweiler (2012) assessed that the total BSi produced in cultivated lands was 29.4 Tmol yr^{-1} namely 35% of total BSi produced annually by terrestrial plants (84±29 Tmol yr^{-1} globally). In the humid tropics, sugarcane and rice, which are particularly efficient in Si accumulation, are the two main cultivated crops.

Table 4-2: Experimental values of Si uptake, Si restitution and Si export rates, and Si in standing biomass in various forest and agricultural ecosystems as measured in the above-ground plant parts. Values for croplands are given for soils that did not receive any Si amendments. Si uptake are lower for the tropical forests on slightly weathered soils than for the tropical forests established on highly weathered soils. Inversely, values of Si uptake are globally larger for the croplands on slightly weathered soils than for the croplands on highly weathered soils. The data present here below are published experimental data from field studies.

Ecosystem	**Climate (MAP in mm)**	**Soil weathering degree**		**Location**	**Si uptake (kg ha^{-1} yr^{-1})**	**Si restitution (kg ha^{-1} yr^{-1})**	**Si export (kg ha^{-1} yr^{-1})**	**Si in standing biomass (kg ha^{-1})**
		WRB class	TRB[a]					
Weakly weathered soils								
Rain forest[1]	Tropical humid (4200)	Leptosol		Reunion Island	7	7	0	17.76
Coniferous forest[2]	Subtropical monsoon (1585)	Leptosol Cambisol		Anhui Province (China)	28	17.5	0	
Rice[2]	Subtropical monsoon (1585)	Cambisol		Anhui Province (China)	218	177.4	41	
Rice[3]	Tropical monsoon (2050)		168	Luzon Island (Philippines)	1470	230	1240	560-760
Rice[3]	Tropical monsoon (2050)		176	Luzon Island (Philippines)	1140	240	900	510-630
Rice[3]	Tropical humid (3670)		167	Luzon Island (Philippines)	600	50	550	600
Highly weathered soils								
Rain forest[4]	Tropical humid (2100)	Ferralsol		Manaus (Brazil)	41	41	0	834
Rain forest[5]	Tropical humid (2100)	Ferralsol		Manaus (Brazil)	51	51	0	

Rain forest[6]	Tropical humid (1500)	Ferralsol		Mayombé (Congo)	58-76	58-76	0	
Campinarana[7]	Tropical humid (2100)	Podzol		Manaus (Brazil)	21	21	0	
Bamboo forest[8]	Tropical humid	Podzol		Reunion Island	453-644	453-644	0	
Rice[3]	Subtropical warm humid (1676)		94	Northern Vietnam	600	110	490	230-370
Rice[3]	Subtropical warm humid (1676)		31	Northern Vietnam	360	90	270	150-210
Rice[3]	Subtropical warm humid (2840)		90	Northern Vietnam	280-390	50-60	230-330	280-390
Rice[3]	Tropical monsoonal (1930)		89	Southern Vietnam	370-470	90-140	280-330	170-240
Rice[9]	Tropical humid (3300)	Acrisol		Karnataka (South India)	234.3	0-189[b]	45.5-234.3	
Rice[9]	Tropical humid (3390)	Acrisol		Karnataka (South India)	129.5	0-108[b]	21.05-129.5	
Rice[10]	Subtropical warm humid (1680)	Acrisol		Northern Vietnam				107
Sugarcane[11]	Tropical humid	Ferralsol		Mauritius Island	248			

[1](Meunier et al., 2010); [2](Yang and Zhang, 2018); [3](Klotzbücher et al., 2016) ; [4](Lucas et al., 1993) ; [5](Cornu, 1995); [6](Alexandre et al., 1997); [7](Cornu et al., 1998); [8](Meunier et al., 1999); [9](Prakash et al., 2011); [10](Marxen et al., 2016); [11](Ross et al., 1974).

4.5.1 Plant Si uptake is largest in croplands established on slightly weathered soils

In slightly weathered soils, plant available DSi is constrained by the reserve of LSi minerals (Figure 4-3 andFigure 4-4). High Si-accumulating plants (e.g. rice, sugarcane or banana) take up very large amounts of Si ranging from 218 to 1470 kg ha^{-1} yr^{-1} (Henriet et al., 2008a, 2008b; Klotzbücher et al., 2016, 2015b; Yang and Zhang, 2018) (Table 4-2 and Table 4-3). Here, the management of non-edible plant parts is crucial as it largely influences the soil-plant Si cycle (Klotzbücher et al., 2015b; Savant et al., 1999, 1996). Rice straws are often removed from the field in South and Southeast Asia, where most of the rice is grown worldwide, for various purposes such as animal fodder, fuel for stoves, or burning (Savant et al., 1996; Seyfferth et al., 2013). As rice straws contain about 86% of total plant Si (Klotzbücher et al., 2015a), their removal strongly influences the soil-plant Si cycle by disrupting the biological silicon feedback loop and therefore enhancing soil desilication (Seyfferth et al., 2013) and LSi/PSi weathering (Yang and Zhang, 2018). The harvest of sugarcane generally involves the export of the stalks while the leaves return to soil either green or burned. As stalks contain about 15-20% of the total plant Si (Ayres, 1966; Kingston, 2008), little Si amount is usually exported in sugarcane croplands. In slightly weathered soils, the biological Si feedback loop is thus very active if high Si-accumulating plants are used, and if non-edible plant parts return to soil.

Table 4-3: Plant Si content in rice, banana, and sugarcane from different cultivated plots established on soils differing in weathering stage. The mean Si concentration is generally larger in the slightly weathered soils than in the highly weathered soils, but some values do not follow this trend.

Plant	Soil type	Plant part	Si %
Weakly weathered soil			
Rice[1]	Vertisol	Plant composite	3.4-3.61
Rice[2]	Cambisol	Straw	3.051
Rice[3]	Cambisol, Luvisol, and Nitosol	Straw	7.6-9.1
Rice[3]	Cambisol, Nitisol, and Vertisol	Straw	6.3-8.1
Rice[3]	Nitosol, and Acrisol	Straw	7.6
Banana[4]	Andosol	Leaf	1.3
Banana[4]	Cambisol	Leaf	1.2
Strongly weathered soil			
Rice[5]	Acrisol	Straw	5.4
Rice[3]	Gleysol	Straw	4-4.1
Rice[3]	Acrisol	Straw	4-4.3
Rice[3]	Acrisol	Straw	4.4-4.8
Rice[3]	Gleysol, and Fluvisol	Straw	2.8-3.2
Rice[6]	Acrisol	Straw	2.6
Rice[6]	Acrisol	Straw	1.53
Rice[1]	Ferralsol	Plant composite	0.24-0.42
Sugarcane[7]	Ferralsol	Leaf	0.42-0.61
Sugarcane[8]	Ferralsol	Plant composite	0.7
Banana[4]	Nitisol	Leaf	0.75
Banana[4]	Ferralsol	Leaf	0.56

[1](Tavakkoli et al., 2011); [2](Yang and Zhang, 2018); [3](Klotzbücher et al., 2016) ; [4](Henriet et al., 2008a) ; [5](Marxen et al., 2016); [6](Prakash et al., 2011); [7](Ross et al., 1974); [8](Rodrigues, 1997).

4.5.2 Plant Si uptake is lowest in croplands established on highly weathered soils

In highly weathered, desilicated soils, the pool of bioavailable Si is low. The annual Si uptake by rice plant varies between 129.5 and 600 kg ha^{-1} yr^{-1} (Table 4-2) (Klotzbücher et al., 2016; Prakash et al., 2011). These values are relatively low (Henriet et al., 2008a, 2008b; Klotzbücher et al., 2015b; Miles et al., 2014) compared to Si uptake by plants cropped on slightly weathered soils (Table 4-2 and Table 4-3, Figure 4-3b). Si is thus considered as "deficient" in highly weathered soils. Si supply has a positive impact on sugarcane and rice crop yields through Si fertilizers (Allorerung, 1989; Ayres, 1966; D'Hotman and Villiers, 1961; Foy, 1992; Kawaguchi, 1966; A. Klotzbücher et al., 2018; Ross et al., 1974; Savant et al., 1999, 1996; Takijima and Gunawardena, 1969) as well as phytolithic biochar (Li et al., 2018).

4.5.3 Land use change impacts hydrology and related Si fluxes

Land use changes greatly impact the hydrology of the soil-plant system (Carlson and Traci Arthur, 2000; Davidson et al., 2012; Kosmas et al., 1997; Piao et al., 2007; Sanchez, 2019), in particular in the tropics (Piao et al., 2007; Sanchez, 2019). Deep rooting of trees in tropical evergreen forests allows to pump deep soil water, and limit water losses (Nepstad et al., 2004, 1994). Moreover, the very large leaf area index of evergreen forest's canopy increases rainfall interception, limiting water losses from the soil-plant system by runoff and infiltration (Bruijnzeel and Sampurno, 1990; Sanchez, 2019).

Converting forest into cropland drastically decreases rooting depth, hence deep soil exploration by roots (Canadell et al., 1996; Jackson et al., 1996; Kleidon and Heimann, 1998), and leaf area index (Sanchez, 2019). This leads to substantial decreases in evapotranspiration and water interception by canopy, hence increasing water losses through runoff and infiltration (Davidson et al., 2012; Piao et al., 2007; Sanchez, 2019). In addition, soil compaction resulting from tillage practices can lead to increased runoff. Finally, irrigation practices in croplands may constitute significant additional water and nutrients inputs, especially for flooded rice (Desplanques et al., 2006; Klotzbücher et al., 2015b; Riotte et al., 2018b). We distinguish here Si inputs to soil from rainfall and irrigation, and Si output by leaching and runoff

(Table 4-4). They are controlled by water fluxes and associated Si concentrations.

Si input from rainfall. Si concentrations in rainfall waters are generally very low (Alexandre et al., 1997; Klotzbücher et al., 2015b; Meunier et al., 2010; Riotte et al., 2018b), leading to negligible Si inputs by rainfall (Table 4-4) (Alexandre et al., 1997; Meunier et al., 2010).

Si input from irrigation. While absent in forests, Si input can be large in flooded rice croplands (Desplanques et al., 2006; Klotzbücher et al., 2015a; Riotte et al., 2018b), in which it depends on irrigation dose and frequency (Klotzbücher et al., 2015b) (Table 4-4). It may also depend on the reserve of weatherable minerals in the catchment area upstream of the irrigated perimeters, since it strongly impacts DSi concentration in rivers downstream (see Cornelis et al. 2011 for a review). Unfortunately, to the best of our knowledge, no experimental data for flooded/irrigated rice croplands are available in highly weathered soils of the humid tropics to test this hypothesis. Riotte et al. (2018a) measured irrigation inputs of Si in moderately weathered soils under a tropical savanna climate (Koppen classification, Mean Annual Rainfall 970mm), i.e. not in the humid tropics. Si irrigation input amounted to 153 kg Si ha^{-1} $season^{-1}$ (Riotte et al., 2018a), which is similar to the values reported by Klotzbücher et al. (2015b) in weakly weathered soils under monsoon climate.

Increase in Si release upon flooding. Such an increase was reported in pot and field experiments under rice cropping (Ma and Takahashi, 1989; Marxen et al., 2016), likely on moderately weathered soils. In the study conducted by Marxen et al. (2016), redox potential rapidly decreased to ~ -160 mV within the first 6 days after flooding. Actually, flooding induces reduction reactions, which involve electron exchange and proton (H^+) consumption, thus inducing pH increase. Regardless of their original pH, most soils reach pH values of 6.5–7.2 rapidly after flooding and remain at that level while submerged: the increase in pH in flooded acid soils may reach 3 pH units in a week (Ponnamperuma, 1972; Sanchez, 2019). Such a pH increase undoubtedly reduces mineral weathering, and thus limits the release of Si from LSi and/or PSi mineral dissolution whereas it may considerably enhance phytolith dissolution in solution (Fraysse et al., 2009) and soil (Li et al., 2019). The impact of flooding on the coupled increase in pH and Si release from

phytolith is, however, unknown, despite its importance on Si fluxes in paddy fields.

Si outputs by leaching or runoff. Si output by leaching or runoff tends to increase when converting forest into rice cropland in weakly weathered soils, except for one very low Si output value due to soil impermeability (Klotzbücher et al., 2015b). Using hydrological modelling, Nguyen et al. (2016) attributed an exceptionally high leachate output of Si (10,000 kg Si ha^{-1} yr^{-1} (Table 4-4)) to high water infiltration rate in soil. In contrast, in natural forests on highly weathered soils, leachate outputs of Si were relatively low (4-26 kg Si ha^{-1} yr^{-1}), and in the same range as the value reported by Meunier et al. (2010) for a forest on a little weathered soil. Thus, available literature data do not allow us to infer about the impact of soil weathering stage on Si output through leaching. As far as land use is concerned, literature data suggest that leachate output of Si should be limited in forests regardless of soil weathering stage, whereas data for rice croplands in highly weathered soils are missing. We therefore hypothesize that Si output through leaching from highly weathered soils is below that in weakly weathered soils since DSi concentration in soil solution decreases with increasing soil weathering stage in cultivated ecosystems (Henriet et al., 2008a, 2008b; Klotzbücher et al., 2015a; Makabe et al., 2009).

Table 4-4: **:** Experimental values of Si input by rainfall, Si input by irrigation, and Si output by leaching or lateral flow in various forest and agricultural ecosystems.

Ecosystem	Climate (MAP in mm)	Soil degree	weathering	Location	Si input by rainfall (kg ha^{-1} yr^{-1})	Si input by irrigation (kg ha^{-1} yr^{-1})[a]	Si output by leaching or lateral flow (kg ha^{-1} yr^{-1})
		WRB class	TRB				
Weakly weathered soils							
Rain forest[1]	Tropical humid (4200)	Leptosol		Reunion Island	1.9	0	15
Rice[2]	Monsoon tropical (2050)		168	Luzon Island (Philippines)	0	78[b]	274
Rice[2]	Monsoon tropical (2050)		168	Luzon Island (Philippines)	0	100[c]	3
Rice[2]	Monsoon tropical (2050)		168	Luzon Island (Philippines)	0	644[d]	805
Rice[3]	Tropical humid (>1600)	Fluvisols		Nothern Vietnam	nd	nd	10,000
Strongly weathered soils							
Rain forest[4]	Tropical humid (2100)	Ferralsol		Manaus (Brazil)	nd	0	11
Rain forest[5]	Tropical huid (2100)	Ferralsol		Manaus (Brazil)	nd	0	26
Rain forest[6]	Tropical humid (1500)	Ferralsol		Mayombé (Congo)	1	0	16
Campinarana[7]	Tropical humid (2100)	Podzol		Manaus (Brazil)	nd	0	4.5
Dry deciduous forest[8]	Tropical subhumid (1100)	Ferralsol		Southern India	nd	0	19.8

[1](Meunier et al., 2010); [2](Klotzbücher et al., 2015b); [3](Nguyen et al., 2016); [4](Lucas et al., 1993); [5](Cornu, 1995); [6](Alexandre et al., 1997); [7](Cornu et al., 1998); [8](Riotte et al., 2018a).

4.6 Soil weathering stage affects the soil-plant cycle of silicon, but depending on land use

Figure 4-4 illustrates graphically the Si plant uptake data presented in Table 4-2 for forest and rice crop, excluding other crops (mainly sugarcane) and bamboo forest: the former are too scarce to draw conclusions, the latter is an exceptional case (Meunier et al., 1999). Si plant uptake is always larger for rice crop than for natural forest (Figure 4-4a), the difference being particularly important on slightly weathered soils. With increasing soil weathering stage, the Si uptake decreases for rice crop (Figure 4-4b) whereas it increases for natural forest (Figure 4-4c). These facts are illustrated in Figure 4-5, which provides a schematic view of the biological Si feedback loop. *On slightly weathered soils*, this loop involves much lesser amounts of Si under forest than rice crop established (Figure 4-5a-b). This much less intense loop is likely because the forest ecosystem shelters few high Si-accumulating plants whereas rice is a high Si-accumulator. Besides, cropping stimulates plant growth and development through fertilizer use and plant protection techniques whereas N and P generally limit the primary production of forest developing on slightly weathered soils (Laliberté et al., 2013). The biological Si feedback loop under rice farming is thus stimulated because of increasing plant growth. *In highly weathered soils*, the biological Si feedback loop is comparable between forest stands and rice croplands, but Si restitutions may be importantly lowered by rice straw exports. A very interesting fact is that soil desilication involves an increase of the biological feedback loop of Si in forests, but a reduction of this loop in cropland. This discrepancy is likely due to the following factors: (i) readily soluble phytoliths make the pool of plant available Si; (ii) forest litter is densely explored by fine roots pumping mineral elements; (iii) deep rooting of forest trees enhances mineral pumping and limits the leaching of dissolved Si; (iv) crop harvesting exports Si out of cultivated ecosystems. Humid tropical forest is one of the biomes with the deepest rooting depth and largest root biomass (Canadell et al., 1996; Jackson et al., 1995, 1996; Kleidon and Heimann, 1998; Nepstad et al., 2004; Schenk and Jackson, 2005, 2002). In contrast, cropland is one of the biomes with the shallowest rooting depth and lowest root biomass (Canadell et al., 1996; Jackson et al., 1996; Kleidon and Heimann, 1998). Maximum rooting depth and root biomass for tropical evergreen forests are 7.3 ± 2.8 m (Canadell et al., 1996) and 5 kg m^{-2} (Jackson et al., 1996), respectively; while they are 2.1 ± 0.2 m (Canadell et al., 1996) and < 1.5 kg m^{-2} (Jackson et

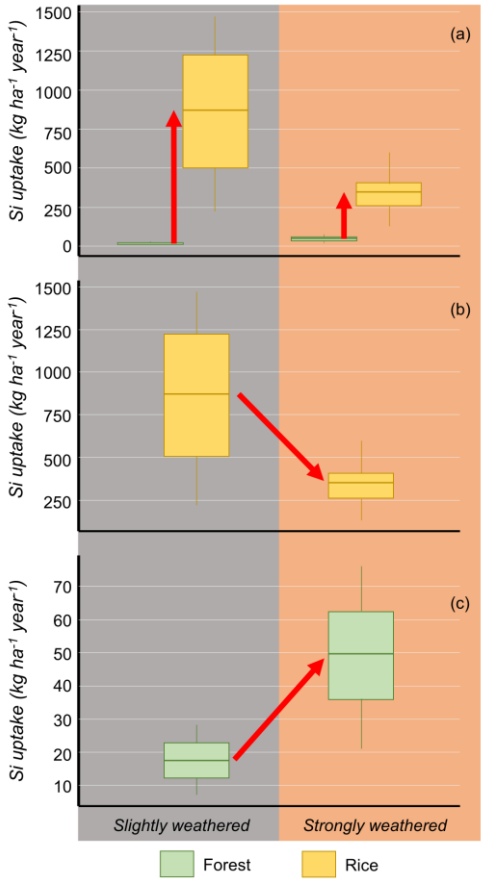

Figure 4-4: Annual Si uptake values for (a) natural forest ecosystems and rice crops, (b) rice crops, and (c) natural forests, established on soils that are slightly (left) or strongly (right) weathered in the humid tropics. The figures from Table 2 (excluding bamboo and sugarcane) were computed with the ggplot function of the R programming language. The graph (a) allows comparison between forest and rice cropping. Graph (b) compares slightly and highly weathered soils for rice crop. Graph (c) compares slightly and highly weathered soils for natural forest ecosystems. Boxes extent represents the values from the first quartile to the third quartile. The line cutting the box is the median. The vertical lines (whiskers) represent the range of values. From (a) we note that rice crop has always larger Si uptake than forest. From (b) we observe that Si uptake by rice plant decreases when soil desilication increases. From (c) we conclude that Si uptake by forest plants increases with increasing soil weathering.

al., 1996), respectively, for croplands. For rice plants, 82% to 99% of the roots are located in the first 30 cm of the soil (Yoshida and Hasegawa, 1982). For

tropical evergreen forests, 69% of the roots are in the first 30 cm of the soil. In forest ecosystems, tree roots are deep enough to absorb nutrients from deep and slightly weathered horizons (Jobbágy and Jackson, 2001; Lucas et al., 1993). Moreover, in the forest ecosystem, the litter forms an environment with a very dense root network in which limiting nutrients are concentrated (Jobbágy and Jackson, 2001), the turnover of C and nutrient cycling is large (Greenland and Nye, 1959), and the dissolution of phytoliths is rapid (Fraysse et al., 2010). This strongly minimizes the loss of elements by leaching (see section 1.5.3) (Lucas et al., 1993), which explains why such weathered soils support evergreen forests with the greatest biodiversity and biomass (Beer et al., 2010; Laliberté et al., 2013; Myers, 1988). Two Si sinks thus occur in natural forest ecosystems while they strongly decrease in croplands: the subsoil LSi pool that is exploited by the deep roots of forest trees; the topsoil PhSi pool that is directly exploited by a very dense root network.

In cropping systems established on highly weathered soils, Si management is thus crucial to substantially increase crop yields in a sustainable way (a.o. Guntzer et al., 2012; Klotzbücher et al., 2018, 2015b, 2015a; Li et al., 2019).

4.7 The impact of liming on the soil-plant Si cycle depends on soil weathering stage

Liming is a common agricultural practice that increases soil pH, depending on soil buffer capacity (Li et al., 2019). The impact of the increase in soil pH on the soil-plant Si cycle is still unclear. Increasing pH either decreases the bioavailability of Si because of increasing Si adsorption (Berthelsen et al., 2003; Haynes and Zhou, 2018; Savant et al., 1999; Tavakkoli et al., 2011), or increases Si bioavailability (Camargo et al., 2007; Li et al., 2019; Mantovani et al., 2016; Miles et al., 2014). As a matter of fact, studies on the impact of liming on the Si soil-plant cycle are still scarce (Guntzer et al., 2012; Haynes and Zhou, 2018; A. Klotzbücher et al., 2018; Tavakkoli et al., 2011), despite soil pH can strongly control Si bio-availability (Meunier et al., 2018).

In humid tropical conditions, LSi and PSi minerals dissolve through acidic hydrolysis (Lindsay, 1979). Increasing soil pH by liming would therefore limit the dissolution of these silicates since the added alkaline agent becomes the privileged consumer of protons. In contrast, increasing soil pH by liming

would increase the dissolution of phytoliths (Fraysse et al., 2010, 2009, 2006; A. Klotzbücher et al., 2018). Besides, increasing soil pH may promote the deprotonation of $H_4SiO_4^0$ but only at very high pH value since it is a very weak acid (pK_a = 9.8), and deprotonation may theoretically favor Si adsorption onto Al and Fe oxides (Haynes and Zhou, 2018; Tavakkoli et al., 2011). The impact of liming on the soil-plant Si cycle depends on four factors: (i) soil buffering capacity, (ii) the reserve of LSi and PSi minerals, (iii) the PhSi pool, and (iv) the pool of secondary Al and Fe oxides; that are all impacted by soil weathering stage. Soil weathering stage may thus influence the impact of liming on the soil-plant Si cycle. However, increasing soil pH may decrease the magnitude of positive charges born by Fe and Al oxides, and thus decrease Si adsorption (Uehara and Gillman, 1981). Considering all the factors influenced by liming that control the Si bioavailability (soil buffer capacity, the reserve in LSi, PSi, PhSi, and secondary Al and Fe oxides), it is extremely complex to predict the impact of liming on the soil-plant Si cycle. Especially for highly weathered soils, whose composition varies greatly depending on the parent material, and the management of non-edible plant parts at harvest. Another alternative is to amend soil with Si fertilizers such as a.o. blast furnace slag (Haynes and Zhou, 2018), ground basalt (Beerling et al., 2018; Haynes and Zhou, 2018), or phytolith-rich biochar (Li et al., 2018; Li et al., 2019). A concomitant increase in soil pH and bioavailable Si pool was observed following application to soils of slags (Camargo et al., 2007; Haynes and Zhou, 2018; Mantovani et al., 2016) and phytolith-rich biochar (Li et al., 2019).

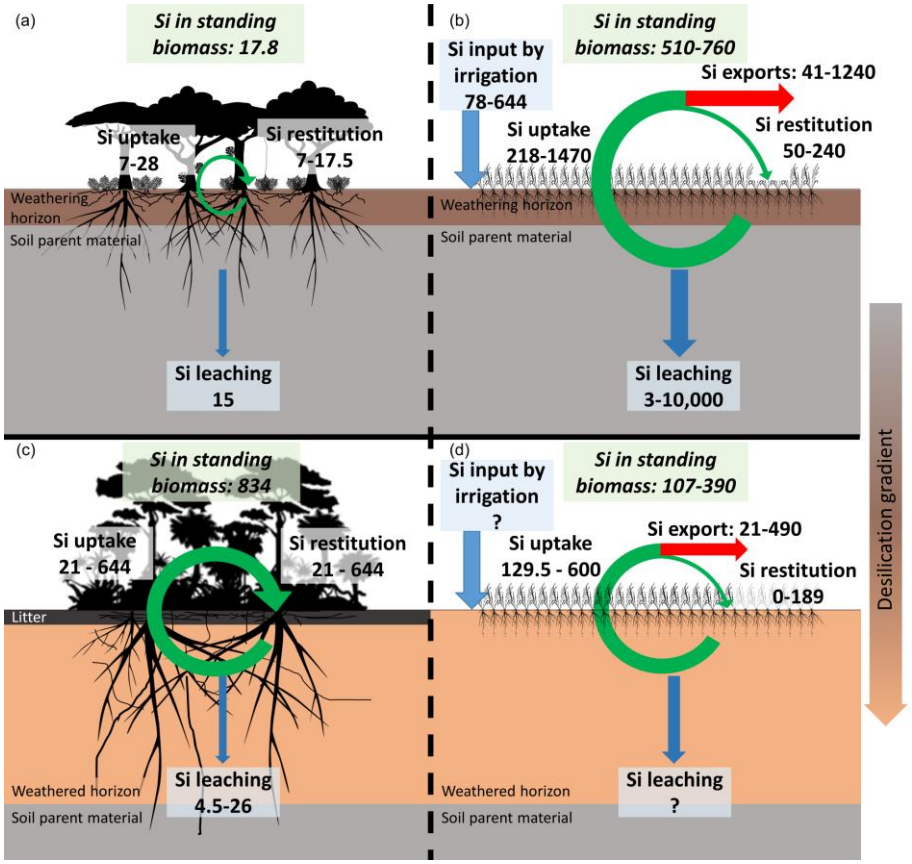

Figure 4-5: Schematic view of the soil-plant cycle of Si under forest (a,c) and rice crop (b,d). (a) and (b) concern the bio-cycling of Si in less weathered soils. (c) and (d) concern the bio-cycling of Si in highly weathered soils. All figures refer to Si fluxes except the values in italics, which refer to reservoirs. Little weathered soil horizons are in grey color while the strongly weathered/desilicated ones are in orange. Soil horizons at intermediate stage of weathering are in brown. In slightly weathered soils, the biocycling of Si is lower in forests than in rice cropland. In highly weathered soils, the biocycling of Si is comparable between forest and rice fields, but Si restitution to soil may be importantly lowered by straw exports out of rice fields. Si in standing biomass evolves in the following order: Forest on highly weathered soil > Rice on slightly weathered soil > Rice on highly weathered soil > Forest on slightly weathered soil. In natural ecosystems, the biocycling of Si is larger for strongly weathered soils while in croplands, the biocycling of Si is larger for slightly weathered soils. References are given in Tables 5-2 and 5-4.

4.8 The transition from forest to rice crop – the Q-I relationship

From all these observations, the Si quantity-intensity relationship can be redrawn for rice cropping systems (Figure 4-6).

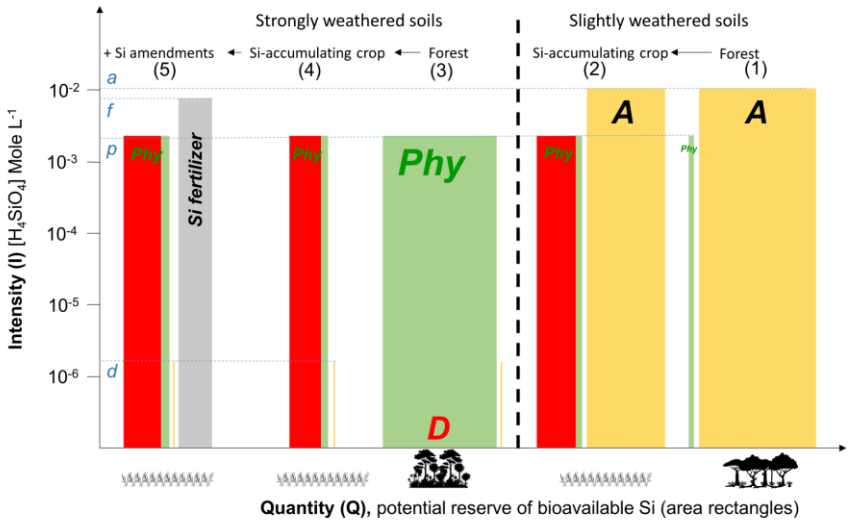

Figure 4-6: Si quantity-intensity (Q-I) relationship under forest and rice field in slightly and highly weathered soils. In slightly weathered soils, converting forest (1) to rice cropland (2) decreases the LSi pool through mineral weathering, which is accelerated because of large Si uptake by rice. The PhSi pool depends on the management of rice straws (the red area corresponds to the potential PhSi pool if rice straws are restituted to soil). In highly weathered soils, converting forest area (3) into rice cropland (4) decreases the PhSi pool. The export of rice straws strongly influences the PhSi pool (red area). If rice straws are exported from the field, the activity of $H_4SiO_4^0$ would abruptly drop from p to d level. Eventually, when Si fertilizers are used (5), a new Si pool (grey area) is created and increases the $H_4SiO_4^0$ activity from d to f. The PhSi pool could therefore slightly increase if straws are not exported as plant Si uptake increases. The size of each rectangle represents the related Si stock.

In slightly weathered soils, converting forest areas into rice croplands results in enhancing the weathering of LSi because of the large uptake of Si by rice (Yang and Zhang, 2018). The LSi pool therefore decreases. The PhSi pool strongly depends on the management of rice straws (Klotzbücher et al., 2016, 2015b; Marxen et al., 2016; Seyfferth et al., 2013). In highly weathered soils, that conversion likely leads to the decrease in the PhSi pool if rice straws are exported out of the field (Klotzbücher et al., 2016, 2015b; Marxen et al., 2016; Seyfferth et al., 2013). In this case, the activity of $H_4SiO_4^0$ could rapidly

drop since the LSi pool is exhausted and can no longer maintain high $H_4SiO_4^0$ concentrations. Finally, Si fertilizer use (Figure 4-6(5)) would increase the $H_4SiO_4^0$ activity from *d* to *f* in Figure 4-6 (Haynes and Zhou, 2018). In this case, the PhSi pool could slightly increase if straws are not exported as the plant uptake of Si increases (Savant et al., 1999, 1996).

4.9 Conclusion

The biological silicon feedback loop strongly differs between natural and cultivated environments in the humid tropics. Soil weathering stage has an opposite impact on the biological silicon feedback loop in natural and cultivated environments. In the former environments, the increase in soil weathering stage tends to raise the importance of the biological silicon feedback loop at the expense of the mineral one. In cultivated environments, an increase in soil weathering stage leads to a decrease in Si biocycling. The conversion of forest into cropland has thus a tremendous impact on the Si soil-plant cycle. The differences between forest area and cropland are attributed to very different rooting depths, litter composition, soil cover, recycling or export of plant parts, density of high Si-accumulating plant species, soil and soil fertility management. Until now, studies on the Si cycle in cultivated ecosystems in the tropics have mostly focused on rice and sugarcane, two high Si-accumulating plant species. Furthermore, our conclusions are only based on the few studies available so far for rice croplands and forest ecosystems in weakly and highly weathered soils in the humid tropics. We expect that the impact of the agricultural land use on the Si cycle would largely differ for non Si-accumulating plants. Further studies are needed to understand deeper the impact of agricultural land use on the Si soil-plant cycle. Taking soil weathering stage into account seems, however, very important to understand the impact of agricultural land use on the Si cycle.

Chapter 5 Banana and sugarcane crops control the bio-availability of the silicon in a gibbsitic Andosol[3]

Abstract

Silicon-accumulating plant species are recognized to impact the soil-plant silicon (Si) cycle. Crop harvests may lead to large Si exports and accelerate soil desilication. For banana and sugarcane crops, inedible plant parts are typically restituted to soil. Their impact could therefore strongly differ from that of other Si-accumulating crops whose crop residues are exported out of cultivated fields. The aim of this study is to quantify the soil-plant Si cycle of banana and sugarcane croplands. Unlike most intensive crops, crop residues of these crops are not exported. The specific view of this chapter is therefore to determine if the crop residues returns to soil could mitigate the impact of agricultural land use on the pool of bioavailable Si in soil.

We selected the banana and sugarcane fields on perhydrated, gibbsitic Andosols in Guadeloupe. Plant, soil, and soil solution samples were collected and analyzed to quantify the soil-plant Si fluxes and pools.

Plant Si uptake, Si export by harvest, and Si returns to soil through crop residues were larger for sugarcane (457.1; 55.3; 401.8 kg ha^{-1} yr^{-1} respectively) than for banana (171.4; 10.06; 161.3 kg ha^{-1} yr^{-1} respectively). Resulting impacts of the biological Si feedback loop on mineral dissolution were larger for sugarcane than for banana. Si exports through leaching amounted to 104.8 and 98.06 kg ha^{-1} yr^{-1} in banana and sugarcane plots, respectively. In both plots, dissolved Si concentrations first decreased from Ap to Bw horizons, then increased from Bw to BC horizons.

We showed that the biological Si feedback loop was particularly active for these two crops. The very large Si uptake, especially for sugarcane, increased mineral weathering. Since inedible plant parts are restituted, Si exports by harvest were limited. In contrast, Si returns to soil were large. The phytogenic Si pool therefore controlled the plant available pool in the topsoil. Our data

[3] Manuscript in preparation for submission in an international peer-reviewed journal.

highlight the crucial importance of the management of crop residues from Si-accumulating plant species.

5.1 Introduction

Lucas et al. (1993) first demonstrated the very important role played by plant nutrients cycling in controlling soil mineralogy. In particular, they demonstrated that plants alleviate soil desilication in highly weathered soils by taking up silicon (Si) in soil through root absorption and returning it as soluble amorphous silica bodies called phytoliths (PhSi). Si absorption, deposition, dissolution and reabsorption define a biological Si feedback loop within the Si soil-plant cycle (Cornelis and Delvaux, 2016). Further, Derry et al. (2005) demonstrated that that loop strongly controls the Si fluxes in rivers from highly weathered watersheds in Hawaii. Si fluxes from continent to ocean greatly influence the oceanic diatom population who represents about 40% of marine primary productivity (Tréguer et al., 2018), and the following capacity of oceans to store carbon (Ragueneau et al., 2006; Tréguer and Pondaven, 2000). Later, studies of Conley et al. (2008) and Struyf et al. (2010) demonstrated for the first time that the conversion of natural forest ecosystems into croplands could greatly influence Si fluxes to the oceans. The harvest of straws of Si-accumulating crops has been pointed out by several authors as the main factor influencing the soil-plant Si cycle under agricultural land use (Barão et al., 2014; Clymans et al., 2011; Guntzer et al., 2012; Vandevenne et al., 2011).

In natural forest ecosystems developed on highly weathered soils, the litter forms an environment with a very dense root network in which limiting nutrients are concentrated (Jobbágy and Jackson, 2001), the turnover of C and nutrient cycling is large (Greenland and Nye, 1959), and the dissolution of phytoliths is rapid (Fraysse et al., 2010). In such soils, when forest is replaced by cropland, the mineralomass that was concentrated in litter and biomass rapidly decreases because of soil erosion and plant exports (Cerdan et al., 2010; Montgomery, 2007; Reusser et al., 2015; Vanacker et al., 2019, 2007). Fertility losses are then compensated by fertilizer use. About Si, silicate fertilizers are rarely used and natural desilication of soil aggravates (*Chapter 4*). At least, this is true for a.o. rice, wheat, barley for which inedible plant parts are commonly harvested (Guntzer et al., 2012; Klotzbücher et al., 2016; Vandevenne et al., 2011). For sugarcane and banana croplands, two Si-accumulating plants, inedible plant parts are commonly restituted to soils. The study of the Si soil-plant cycle under these crops would therefore allow to determine if the long-term restitution of inedible plant parts on the soil

can prevent soil desilication as first observed by Lucas et al. (1993) in natural ecosystems. This study thus aims to quantify the soil-plant Si cycle in banana and sugarcane croplands on plots that were long cultivated in order to assess the role of restitution of crop residues in alleviating or preventing soil desilication.

5.2 Environmental framework

The studied zone is located on the Pères River catchment on the east flank of *La Soufrière* volcano in the south east of the Basse-Terre Island in Guadeloupe (16°N, 61°W) (Figure 5-2a,b). *La Soufrière* active volcano is mostly surrounded by Andosols that are poorly weathered on the west flank of the volcano (Vitric Andosols) and already well developed on the east flank (Silandic Andosols) with high desilication degree as depicted by the presence of gibbsite (*Chapter 2*). The very humid trade winds blowing from east to west are intercepted by the volcanic chain of the Basse-Terre Island, generating an orographic lift that promotes the formation of clouds and rainfalls on windward slopes. The mean annual rainfall (MAR) evolves from 2500 mm at the sea level to up to 7000 mm at the top of the volcano. Soils formed from pyroclastic deposits (30,000 to 18,000 years BP) of andesitic-dacitic composition with plagioclase, pyroxene and volcanic glass as the dominant weatherable minerals (Boudon et al., 1987; Dagain, 1981; Komorowski et al., 2005; Ndayiragije, 1996). Under such climatic conditions, these volcanic deposits quickly weathered, especially volcanic glasses that are completely weathered in the surface horizon on the studied catchment (*Chapter 2*). Croplands and forests cover 56.7% and 17.4% of the total surface of the catchment respectively. The intensive banana production and the intensive sugarcane production represent 60.1% and 11.4% of the croplands. The catchment is probably mostly cultivated since the late seventeenth century AD (Doumenge, 1985).

5.3 Material and methods

5.3.1 Studied plots and general sampling scheme

A banana (*Musa acuminata* L. cv. JAFFA) plot and a sugarcane (*Saccharum officinarum* L. cv. B69.566) plot have been selected next to each other at mean altitude of 173 m above sea level (asl) (plot BA-173) and 180 m asl

respectively (plot SC-180) (Figure 5-2b,c). MAR is 3220 mm under the BA-173 plot and 3280 mm under the SC-180 plot.

"*L'Habitation Le Fromager*" is an ancient, long-established sugar industry built in 1669 belonging to Nicolas Leroy Dumé. The lands of the studied watershed were most probably cultivated with sugarcane from that period. An orthophoto map confirms the presence of sugarcane in both studied plots in 1950. IGN© maps also confirm the presence of sugarcane in both plots in 1963 and 1969. Land use maps of 1976 (Colmet-Daage, 1977) and 1980 (Bernard et al., 1980), IGN© map of 1985, and orthophoto maps of 1984, 2000 and 2004 allowed us to identify banana crop on the studied plots during that period. An orthophoto map of 2006 showed that sugarcane replaced the banana crop on the SC-180 plot between 2004 and 2006. An interview with the farmer confirmed that plot SC-180 has been cultivated with sugarcane since 2006 The BA-173 plot is cultivated with banana (including some fallows between cultivation cycles) since at least 1976 (Colmet-Daage, 1977). Therefore, we can consider that both plots studied had similar land uses except since 2006 (Figure 5-1).

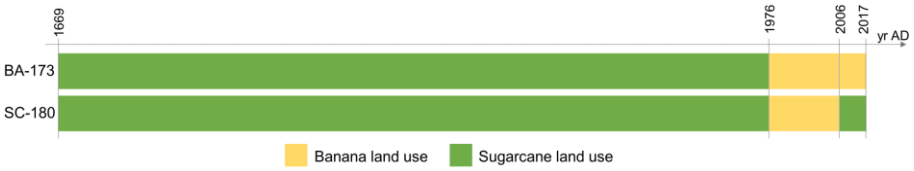

Figure 5-1: Historic of the land use of the two studied plots: BA-173 and SC-180. The green color refers to sugarcane land use and the yellow color to the banana land use.

For each plot, plant, soil and gravity water were sampled in order to estimate pools and fluxes of the soil-plant Si cycle

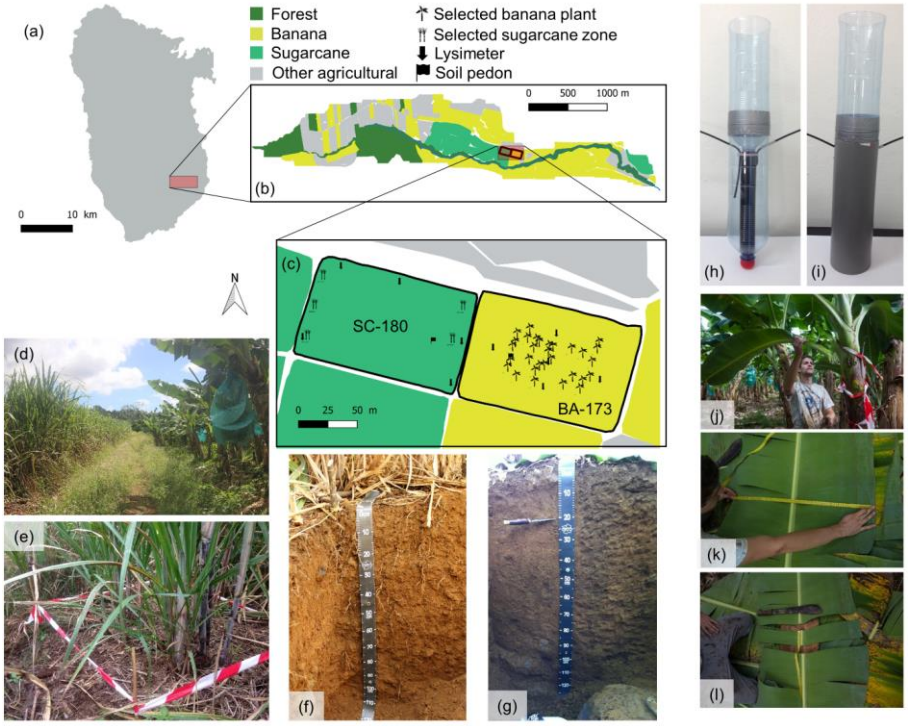

Figure 5-2: (a) Location of the Pères River watershed on the Basse-Terre Island; (b) Land use map of the Pères River watershed and location of the studied plots; (c) Location of the selected banana plants, sugarcane subplots, lysimeters, and soil pedons; (d) path separating the two plots; (e) a sugarcane zone after dead leaves sampling; (f) the sugarcane soil profile; (g) the banana soil profile; a lysimeter (i) with and (h) without its protective sheath, (j-k-l) a fungal diseased banana leaf sampling.

5.3.1.1 Plant sampling

BA-173 plot

Thirty banana plants were randomly selected and divided into five groups to constitute composite samples by group. Plant samples were regularly collected from May 2016 to December 2016. Once one of the 30 banana plants reached harvesting stage: banana fruits, leaves, pseudostem and peduncle were weighed. For each plant part, a sample was collected, weighted, washed with deionized water, dried in a stove at 70°C during one week, and weighted after drying. For banana fruit, a banana of the second hand of the bunch was prevailed. For the leaves, length and width of each leaf were measured in the field to assess their total fresh weight (Figure 5-2k) thanks to a relation established based on measurements on 70 leaves of

diverse sizes taken randomly in the BA-173 plot just before the sampling period (FW = 0.58 x L x W, R^2=0.96; FW = fresh weight (kg), L = length (m), W = width (m)). The central part of each leaf was then collected (Figure 5-2l). For the pseudostem, a slice of 5 cm of thickness was collected at half the length of the pseudostem. For the peduncle, a slice of 5 cm of thickness was sampled at half the length of the peduncle. Moreover, leaves affected by fungal diseases were also collected every two weeks with the same measurement and sampling method as at harvest. For each plant part, all the samples belonging to the same group were assembled to form one composite sample per group and per plant part for further analyses.

SC-180 plot

Five sugarcane subplots of 3 m^2 were delimited in different parts of the SC-180 plot to be as representative as possible of the entire SC-180 plot and easily accessible to facilitate regular sampling as well (Figure 5-2c). For each of this subplot, dead leaves were collected every month between May 2016 and April 2017 (Figure 5-2e). At each sampling time, all the collected leaves were weighted to determine the total fresh weight on each subplot. Then, for each subplot, 5 leaves were randomly selected, washed with deionized water and weighted before and after drying at 70°C during 1 week to determine the water content. Just before the harvest of the SC-180 plot by the farmer, all the stalks and leaves of each subplot were prevailed. Leaves were separated in green leaves and dead leaves as different Si concentrations are expected between these two groups. All the stalks, green leaves and dead leaves were then weighted. Then, a piece of 10 cm long of each stalk was prevailed at half the length of the later, washed with deionized water and weighted before and after drying at 70°C during 1 week to determine the water content. Thirty green leaves and thirty dead leaves were randomly selected for each subplot, washed with deionized water and weighted before and after drying in a stove at 70°C to determine the water content. For each plant part, all the samples belonging to the same subplot were assembled to form one composite sample per subplot and per plant part for further analyses. In total, 25 composite samples for the BA-173 plot and 15 composite samples for the SC-180 plot were generated.

5.3.1.2 Soil sampling

BA-173 plot

One sample of the 20 first cm of soil was prevailed at 40 cm of the foot of each of the thirty selected banana plants. The thirty soil samples were then assembled into composite samples respecting the same grouping as for the plant samples. A soil profile has also been described and sampled down to 130 cm depth. Each horizon was sampled leading to a total of 7 samples. Undisturbed soil samples were collected (Kopecky) to determine bulk density: one Kopecky at the foot of each selected banana plant and three in each soil horizon. Bulk density was measured at field soil moisture and dry.

SC-180 plot

Six topsoil samples (00-20 cm) were collected in each selected subplot, then further assembled to form one composite sample for each subplot. A soil profile has also been described and sampled down to 130 cm depth. Each horizon was sampled leading to a total of 6 samples. Undisturbed soil was collected (Kopecky) in each selected subplot and in each of soil horizon to determine soil bulk density, both at field soil moisture and after drying at 105° during 48 h.

5.3.1.3 Drainage water sampling

In each plot, 10 no-suction lysimeters have been settled to collect drainage water from the 60 first cm as most of the banana and sugarcane rooting systems develop in the corresponding volume (Gousseland, 1983a; Smith et al., 2005). Water was collected every ~200 mm of rainfall from July 2016 to April 2017. Water was then filtered through a 0.2 μm polycarbonate membrane and acidified at 0.25% Suprapur nitric acid. For each plot, 20 samples collected at two different times were then selected for analyses.

5.3.2 Plant analysis

For the 40 plant composite samples, mineral analysis was carried out after calcination at 450°C for 1 day and fusion in Li-metaborate + Li-tetraborate at 1,000°C (Chao and Sanzolone, 1992), followed by ash dissolution with Suprapur HNO_3. Nutrient and Si concentrations were measured by inductively coupled plasma-atomic emission spectrometry (ICP-AES).

5.3.3 Soil analyses

5.3.3.1 Basic analyses.

Analyses were carried on the fine earth (<2 mm) of the 23 composite soil samples. The following parameters were measured. pH was measured in H_2O and 1M KCl solution in 1:5 soil:solution suspensions. Cation exchange capacity (CEC) and exchangeable bases by the 1 M ammonium acetate (NH_4OAc) pH 7 method (Olsen et al., 1982). Total C and N contents were determined by high temperature dry combustion using a Vario EL Cube elemental analyzer. The phosphate retention was measured according to Blakemore (1983). Total elemental contents by ICP-AES after fusion in Li-metaborate and Li-tetraborate at 1000°C (Chao and Sanzolone, 1992). The contents of major alkaline and alkaline-earth cations were summed up to compute the Total Reserve in Bases (TRB) (Herbillon 1986).

Dark oxalate-extractable (o), dithionite-citrate-bicarbonate (DCB) extractable (d) and pyrophosphate-extractable (p) contents of Si, Al and Fe were determined in the respective extracts by ICP–AES following the methods compiled in Dahlgren (1994). These selective extractions estimate the contents of different soil components. Using the values of $(Al_o\text{-}Al_p)/Si_o$ allowed to estimate allophane contents (Parfitt and Wilson, 1985). Fe_o estimates ferrihydrite content (Mizota and Van Reeuwijk, 1989). Fe_t, Fe_d and Fe_o estimate the quantity of Fe in silicate minerals ($Fe_t\text{-}Fe_d$) and in crystalline Fe oxides ($Fe_d\text{-}Fe_o$), and the degree of individualization of free iron (Fe_d/Fe_t). Al_p refers to the quantity of Al that is adsorbed onto the soil organic matter.

5.3.3.2 Specific Si extraction.

The bio-available Si content was estimated by an extraction with a $CaCl_2$ 0.01 M solution (4g of soil for 40 ml of solution) (Sauer et al., 2006) and will further be called $CaCl_2$-Si. After 6h of shaking, the soil-solution suspension was centrifuged at 4000 rpm during 10 min after what 1 ml of the supernatant was prevailed, diluted 10 times and neutralized by 50 µl of a 15 M HNO_3 solution to finally measure the Si content by ICP-AES.

The phytolithic Si pool was estimated by a kinetical extraction method modified from DeMaster (1981). Forty milligrams of soil pretreated by a dark oxalate extraction (Dahlgren, 1994) and by a 6h rinsing with a $CaCl_2$ 0.01 M

solution was mixed with 40 ml of 0.1 M Na_2CO_3 at 85°C during 7h (*Chapter 3*) One milliliter of solution was prevailed after 15, 60, 120, 180, 240, 300, 360, and 420 min, diluted with 9 ml of deionized water and acidified with 50 µl of Suprapur HNO_3. Si, Al, Fe, and Mg concentrations were measured at each time. From the kinetical extraction, the amorphous Si pool was estimated using the dissolution rate method presented in *Chapter 3*.

The here quantified amorphous Si pool – further called ox-Na_2CO_3-Si – includes the phytogenic Si, and may be represented by some lithogenic silicates (LSi) (*Chapter 3*). Until now, no method allows to discern phytolithic Si and lithogenic Si pools in such soils. We therefore decided to consider the ox-Na_2CO_3-Si pool as mainly represented by PhSi in surface horizons and LSi in deeper horizons.

5.3.4 Drainage water analysis

Major element concentrations (Al, Fe, Si, Ca, Mg, K, Na, Mn, P and S) were determined by ICP-AES. Detection limit (ppb) was 10, 2, 5, 10, and 10 for Si, Ca, Mg, K, and Na respectively, and precision is <0.5%.

5.3.5 Calculation of the pools and fluxes

5.3.5.1 Estimation of Si pools

Three Si pools of the soil were quantified (Figure 5-3). The soil inorganic Si pool that includes the lithogenic and pedogenic Si pools, the phytolithic Si pool, and the dissolved Si pool. The phytolithic Si and dissolved Si pools per hectare were estimated with the Equation (1).

$$Pool_i = Concentration_i \times \rho_d \times depth \times surface\ [kg\ ha^{-1}]\ \ Eq\ (1)$$

$Pool_i$ is the Si pool of the component i (kg ha^{-1}); $Concentration_i$ is the Si concentration of the component i (kg [kg of dry soil]$^{-1}$); ρ_d is the dry soil bulk density (kg m^{-3}); *depth* is the depth of the soil considered (in our case 20 cm); *surface* is the surface considered (in our case 1 ha or 10,000 m^2). For the PhSi pool, concentration was estimated by the mean ox-Na_2CO_3-Si concentration in the 00-20 cm soil layer. The ox-Na_2CO_3-Si pool thus represented the phytolithic Si pool since amorphous pedogenic Si (PSi) pools were previously removed by a dark oxalate extraction (*Chapter 2* and *Chapter 3*). The

concentration of dissolved Si (DSi) was estimated by the mean $CaCl_2$-Si concentration.

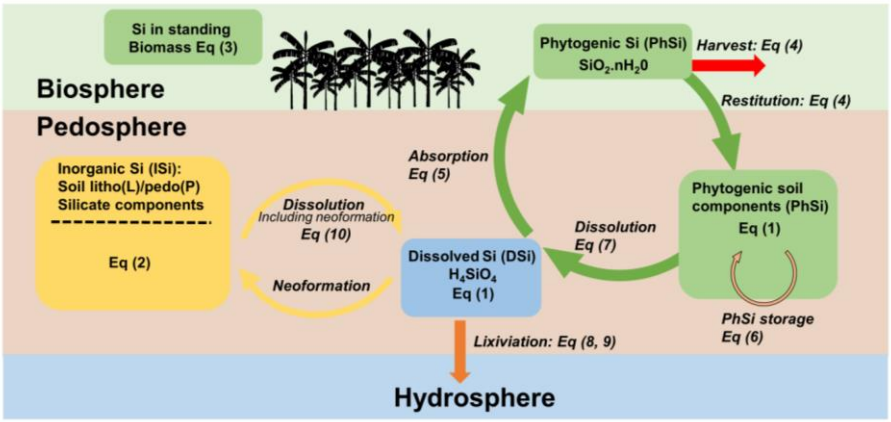

Figure 5-3: Conceptual scheme of Si pools and fluxes in the soil-plant system (adapted from Cornelis and Delvaux (2016)). Fluxes are represented by arrows and italic text. Pools are represented by boxes and bold text. Equation numbers are given for each pool and flux.

The inorganic Si (ISi) pool was estimated by Equation (2).

$$ISi = TSi - PhSi\ [kg\ ha^{-1}] \quad Eq\ (2)$$

ISi represents the inorganic Si pool in the 00-20 cm soil layer (kg ha^{-1}); *TSi* is the total Si pool in the 00-20 cm soil depth (kg ha^{-1}); *PhSi* is the phytolithic Si pool in the 00-20 cm soil layer as estimated by ox-Na_2CO_3-Si (kg ha^{-1}).

The Si in standing biomass at harvest was estimated with Equation (3).

$$Biomass_{Si} = \sum_{j=1}^{n} (Concentration_{Si} \times Dry\ weight)_j\ [kg\ ha^{-1}] \quad Eq\ (3)$$

$Biomass_{Si}$ is the mineralomass of Si at harvest (kg ha^{-1}); $Concentration_{Si,j}$ is the mean concentration of Si in the plant part j at harvest (kg [kg of plant part j]$^{-1}$); $Dry\ weight_j$ is the mean total dry weight of the plant part j at harvest ([kg of plant part j] ha^{-1}). The sum of the n different plant parts estimates the total mineralomass.

For BA-173, the mean dry weight was estimated for each plant part per plant. The total dry weight was then calculated by multiplying the mean dry weight

of each plant part per plant by the planting density of 1800 plants ha^{-1} used by the farmer. For SC-180, two methods were used to estimate the dry weight for each plant part: M1 and M2. For M1, the mean dry weight per ha was extrapolated from the measurements of weights at harvest on the five 3 m^2 subplots. For M2, the mean [green leaves weight/stalk weight] and [dead leaves weight/stalk weight] ratios at harvest were estimated through the weight measurements at harvest. The total stalk weight at harvest was furnished by the farmer as the harvested stalks were weighed when arriving at the distillery. The green leaves and dead leaves weights at harvest were therefore estimated thanks to the [green leaves weight/stalk weight] and [dead leaves weight/stalk weight] ratios at harvest. M2 has the advantage of being more representative of the whole plot.

5.3.5.2 Estimation of Si fluxes

Quantified Si fluxes are illustrated in Figure 5-3. Si fluxes were estimated considering a steasy-state Si cycle (Alexandre et al., 2011, 1997; Blecker et al., 2006). The steady-state Si cycle is based on the hypothesis that annual DSi outputs equal annual DSi inputs. Annual DSi outputs include (i) the uptake of the DSi by plants and (ii) the lixiviation of DSi towards the hydrosphere. Annual DSi inputs include: (i) the dissolution of phytoliths and (ii) the mineral weathering of the LSi pool. Si inputs from rainfall and dusts can also be considered but we decided to ignore them in this study as they were negligible in most of the studies in which they were quantified (Bernhard Reversat et al., 1978; Desplanques et al., 2006; Klotzbücher et al., 2015b; Lucas et al., 1993; Michael Sommer et al., 2013; Yang and Zhang, 2018).

Fluxes from plants to soil or exported by harvest were estimated with Equation (4).

$$Flux_{Si} = \sum_{j=1}^{n} (Concentration_{Si} \times Dry\ weight)_j \ [kg\ ha^{-1} yr^{-1}] \qquad Eq\ (4)$$

$Flux_{Si}$ is the flux of Si (kg ha^{-1} yr^{-1}); $Concentration_{Si,j}$ is the mean concentration of Si in the plant part j (kg [kg of plant part j]$^{-1}$); $Dry\ weight_j$ is the mean total dry weight of the plant part j that is restituted on soil or exported with harvest ([kg of plant part j] ha^{-1} yr^{-1}). The sum of the n different plant parts estimates the total annual flux.

For the BA-173 plot, the mean dry weight was estimated for each plant part per plant. Plant parts concerned by Si fluxes from plants to soil are (i) the leaves at harvest, (ii) the leaves affected by fungal disease, (iii) the pseudostem, and (iv) the peduncle. Plant part concerned by Si exports by harvest is the banana bunch. The total dry weight was then calculated by multiplying the mean dry weight of each plant part per plant by the planting density of 1800 plants ha^{-1} used by the farmer. For the SC-180 plot, the mean dry weights were estimated using M1 and M2 described for the calculation of the Si pool in the standing biomass at harvest. The only difference is that dead leaves collected during the year were included in the [dead leaves weight/stalk weight] ratio. Plant parts concerned by Si fluxes from plants to soil are (i) green leaves and (ii) dead leaves. Plant part concerned by Si exports by harvest is the stalk.

The annual absorption of DSi by plants was estimated with Equation (5).

$$Absorption = Harvest + Restitution \ [kg\ ha^{-1}yr^{-1}] \ Eq\ (5)$$

The PhSi storage flux was estimated with Equation (6).

$$PhSi\ storage = Restitution \times \%\ of\ PhSi\ stored\ [kg\ ha^{-1}yr^{-1}] \ \ Eq\ (6)$$

The PhSi dissolution flux was estimated with Equation (7).

$$Dissolution_{PhSi} = Restitution - PhSi\ storage\ [kg\ ha^{-1}yr^{-1}]\ Eq\ (7)$$

Fluxes with drainage waters were estimated with the Equation (8).

$$Flux_{Si} = Concentration_{Si} \times \ Water\ infiltration\ [kg\ ha^{-1}yr^{-1}]\ Eq\ (8)$$

$Flux_i$ is the flux of Si (kg ha^{-1} yr^{-1}); $Concentration_{Si}$ is the mean concentration of Si in the drainage water (kg l^{-1}); *Water infiltation* is the total volume of water that infiltrates annually per ha on the respective plot (l ha^{-1} yr^{-1}).

The water infiltration was estimated based on MAR, evapotranspiration and runoff data (Equation (9)).

$$Water\ infiltration = Rainfall - Evapotranspiration - Runoff\ [m^3 ha^{-1} yr^{-1}]\ Eq\ (9)$$

Evapotranspiration (ET) was assessed following Crabit et al. (2016). In particular, actual ET is considered equal to ET_0 as (i) the plots were covered by crops for which the crop coefficient Kc was equal to unity (1), and (ii) the soils were never dry during the year, so the water stress coefficient Ks was equal to 1 (Cattan et al., 2007; Charlier, 2007; Crabit et al., 2016). The annual ET_0 was then estimated for each plot by using the relationship defined by Vittecoq et al. (2010) and calibrated using the ET_0 at the Neufchâteau station using the relation found by Morell and Jérémie (1994) (Equation 10).

$$ET_0 = -0.7205\ A + 1406\ [mm\ yr^{-1}]\ Eq\ (10)$$

ET_0 is the annual reference evapotranspiration, and A is the altitude. Equation 9 and the mean altitude of each plot were used to compute the annual ET_0 of each plot.

To simplify the model, we hypothesized that runoff was negligible on the studied plots. Indeed, measurements of infiltration at saturation with double ring infiltrometer (method in: Bouwer, 1986) showed very high infiltration capacity (39.9 ± 7.7 mm h^{-1}) as measured on similar soils in Guadeloupe (Cattan et al., 2007; Charlier et al., 2008).

Fluxes corresponding to the weathering of the inorganic Si pool taking into account the neoformation of the secondary minerals were estimated by considering a steady state of the Si soil-plant cycle with Equation (11).

$$Dissolution_{ISi} = (Absorption + Lixiviation) - Dissolution_{PhSi}\ [kg\ ha^{-1} yr^{-1}]\ Eq\ (11)$$

5.3.6 Statistical analyses

The significance of the difference between the different concentrations, pools and fluxes has been tested thanks to ANOVA 1 statistical tests performed with the *aov* function of the R programing language.

5.4 Results

5.4.1 Soil properties

Table 5-1 gives the results of the main physico-chemical analyses of the different horizons of BA-173 and SC-180 soil pedon. Soil pedons of BA-173 and SC-180 were quite similar. Within the soil pedons, two ash layers were identified. Soil texture was clay and clay loam. Soil bulk density was < 0.9 g cm^{-3} in all horizons. pH H_2O values ranged from 5.5 to 5.7 in the BA-173 pedon, and from 5.4 and 6.1 in the SC-180 pedon. pH KCl values were always lower than pH H_2O values. Carbon content was the largest in surface horizon and then decreased with depth. CEC values were comprised between 47 and 58 $cmol_c\ kg^{-1}$ in the BA-173 pedon, and 51 and 62 $cmol_c\ kg^{-1}$ in the SC-180 pedon. Calcium was the dominant cation on the exchange complex (from 0.66 to 5.4 $cmol_c\ kg^{-1}$ in the BA-173 pedon, and from 0.59 and 5.4 $cmol_c\ kg^{-1}$ in the SC-180 pedon), followed by Mg (from 0.69 to 2.8 $cmol_c\ kg^{-1}$ in the BA-173 pedon, and from 0.56 and 4.8 $cmol_c\ kg^{-1}$ in the SC-180 pedon). The exchange complex was desaturated in all horizons. Allophane content increased with soil depth and ranged from 13.7% to 34.7% in the BA-173 pedon, and from 10.5% to 26.8% in the SC-180 pedon. Fe_d/Fe_t ratios showed decreasing values with increasing soil depth and ranged from 0.50 to 0.37 in the BA-173 pedon and from 0.58 to 0.44 in the SC-180 pedon. In contrast, TRB increased with increasing soil depth and ranged from 89.5 to 161 $cmol_c\ kg^{-1}$ in the upper ash layer and from 75.7 to 87.6 $cmol_c\ kg^{-1}$ in the buried ash layer of the BA-173 pedon, and from 73.5 to 121 $cmol_c\ kg^{-1}$ in the upper layer and 97.8 $cmol_c\ kg^{-1}$ in the buried layer of the SC-180 pedon. The DSi concentrations were relatively large in the Ap horizons (2.63×10^{-3} and 2.68×10^{-3} mol l^{-1} for BA-173 and SC-180 respectively), AB horizons (2.73×10^{-3} mol l^{-1} and 1.89×10^{-3} mol l^{-1} for BA-173 and SC-180 respectively), and BC horizons (2.27×10^{-3} and 2.13×10^{-3} mol l^{-1} for BA-173 and SC-180 respectively), while they were relatively low in Bw horizons (<2×10^{-3} mol l^{-1}).

Table 5-1: Basic soil properties of soil horizons of banana plot (BA-173) and sugarcane plot (SC-180) profiles: texture, bulk density, pH, contents of organic C, allophane, ferrihydrite, CEC, and contents of exchangeable bases, Fe_d/Fe_t, Total Reserve in Bases (TRB), and $CaCl_2$-extractable Si ($CaCl_2$-Si).

Hor	Depth	Texture (%)			Bulk density	pH		C	CEC	Exch Bases ($cmol_c\ kg^{-1}$)				Allo-phane[a]	Ferri-hydrite[b]	Fe_d/Fe_t	TRB	$CaCl_2$-Si[c]
	cm	clay	silt	sand	$g\ cm^{-3}$	KCl	H_2O	%	$cmol_c\ kg^{-1}$	Ca	Mg	K	Na	%	%		$cmol_c\ kg^{-1}$	$log_{10}(Si)\ mol\ l^{-1}$
BA-173 profile																		
Ap	0-12	48	21	31	0.62	4.7	5.5	6.01	58	5.4	2.8	2.0	0.10	13.7	2.93	0.50	89.5	-2.58
AB	12-23	38	23	39	0.67	4.7	5.5	4.39	47	1.8	1.2	1.3	0.07	15.8	3.14	0.50	86.6	-2.56
Bw	24-45	55	14	31	0.59	5.0	5.4	2.52	52	0.66	0.69	0.15	0.16	23.6	3.39	0.45	97.7	-2.81
BC	46-62	39	18	43	0.64	5.3	5.5	0.94	49	0.86	1.2	0.20	0.23	34.7	3.23	0.43	161	-2.64
2Bw1	63-80	nd	nd	nd	0.64	5.0	5.6	1.19	58	1.8	2.3	0.79	0.67	19.1	2.32	0.49	75.7	-2.70
2Bw2	81-95	nd	nd	nd	0.60	5.3	5.6	0.98	56	1.5	2.0	0.47	0.33	27.8	2.93	0.44	84.7	-2.80
2BC	96-128	nd	nd	nd	n.d.	5.3	5.7	1.05	52	1.5	1.8	0.95	0.53	28.6	2.42	0.37	87.6	n.d.
SC-180 profile																		
Ap	0-5	52	28	20	0.54	4.6	5.7	8.06	62	5.4	4.8	2.6	0.19	10.5	2.64	0.58	73.5	-2.57
AB	6-24	56	16	28	0.66	4.6	5.7	4.95	51	2.0	1.8	1.8	0.14	12.4	2.87	0.52	74.1	-2.72
Bw1	25-36	56	21	23	0.81	4.5	5.7	3.68	52	0.75	0.61	0.49	0.27	14.7	2.73	0.50	78.7	-2.86
Bw2	37-63	nd	nd	nd	0.70	4.5	5.4	2.22	54	0.59	0.56	0.64	0.32	20.7	2.42	0.47	98.5	-2.76
BC	64-85	61	15	24	0.70	4.9	5.5	1.08	56	0.92	1.2	1.5	0.23	26.8	2.11	0.40	121	-2.67
2Bw1	86-110	nd	nd	nd	n.d.	5.5	6.1	1.22	62	2.2	1.6	2.5	0.23	23.9	2.46	0.44	97.8	n.d.

[a]Allophane content was estimated according to Parfitt and Wilson (1985), using $(Al_o\text{-}Al_p)/Si_o$ ratios (results of the total analyses, oxalate, DCB, and pyrophosphate analyses are presented in Table 5-S1).

[b]Ferrihydrite content was estimated according to Parfitt and Childs (1988) assuming complete dissolution with dark acid oxalate, using 1.7 x Fe_o.

[c] $CaCl_2$-Si concentration was determined from $CaCl_2$-Si content in soil and soil moisture content at sampling time.

5.4.2 Plant analyses

Table 5-2 and Table 5-3 show the results that concern the plant analyses from BA-173 and SC-180 plots respectively. The Si concentrations, the mass fluxes, the Si fluxes, and the Si mineralomass are given for the different plant parts. For the SC-180 plot, mass fluxes, Si fluxes, and Si mineralomass are given for method 1 (M1) and method 2 (M2) as here-above explained (see Section 5.3.5).

Table 5-2: Average Si concentrations, mass fluxes (dry weight), Si fluxes, and Si mineralomass at harvest of the different banana plant parts.

	Banana fruits	**Harvest leaves**	**Pseudostem**	**Peduncle**	**FD[a] leaves**
Si conc ($g\ kg^{-1}$)	0.77 (0.03)	21.47 (2.20)	5.56 (0.21)	6.90 (0.25)	8.99 (0.16)
Mass flux ($t\ ha^{-1}\ yr^{-1}$)	-13.10 (0.72)	2.36 (0.35)	8.01 (0.32)	0.46 (0.03)	6.99 (0.37)
Si fluxes ($kg\ ha^{-1}\ yr^{-1}$)	-10.06 (0.99)	50.64 (12.68)	44.56 (3.48)	3.19 (0.30)	62.89 (4.25)
Si in biomass ($kg\ ha^{-1}$)	5.03 (0.49)	25.32 (6.34)	22.28 (1.74)	1.60 (0.15)	0

[a]FD corresponds to Fungal Disease.
Values in parentheses are standard errors.
Minus indicate fluxes going out of the studied soil-plant system (harvested parts).

For the BA-173 plot (Table 5-2), the Si concentration in plant increased in the sequence banana fruits < peduncle < pseudostem < fungal diseased leaves < harvest leaves. Differences were always significant (p-value < 0.01). Mass fluxes increased in the sequence peduncle < harvest leaves < fungal diseased leaves < pseudostem < banana fruits. Si fluxes increased in the sequence peduncle < banana fruits < pseudostem < harvest leaves < fungal diseased leaves. The addition of all the positive Si fluxes gives the total Si flux that is restituted on soil (see Table 5-5). The restituted Si flux was significantly larger than the exported Si flux (p-value < 0.001). The addition of the Si mineralomass of all the plant parts gives the total Si in standing biomass at harvest. It amounted to 54.24 $kg\ ha^{-1}$.

For the SC-180 plot (Table 5-3), the Si concentration in plant increased in the sequence stalks < green leaves < dead leaves. Concentrations of stalks and dead leaves or green leaves were both significantly different (p-value < 0.001). Concentrations of dead leaves and green leaves were not significantly

different. Mass fluxes evolved in the sequence dead leaves ~ green leaves < stalks for both M1 and M2 that were not significantly different. Si fluxes increased in the sequence stalks < green leaves ≤ dead leaves for both M1 and M2 even if differences between dead leaves and green leaves were not significant. Si fluxes estimated with M1 and M2 were not significantly different. The addition of the green leaves and dead leaves Si fluxes gives the total Si flux that is restituted on soil. The restituted Si flux was significantly larger than the exported Si flux (p-value < 0.001). The addition of the Si mineralomass of all the plant parts gives the total Si in standing biomass at harvest. It amounted to 310.4 and 264.5 kg ha^{-1} with M1 and M2 respectively.

Table 5-3: Average Si concentrations, mass fluxes (dry weight) estimated with method 1 (M1) and method 2 (M2), Si fluxes estimated with M1 and M2, and Si mineralomass at harvest estimated with M1 and M2 of the different sugarcane plant parts.

	Stalks	**Dead leaves**	**Green leaves**
Si concentration (g kg^{-1})	2.96 (0.37)	25.67 (0.94)	20.36 (3.58)
Mass flux M1 (t ha^{-1} yr^{-1})	-21.94 (3.68)	9.58 (0.97)	10.03 (1.62)
Mass flux M2 (t ha^{-1} yr^{-1})	-18.69	8.89 (1.27)	8.53 (0.44)
Si fluxes M1 (kg ha^{-1} yr^{-1})	-64.93 (18.93)	246.0 (33.85)	204.3 (68.83)
Si fluxes M2 (kg ha^{-1} yr^{-1})	-55.30 (6.855)	228.2 (40.84)	173.6 (39.42)
Si mineralomass M1 (kg ha^{-1})	64.93 (18.93)	41.14 (11.40)	204.3 (68.83)
Si mineralomass M2 (kg ha^{-1})	55.30 (6.855)	35.64 (6.787)	173.6 (39.42)

Minus indicate fluxes going out of the studied soil-plant system (harvested parts).
Values in parentheses are standard errors.

5.4.3 Soil Si pools

The quantified soil Si pools are the ISi pool that includes the LSi and PSi pools, the ox-Na_2CO_3-Si pool mainly composed by the PhSi pool, and the $CaCl_2$-Si pool that represents the DSi pool. All these pools are given for the 20 first cm of soil of the BA-173 and SC-180 plots in Table 5-4. The ISi pool was significantly larger in the BA-173 soil (188.7 t ha^{-1} 20 cm^{-1}) than in the SC-180 soil (175.3 t ha^{-1} 20 cm^{-1}). The ox-Na_2CO_3-Si pools in BA-173 and SC-180 plots amounted to 3659 and to 3907 t ha^{-1} 20 cm^{-1}, respectively, and did not significantly differ. The DSi pool was significantly larger in BA-173 (56.35 t ha^{-1} 20 cm^{-1}) than in SC-180 soil (32.74 t ha^{-1} 20 cm^{-1}).

Table 5-4: Average contents of total Si, ox-Na_2CO_3-Si, inorganic (LSi + PSi), and $CaCl_2$-Si pools in the topsoil (00-20 cm) in the banana (BA-173) and sugarcane (SC-180) plots.

	Total Si	**ox-Na_2CO_3-Si**	**LSi + PSi**	**$CaCl_2$-Si**
	t ha^{-1}	**t ha^{-1}**	**t ha^{-1}**	**kg ha^{-1}**
BA-173	194.3 (3.39)	3.66 (0.22)	190.6 (3.53)	56.35 (4.77)
SC-180	180.6 (4.59)	3.91 (0.25)	176.7 (1.97)	32.74 (1.21)

Values in parentheses are standard errors.

5.5 Discussion

5.5.1 Andosol properties of the soil and soil weathering stage

Analyses of the soil pedons pointed both soils as Aluandic Dystric Andosols according to the WRB classification system (IUSS 2014). TRB values were quite low (< 100 $cmol_c$ kg^{-1} excepted in the BC horizons) showing the advanced soil weathering stage despite pyroclastic deposits were relatively recent (Boudon et al., 1987; Dagain, 1981; Komorowski et al., 2005). This demonstrated that in such climatic conditions (high rainfall and temperatures), soil desilication and weathering were rapid (Chadwick et al., 2003) for lapilli pyroclasts; especially for the volcanic glasses as observed in other studies on relatively young soils in Guadeloupe (Jongmans et al., 1999; Ndayiragije and Delvaux, 2003). Increasing TRB values and decreasing degrees of individualization of free iron (Fe_d/Fe_t ratios) (Table 5-1) with soil depth down to BC horizons both indicated that weathering was the most advanced at surface horizon. Beneath BC, TRB decreased while Fe_d/Fe_t increased in both profiles, testifying that these horizons originated from a buried Andosol. The increase in C content in soil horizons beneath BC also supported this statement. The following discussion will only concern the upper layer (horizons Ap, AB, Bw and BC). In BC horizons, Mg was the dominant cation in TRB (76% in TRB for BA-173 and 83% in TRB for SC-180) followed by Ca (16% and 10% in TRB for BA-173 and SC-180 profiles, respectively), Na (5.5% and 4% in TRB for BA-173 and SC-180 profiles, respectively), and K (2.5% and 3% in TRB for BA-173 and SC-180 profiles, respectively). This cation distribution corresponds to the mineralogical composition of unweathered parent pyroclasts (mainly pyroxenes, plagioclases and volcanic glasses) (Dagain, 1981).

Allophane content increased with depth in both profiles (from 13.7% to 34.7% in the BA-173 profile and from 10.5% to 26.8% in the SC-180 profile) while Al_p/Al_o drastically decreased at depth in both profiles (from 0.25 to 0.04 in the BA-173 profile and from 0.36 to 0.05 in the SC-180 profile). Moreover, allophane and carbon contents were inversely correlated ($r = -0.83$ p-value < 0.001). This indicates that, in A and AB horizons, Al was mostly complexed with organic matter causing an anti-allophanic effect (Shoji et al., 1993) while in Bw and BC horizons, Al was incorporated in allophane. Contrasting allophane contents between A and B horizons is usual in Andosols in which organic matter content in the A horizon may induce an anti-allophanic effect (Adjadeh and Inoue, 1999; Madeira et al., 1994; Mizota and Van Reeuwijk, 1989; Ndayiragije and Delvaux, 2003).

5.5.2 Si accumulating plants

The Si repartition between the different plant samples (Table 5-2: Banana fruit < pseudostem < peduncle < fungal disease leaf < harvest leaf for the banana plant, and Table 5-3: stalks < green leaf < dead leaf for the sugarcane plant) illustrates that the transpiration stream carries monosilicic acid from roots towards shoot transpiration termini (Henriet et al., 2006; Raven, 2001, 1983). Si concentrations in old leaves (harvest leaves for banana and dead leaves for sugarcane) were larger than Si concentrations in relatively young leaves (FD leaves for banana and green leaves for sugarcane) as older leaves have evaporated water over a longer period of time than younger leaves (Henriet et al., 2006). Banana and sugarcane plants are known as Si-accumulating species as active mechanisms of Si absorption have been demonstrated for these plants (Henriet et al., 2006; Hodson et al., 2005; Ma and Takahashi, 2002; Savant et al., 1999). The large Si concentrations in the banana leaves (0.9% in fungal disease leaves and 2.2% in harvest leaves), and in the sugarcane leaves (2.0% in the green leaves and 2.6% in the dead leaves) corroborate the Si active absorption mechanisms of these plant species.

5.5.3 The soil PhSi pool

The PhSi pools of BA-173 and SC-180 soils did not significantly differ. Since soils were cultivated (about 347 years BP), sugarcane is probably the crop that was mainly cultivated. Land use was likely different between both plots

since 2006 only (see Section 5.3.1). It is therefore not surprising that soil PhSi pools were not significantly different between the two plots.

Part of phytoliths that are returned to soil is stabilized in soil and may further migrate at depth (Alexandre et al., 2011, 1997). The PhSi storage flux may be estimated by quantifying the PhSi pool evolution with soil depth (Alexandre et al., 2011, 1997). At depth, the PhSi pool generally decreases progressively until reaching a constant value which represents the stable pool of PhSi (Alexandre et al., 2011, 1997; Blecker et al., 2006; Yang and Zhang, 2018). The proportion of PhSi that is annually stabilized is therefore estimated with the ratio [PhSi pool in depth/PhSi pool in surface] (Alexandre et al., 1997). However, for the studied soils, there is no method to quantify the PhSi pool in deep horizons. The ox-Na_2CO_3-Si pool may be composed of PhSi and amorphous LSi in proportions that we were unable to determine. Therefore, we were not able to quantify the evolution of the PhSi pool at depth.

The PhSi storage in soil depends on climatic factors (Blecker et al., 2006), on phytoliths morphology (Alexandre et al., 2011), and on plant species (Bartoli, 1983; Gérard et al., 2008; Sommer et al., 2013; Yang and Zhang, 2018). Blecker et al. (2006) reported that the percentage of phytoliths that was annually stabilized was inversely proportional to annual rainfall. Alexandre et al. (2011) found a strong relationship between the globular granulate phytolith pool and the total phytolith pool, demonstrating that this particular phytolith morphotype stabilized in soil. Comparison between different studies reveals that coniferous phytoliths are particularly stable in soils (Bartoli, 1983; Gérard et al., 2008; Yang and Zhang, 2018).

In the absence of quantifiable data for PhSi storage in soils, two scenarios were assumed based on literature data (Table 5-5; Figure 5-4), as follows: Scenario (1): PhSi storage of 8%, the lowest PhSi storage reported in literature (Alexandre et al., 1997); Scenario (2): PhSi storage of 31%, the largest PhSi storage reported in literature (Blecker et al., 2006) excluding coniferous. We decided to exclude data from coniferous species as they are out of the range of other studies.

Depending on the scenario, PhSi storage ranged from 12.91 (Scenario 1) to 50.02 kg ha^{-1} yr^{-1} (Scenario 2) for the BA-173 plot, and from 32.14 (Scenario 1) to 124.6 kg ha^{-1} yr^{-1} (Scenario 2) for the SC-180 plot. Resulting PhSi

dissolution (see Equation 6, Section 5.3.5) ranged from 111.3 (Scenario 2) to 148.4 kg ha^{-1} yr^{-1} (Scenario 1) for the BA-173 plot, and from 277.2 (Scenario 2) to 369.7 kg ha^{-1} yr^{-1} (Scenario 1) for the SC-180 plot. Phytolith dissolution contributes more to the DSi pool in the SC-180 soil than in the BA-173 soil because the phytolith input from plants to soil was greater in the SC-180 plot. Considering that banana and sugarcane phytoliths may exhibit similar dissolution rates, a greater soluble phytolith pool was thus returned on soil in the SC-180 soil.

Table 5-5: Si fluxes estimated for the banana (BA-173) and sugarcane (SC-180) plots assuming PhSi storage of 8 and 31%.

	PhSi storage	DSi uptake by plants	PhSi input to soil	PhSi output by harvests	PhSi dissolution in soil	DSi output by lixiviation	Mineral dissolution[1]
	%	kg ha^{-1} yr^{-1}					
BA-173	8	171.4	161.3	10.06	148.4	106.3	129.3
		(21.70)	(20.71)	(0.99)	(19.05)	(5.65)	(8.30)
BA-173	31	171.4	161.3	10.06	111.3	106.3	166.4
		(21.70)	(20.71)	(0.99)	(14.29)	(5.65)	(13.06)
SC-180	8	457.1	401.8	55.30	369.7	99.80	187.2
		(87.12)	(80.26)	(6.86)	(73.84)	(9.52)	(22.80)
SC-180	31	457.1	401.8	55.30	277.2	99.80	279.7
		(87.12)	(80.26)	(6.86)	(55.38)	(9.52)	(41.26)

5.5.4 The inorganic Si pool

The inorganic Si pool was significantly larger ($p < 0.01$) in the BA-173 soil (190.6 t ha^{-1}) than in the SC-180 soil (176.7 t ha^{-1}). Both plots studied had similar land uses except since 2006. From 2006 to 2016, the SC-180 plot was cultivated with sugarcane while the BA-173 plot was cultivated with banana. As DSi output by leaching were not significantly different between BA-173 and SC-180 plots, we can consider that, on that period of time, the larger annual Si uptakes by the sugarcane plants favored the dissolution of the inorganic Si pool. From 2006 to 2016, supplementary 690 kg of Si ha^{-1} were released from the dissolution of the inorganic Si pool in the SC-180 plot compared to the BA-173 plot. As the difference between the inorganic Si pool of the BA-173 and SC-180 plots amounted to 13,400 kg of Si, we understand

that the difference in land use on the last 10 years can not explain the difference in size of the ISi pools. The larger MAR on the SC-180 plot is the most likely factor that could have significantly impacted the ISi pool (Chadwick et al., 2003). We must recall here that these two neighbouring plots share an identical soil cover, the same soil mapping unit as identified by a detailed soil survey (Colmet-Daage et Lagache, 1965; Colmet-Daage et Lagache, 1969). Besides they exhibit similar basic soil properties as shown in the present study.

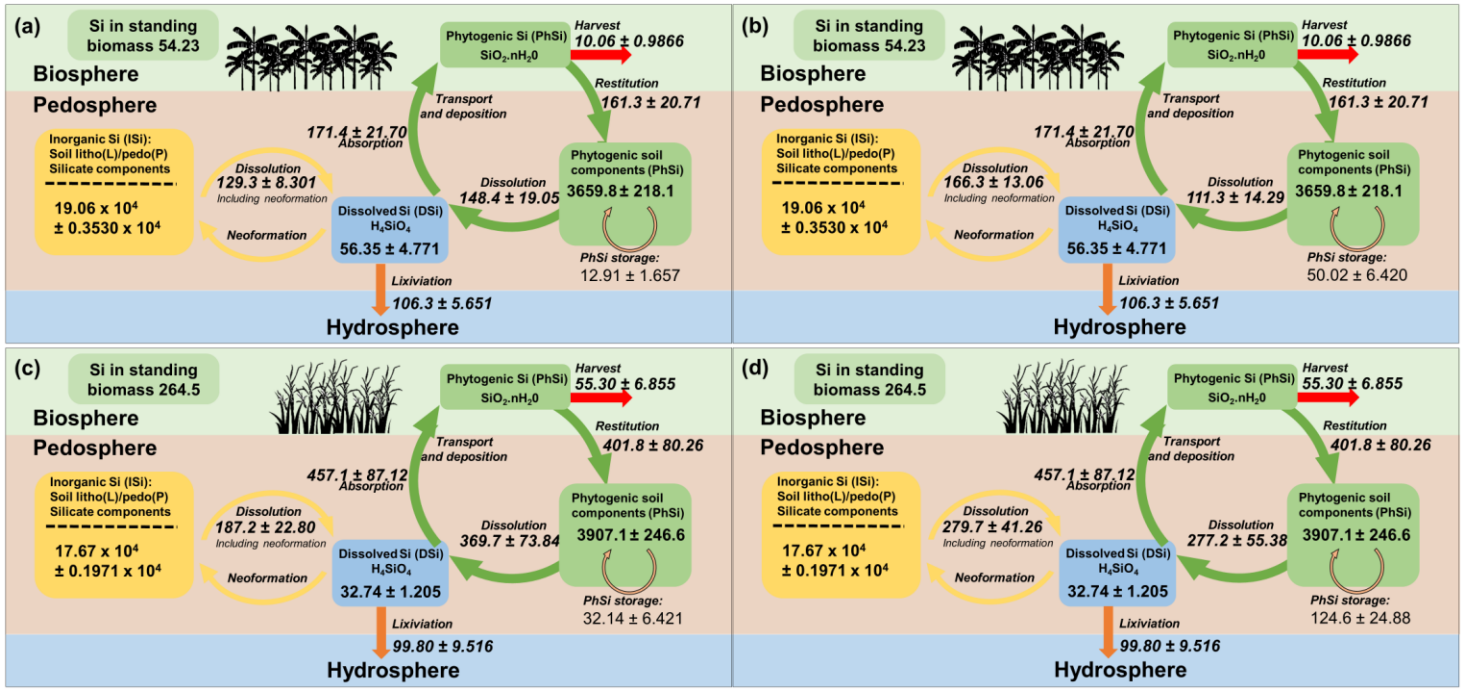

Figure 5-4: Steady-state soil-plant Si cycle established for the BA-173 (a,b) and SC-180 (c,d) plots assuming (a and c) 8% of PhSi storage, and (b and d) 31% of PhSi storage.

5.5.5 Impact of the plant Si cycling on the mineral dissolution

Plants favor the mineral dissolution through the uptake of Si from the soil solution (Alexandre et al., 1997; Blecker et al., 2006; J-T Cornelis et al., 2011; Drever, 1994; Moulton et al., 2000). Under sugarcane the Si uptake by plants amounted to 457 kg ha^{-1} yr^{-1} which was significantly larger than the quantity of Si taken up by the banana plants (171 kg ha^{-1} yr^{-1}). The reason why the absorption of Si was more important for sugarcane was twofold. Firstly, the above ground biomass production was larger for sugarcane plants (416 t ha^{-1} yr^{-1} with M1 and 361 t ha^{-1} yr^{-1} with M2) than for banana plants (309 t ha^{-1} yr^{-1}). Secondly, the mean Si concentration in sugarcane plant (M1: 1.24% and M2: 1.27%) was larger than the mean Si concentration in the banana plant (0.55%). Si uptakes by sugarcane plants in literature amounted to 160 kg ha^{-1} yr^{-1} (Tubana et al., 2016), 248 kg ha^{-1} yr^{-1} (Ross et al., 1974), 300 kg ha^{-1} yr^{-1} (Meyer and Keeping, 2005 from Tubana et al., 2016), 379 kg ha^{-1} yr^{-1} (Samuels, 1969), or even 408 kg ha^{-1} yr^{-1} and 509 kg ha^{-1} yr^{-1} (Ross et al., 1974) when Si amendments were brought to soil. In our study, Si uptake by sugarcane plants was thus important as compared to literature data. Si uptake by banana plant has never been quantified yet. Therefore, we can not compare our results to literature data.

When phytolith dissolution is not sufficient to match annual plant Si uptake, Si from mineral dissolution compensates (Blecker et al., 2006). Since part of absorbed Si was mostly stored for long periods, and formed a stable phytolith pool in soil (Alexandre et al., 2011, 1997; Blecker et al., 2006; Yang and Zhang, 2018), phytolith dissolution did not match Si quantities taken up by plants. Therefore, plant Si cycling favored mineral dissolution (Alexandre et al., 2011, 1997; Bartoli, 1983; Blecker et al., 2006; Lucas et al., 1993; Yang and Zhang, 2018). In the studied plots, without any plant Si cycling, mineral dissolution would amount to 106.3 and 99.80 kg Si ha^{-1} yr^{-1} for the BA-173 and SC-180 plots respectively.

However, when we considered plant Si cycling, depending on the scenario, ISi dissolution fluxes ranged from 129.3 (Scenario 1) to 166.4 kg ha^{-1} yr^{-1} (Scenario 2) for BA-173, and from 187.2 (Scenario 1) to 279.7 kg ha^{-1} yr^{-1} (Scenario 2) for SC-180. Sugarcane plants were particularly efficient to accelerate the ISi dissolution as very important amounts of Si were prevailed by plants. Table 5-6 (adapted from Blecker et al. 2006) illustrates the impact

of the biological Si feedback loop on mineral dissolution. Cultivated environments indeed promote mineral dissolution. The impact of the biological Si feedback loop on mineral weathering decreases in the order: **sugarcane** (with large PhSi storage) > **sugarcane** (with low PhSi storage) > savanna (with high Si exports) > **banana** (with large PhSi storage) > **rice** > savanna (with low Si exports) > **banana** (with low PhSi storage) > subtropical forest > tall grass > mixed grass > short grass ≥ deciduous temperate forest ≥ tropical rainforest > coniferous forest.

The cultivated plants are particularly efficient in enhancing mineral weathering because they are high Si-accumulators and because harvest of plant parts that contain Si increases the difference between the Si uptake and Si release by phytolith dissolution. Alexandre et al. (2011) have particularly evidenced the impact of the amplitude of the Si exports on mineral dissolution. Comparing scenarios of ash exports after savanna burning, these authors have shown that, the more the exports, the more the mineral dissolution. Considering a steady state cycle, the principle is applicable to exports through the harvest of plant parts that contain phytoliths in cultivated environments (see Equations 6 and 9 in section 5.3.5). In rice fields for example, the export of Si –rich rice straws can be very high (up to 1240 kg ha^{-1} yr^{-1} (Klotzbücher et al., 2016)), and strongly impact mineral weathering. The subtropical forest in Table 5-6 particularly enhances mineral dissolution as bamboo, a well-known high Si accumulator (e.g. Li et al., 2006), is present in the studied forest (Yang and Zhang, 2018). Differences between different grasslands is due to differences in biomass production between the tall, mixed, and short grasses (Blecker et al., 2006; Cornelis and Delvaux, 2016). Grasses are particularly efficient in taking up Si in soil, and therefore in accelerating mineral dissolution, because of the high density of high Si accumulators. In forest ecosystems, the impact of the biological Si feedback loop mainly depends on plant species, but also on soil weathering degree (Cornelis and Delvaux, 2016).

Table 5-6: Comparison of the impact of the biological Si feedback loop on mineral dissolution of Si between the studied plots and other ecosystems on an annual basis (adapted from Blecker et al. 2006).

	Mineral dissolution (kg Si ha^{-1} yr^{-1})		
	Without plant cycling Inputs – Outputs	**With plant cycling (Input + Phytolith dissolution) – (Outputs + plant uptake)**	**Phytolith dissolution – plant uptake**
Sugarcane Scenario 1	-99.80	-187.2	-87.4
Sugarcane Scenario 2	-99.80	-279.7	-179.9
Banana Scenario 1	-106.3	-129.3	-23.0
Banana Scenario 2	-106.3	-166.4	-60.1
Subtropical forest + rice[a]	-50.1	-86.4	-36.3
Subtropical forest + rice[a]	-50.5	-77.9	-27.3
Savanna[b]	-9	-85	-76
Savanna[b]	-9	-62	-53
Savanna[b]	-9	-33	-24
Tall grass[c]	-9	-25	-16
Tall grass[c]	-4.3	-14.3	-10
Mixed grass[c]	1.7	-11.3	-13
Mixed grass[c]	0.5	-11.5	-12
Mixed grass[c]	0.3	-3.7	-4
Short grass[c]	1.8	-7.2	-9
Short grass[c]	1.5	-4.5	-6
Subtropical forest[a]	-48.7	-69.5	-20.8
Deciduous forest[d]	n.d.	n.d.	-6.0
Coniferous forest[d]	-24.5	-28.5	-4.0
Tropical rainforest[e]	-15.0	-21.0	-6.0

Positive values represent a net increase in Si; however this is not to imply that mineral weathering is not occurring. Negative values represent a hypothesized increase in mineral dissolution. (Inputs = atmospheric deposition; outputs = leaching export; phytolith dissolution = Si addition through dissolution of labile phytoliths; plant uptake = Si uptake stored in aboveground biomass). Here. n.d. denotes not determined due to insufficient data.
[a]Yang and Zhang (2018) ; [b]Alexandre et al. (2011) ; [c]Blecker et al. (2006) ; [d]Bartoli (1983) ; [e]Alexandre et al. (1997)

5.5.6 Desilication due to harvest

Harvest exports of Si are problematic for some Si accumulating species as it could accelerate soil desilication and impact crop yields (e.g. rice or sugarcane – Berthelsen et al., 2001; Klotzbücher et al., 2016). Si exports for sugarcane are known to be less problematic than for other crops as stalks is generally the only plant organ that is exported while leaves are typically returned on the ground (Ayres, 1966; Kingston, 2008). For banana, only the

banana bunch is exported while other plant parts return to soil. Si exports by sugarcane stalks amounted to 55 kg ha^{-1} yr^{-1}. Si exports by banana bunches amounted to 10 kg ha^{-1} yr^{-1}. For rice, Si exports by straw harvest can reach 1240 kg ha^{-1} yr^{-1} (Klotzbücher et al., 2016), but are commonly comprised between 50 and 500 kg ha^{-1} yr^{-1} depending on the straw management and the size of the bio-available Si pool (Klotzbücher et al., 2016; Prakash et al., 2011; Yang and Zhang, 2018). For maize, wheat, triticale, oat, barley, potato, sugar beet, and flax, Si exports (kg ha^{-1} yr^{-1}) can be 112-127, 37-113, 36-44, 19-27, 15-24, 3-7, 3-8, and 1, respectively (Vandevenne et al., 2011). Si exports by banana harvests were thus relatively low and in the same range as low Si-accumulators. This can be explained by the low proportion of absorbed Si that was exported through harvest (5.9%) as compared to the proportion that was restituted to soil (94.1%). Banana fruits have extremely low Si concentrations (Table 5-2) compared to leaves that are restituted to soil. Sugarcane harvest exported slightly larger Si quantities but still low as compared to Si quantities returned to soil (12% of the total absorbed Si was exported while 88% was restituted to soil). Banana and sugarcane are thus relatively low "desilicating" crops.

5.5.7 Control of the DSi concentration in the soil solution

The DSi concentration in the soil solution along the banana and sugarcane soil pedons first decreased with soil depth from the Ap to Bw horizons, and then increased in BC horizons (Figure 5-5). Regarding the evolution of TRB and considering the solubility of amorphous silica (0.002 mol l^{-1}), we can interpret the DSi concentration in soil solution of BC horizons as being controlled by the LSi pool. However, the large DSi concentration in soil solution from topsoil was likely controlled by the PhSi pool (Georgiadis et al., 2013). As depicted by low TRB values and high Fe_d/Fe_t, the easily weatherable primary minerals were probably exhausted in topsoil horizons (see XRD patterns – Figures 5-S1 and 5-S2), and unlikely controlled large DSi concentrations. Moreover, in Bw horizons, where TRB values were comparable to the one of Ap and AB horizons and in which the PhSi pool was probably negligible, DSi concentrations were low (< 2 mol l^{-1}) and probably controlled by the PSi pool. Expected DSi concentration without biological Si-cycling were therefore lower than actual DSi concentrations in Ap and AB horizons (Figure 5-5). Our results therefore highlight the importance of the biological Si feedback loop in maintaining large DSi concentration and soil

fertility in topsoil horizons. This plant characteristic was first observed in a tropical forest in the Amazon basin (Lucas et al., 1993), and was further described in other natural environments (a.o. Alexandre et al., 1997; Gérard

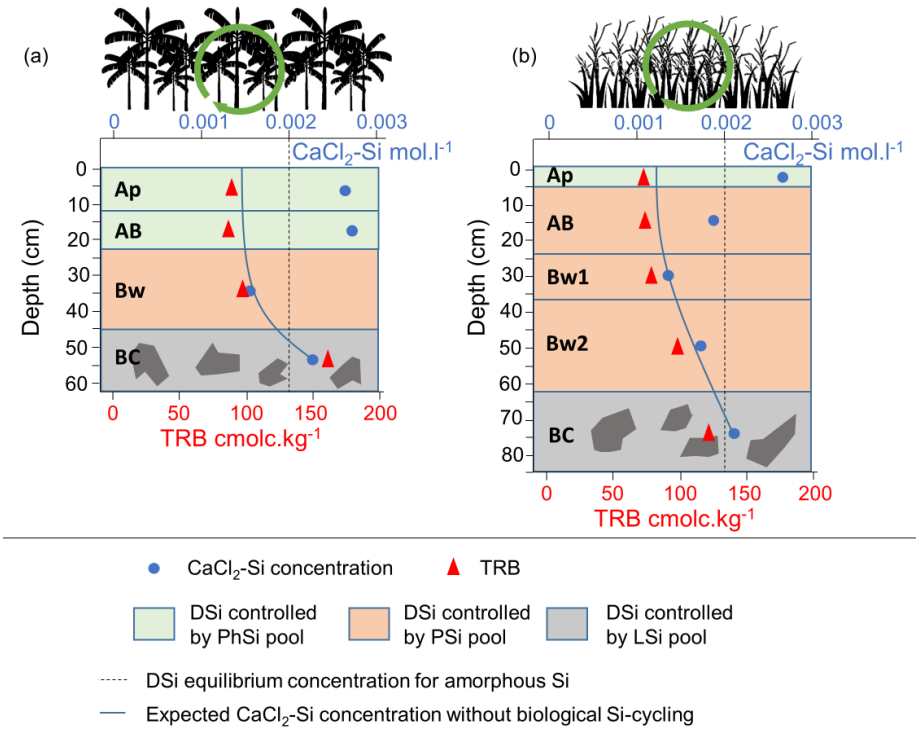

Figure 5-5: $CaCl_2$-Si concentration and total reserve in bases (TRB) in the soil horizons of the *(a) BA-173* and *(b) SC-180* soil pedons. The color of the horizon indicates what soil component controls the $CaCl_2$-Si concentration. The dotted lines represent the solubility of amorphous silica (0.002 mol l^{-1}). The blue lines illustrate the expected evolution of $CaCl_2$-Si concentrations with soil depth without any biological Si cycling as calibrated from TRB values.

et al., 2008; Sommer et al., 2013) as well as in banana croplands established on basaltic ash soils (Opfergelt et al., 2010). We think that this was particularly due to two facts. First, the dominance of Si-accumulating plants over the three last centuries (mainly sugarcane) on that plots. Second, the large proportion of the Si absorbed by plants that was returned on soil instead of being exported in harvest products as it is commonly done for other crops. This demonstrated the importance of the management of the inedible plant part of Si accumulating crops at harvest.

5.6 Conclusion

The distributions of Si among the banana and sugarcane plant parts were explained by the differences of total evaporated water volumes.

We showed that the biological Si feedback loop was highly active in the studied soil-plant system involving Si accumulating plant species and Andosols at advanced weathering stage. This active loop significantly accelerated mineral weathering. In the studied cultivated plots, DSi concentrations in topsoil solution were controlled by phytolith dissolution. We attribute this to two main facts. Firstly, the dominance of Si accumulating crops on the three last centuries. Secondly, the restitution of the inedible plan parts on soil. The management of the inedible plant parts at harvest is therefore a key factor to maintain large DSi concentrations in the top soil horizons and soil fertility.

Chapter 6 The silicon soil-plant cycle in a tropical rainforest and a nearby banana field[4]

Abstract

Land use impacts the soil-plant cycle of silicon (Si). In particular, the transition from forest into cropland may lead to a drastic decrease of the soil phytogenic Si pool due to crop harvest. However, this decrease is related to the management of inedible plant parts in cultivated ecosystems. The aim of this chapter is to determine the impact of the transition from an evergreen tropical forest to an intensive banana cropland on the soil-plant Si cycle developing on desilicated Andosols.

We studied the soil-plant Si cycle in an evergreen tropical forest on the Eastern flank of *La Soufrière* volcano in Guadeloupe. Si taken up by plants was measured for leaves of *Swietenia macrophylla* (the dominant species), *Myrcia deflexa* (the species with the largest Si concentrations), and of all the other species mixed, and for non-foliar samples. Si leached out was also measured through lysimetry. Si in standing biomass was estimated. Soil Si pools were quantified with specific chemical extractions. Si fluxes were further compared to the one of a banana plot located 2.8 km from the forest plot. Soil Si pools were compared to the one of a banana plot located 0.4 km from the forest plot.

Total Si uptake by plants amounted to 43 kg ha^{-1} yr^{-1} in the forest plot. *Swietenia macrophylla* and *Myrcia deflexa* uptakes represented ~70% and ~17% of the total Si uptakes respectively, while other species leaves and non-foliar items only represented ~7% and ~6% of the total Si uptakes respectively. Si in standing biomass amounted to 836 kg ha^{-1}. Plant Si uptake in the banana plot amounted to 171 kg ha^{-1} yr^{-1}. Si in standing biomass in the banana plot at harvest was 54 kg ha^{-1}. The soil-plant Si cycle of the studied tropical evergreen forest is strongly controlled by two species. When forest is transformed into banana cropland, Si in standing biomass greatly decreases while the Si bio-cycling becomes much more intense, which increases the dissolution of the lithogenic and pedogenic Si pools.

[4] Manuscript in preparation for submission in an international peer-reviewed journal.

6.1 Introduction

The soil-plant silicon (Si) cycle widely differs among Earth's ecosystems depending on soil properties and processes, climate, plant species, and human management practices. Vegetation is well known to impact the soil-plant Si cycle through the absorption of dissolved Si (DSi) in the soil solution, the formation of amorphous silica bodies called phytolith (PhSi), and the return of highly soluble phytolith on soil by litterfall (a.o. Alexandre et al., 1997; Bartoli, 1983; Lucas et al., 1993; Meunier et al., 1999). Si taken up by plants ranges from 0.7 to 1470 kg Si ha^{-1} yr^{-1} among different terrestrial ecosystems (*Chapter 4*) depending mainly on plant species (Cornelis et al., 2010; Meunier et al., 2010), soil weathering stage (Cornelis and Delvaux, 2016; Henriet et al., 2008a; *Chapter 4*), and climate conditions (Blecker et al., 2006; Quigley et al., 2017). The impact of plant species is particularly highlighted in environments rich in high Si-accumulating species such as bamboo forests (Li et al., 2006; Meunier et al., 1999), or rice croplands (Desplanques et al., 2006; Klotzbücher et al., 2016; Makabe et al., 2009). Converting evergreen tropical forest into rice croplands changes the soil-plant Si cycle (Klotzbücher et al., 2016; Yang and Zhang, 2018). The density of high Si-accumulating species drastically increases, crop harvest exports large amounts of Si, and irrigation can constitute important inputs of Si (a.o. Desplanques et al., 2006; Klotzbücher et al., 2015, 2016, 2018; Riotte et al., 2018). However, little is known about the impact of deforestation at the expense of other crops in tropical environments. In particular, the impact of the conversion of tropical evergreen forest into banana crop is still unknown. To fill this gap, we compared the soil-plant Si cycle of an evergreen tropical forest to that of neighboring banana plantations.

6.2 Environmental framework

This study was conducted in the Southern part of the volcanic island of Basse-Terre in Guadeloupe (16°N, 61°W) (Figure 6-1a). This region was shaped by The Grande Découverte Volcanic Complex (GDVC) from about 200 ka BP to 1440 AD (Carlut et al., 2000; Komorowski et al., 2005; Samper et al., 2007). Soil weathering stage of the flanks of the volcano depends mainly on the age of the pyroclastic deposits, and on mean annual rainfall (MAR). Soils are slightly weathered on the Western flank of the volcano (Vitric Andosol) and already well developed on the Eastern flank (Silandic Andosols) with high

desilication degree as depicted by the presence of gibbsite (*Chapter 2*). Soils formed from pyroclastic deposits of andesitic-dacitic composition with plagioclase, pyroxene and volcanic glass as the dominant weatherable minerals (Boudon et al., 1987; Dagain, 1981; Komorowski et al., 2005; Ndayiragije, 1996).

6.3 Material and methods

6.3.1 Studied plots and general sampling scheme

An evergreen tropical forest plot (0.73 ha) at mean altitude of 396 m above sea level (asl) (FO-396) and a banana (*Musa acuminate* L. cv. ASIA) plot (0.5 ha) at mean altitude of 343 m asl (BA-343) close to each other were selected on the Eastern flank of the volcanic massif (Figure 6-1a, b). MAR is 4400 mm under the FO-396 plot and 4200 mm under the BA-343 plot. Soils are described as perhydrated Andosols on the soil map (Colmet-Daage and Lagache, 1969) and developed from lapilli pyroclastic deposits of andesitic-dacitic composition of 30,000 to 18,000 year old. The cultivated plots of this area are called “the concessions” because they were granted to former slaves following the abolition of slavery in Guadeloupe in 1848. We can therefore estimate that the BA-343 plot is cultivated since at least this date even if banana plantations did not appear before the beginning of the twentieth century. Before being planted for bananas, these plots were probably used for household food production. They were therefore probably relatively diversified: orchards, vegetable gardens, livestock, etc.

Mahogany (*Swietenia macrophylla*) were planted on the FO-396 plot in the 1960s for logging. However, this logging has never been exploited and is now abandoned. Plant species were inventoried and trees with a diameter at breast height (dbh) of more than 10 cm were counted (Table 6-1). Thirty-four different plant species were identified. Three species were largely dominant in term of population size. *Swietenia macrophylla* (35%), *Cyathea muricata* (22%), *Sterculia caribaea* (12%). One species was not very present in the tree stratum (dbh > 10 cm) but was predominant in the shrub stratum (*Myrcia deflexa*).

For the FO-396 plot, plant, soil and drainage water samples were collected in order to estimate pools and fluxes of the soil-plant Si cycle. For the BA-343 plot, plant and soil samples were collected in order to measure the Si concentration in banana leaves, and estimate the soil Si pools.

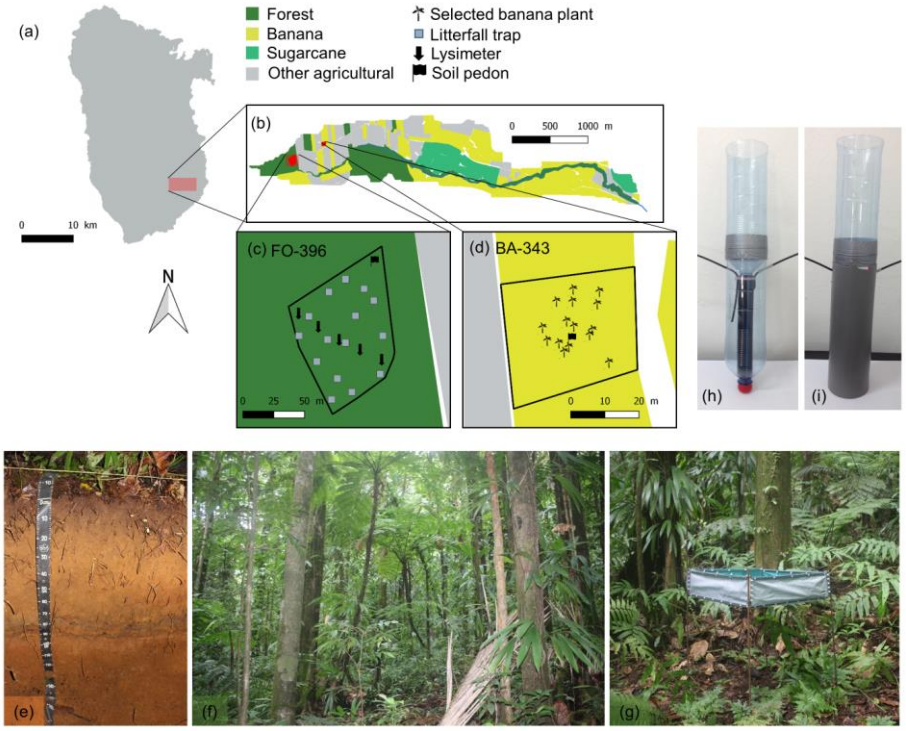

Figure 6-1: (a) Location of the Pères River watershed on the Basse Terre Island; (b) Land use map of the Pères River watershed and location of the studied plots; (c) Location of the litterfall traps, lysimeters, and soil pedon on the *FO-396* plot; (d) Location of the selected banana plants, and soil pedon on the *BA-343* plot; pictures of (e) the *FO-396* soil pedon, (f) *FO-396* plot, (g) a litterfall trap, (h) a lysimeter without its protective sheath, (i) a lysimeter with its protective sheath.

Table 6-1: Inventory of the plant species of the forest plot, and, for each species, the number of trees with a diameter at breast height (dbh) above 10 cm.

Species	**Number of tree with dbh > 10 cm**
Aniba bracteata	0
Asplundia rigida	0
Aspnudia insignis	0
Byrsonima trinitensis	0
Cecropia schreberiana	6
Cedrela odorata	0
Chimarrhis cymosa	12
Cordia sulcata	3
Cyathea muricata	141
Eugenia trinervia	0
Garcinia humilis	1
Guatteria caribaea	0
Inga ingoides	2
Miconia mirabilis	10
Myrcia deflexa	1
Nephrolepis rivularis	0
Ocotea leucoxylon	2
Ormosia monosperma	2
Philodendron gigantea	0
Phyllanthus mimosoides	0
Prestoea montana	36
Psychotria urbaniana	0
Richeria grandis	0
Rudgea citrifolia	5
Salpichlaena volubilis	0
Sapium glandulosum	1
Selaginnalla flabellata	0
Simarouba amara	17
Sloanea dentata	12
Sloanea massonii	17
Sterculia caribaea	75
Swietenia macrophylla	226
Tapura latifolia	8
Thelypteris reticulata	0

6.3.1.1 Plant sampling

FO-396 plot

Fifteen litterfall traps (0.75cm x 0.75cm) were randomly set so that there was at least 10 meters between them (Figure 6-1c,d). They were sampled regularly (maximum 3 weeks between two sampling) during 9 months from January 2017 to October 2017. Litterfall traps were randomly divided into

five groups. At sampling, litterfall traps were collected in bags corresponding to their group. At the laboratory, foliar samples were separated from non-foliar one. Leaves were then separated into three groups: *Swietenia macrophylla* (SM) leaves, *Myrcia deflexa* (MD) leaves, and other species (OS) leaves. SM leaves were separated from other species as SM was the dominant species. MD leaves were separated because of their particular high Si concentration. All other leaves were gathered into one composite samples because they had intermediate Si concentrations. Samples were weighted fresh, washed with deionized water, and weighted after drying in a stove at 70°C for one week. At the end of the sampling period, all samples belonging to the same group were gathered for analysis. Twenty composite samples were therefore generated: 5 non-foliar samples, 5 SM leaves samples, 5 MD leaves samples, and 5 OS leaves samples.

BA-343 plot

We selected fifteen banana plants of similar crop yield potential at flowering stage (Figure 6-1d). For each plant, we sampled the center (100 mm width) of the antepenultimate leaf (leaf III), following the international standard set up for banana foliar diagnosis (Martin-Prével, 1980). The fifteen plants were further randomly divided in five groups. Samples belonging to the same group were mixed up as a composite leaf sample.

6.3.1.2 Soil sampling

FO-396 plot

Two topsoil (00-20 cm) samples were collected close to each litterfall trap. The thirty soil samples were then assembled into composite samples respecting the same group as for the litterfall samples. A soil pedon was also described and sampled down to 120 cm depth. Each horizon was sampled, leading to a total of 7 samples. Undisturbed soil samples were collected (Kopecky) to determine the soil bulk density, at field soil moisture and dry.

BA-343 plot

Two topsoil (00-20 cm) samples were collected at 40 cm of the foot of each of the fifteen selected banana plants. The thirty soil samples were then assembled into composite samples respecting the same grouping as for the

plant samples. A soil pedon was also described and sampled down to 80 cm depth. Each horizon was sampled, leading to a total of 4 samples. Undisturbed soil samples were collected (Kopecky) to determine soil bulk density, at field soil moisture, and dry.

6.3.1.3 Sampling of gravity water under forest

Five zero-tension lysimeters were settled to collect gravity water at 60 cm depth. Water was collected in the lysimeters every ~200 mm of rainfall from January 2017 to July 2017. Collected water was then filtered through a 0.2 μm polycarbonate membrane and acidified at 0.25% Suprapur nitric acid. For each plot, 20 samples collected at two different times were then selected for analyses.

6.3.2 Plant analysis

For the 25 plant composite samples (20 for the FO-396 plot and 5 for the BA-343 plot), mineral analysis was carried out after calcination at 450°C for 1 day and fusion in Li-metaborate + Li-tetraborate at 1,000°C (Chao and Sanzolone, 1992), followed by ash dissolution with Suprapur HNO_3. Nutrient and Si concentrations were measured by inductively coupled plasma-atomic emission spectrometry (ICP-AES).

6.3.3 Soil analysis

6.3.3.1 Basic analyses

Analyses were carried on the fine earth (<2 mm) of the 21 soil samples. pH was measured in H_2O and 1 M KCl in 1:5 soil:solution suspensions. Cation exchange capacity (CEC) and exchangeable bases were measured using a 1 M ammonium acetate pH 7 solution (Olsen et al., 1982). Total C contents were determined by high temperature dry combustion using a Vario EL Cube elemental analyzer. Total elemental contents were measured by inductively coupled plasma-atomic emission spectrometry (ICP-AES) after fusion in Li-metaborate and Li-tetraborate at 1000°C and further dissolution of the cooled melt in 2 M Suprapur HNO_3 (Chao and Sanzolone, 1992). The contents of major alkaline and alkaline-earth cations were summed up to compute the Total Reserve in Bases (TRB) (Herbillon 1986). Dark oxalate-extractable (o), dithionite-citrate-bicarbonate (DCB) extractable (d) and pyrophosphate-extractable (p) contents of Si, Al and Fe were determined in the respective

extracts by ICP–AES following the methods compiled in Dahlgren (1994). These selective extractions are used to estimate the amounts of different soil components. Using the $(Al_o\text{-}Al_p)/Si_o$ values allowed to estimate allophane content (Parfitt and Henmi, 1982; Parfitt and Wilson, 1985). Fe_o values estimate the ferrihydrite content (Mizota and Van Reeuwijk, 1989). Fe_t, Fe_d and Fe_o values estimate the quantity of Fe in silicate minerals (Fe_t-Fe_d) and in crystalline sesquioxides (Fe_d-Fe_o) and the degree of individualization of free iron (Fe_d/Fe_t). Al_p refers to Al complexed by organic matter.

6.3.3.2 Specific Si extractions

$CaCl_2$. $CaCl_2$-extractable Si content ($CaCl_2$-Si) is considered to assess the bioavailable Si pool in soils (Haysom and Chapman, 1975; Sauer et al., 2006). It was estimated in a 0.01 M $CaCl_2$ solution (4g of soil for 40 ml of solution) after 6h of shaking (Cornelis et al., 2011; Sauer et al., 2006). Si concentration is measured by ICP-AES after having diluted 10 times and acidified the solution.

Na_2CO_3. Na_2CO_3 extractable Si (Na_2CO_3-Si) was estimated by a kinetical extraction method modified from DeMaster (1981). Forty milligrams of soil pretreated by a dark oxalate extraction (Dahlgren, 1994) and by a 6h rinsing with a $CaCl_2$ 0.01 M solution was mixed with 40 ml of 0.1 M Na_2CO_3 at 85°C during 7h (*Chapter 3*). One milliliter of solution was collected after 15, 60, 120, 180, 240, 300, 360, and 420 min, diluted with 9 ml of deionized water and acidified with 50 µl of Suprapur HNO_3. Si, Al, Fe, and Mg concentrations were measured at each time. From the kinetical extraction, the amorphous Si content was estimated using the dissolution rate method presented in the *Chapter 3* of this thesis. This content is named ox-Na_2CO_3-Si. The ox-Na_2CO_3-Si pool only includes the PhSi pool and possibly Na_2CO_3 extractable lithogenic silicates (LSi) as amorphous pedogenic silicates (PSi) were removed by dark oxalate extraction. Until now, no method allows to discern PhSi and Na_2CO_3 extractable LSi pools in such soils. We therefore decided to consider the ox-Na_2CO_3-Si pool as mainly composed of PhSi in surface horizons and LSi in deeper horizons.

6.3.4 Drainage water analysis

Major element concentrations (Al, Fe, Si, Ca, Mg, K, Na, Mn, P and S) were determined by ICP-AES. Detection limit (ppb) was 10, 2, 5, 10, and 10 for Si, Ca, Mg, K, and Na respectively, and precision is <0.5%.

6.3.5 Calculation of the Si pools and fluxes

6.3.5.1 Si pools.

The soil Si pool that includes the LSi and PSi pools, PhSi pool, and DSi pool were quantified as described in the *Chapter 5* of this thesis (Equation 1).

$$Pool_i = Concentration_i \times \rho_d \times depth \times surface\ [kg\ ha^{-1}] \quad Eq\ (1)$$

$Pool_i$ is the Si pool of the component i (kg ha^{-1}); $Concentration_i$ is the Si concentration of the component i (kg [kg of dry soil]$^{-1}$); ρ_d is the dry bulk density of the soil ([kg of dry soil] m^{-3}); *depth* is the depth of the soil considered (in our case 20 cm); *surface* is the surface considered (in our case 1 ha or 10,000 m^2). For the PhSi pool, the concentration was the mean ox-Na_2CO_3-Si concentration in the topsoil (00-20 cm). The ox-Na_2CO_3-Si pool in the topsoil is mainly represented by the PhSi pool as Na_2CO_3 extractable PSi pools have been previously removed by dark oxalate, and Na_2CO_3 extractable LSi pools can be neglected in topsoil samples (as discussed in *Chapter 2* and *Chapter 3*). The DSi concentration was the mean $CaCl_2$-Si concentration.

The inorganic Si (ISi) pool was roughly estimated with Equation (2).

$$ISi = TSi - oxNa_2CO_3Si\ \ [kg\ ha^{-1}]\ \ Eq\ (2)$$

The Si in standing biomass was estimated for the FO-396 plot by multiplying the standing biomass reported for hygrophile forest in Guadeloupe (747 t ha^{-1} FAO, 2010) to the concentration of Si in non-foliar samples.

6.3.5.2 Si fluxes of the forest

Si fluxes in the soil-plant system are: Si absorbed by plants, PhSi restituted to soil, PhSi dissolution, dissolution of LSi and PSi minerals including PSi neoformation, and the leaching of DSi to the hydrosphere. We can directly quantify the PhSi restitution to soil, and the Si leached out. The amount of Si absorbed by the plants was estimated by considering an annual net primary

productivity of zero and no exports of plant materials. The quantity of Si released by the dissolution of PhSi and by the dissolution of the ISi pool was thereafter estimated by considering a steady-state soil-plant Si cycle.

Fluxes from plants to soil were estimated with Equation (3).

$$Flux_{Si} = \sum_{j=1}^{n} (Concentration_{Si} \times Dry\ weight)_j \ \ [kg\ ha^{-1} yr^{-1}]\ Eq\ (3)$$

Flux$_{Si}$ is the flux of Si (kg ha^{-1} yr^{-1}); *Concentration*$_{Si,j}$ is the mean concentration of Si in the sample j (kg [kg of sample j]$^{-1}$); *Dry weight*$_j$ is the mean total dry weight of the sample j that is restituted on soil ([kg of sample j] ha^{-1} yr^{-1}). The sum of the n different samples allowed to estimate the total annual flux.

Fluxes with drainage waters were estimated by Equation (4).

$$Flux_{Si} = Concentration_{Si} \times Water\ infiltration\ [kg\ ha^{-1} yr^{-1}]\ Eq\ (4)$$

Flux$_{Si}$ is the flux of Si (kg ha^{-1} yr^{-1}); *Concentration*$_{Si}$ is the mean concentration of Si in the drainage water (kg l^{-1}); *Water infiltation* is the total volume of water that infiltrates per ha on the respective plot (l ha^{-1} yr^{-1}).

The water infiltration is estimated based on mean annual rainfall, evapotranspiration and runoff data (Equation (5)).

$$Water\ infiltration = Rainfall - Evapotranspiration - Runoff\ [m^3 ha^{-1} yr^{-1}]\ Eq\ (5)$$

Evapotranspiration (ET) was assessed following Crabit et al. (2016) and as explained in the *Chapter 5* of this thesis (Equation 6).

$$ET_0 = -0.7205\ A + 1406\ [mm\ yr^{-1}]\ Eq\ (6)$$

ET_0 is the annual reference evapotranspiration, and A is the altitude. Equation 6 and the mean altitude of the FO-396 plot were used to compute the annual ET_0.

To simplify the model, we hypothesized that runoff is negligible on the studied plot. Indeed, infiltration at saturation of soils of the studied zone is large and runoff is a rare phenomenon (Cattan et al., 2007; Charlier et al., 2008).

6.3.6 Statistical analyses

The significance of the difference between the different concentrations, pools and fluxes were tested through ANOVA 1 statistical tests performed with the *aov* function of the R programing language.

6.4 Results

6.4.1 Soil properties

The main physico-chemical characteristics of soil horizons under forest and banana are given in Table 6-2. In the forest soil pedon, pH-H_2O increased at depth from 4.1 in Ah1 to 5.7 in Bw2, and 5.6 in 2BC. pH-KCl followed the same trend and is always below pH H_2O. In the banana soil pedon, pH-H_2O was rather constant in all horizons (from 5.3 to 5.5), and pH-KCl followed the same trend being always below pH-H_2O. Soil organic carbon (SOC) content decreased at depth in the two pedons: from 167 g kg^{-1} in Ah1 to 6.1 g kg^{-1} in 2BC under forest, and from 6.42 g kg^{-1} in AB to 0.92 g kg^{-1} in BC under banana. In the forest soil pedon, CEC ranged between 35.8 and 61.3 $cmol_c$ kg^{-1}. In the banana soil pedon, CEC ranged between 45.1 and 52.1 $cmol_c$ kg^{-1}. The exchange complex was desaturated in all horizons. Ca and Mg were the dominant cations on the exchange complex. In the forest soil pedon, allophane content was very low in Ah1, Ah2, and AB horizons, and relatively high in Bw1, Bw2, and 2BC horizons. In the banana soil pedon, allophane content increased from 7.2% in AB to 33.2% in BC. TRB fluctuated along the forest soil pedon from 67 to 173 $cmol_c$ kg^{-1}. In the banana soil pedon, TRB ($cmol_c$ kg^{-1}) increased from 123 in AB to 165 in Bw, and 152 in BC. Fe_d/Fe_t was minimal in 2BC of the forest soil pedon (0.24), and fluctuated between 0.52 and 0.60 in the other horizons. In the banana soil pedon, Fe_d/Fe_t decreased from 0.53 in AB to 0.37 in BC and 2A horizons. Mg was the dominant cation on the TRB in all horizons (from 67.8% to 84.8%), followed by Ca (from 10.1% to 25.8%), Na (from 3.20% to 7.01%), and K (from 1.60% to 6.21%).

Table 6-2: Main soil properties of soil horizons of forest plot (FO-173) and banana plot (BA-343) pdeons: Texture, bulk density, pH, contents of OC, allophane, ferrihydrite and TRB with the cation proportions in TRB, Fe_d/Fe_t ratio, CEC and contents of exchangable bases.

Hor	Depth	Texture (%)			Bulk density	pH		C	CEC	Exch Bases ($cmol_c\ kg^{-1}$)				Allo-phane[a]	Ferri-hydrite[b]	Fe_d/Fe_t	Al_p/Al_o	TRB	Contribution on TRB (%)[c]			
	cm	clay	silt	sand	g cm^{-3}	H_2O	KCl	g kg^{-1}	$cmol_c$ kg^{-1}	Ca	Mg	K	Na	%	%			$cmol_c$ kg^{-1}	Ca	Mg	K	Na
FO-396 soil pedon																						
Ah1	0-8	36	46	18	0.28	4.2	4.1	167	61.3	2.32	1.37	0.32	0.31	1.9	3.35	0.60	0.79	173	25.8	67.8	1.60	4.72
Ah2	8-16	45	32	23	0.32	4.4	4.2	112	54.1	0.45	0.30	0.20	0.22	2.6	3.71	0.60	0.75	102	14.6	73.4	5.19	6.89
AB	16-30	56	26	18	0.37	5.0	4.6	62.7	35.8	0.13	0.13	0.14	0.15	4.9	4.61	0.52	0.59	119	14.3	77.4	3.94	4.44
Bw1	30-55	65	20	15	0.52	5.2	4.9	43.4	49.2	0.05	0.07	0.09	0.17	24.0	5.43	0.61	0.18	67	12.3	74.9	6.21	6.60
Bw2	55-70	51	23	26	0.46	5.7	5.4	25.0	50.0	0.03	0.05	0.15	0.10	35.3	4.28	0.55	0.08	99	13.5	73.8	6.06	6.66
2BC	70-88	34	22	37	nd	5.6	5.2	6.1	42.9	0.22	0.26	0.09	0.15	18.7	1.64	0.24	0.05	116	10.1	84.8	1.92	3.20
3A	88-90	62	21	17	nd	5.3	4.2	7.2	41.9	1.19	3.28	0.09	0.52	5.9	1.41	0.53	0.18	106	14.1	72.2	6.75	7.01
3 Bw	90-120	nd	nd	nd	nd	5.3	5.4	23.4	nd	nd	nd	nd	nd	22.9	0.91	nd	0.07	nd	nd	nd	nd	nd
BA-343 soil pedon																						
AB	0-45	48	12	24	nd	5.3	4.6	64.2	52.1	2.04	0.79	0.55	0.19	7.2	2.61	0.53	0.49	123	15.6	74.3	4.90	5.12
Bw	45-55	47	40	13	nd	5.5	5.0	12.1	49.6	0.74	0.57	0.54	0.17	15.3	1.45	0.51	0.18	165	16.6	75.8	3.69	3.99
BC	55-70	46	30	24	nd	5.5	5.4	9.2	53.9	0.33	0.28	0.16	0.09	33.2	2.68	0.37	0.04	152	16.4	76.3	3.73	3.50
2A	70-80	66	13	16	nd	5.4	4.4	12.9	45.1	1.06	1.39	0.55	0.53	8.2	1.63	0.37	0.14	133	11.8	77.9	4.75	5.63

Values in parentheses are standard errors.

[a]Allophane content was estimated according to Parfitt and Wilson (1985), using $(Al_o\text{-}Al_p)/Si_o$ ratios. Results of DCB, oxalate, and pyrophosphate analyses are presented in Table 6-S1.

[b]Ferrihydrite content was estimated according to Parfitt and Childs (1988) assuming complete dissolution with dark acid oxalate, using 1.7 x Feo.

cContribution on TRB were calculated using total contents of Ca, Mg, K, and Na (results of total analysis are given in Table 6-S2).

6.4.2 Plant analyses

Plant mineral contents are given in Table 6-3, where Si concentrations, mass fluxes and Si fluxes are given. Si concentration (g kg^{-1}) increased in the order: non-foliar (1.119±0.3331) < other species leaves (1.620±0.0959) < banana leaves III (5.583±0.825) < *Swietenia macrophylla* leaves (9.575±3.128) < *Myrcia deflexa* leaves (40.61±5.739). Mass flux from plant to soil (kg ha^{-1} yr^{-1}) increased in the order: *Myrcia deflexa* leaves (174.9±33.44) < other species leaves (1816±363.6) < non-foliar (2473±606.2) < *Swietenia macrophylla* leaves (3102±1509). Resulting Si fluxes from plants to soil (kg ha^{-1} yr^{-1}) increased in the order: non-foliar (2.767±1.502) < other species leaves (2.942±0.7633) < *Myrcia deflexa* leaves (7.104±2.362) < *Swietenia macrophylla* leaves (29.71±24.15). In the FO-396 plot, the total Si flux from plant to soil amounted to 42.52 kg ha^{-1} yr^{-1}. The Si in standing biomass of the FO-396 plot was 836 kg ha^{-1}.

Table 6-3: Si concentrations, mass fluxes, and Si fluxes of the different plant samples of the forest.

	Non-foliar	SM[a] leaves	MD[b] leaves	OS[c] leaves	Banana leaves
Si concentration (g kg^{-1})	1.12 (0.33)	9.58 (3.13)	40.61 (5.74)	1.62 (0.10)	5.58 (0.83)
Mass flux (kg ha^{-1} yr^{-1})	2473 (606.2)	3103 (1509)	174.9 (33.44)	1816 (363.6)	nd
Si fluxes (kg ha^{-1} yr^{-1})	2.77 (1.50)	29.71 (24.15)	7.10 (2.36)	2.94 (0.76)	nd

[a]SM corresponds to *Swietenia macrophylla*, [b]MD corresponds to *Myrcia deflexa*, [c]OS corresponds to other species.
Values in parentheses are standard errors

6.4.3 Soil Si pools

The quantified soil Si pools are the ISi pool that includes the LSi and PSi pools, the ox-Na_2CO_3-Si pool mainly composed of the PhSi pool, and the $CaCl_2$-Si pool that represents the DSi pool. All these pools are given for the topsoil (00-20 cm) of the FO-396 and BA-343 plots in Table 6-4. All these pools were significantly ($p < 0.001$) larger in the banana topsoil than in the forest topsoil. However, the PhSi and DSi concentrations (mg kg^{-1}) were larger in the forest topsoil (6001 and 14.35, respectively) than in the banana topsoil (5024 and

12.72, respectively); the ISi concentration (g kg^{-1}) was larger in the banana topsoil (139.4) than in the forest topsoil (121.7).

Table 6-4: Average inorganic (LSi + PSi), phytogenic (PhSi), and dissolved Si (DSi) pools in the topsoil (00-20 cm) in the FO-396 and BA-343 plots.

	ISi (LSi + PSi)		**PhSi (ox-Na_2CO_3-Si)**		**DSi ($CaCl_2$-Si)**	
	t ha^{-1}	**g kg^{-1}**	**kg ha^{-1}**	**mg kg^{-1}**	**kg ha^{-1}**	**mg kg^{-1}**
FO-396	68.15 (1.337)	121.7 (2.387)	3361 (181.8)	6002 (324.6)	8.035 (0.3995)	14.35 (0.7135)
BA-343	170.8 (8.409)	139.4 (6.859)	6160 (661.9)	5024 (539.9)	15.59 (1.021)	12.72 (0.8331)

Values in parentheses are standard errors.

6.5 Discussion

6.5.1 Andosol properties

Analyses of the soil pedons pointed the forest soil as an Aluandic Hydric Dystric Andosol (Fulvic), and the banana soil as Silandic Dystric Andosol according to the WRB classification system (IUSS 2014). In the forest soil, the very large content in SOC in Ah1, Ah2, and AB horizons greatly influenced the properties of these horizons. Aluminum cation was mainly complexed with soil organic matter (SOM), preventing the formation of short range-ordered (SRO) minerals (Shoji et al., 1993) as illustrated by the high Al_p/Al_o ratios, and the low allophane content (<5%). Micro-aggregation involving organo-mineral associations as well as SRO minerals resulted in a low bulk density. In mineral horizons, allophane content was larger as the SOC content decreased. The soil exchange complex was desaturated in all horizons. In Ah1, exchangeable and total Ca, Mg, and K cations were larger than in other horizons (Table 6-2 and 6-S2). This is likely due to the uptake of these cations by plants that further return it on the topsoil by litterfall.

TRB and Fe_d/Fe_t can be used as indicators of the soil weathering stage (Herbillon, 1986). The regular decrease in SOC from Ah1 to Bw2 suggests that these horizons could belong to the same weathered ash layer. The progressive decrease in TRB from Ah1 to Bw1 may account for an enrichment of fresh ash in the topsoil or the biological cycle of nutrients (Jobbágy and Jackson, 2001). From Bw2 to 3Bw, TRB varies in a narrow range (99-116 $cmol_c$ kg^{-1}). The depth-variation of Fe_d/Fe_t supports that the sequence Ah1-Bw2

(Fe_d/Fe_t = 0.5-0.6) belongs to the same weathered ash deposit. This ratio abruptly decreased in 2BC (0.24), then increased in 3A (0.53).

The banana pedon had a thick AB horizon resulting from tillage practices. SOC progressively decreased from AB to BC.

6.5.2 In the forest, the biological Si feedback loop is controlled by two species

In the studied forest, the annual Si uptake by plants (kg ha^{-1} yr^{-1}) amounted to 42.52. Annual Si uptakes by tropical forests (kg ha^{-1} yr^{-1}) amounted to 7 (Meunier et al., 2010), 21-50 (Lucas, 2001), 58-76 (Alexandre et al., 1997), or even 450-670 in the particular case of a bamboo forest (Meunier et al., 1999). In our study, Si plant uptake was thus in the same range as that reported by Alexandre et al. (1997) and Lucas (2001) for tropical forests that developed on Ferralsols. In our case, two species (*Myrcia deflexa* and *Swietenia macrophylla*) contributed to 86.6% of total Si uptake and Si restitution on soil. *Myrcia deflexa* was rather negligible in terms of mass fluxes, but accumulated important amounts of Si. *Swietenia macrophylla* was the dominant species in terms of mass fluxes, and accumulated important amounts of Si, and therefore contributed to 69.9% of the total Si bio-cycling. In the studied forest, Si bio-cycling therefore greatly depended on *Swietenia macrophylla* as dominant species. As *Swietenia macrophylla* trees were planted about fifty years ago, we can consider that Si bio-cycling is strongly disturbed by human forest management. Excluding this species, Si bio-cycling would amount to 12.81 kg ha^{-1} yr^{-1}, which is closer to the Si bio-cycling measured by Meunier et al. (2010) in a tropical forest that developed on poorly weathered volcanic soils. Therefore, Si fluxes in the studied forest are controlled by plant species because of human forest management. The abundance of high Si-accumulating species in forest ecosystems is thus a very important factor impacting plant Si uptakes. Extreme cases are bamboo forests, the natural environments with the highest density of high Si-accumulating plants. They recycle the largest Si quantities through plant uptake and litterfall (Li et al., 2006; Meunier et al., 1999; Umemura and Takenaka, 2014), and may impressively impact the PhSi storage in soil (Meunier et al., 1999).

6.5.3 The PhSi storage in soil and resultant Si fluxes

Part of the phytoliths returned to soil is stabilized in soil and may further migrate in the soil profile (Alexandre et al., 2011, 1997; Blecker et al., 2006). However, we were not able to estimate this part in the studied soils (*Chapter 5* for justifications). Therefore, two scenarios were assumed, as based on literature data (Table 6-5): Scenario (1): PhSi storage of 8% (Alexandre et al., 1997); Scenario (2): PhSi storage of 31% (Blecker et al., 2006) (*Chapter 5*).

Depending on the scenario, PhSi storage ranged from 3.64 (Scenario 1) to 13.18 kg ha^{-1} yr^{-1} (Scenario 2). Resulting PhSi dissolution ranged from 29.34 (Scenario 2) to 39.12 kg ha^{-1} yr^{-1} (Scenario 1) (Figure 6-2). Considering a steady-state Si cycle, the dissolution of LSi and PSi pools, including neoformation of PSi minerals, amounted to 87.79 kg ha^{-1} yr^{-1} with Scenario 1, and 97.57 kg ha^{-1} yr^{-1} with Scenario 2 (Figure 6-2).

Table 6-5: Si fluxes estimated for the FO-396 plot assuming PhSi storage of 8 and 31%.

	PhSi storage	**DSi uptake by plants**	**PhSi input to soil**	**PhSi dissolution in soil**	**DSi output by lixiviation**	**Mineral dissolution[1]**
	%			**kg ha^{-1} yr^{-1}**		
FO-396	8	42.52	42.52	39.12	84.39	87.79
		(28.78)	(28.78)	(26.48)	(5.752)	(8.052)
FO-396	31	42.52	42.52	29.34	84.39	97.57
		(28.78)	(28.78)	(19.86)	(5.752)	(14.67)

[1]The mineral dissolution includes the neoformation of secondary silicates.
Values in parentheses are standard errors.

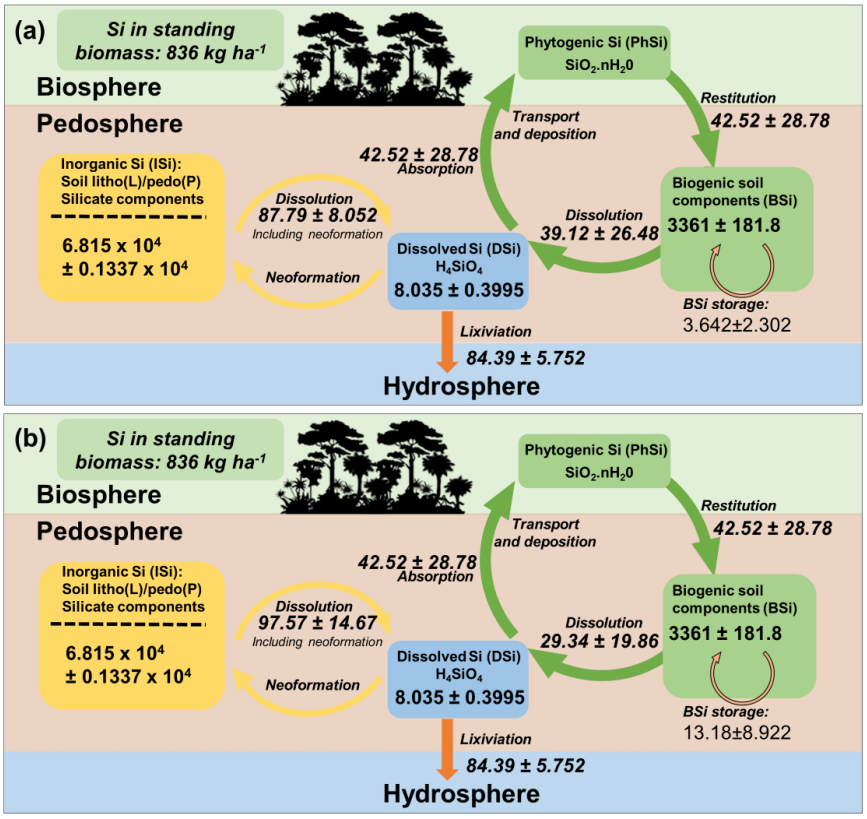

Figure 6-2: Steady-state soil-plant Si cycle established for the forest plot assuming (a) 8% of PhSi storage, and (b) 31% of PhSi storage.

6.5.4 How do plants impact the mineral Si feedback loop?

Plants promote mineral weathering through Si uptake from soil solution (Alexandre et al., 1997; Blecker et al., 2006; J-T Cornelis et al., 2011; Drever, 1994; Moulton et al., 2000). When phytolith dissolution does not match the plant uptake, the Si deficit is compensated through LSi and PSi weathering (Blecker et al., 2006). As a part of plant Si is mostly stored for long periods (Alexandre et al., 2011, 1997; Blecker et al., 2006; Yang and Zhang, 2018), phytolith dissolution does not match Si plant uptake. Therefore, the biological Si feedback loop promotes LSi and PSi dissolution (Alexandre et al., 2011, 1997; Bartoli, 1983; Blecker et al., 2006; Lucas et al., 1993; Yang and Zhang, 2018). In the FO-396 plot, without any biological Si feedback loop, LSi

and PSi dissolution would amount to 84.4 kg ha^{-1} yr^{-1}. However, when we considered the biological Si feedback loop, depending on the scenario, LSi and PSi dissolution ranged from 87.79 (Scenario 1) to 97.57 kg ha^{-1} yr^{-1} (Scenario 2) (Figure 6-2 and Table 6-5). Plant Si uptake therefore increased LSi and PSi dissolution from 3.4 to 13.18 kg ha^{-1} yr^{-1}, depending on the scenario. This is in the same range of values as the ones reported for tropical forest (6 kg ha^{-1} yr^{-1}, Alexandre et al. 1997), grasslands (4 to 16 kg ha^{-1} yr^{-1}, Blecker et al. 2006), temperate forests (4 to 6 kg ha^{-1} yr^{-1}, Bartoli 1983), but lower than savanna ecosystems (24 to 76 kg ha^{-1} yr^{-1}, Alexandre et al. 2011). This can be explained by a combination of two factors that favor LSi and PSi dissolution in savanna ecosystems: (i) the dominance of high Si-accumulating plants in these ecosystems, and (ii) the exports of Si by ash exportations resulting from human fires.

6.5.5 The transition from forest to banana plantation: impacts on the Si cycle

Converting forest into cropland impacts the Si cycle (Barão et al., 2014; Guntzer et al., 2012; Struyf et al., 2010; Vandevenne et al., 2015; *Chapter 4*). Here, forest Si uptake and return to soil are compared to the ones of a banana plot located 2.8 km away from the FO-396 plot (*Chapter 5*), named BA-173 (altitude in m asl). The soils from FO-396 and BA-173 plots did not differ in weathering stage (TRB BA-173 = 94.3 $cmol_c$ kg^{-1} and TRB FO-396 = 106.3 $cmol_c$ kg^{-1}). The banana leaf Si content did not significantly differ between BA-343 and BA-173, although the pool of $CaCl_2$-Si was significantly lower in BA-343 (15.6 ± 1.02 kg ha^{-1}) than in the BA-173 (48.5 ± 14.3 kg ha^{-1}). Comparison between the soil-plant Si cycle between BA-173 and FO-396 would therefore allow us to determine the impact of land use on this cycle.

Table 6-6: Mean Si concentrations in banana leaf III of BA-343 and BA-173 plots.

	BA-345	**BA-173**
Si banana leaf III (g kg^{-1})	5.56 (0.83)	4.98 (0.34)

Values in parentheses are standard deviations.

The forest ecosystem exhibits a very large standing biomass (747 t ha^{-1}, FAO 2010 see Section 6.3.5), whereas the cultivated ecosystem has a lower biomass (about 14.3 t ha^{-1}, *Chapter 5*). The Si mineralomass in standing forest biomass was estimated from the standing biomass given for hygrophile

forest in Guadeloupe (FAO, 2010) and the average Si concentration in non-foliar samples (1.1 g kg^{-1}). It amounted to 836 kg Si ha^{-1}. The Si mineralomass in BA-173 at harvest amounted to 54 kg Si ha^{-1}.

However, annual net primary productivity was lower in FO-396 (about 7.6 t ha^{-1} yr^{-1} – estimated with annual biomass return in litterfall traps and considering steady-state) than in BA-173 (about 28.6 t ha^{-1} yr^{-1} – estimated with the total biomass at harvest and considering two harvests per year). Firstly, because wood production requires much more energy than that of non-ligneous banana shoots. Secondly, because biomass production in croplands is enhanced by the use of fertilizers and phytosanitary products. Annual plant Si uptakes (kg ha^{-1} yr^{-1}) were therefore four times larger in BA-173 (171.4±21.70) than in FO-396 (42.52±28.78). Since Si exports by harvest were relatively low for BA-173 (see *Chapter 5*), annual Si restitutions on soil (kg ha^{-1} yr^{-1}) for the BA-173 (161.3±20.71) were also ~4 times larger than for FO-396 (42.52±28.78).

Finally, Si leaching amounted to 84.4 kg ha^{-1} yr^{-1} for FO-396 and to 106.3 kg ha^{-1} yr^{-1} for BA-173. In the forest, Si leaching beneath the trees root systems might be below the estimated value since tree rooting systems are much deeper than 60 cm (Canadell et al., 1996). The value given here is therefore a maximum. In contrast, banana crop has a very shallow root system (~85% of the roots in the top 35 cm) (Delvaux and Guyot, 1989; Gousseland, 1983b). The large total soil Ca, Mg, and K contents in the upper horizons of the FO-396 plot may be due to biological pumping, which uplifts nutrients from deep to surface horizons (Jobbágy and Jackson, 2001) through root uptake and further litterfall (see Section 6.5.1). We think that the slightly lower Si leaching at 60 cm depth under the forest could be due to two reasons. Firstly, in the forest, the litter forms an environment with a very dense root network (Figure 6-3) in which limiting nutrients are concentrated (Jobbágy and Jackson, 2001), and the turnover of C and nutrients is large (Greenland and Nye, 1959). This could partly explain the lower Si output by leaching in the FO-396 plot. However, as the banana crop ecosystem was exclusively covered by Si-accumulating plants, Si uptake was still larger for the BA-173 plot than for the FO-396 plot despite the more efficient rooting systems of the forest. Secondly, DSi is highly mobile in well drained soils as it is uncharged ($H_4SiO_4^0$) (Nguyen et al., 2016). Therefore, rainfall strongly affects

the Si concentration in the soil solution (*Chapter 2*), affecting Si exports through leaching.

Figure 6-3: Picture of the very dense root network of the litter in the FO-396 plot.

Therefore, land use greatly impacts the soil-plant Si cycle in our case study. In the forest ecosystem, Si was mainly stored in the standing biomass, with relatively low Si bio-cycling. In the banana crop ecosystem, Si bio-cycling was intense but with little Si in the standing biomass (Figure 6-4).

In the BA-173 plot, the biological Si feedback loop increased mineral weathering from 23.0 to 60.1 kg Si ha^{-1} yr^{-1} depending on the scenario (*Chapter 5*). These values were therefore larger than for the forest ecosystem (from 3.4 to 13.2 kg Si ha^{-1} yr^{-1}). This is due to the larger Si uptake by plants in the BA-173 plot than in the FO-396 plot, and to the Si exports through harvest in the BA-173 plot. Forest and banana crop land use therefore also impacted the dissolution of the LSi and PSi minerals. The ISi, ox-Na_2CO_3-Si, and $CaCl_2$-Si pools (kg ha^{-1}) in topsoil were all larger in the BA-343 plot (170800±8409; 6160±661.9; 15.59±1.021, respectively) than in the FO-396 plot (68150±1337; 3361±181.8; 8.035±0.3995, respectively) (Table 6-4). However, this was mainly due to the very low bulk density of the forest topsoil as ISi, ox-Na_2CO_3-Si, and $CaCl_2$-Si concentrations (mg kg^{-1}) in the BA-343 plot topsoil (139400±6859; 5024±539.9; 12.72±0.8331, respectively) were more comparable to ISi, ox-Na_2CO_3-Si, and $CaCl_2$-Si concentrations (mg kg^{-1}) in the FO-396 plot topsoil (121700±2387; 6002±324.6; 14.35±0.7135, respectively). Converting forest to cropland decreases SOC content, impacting soil aggregation, and bulk density. Moreover, tillage practices can also promote soil compaction. Soil ISi, PhSi and DSi pools (Table 6-4) in the

topsoil (00-20 cm) were much larger in the BA-343 plot likely because of the increase in bulk density due to management practices (Dorel et al., 2000).

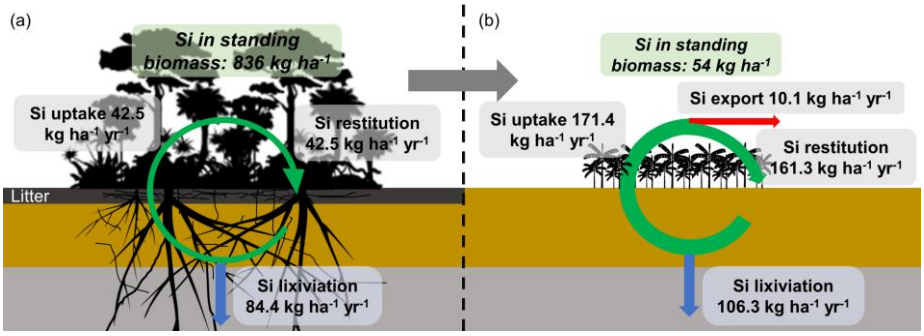

Figure 6-4: Comparison between the biological Si feedback loop of (a) the FO-396 plot, and (b) of the BA-173 plot. Si in standing biomass is much larger in the forest ecosystem than in the banana cropland. However, plant Si uptakes, and Si returns on soil by plants are much larger in the banana cropland than in the forest ecosystem. Si leaching is in the range of value even if slightly larger for the banana cropland.

6.6 Conclusion

The soil-plant Si cycle in the FO-396 plot was controlled by two plant species: *Swietenia macrophylla* and *Myrcia deflexa*. This demonstrated that species composition of a forest tremendously impacts the soil-plant Si cycle. Converting forest into banana cropland greatly impacts the soil-plant cycle of Si. In the forest ecosystem, Si is largely stored in the standing biomass, and the biological Si feedback loop is rather weak. In contrast, in the banana crop ecosystem, the biological Si feedback loop is intense, and strongly impacts mineral weathering, thus affecting LSi and PSi pools.

Chapter 7 Tracing silicon fluxes from forested and cultivated volcanic watersheds using Ge/Si ratio[5]

Abstract

Among the factors influencing silicon (Si) fluxes from continent to ocean, land use is determinant in temperate environments. These fluxes are expected to be particularly important from tropical volcanic islands. Here, we determined elemental concentrations and Ge/Si ratio in aqueous samples including groundwater, soil solution, river at base flow and during flood events within watersheds differing in land use, and covered by gibbsite-rich Andosols in Guadeloupe. Ge/Si ratios, Si and Al concentrations of soil solution indicate that phytoliths and lithogenic silicates were likely the main contributors of dissolved Si in soil solution. Simulations from a two components mixing model suggest that phytolith dissolution contributed to ~70-95% of dissolved Si in soil solution whatever the land use: banana, sugarcane or forest. Thus, here, land use did not influence the relative contribution of phytoliths to dissolved Si in soil solution. This is in agreement with previous results showing that, in the studied croplands, the exported quantity of phytoliths through crop harvest was negligible compared to the one returned to soil with plant residues. At base flow, Si fluxes toward river were controlled by groundwater, hence by mineral weathering. In contrast, during flood events, soil solution could impact the Si fluxes exported into rivers. The contribution of soil solution and/or runoff in croplands during intense flood events could be significant in small watersheds that were exclusively cultivated, but was not significant in large watersheds where forest dominated the upstream positions.

[5] Manuscript in preparation for submission in an international peer-reviewed journal.

7.1 Introduction

Silicon (Si) plays major ecological roles related to eminent global problematics in continental and marine ecosystems. In the latter, Si is a major nutrient for diatoms (photosynthetic phytoplankton). Si fluxes from terrestrial ecosystems to watersheds therefore impact the ocean capacity to fix C by controlling the diatom population (a.o. Ragueneau et al., 2006; Tréguer and Pondaven, 2000; Tréguer et al., 2018). Upstream, in coastal areas, the ratio of Si to nitrogen (N) and phosphorus (P) of river waters is a crucial factor in eutrophication (Cloern, 2001; Schelske and Stoermer, 1971). Overall, Si fluxes toward rivers firstly depend on the pools of weatherable silicate minerals. Mineral weathering further depends on the residence time of water in soils and rocks, , temperature, rainfall, in particular the amount of water available to leach solutes, topography, and land use (Conley et al., 2008; Cornelis et al., 2011; Dürr et al., 2011; Jennerjahn et al., 2006; Struyf et al., 2010). Converting forest into cropland affects the Si fluxes from continent to ocean (Ameijeiras-Mariño et al., 2018; J. C. Carey and Fulweiler, 2012; Conley et al., 2008; Struyf et al., 2010). This conversion first increases Si fluxes toward rivers because (1) the pool of phytogenic Si (PhSi) is progressively depleted under cropping (Conley et al., 2008; Struyf et al., 2010) and (2) erosion of cultivated lands exports particulate Si (Clymans et al., 2015b; Mangalaa et al., 2017). In the long term, however, Si exports from croplands may decrease at lower levels than in forest (Jennerjahn et al., 2006; Struyf et al., 2010) since successive harvests deplete the PhSi pool in soil and progressively the total Si pool (Barão et al., 2014; Struyf et al., 2010; Vandevenne et al., 2011, 2015).

The volcanic island of Basse-Terre in Guadeloupe has among the highest chemical weathering rate worldwide since high precipitation and temperatures, permeable volcanic rocks, and dense vegetation all favor chemical weathering (Gaillardet et al., 2011a, 2011b; Rad et al., 2013, 2011). Extreme meteorological events such as hurricane or tropical storm lead to floods. Though occurring during 10% of the time (Lloret et al., 2011), these floods account for ~40% of the annual water flux (Lloret et al., 2013), and for 21 to 31% of annual chemical weathering fluxes (Dessert et al., 2015). This island is largely cultivated at low altitude since pedo-climatic conditions are favorable to intensive cropping (Dorel et al., 2000). Banana and sugarcane are Si accumulating plant species (Henriet et al., 2006; Hodson et al., 2005),

and are the main crops in Guadeloupe. Banana and sugarcane cropping strongly impacts the soil-plant cycle of Si (*Chapter 5* and *Chapter 6*). These plant species take up high amounts of Si, accelerating mineral weathering, and return large amounts of PhSi to topsoil since little PhSi is exported through crop harvest (*Chapter 5*). The PhSi pool thus controls the dissolved silicon (DSi) concentration in the topsoil. Banana and sugarcane croplands could therefore impact Si fluxes toward watersheds. The impact of agricultural land use on these Si fluxes has been investigated in temperate areas (Conley et al., 2008; Hood and Van Cappellen, 2014; Struyf et al., 2010), but not in the humid tropics. The precise identification of land use impact on Si fluxes toward rivers is an acute challenge since Si sources are multiple (Ameijeiras-Mariño et al., 2018; Cornelis et al., 2011; Georg et al., 2006; Kurtz et al., 2011; Robinet et al., 2018). The aqueous continuum from soil to spring involves surface water, soil solution, and groundwater. The solid phase encompasses a number of silicates of lithogenic, pedogenic and biogenic origin. Besides, processes controlling Si concentrations are numerous (Garrels and Christ, 1965; Lindsay, 1979; Rai and Kittrick, 1989): dissolution of lithogenic and pedogenic silicates (LSi and PSi), as well as biogenic silica, and sorption/desorption on oxide surfaces. However, the use of the germanium to silicon ratio (Ge/Si) as a tracer may overcome this problem as reviewed by Cornelis et al. (2011). PhSi particles have amongst the lowest Ge/Si ratio since plants discriminate Si against Ge (Blecker et al., 2007; Cornelis et al., 2011; Delvigne et al., 2009; Derry et al., 2005). During PSi neoformation, Ge substitutes for Si and PSi minerals are therefore enriched in Ge as compared to parent rock (Kurtz et al., 2002; Murnane and Stallard, 1990). Consequently, the Ge/Si ratio of soil solution and streams is below that of the parent rock (Mortlock and Frohlich, 1987). Therefore, the Ge/Si ratio of river waters depends on the relative contribution of PhSi, PSi, and LSi to DSi exported to rivers. The Ge/Si ratio can thus be used as a geochemical tracer of land use impact on Si fluxes toward rivers.

Here, we studied the Si concentrations, Si fluxes, and Ge/Si ratios in river waters at base flow and during flood events at different gauging stations within watersheds differing in geomorphological properties and land use in Guadeloupe (forest, sugarcane, and banana). We characterized these parameters in the aqueous continuum from soil to spring: soil solution, runoff water, groundwater, and tributaries.

7.2 Environmental framework

The two watersheds are located in the Southern part of the Basse-Terre Island in Guadeloupe (16°N 61°W): the Pères River watershed (8.95 km²), and the Pérou River watershed (12.15 km²) (Figure 7-1; Crabit et al. (2016), Pépin et al. (2017)). These watersheds differ in area, topography, base flow discharge, flood discharge, and rainfall (Table 7-1). Both watersheds are monitored at gauging stations (GS) within the "Observatoire sur la Pollution agricole aux AntilLEs (OPALE)" framework by CIRAD, BRGM, IRD, and INRA organisms. The climate is tropical monsoon (Köppen classification). Average

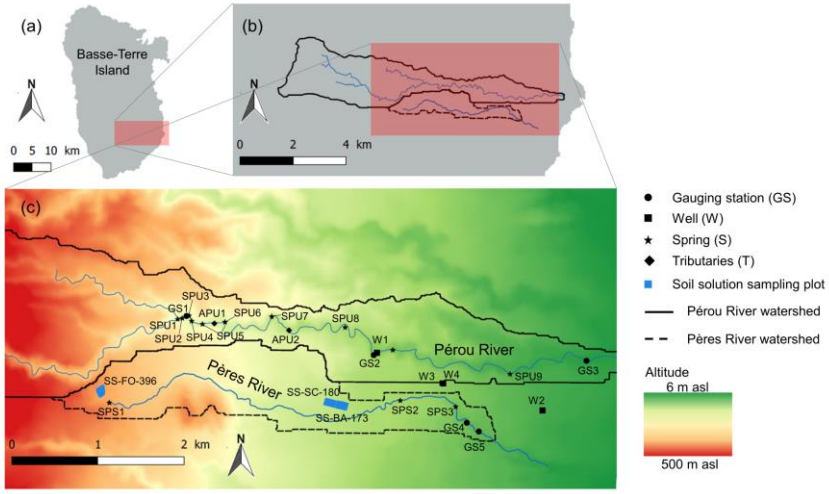

Figure 7-1: Location of the Pérou River and Pères River watersheds on the Basse-Terre Island (a,b), and location of sampling points on the background of the elevation map (c). Solid circles are stream gauging stations of the Pérou River (GS1, GS2, GS3), and Pères River (GS4, GS5), solid squares are wells (W1, W2, W3, W4), stars are springs of the Pérou River (SPU1-8) and of the Pères River (SPS1-3), solid diamonds are the tributaries of the Pérou River (TPU1, TPU2), and blue shapes are the plots where soil solutions were sampled. Soil solutions were collected under a banana plot (SS-BA-173), a sugarcane plot (SS-SC-180), and a forest plot (SS-FO-396). Runoff waters were collected in the banana plot (RW-BA-173).

annual rainfall (MAR) (from 1929 to 1978; ORSTOM) is ~ 4700 mm on the Pérou River watershed (which drains the volcano from the highest altitudes), and ~ 3600 mm on the Pères River watershed (which drains mainly the cultivated area at low altitudes). MAR increases with increasing altitude due to the orographic lift of the trade winds from the Atlantic Ocean (from 2500 mm at sea level to 4500 mm at the head of the Pères River watershed, and

7000 mm at the head of the Pérou River watershed). Two seasons are distinguished: a dry season (December-May), characterized by brief showers, and a rainy season (hurricane season), from June to November, characterized by heavy rains and tropical waves.

Main characteristics of the basins can be described from the downstream gauging stations (GS3 and GS4 in Table 7-1). Annual runoff was 3833 mm on the Pérou River watershed (measured from October 2009 to September 2010 (Crabit et al., 2016)), and 416 mm on the Pères River watershed (measured from November 2013 to October 2014 (Pépin et al., 2017)). Evapotranspiration (ET), estimated following Crabit et al. (2016), was 1012 mm on the Pérou River watershed, and 1234 mm on the Pères River watershed. For the Pérou River watershed, most of the slopes are moderate (0-24%), even if 33% are steep (slope >48%), mostly at high altitudes (Crabit et al., 2016). For the Pères River watershed, most of the slopes are moderate (<9%). Mean annual discharges are 0.95 $m^3 s^{-1}$ and 0.07 $m^3 s^{-1}$ at base flow for the Pérou and Pères rivers respectively (Crabit et al., 2016; Pépin et al., 2017). Measured peak annual discharges are 127 $m^3 s^{-1}$ and 3.6 $m^3 s^{-1}$ for the Pérou and Pères rivers respectively (Pépin et al., 2017; OPALE). Most of the Pérou River watershed is covered by forest (~75%), while croplands covers ~19% of the surface of the watershed. Most of the Pères River watershed is covered by cultivated lands (~57%), while forest covers ~17% of the surface of the watershed. Forest is an evergreen tropical rainforest with a.o. *Sterculia caribaea, Sloaena dentate, Sloaena massonii, Thelypteris reticulate, Prestoea montana*. Croplands are intensively used for the productions of dessert banana (*Musa acuminata*) and sugarcane (*Saccharum officinarum*).

The watersheds are underlain by three geological formations (Charlier et al., 2015). (1) The fractured andesitic lavas of the Capesterre Mountain, which outcrop mostly at the left bank of the Pérou River (1023-435 kyr); (2) the less permeable formation of debris flows that have filled a paleo valley at the right bank of the Saint Denis River (< 0.5 Myr); (3) pyroclastic deposits (< 0.2-0.5 Myr). These deposits were covered more recently (30,000-18,000 years BP) by successive pumice lapilli of several meters thick (Charlier, 2007) containing plagioclase, pyroxene and volcanic glass as the dominant weatherable minerals (Dagain, 1981; Ndayiragije, 1996). The soils are Andosols (Colmet-Daage and Lagache, 1969). They are strongly desilicated

and contain gibbsite. However, desilication increases with increasing altitude because of increasing rainfall (*Chapter 2*). At low altitude, allophane and halloysite are the main secondary minerals. With increasing altitude, the proportion of gibbsite and organo-mineral complexes increases.

Table 7-1: Main characteristics of the studied watersheds. Altitude above sea level of the gauging station. Surface area and slopes of the watersheds. Hydrologic characteristics: operating period of gauging stations, discharge during base flow and flood (mean±SD), and mean annual rainfall, runoff, evapotranspiration, and gain of water for groundwater. Data of GS1, GS2, and GS3 come from (Crabit et al., 2016), and data of GS4 come from (Pépin et al., 2017).

	River	**Altitude**	**Area**	**Part of watershed where slopes are**			**Operating period[1]**	**Mean base flow**	**Mean flood**	**Mean annual**			
		m	**km²**	**9-24**	**25-48**	**49-99**		**Discharge**	**Discharge**	**Rainfall**	**Runoff**	**ET[2]**	**Gain[3]**
				%	**%**	**%**		**$m^3 s^{-1}$**	**$m^3 s^{-1}$**	**$mm yr^{-1}$**			
GS1	Pérou	230	9.06	45	35	4.0	Oct 2009 to Sept 2010	0.76±0.59	6.30±4.37	6621	4699	915	1007
GS2	Pérou	110	10.49	45	33	3.5	Oct 2009 to Sept 2010	0.75±0.60	6.48±4.36	6210	4071	961	1178
GS3	Pérou	20	11.92	44	28	2.9	Oct 2009 to Sept 2010	0.95±0.66	6.56±6.27	5686	3833	1012	841
GS4	Pères	76	6.43	16	3.9	0.0	Nov 2013 to Oct 2014	0.07±0.03	0.218±0.221	3630	416	1234	1980

[1]Operating period corresponds to the period during which data were collected.
[2]ET corresponds to evapotranspiration. It was calculated following Crabit et al. (2016).
[3]Gain corresponds to the annual change in storage. They were obtained following Crabit et al. (2016) (Gain = Rainfall – ET – annual runoff).

7.3 Material and method

7.3.1 Sampling

7.3.1.1 Stream water

Five gauging stations (Figure 7-1) were settled by CIRAD, INRA, BRGM and IRD firstly within the ANR Chlordexo project and further the OPALE project in the Pérou and Pères rivers. They are used to measure water discharges, pH, electrical conductivity, and temperature (Figure 7-1c). Three stations are in the Pérou River, and two stations are in the Pères River. Stations are located upstream of croplands (GS1), in the middle of croplands (GS2), and downstream of croplands (GS3) in the Pérou River. Stations are located downstream of croplands in the Pères River (GS4 and GS5) (Figure 7-1). The respective surfaces drained in each gauging station increases from GS1 to GS3 (9.06, 10.49, 11.92 km², respectively; (Crabit et al., 2016)), and from GS4 to GS5 (6.43, 8.95 km², respectively). GS4 was replaced in July 2016 by GS5 due to logistical issues. GS5 is located 130 m downstream of GS4.

Stream water samples were collected at base flow at stations GS1, GS2, GS3, and GS5, and during flood events at stations GS3 and GS5. Water samples were collected at base flow from June 2016 to July 2017 at least twice a month. For each station, 12 base flow samples were selected for analyses at 12 different dates. The samples selected were those for which rainfall was minimal during the 24 hours prior to sampling.

From April 2017 to June 2017, stream water samples were collected with automatic samplers (SIGMA SD900) during six flood events at the downstream stations of the Pérou (GS3) and Pères rivers (GS5). The sampling included flood events with low and high change in stream discharge. During one flood event, sampling started when the water level exceeded a pre-defined level and 8 samples were collected at fixed increments or after 45 min if the level increment had not reached the preset value.

Water samples from two tributaries of the Pérou River (TPU1 and TPU2 – Figure 7-1c) were collected during base flow periods. Tributaries were sampled at their outlets (i.e. before their confluence with the Pérou River).

7.3.1.2 Groundwater

Water samples from 8 springs located in the Pérou River bed (SPU1 to SPU8 – Figure 7-1c) were collected, as well as from 3 springs in the Pères River bed (SPS1 to SPS3 – Figure 7-1c).

Groundwater was also collected in four different wells (W1, W2, W3, and W4 – Figure 7-1c) reaching aquifers from different geological layers. W1 allowed to collect water from the fractured andesitic lavas influenced by surface or soil infiltrations, W2 allowed to sample water from pyroclastic deposits, W3 from fractured andesitic lavas, and W4 from pyroclastic deposits of a different origin from W1 (Charlier et al., 2015). Water was sampled after one hour of pumping.

7.3.1.3 Soil solution

Three plots were selected on the Pères River watershed: (i) banana and (ii) sugarcane plots next to each other at 173 m (BA-173) and 180 m asl (SC-180), respectively, and (iii) one forest plot at 396 m asl (FO-396) (Figure 7-1c). Twenty five zero-tension lysimeters were settled in all plots (10 under BA-173 and SC-180, 5 under FO-396) at 60 cm depth. The lysimeters were placed as illustrated in Figure 7-S1a-e. (1) A hole was dug by augering to 89 cm depth (Figure 7-S1c-d). (2) The upper part of the lysimeter (Figure 7-S1b) was then filled with soil material of corresponding depth. (3) Finally, the lysimeter was driven into the hole, and the hole was carefully plugged back in with soil material while respecting the respective depths. Zero-tension lysimeters collect gravity water that mostly contributes to groundwater. Lysimeter waters were collected every ~200 mm of rainfall from July 2016 to April 2017 in BA-173 and SC-180 plots, and from January 2017 to July 2017 in the FO-396 plot. The first three samples were discarded to allow soil recovery from set up disturbance. In each plot, 20 soil solution samples (SS) were selected for analyses.

7.3.1.4 Runoff waters at the plot scale

Surface runoff waters (RW) were collected in the BA-173 plot (RW-BA-173) in October 2016. Three samples were selected for analyses. Runoff water was collected through a device set up in a gully (see Figure 7-S1f,g). A metal plate pierced in its center prevented water from flowing into the gully. A pipe connecting the hole in the plate to a tank was used to collect runoff water. Water was then collected in the tank within the 24 h following the rain event.

7.3.2 Hydrological variations of the sampled flood events

The hydrographs of the flood events at GS3 on 9 May 2017 (FPU1), 14 June 2017 (FPU2), and 18 June 2017 (FPU3), and at GS5 of the 28 April 2017 (FPS1), 11 May 2017 (FPS2), and 18 June 2017 (FPS3) are shown in Figure 7-2. Dates of sampling differ between both stations for several reasons. Firstly, similar rainfalls in height, duration and intensity did not result in similar water levels at stations GS3 and GS5. Secondly, the predefined water level for the initiation of sampling was adjusted to each GS. Thirdly, technical problems may have led to the interruption of sampling at one of the two GS while the other was still operating.

In the Pérou River, the flood FPU1 (Figure 7-2a) was a high intensity event (3 similar events occurred from October 2009 to September 2010). Water discharge before the flood was 3.9 $m^3 s^{-1}$. Water discharge increased 12.6 times at the first peak (49 $m^3 s^{-1}$), and 15.6 times at the second peak (61 $m^3 s^{-1}$). FPU2 (Figure 7-2b) was less intense and a little more frequent as 11 floods reached similar discharges from October 2009 to September 2010. Water discharge was 2.7 $m^3 s^{-1}$ before the flood and water discharge at peak flow was 12.6 times larger (34 $m^3 s^{-1}$). Rainfall at the gauging station stayed rather low and the event was probably generated by rainfall at higher altitude. FPU3 (Figure 7-2c) was a very common event as 47 floods reached similar discharges from October 2009 to September 2010. Water discharge was 2.6 $m^3 s^{-1}$ before the flood and reached 10 $m^3 s^{-1}$ at peak.

For floods in the Pères River, available water discharges at station GS5 are from July 2016 until January 2017 (Pépin et al., 2017). Therefore, the intensity classification between small, medium and high intensity events is not as precise as at station GS3. However, 39 floods were recorded during this period (Pépin et al., 2017). From these 39 floods, data on the 10 most intense events are available (Pépin et al., 2017) and indicate that the first flood (following an order according to peak water discharge) reached a peak water discharge of 11.7 $m^3 s^{-1}$, while the tenth flood reached a peak water discharge of 0.95 $m^3 s^{-1}$. Mean peak water discharge of the ten biggest flood events was 3.71 $m^3 s^{-1}$. This information was used to classify floods FPS1, FPS2, and FPS3. For FPS1 (Figure 7-2d), stream water discharge increases 4.7

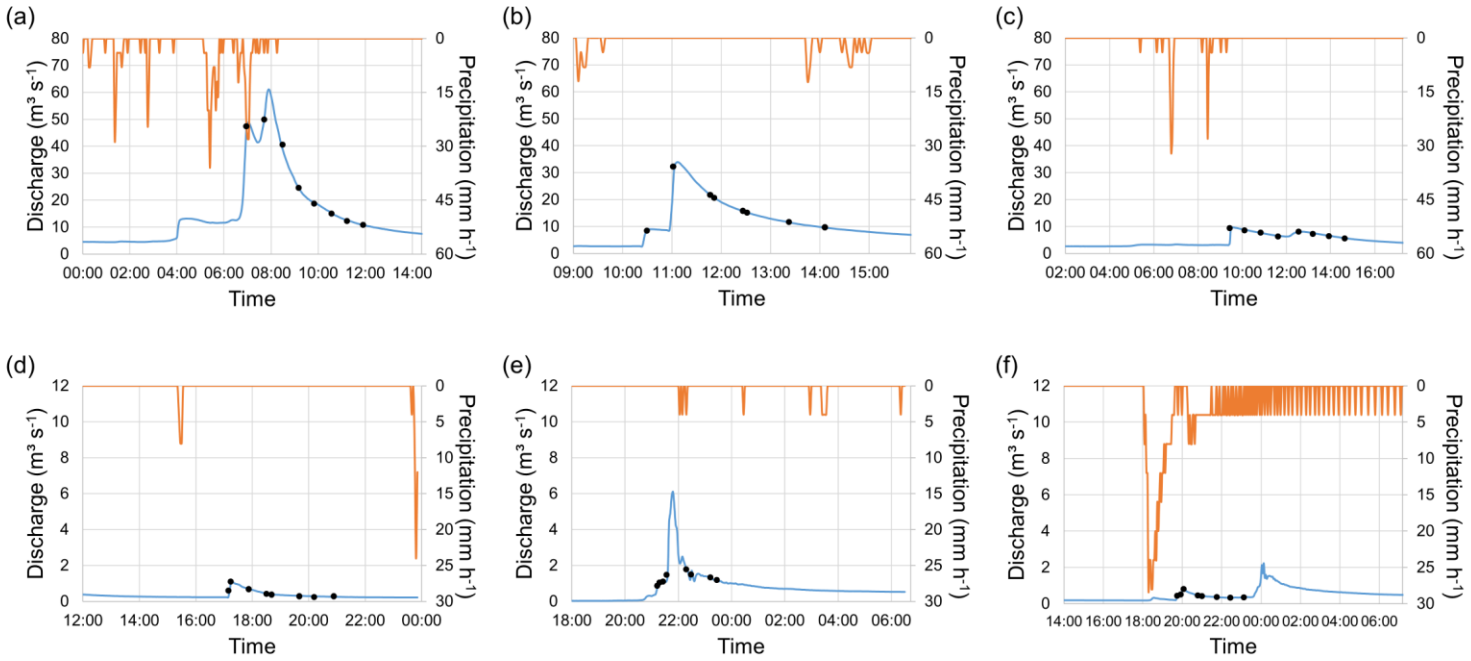

Figure 7-2: Stream hydrographs for (a) the 9 May 2017 (FPU1), (b) the 14 June 2017 (FPU2), (c) the 18 June 2017 (FPU3) flood events at GS3, (d) the 28 April 2017 (FPS1), the 11 May 2017 (FPS2), and 18 June 2017 (FPS3) flood events at GS5. Blue curves represent the stream discharge, orange curves represent precipitation intensity, and the solid circles represent the water samples collected during the events. Precise description of the floods is given in section 7.3.2.

times (from 0.23 m^3 s^{-1} prior to the event up to 1.08 m^3 s^{-1} at peak). FPS2 (Figure 7-2e) was bigger. Discharge was 0.04 m^3 s^{-1} prior to the event, and increased 153 times to reach 6.1 m^3 s^{-1} at peak. No rainfall was measured prior to the event, meaning that flood could result from rainfall at higher altitude only. However, this is little surprising given the intensity of the flood. Moreover, rainfall data were not always reliable and a malfunction of the rain gauge could also justify this. For FPS3 (Figure 7-2f), the flood event resulted from rainfall at low altitude that reached an intensity of 28 mm h^{-1}. Resulting water discharge increased from 0.19 m^3 s^{-1} to 2.23 m^3 s^{-1} at peak.

7.3.3 Water elemental analyses

Within 24h after sampling, water was filtered through a 0.2 µm polycarbonate membrane and acidified at 0.25% Suprapur nitric acid. The analyses were carried out on all aqueous samples listed above.

7.3.3.1 Major elements

The concentration of major elements (Si, Al, Fe, Ca, Mg, K, and Na) were determined on all types of water by inductively coupled plasma-atomic emission spectrometry (ICP-AES; iCAP 6500 Thermo Fisher Scientific). Detection limit (ppb) was 10, 2, 5, 10, and 10 for Si, Ca, Mg, K, and Na respectively, and precision is <0.5%.

7.3.3.2 Ge measurement and Ge/Si ratio

Ge concentration was measured by inductively coupled plasma mass spectrometry (ICP-MS; iCAP Q Thermo Scientific) using ^{74}Ge isotope. Detection limit was 0.003 ppb. For each set of measures, Ge concentration was measured in blanks, Ge standards (0.05 ppb, 0.1 ppb, 0.2 ppb, 0.4 ppb), and a reference material (SLRS-6). The precision is 8% for concentrations below 0.001 ppb and from 3 to 4% for concentration above 0.001 ppb. Ge/Si ratios were calculated and expressed in µmol mol^{-1}.

7.3.4 Estimation of Si fluxes in rivers

Si fluxes were estimated at stations GS1, GS2, GS3, and GS4. Discharge was measured at gauging stations as water level was measured every 3 min with a pressure detector. Gauging campaigns were regularly conducted to adjust the calibration curves relating discharge with water level (Pépin et al., 2017). Discharge data were collected for a complete year operating period for each

gauging station (Crabit et al., 2016; Pépin et al., 2017). Namely from October 2009 to September 2010 for GS1, GS2, and GS3 (Crabit et al., 2016), and from November 2013 to October 2014 for GS4 (Pépin et al., 2017). For GS5 discharge was measured from July 2016. Based on the discharge dataset at GS1, GS2, GS3, and GS4, we estimated the mean discharge value for base flow and for flood conditions (Table 7-1). Due to a lack of data for station GS5, we could not estimate the mean discharge value for base flow and flood conditions at that station. To differentiate the base from the flood flow, we proceeded as indicated in Lloret et al. (2011). More specifically, the discharge was plotted against frequency for each station. Two hydrological periods were evidenced. A first period that includes 90% of the annual flux corresponded to the base flow levels. The second period that included the last 10% of the annual flux corresponded to the flood water levels.

Annual Si fluxes at base flow were estimated at GS1, GS2, GS3, and GS4 by multiplying mean Si concentration by the mean discharge and the occurrence of base flow (90%). This was a first estimate based on available data. Yet, uncertainties remain given that the precision on river discharge is highly dependent on fixed parameters at which the water level is measured, which may vary depending on the size of the river bed. For the Pères River, we used Si concentrations at station GS5 (where water samples were collected) and mean discharge levels at GS4 (due to the lack of data to estimate the mean annual discharge at GS5) to estimate Si fluxes at base flow. GS4 and GS5 are located close to each other (130 m), and no springs or tributaries were identified between these two stations. Therefore, we do not expect that water discharge or Si concentration would significantly differ between GS4 and GS5 at base flow.

Annual Si fluxes during floods were estimated by multiplying the mean Si concentration during each event by the mean discharge at flood water levels and the occurrence of floods (10%). However, during flood events, pipelines collecting runoff water from cultivated and inhabited areas contributed to the river between GS4 (where discharge was measured) and GS5 (where Si concentrations have been measured), and could have significantly increased the river discharge and influence Si concentration. Therefore, the mean water discharge of flood conditions at GS4 are considered as the minimum discharge value for GS5 during floods. We estimate annual Si fluxes during

floods using mean water discharge in flood conditions at GS4 and mean Si concentration during flood at GS5.

Total annual Si fluxes were estimated at GS3 and GS4 by adding the annual Si fluxes at base flow to the annual Si fluxes during floods.

7.3.5 Two components mixing model

The two components mixing model is used to determine the relative importance of two Si sources to a solution sample (Derry et al., 2005; Kurtz et al., 2011). It is based on the Ge/Si ratio of the Si sources and on the resulting Ge/Si ratio of the aqueous sample (Equation 1). It can be used if only two Si sources with contrasting Ge/Si ratios are expected to contribute, and if no processes preferentially incorporating Ge relative to Si (or Si relative to Ge) occurs (Derry et al., 2005).

$$Ge/Si_{sample} = x\ Ge/Si_{comp1} + (1 - x)Ge/Si_{comp2} \quad Eq\ 1$$

Ge/Si_{sample} corresponds to the Ge/Si ratio of the aqueous sample, x is the relative contribution of component 1 (comprised between 0 and 1), Ge/Si_{comp1} is the Ge/Si ratio of the component 1, and Ge/Si_{comp2} is the Ge/Si ratio of the component 2. Relative contribution of component 2 is deduced by 1-x.

This model was used here to determine the relative contribution in soil solution samples of PhSi dissolution (component 1) considering that LSi was component 2 (Scenario 1), or that PSi was component 2 (Scenario 2). We expect that the dissolution of PhSi, LSi, and PSi contribute concomitantly to the DSi in soil solution. Therefore, the real contribution of PhSi dissolution is likely comprised between the one obtained with Scenario 1 and Scenario 2. Phytoliths have low Ge/Si ratios ranging from 0.03 to 0.5 (Blecker et al., 2007; Delvigne et al., 2009; Derry et al., 2005; Lugolobi et al., 2010). LSi minerals, however, have a Ge/Si ratio commonly ranging from 2.3 to 2.9 µmol mol^{-1} (Ameijeiras-Mariño et al., 2018; Derry et al., 2005; Kurtz et al., 2002; Lugolobi et al., 2010). PSi minerals of the studied soils are mainly SRO aluminosilicates of the allophane-imogolite series (most probably Al-rich allophane). Kurtz et al. (2002) reported a Ge/Si ratio for allophane ranging from 10 to 15 µmol mol^{-1}. The mixing model considers that DSi in soil solution samples represents a contribution from the dissolution of PhSi (Component 1; x in Equation 1)

with a mean Ge/Si ratio of 0.25 µmol mol^{-1} ($Ge/Si_{comp1:}$ Derry et al., 2005) and from the dissolution of: *Scenario (1)* primary minerals (Component 2: 1-x in Equation 1), i.e. the "weathering-derived Si" with a mean Ge/Si ratio of 2.6 µmol mol^{-1} (Ge/Si_{comp2}: Derry et al., 2005), or *Scenario (2)* pedogenic minerals (Component 2: 1-x in Equation 1), with a mean Ge/Si ratio of 12.5 µmol mol^{-1} (Ge/Si_{comp2}: Kurtz et al., 2002).

This model was also used to determine the relative contribution of soil solution/runoff waters at the plot scale (Component 1), and groundwater (Component 2) to the DSi in stream waters samples during floods. Mean Ge/Si ratio of soil solutions/runoff waters were used to characterize Component 1. Mean Ge/Si ratio of stream water at base flow were used to characterize Component 2.

7.4 Results

7.4.1 Elemental composition of the water during low-flow periods

Mean Na, K, Mg, Ca, Al and Si concentrations in stream waters at base flow, tributaries, springs, groundwater, soil solution, and runoff waters are given in Table 7-2. Data for each date of sampling are available in the Supplementary Table 7-S1. In river waters at base flow, elemental concentrations slightly increase from upstream station (GS1) to downstream one (GS3). Elemental concentrations were from 1.6 to 3.3 times larger in the Pères River station (GS5) than in the Pérou River stations (GS1-2-3). Elemental compositions of groundwater in springs and wells differed largely from one site to another. Elemental concentrations of soil solutions were larger in SS-BA-173 and SS-SC-180 than SS-FO-196, and are globally lower than in springs and groundwater. In runoff at plot scale, Si concentrations were slightly lower than the one of soil solutions SS-BA-173 and SS-SC-180, while Na, Mg, and Ca concentrations were strongly lower than the one of soil solutions SS-BA-173 and SS-SC-180.

Table 7-2: Na, K, Mg, Ca, Al, Si, Ge concentrations, and Ge/Si ratios of aqueous samples collected from: (1) the Pérou River at three different gauging station (GS1, GS2, GS3), and the Pères River at one gauging station (GS5) during base flow (bf), and flood (fl); (2) two tributaries (T) of the Pérou (PU) River (TPU1-2); (3) eight springs (S) of the Pérou River (SPU1-8); (4) three springs of the Pères (PS) River (SPS1-3); (5) four groundwater coming from four different wells (W1-4); (6) soil solutions collected at 60 cm depth in a banana plot (SS-BA-173), sugarcane plot (SS-SC-180), and forest plot (SS-FO-396); and (7) runoff waters at the plot scale collected in the same banana plot as for soil solution (RW-BA-173). Values are means ± standard deviations. For GSx bf n = 12, for GSx fl n = 24, For SS-XX-XXX n = 10, and for RW-BA-173 n = 3. Complete data are available in the supplementary material Table 7-S1.

	Na	K	Mg	Ca	Al	Si	Ge	Ge/Si
				µmol l^{-1}			pmol l^{-1}	µmol mol^{-1}
	(1) River water at base flow							
GS1 bf	247 ± 20	23 ± 6	65 ± 6	133 ± 25	<dl	471 ± 46	100 ± 6	0.21 ± 0.03
GS2 bf	276 ± 64	28 ± 16	79 ± 31	162 ± 92	<dl	515 ± 141	91 ± 16	0.18 ± 0.03
GS3 bf	286 ± 31	27 ± 2	81 ± 11	157 ± 22	<dl	517 ± 52	89 ± 8	0.17 ± 0.03
GS5 bf	469 ± 67	77 ± 17	178 ± 33	435 ± 95	<dl	916 ± 134	118 ± 34	0.13 ± 0.04
	(2) River water during flood							
GS3 fl	202 ± 67	21 ± 5	48 ± 23	106 ± 43	1.05 ± 0.95	297 ± 160	nd	nd
GS5 fl	301 ± 122	106 ± 35	105 ± 41	368 ± 116	2.25 ± 1.26	507 ± 230	nd	nd
	(3) Tributaries of Pérou River							
TPU1	368	53	129	321	<dl	748	56	0.07
TPU2	325	66	53	291	<dl	626	139	0.22
	(4) Springs of Pérou River							
SPU1	375	45	155	451	<dl	641	111	0.17
SPU2	446	5	219	266	<dl	962		nd
SPU3	367	27	54	644	<dl	576	56	0.09
SPU4	447	40	170	421	<dl	826	83	0.10
SPU5	259	59	42	312	<dl	262	83	0.32
SPU6	484	39	57	260	<dl	753	167	0.22

SPU7	550	30	51	178	<dl	597	56	0.09
SPU8	1016	105	412	731	<dl	1447	361	0.24
	(5) Springs of Pères River							
SPS1	307	18	107	205	<dl	555	194	0.26
SPS2	672	75	267	661	<dl	1080	250	0.22
SPS3	710	63	293	413	<dl	1367	361	0.25
	(6) Groundwater							
W1	449	30	118	199	<dl	738	222	0.30
W2	766	113	370	642	<dl	1428	417	0.29
W3	464	47	134	303	<dl	906	778	0.85
W4	708	120	304	691	<dl	1419	417	0.29
	(7) Soil solution at 60 cm depth							
SS-BA-173[1]	231 ± 51	81 ± 50	213 ± 92	182 ± 85	0.54 ± 0.49	190 ± 23	100 ± 27	0.92 ± 0.11
SS-SC-180[2]	195 ± 55	366 ± 542	212 ± 199	248 ± 238	0.51 ± 1.01	183 ± 39	171 ± 21	0.95 ± 014
SS-FO-396[3]	199 ± 45	14 ± 14	43 ± 15	43 ± 7	1.82 ± 1.35	92 ± 14	176 ± 33	1.10 ± 0.30
	(8) Runoff water							
RW-BA-173	83 ± 9	243 ± 50	43 ± 7	51 ± 6	5.2 ± 1	140 ± 1	156 ± 8	1.11 ± 0.07

[1]SS-BA-173 = soil solution of banana plot (BA-173), [2]SS-SC-180 = soil solution of sugarcane plot (SC-180), [3]SS-FO-396 = soil solution of forest plot (FO-396).[4]dl = detection limit

7.4.2 Ge/Si ratios in water during low-flow periods

The values of Ge/Si ratio of stream waters during base flow periods and end-members are given in Figure 7-3. The Ge/Si ratios of the rivers and tributaries (ranging from 0.07 to 0.26 µmol mol^{-1}) were in the same order of values as in groundwater (except the 0.85 µmol mol^{-1} value for W3). In contrast, Ge/Si ratios of soil solution and runoff from plots were higher (ranging from 0.71 to 1.64 µmol mol^{-1}). This is coherent with the export of groundwater into rivers during base flow periods, the soil compartment being not a major contributor of water in such periods.

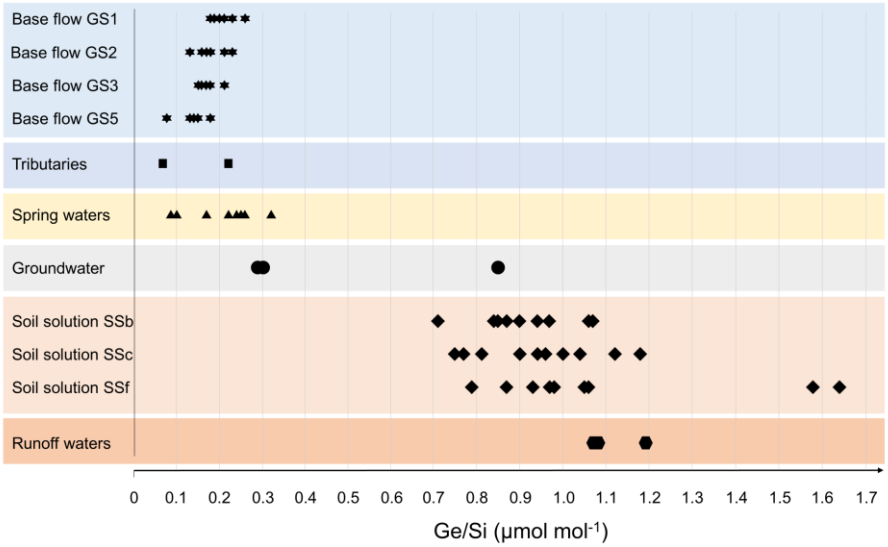

Figure 7-3: Ge/Si ratios of the river water at base flow (✸), tributaries (■), and from the different end-members (springs ▲, groundwater ●; soil solutions ♦; runoff waters ⬣).

7.4.3 Evolution of the Si concentration and Ge/Si ratio during flood events

The values of Si concentration and Ge/Si ratio of the stream water samples collected during the flood events PU1-2-3 at GS3, and PS1-2-3 at GS5 are shown in Figure 7-4 and Figure 7-5. Analytical data are available in Table 7-S2.

For each flood, the concentration of dissolved Si in stream water was lower at the end of the flood even if the discharge had returned to its initial state. Considering average concentrations of Si before the floods of 517 and 916

µmol l^{-1} at GS3 and GS5 respectively (Table 7-2), Si concentrations did not strongly change during the rising limb (508, 537, 883 µmol l^{-1} for FPU1, FPU2, and FPS3 respectively). In contrast Si concentrations decreased during the rising limb for FPU3, FPS1, and FPS2 (274, 573, and 192 µmol l^{-1} for FPU3, FPS1, and FPS2 respectively). During the falling limb, Si concentration first decreased for all floods, and finally increased for FPU2, FPU3, FPS1, and FPS2. Thus, two periods are distinguished: a first period of relatively constant Si concentration at the beginning of the flood, followed by a Si dilution period after the peak flow, meaning that different processes contribute to the flood generation. It is also interesting to note that the higher the peak flow, the higher the decrease in Si concentration. In fact, while water discharge increased by factors of 15.6, 12.6, 153, and 11.7 for FPU1, FPU2, FPS2, and FPS3, the Si concentration decreased by factors of 1.3, 2.7, 5.5, and 2.1 for FPU1, FPU2, FPS2, and FPS3, respectively. For FPU3 and FPS1 water discharge increased by factors of 3.8 and 4.7, respectively, and Si concentration decreased by factors of 5.5 and 5.2, respectively.

Ge/Si ratio in stream waters first increased during the flood, and then decreased at the end of the flood when water discharge progressively approached base flow water discharge. The increase in the Ge/Si ratio in stream waters was always larger when the increase in water discharge was less, especially at GS3.

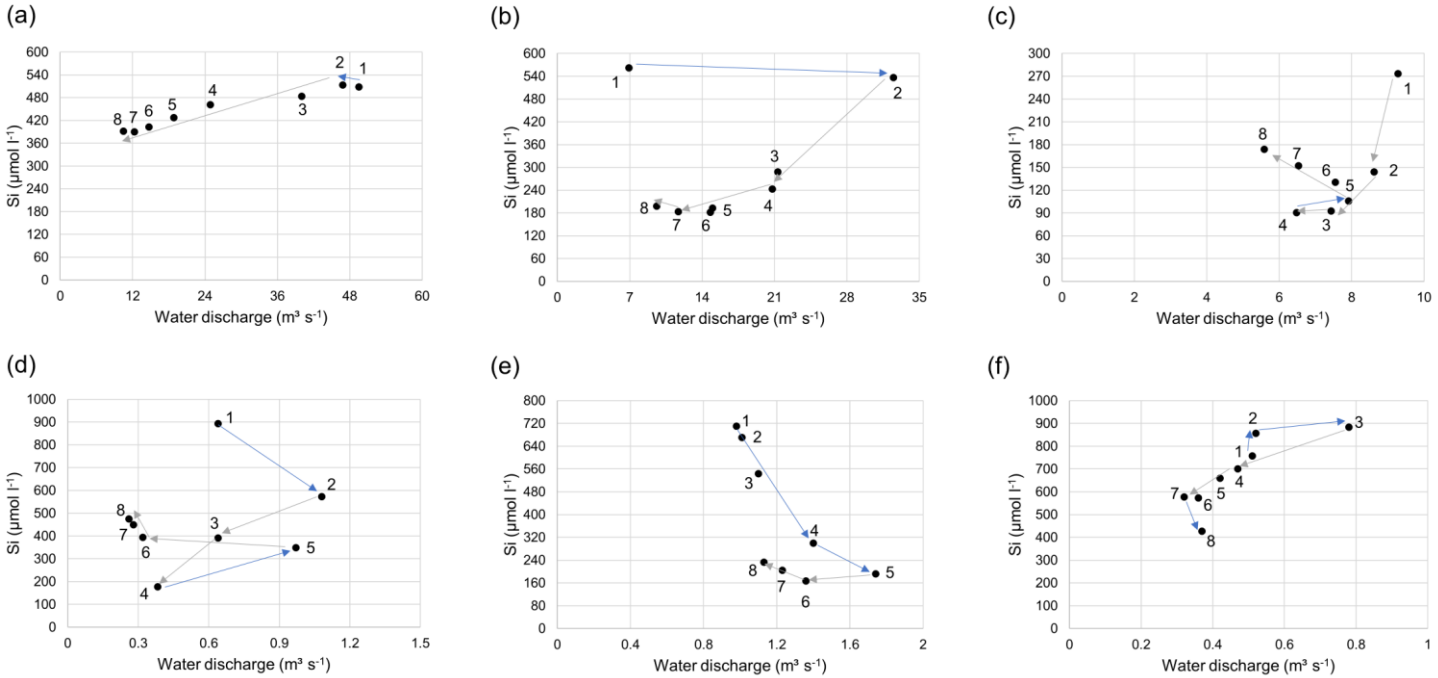

Figure 7-4: Concentration-discharge curves for (a) FPU1, (b) FPU2, (c) FPU3 flood events in the Pérou River (GS3), (d) FPS1, (e) FPS2, and (f) FPS3 flood events in the Pères River (GS5) (numbers = temporal evolution of sampling, blue arrows represent the rising limb, grey arrows represent the falling limb).

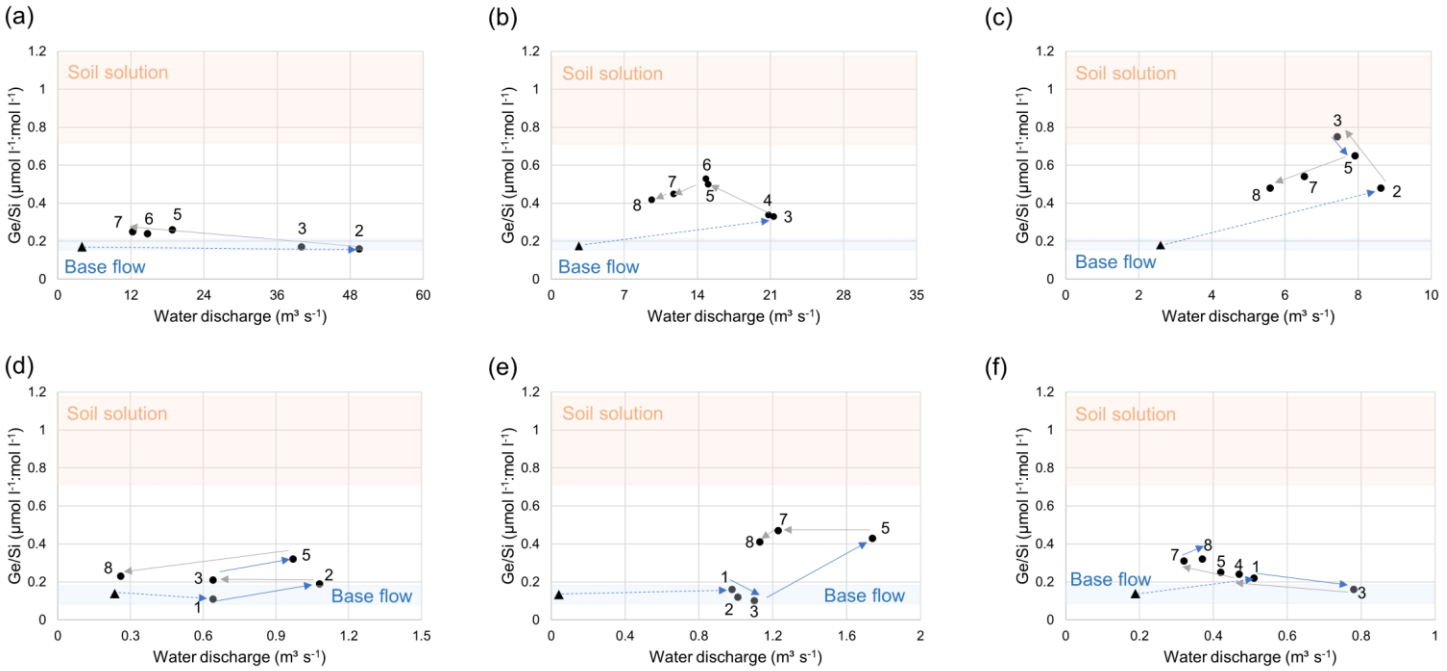

Figure 7-5: Ge/Si ratio-discharge curves for (a) FPU1, (b) FPU2, (c) FPU3 flood events at GS3, (d) FPS1, (e) FPS2, and (f) FPS3 flood events at GS5 (numbers = temporal evolution of sampling, triangle = fictive initial Ge/Si ratio before the flood as estimated from the mean Ge/Si ration at each station at base flow, doted arrow = corresponding fictive evolution of the Ge/Si ratio, blue arrows represent the rising limb, grey arrows represent the falling limb).

7.4.4 Annual elemental fluxes in rivers

From mean elemental concentrations in river waters during base flow periods (Table 7-2) and mean annual discharge (Table 7-1), elemental annual fluxes for each gauging station were estimated for these periods. Such as for elemental concentrations, Si fluxes were always larger than fluxes of other elements. Si fluxes at base flow were 312, 292, 322, and 80 kg ha^{-1} yr^{-1} at GS1, GS2, GS3, and GS4 respectively. From mean Si concentrations during the six flood events (FPU1-2-3, FPS1-2-3; Table 7-2), and from the mean water discharge during flood events (Table 7-1), annual Si fluxes during floods were estimated at 142 and 15.2 kg ha^{-1} yr^{-1} and accounted for 31 and 16% of the total annual Si fluxes at GS3 and GS4, respectively. Annual Si fluxes during floods at GS4 were minimal values, but they reflect the geomorphological properties of both watersheds with less important flooding at GS4 (smallest watershed without large upstream rainy area).

Table 7-3: Annual Na, K, Mg, Ca, and Si fluxes at base flow in Pérou River (gauging stations GS1, GS2, GS3) and Pères River (GS4), during floods in Pérou River (GS3) and Pères River (GS4), and deduced total annual fluxes in Pérou River (GS3) and Pères River (GS4). Values are means ± standard deviations.

	Discharge	Na	K	Mg	Ca	Si
	m^3 s^{-1}			kg ha^{-1} yr^{-1}		
			Base flow			
GS1	0.76	133.9	21.1	37.5	125.5	312.3
	± 0.59	± 8.5	± 4.4	± 2.8	± 18.4	± 24.0
GS2	0.75	128.3	22.2	38.8	131.2	292.0
	± 0.60	± 23.7	± 10.1	± 12.3	± 59.8	± 64.0
GS3	0.95	145.8	23.6	43.8	139.7	321.9
	± 0.66	± 10.8	± 1.4	± 4.1	± 13.4	± 22.6
GS4	0.07	33.3	9.2	13.3	53.9	79.5
	± 0.03	± 2.0	± 0.9	± 1.1	± 5.0	± 5.0
			Flood			
GS3	6.56	79.0	14.2	19.7	72.1	142.0
	± 6.27	± 25.0	±3.4	± 9.0	± 27.8	± 72.9
GS4	0.218	7.39	4.43	2.73	15.8	15.2
	± 0.221	± 3.04	± 1.48	± 1.08	± 5.04	± 7.00
			Total (base flow + flood)			
GS3	1.51	224.8	37.8	63.5	211.8	463.9
	± 1.22	± 35.8	± 4.8	± 13.1	± 41.2	± 95.5
GS4	0.085	40.7	13.7	16.1	69.6	94.7
	± 0.05	± 5.1	± 2.3	± 2.1	± 10.1	± 12.0

7.4.5 Two components mixing model

7.4.5.1 Soil solution

Results of the model are shown in Figure 7-6. The two samples with higher values of Ge/Si of the SS-FO-396 were excluded from the simulation because they were out of the range of other values (see Section 7.5.2 for explanations). Based on the mean Ge/Si ratios in soil solution of 0.92, 0.95, and 0.95 µmol mol^{-1} for BA-173, SC-180, and FO-396 plots respectively, and considering *Scenario 1* (component 2 is represented by LSi, see Section 7.3.5) the mixing model suggests that PhSi (component 1) contributed to 71, 70,

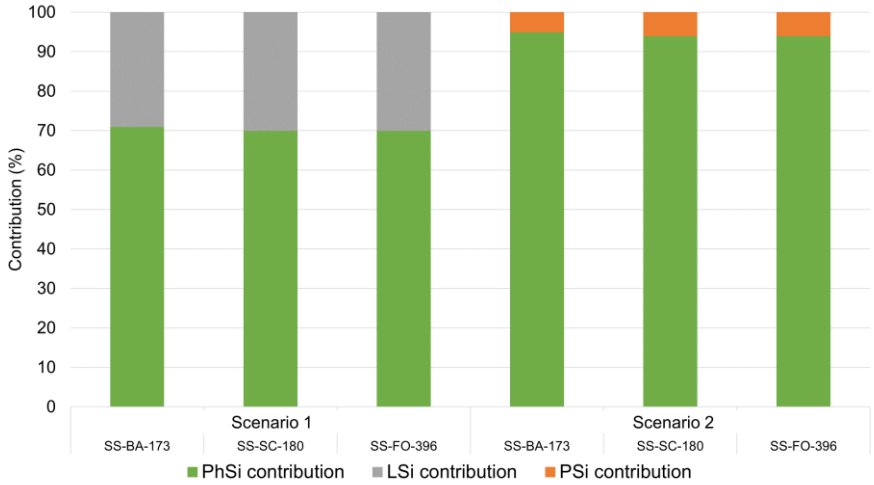

Figure 7-6: Relative contribution of the phytolith dissolution (PhSi), of the lithogenic silicates (LSi) (Scenario 1), and of the pedogenic silicates (PSi) (Scenario 2) to the dissolved Si in the soil solution of banana (SS-BA-173), sugarcane (SS-SC-180), and forest (SS-FO-396) plots as obtained with the two component mixing model following Derry et al. (2005).

and 70% of Si collected in soil solutions, respectively. Considering *Scenario 2* (component 2 is represented by PSi, see section 7.3.5), the mixing model suggests that PhSi contributed to 95, 94, and 94% of Si collected in soil solutions for BA-173, SC-180, and FO-396 plots respectively. These scenarios indicate that, whatever the plot, PhSi contribution to DSi in soil solution is comprised between 71 and 95% for the BA-173 plot, and between 70 and 94% for the SC-180 and FO-396 plots.

7.4.5.2 Stream water during flood

Results of the simulation are shown in Figure 7-7. For the Pérou River, in the big flood FPU1, soil water did not contribute to Si fluxes when water discharge were 9 and 11 times larger than before the flood, and only contributes to ~10% at the end of the falling limb. During the middle flood event FPU2, contribution from soil water was larger than during FPU1: maximum contribution from soil water was ~46% and occurred during the falling limb. During the small flood event FPU3 contribution from soil water reached ~74% at the start of the falling limb. Thereafter it decreased to reach about 40% at the end of the flood.

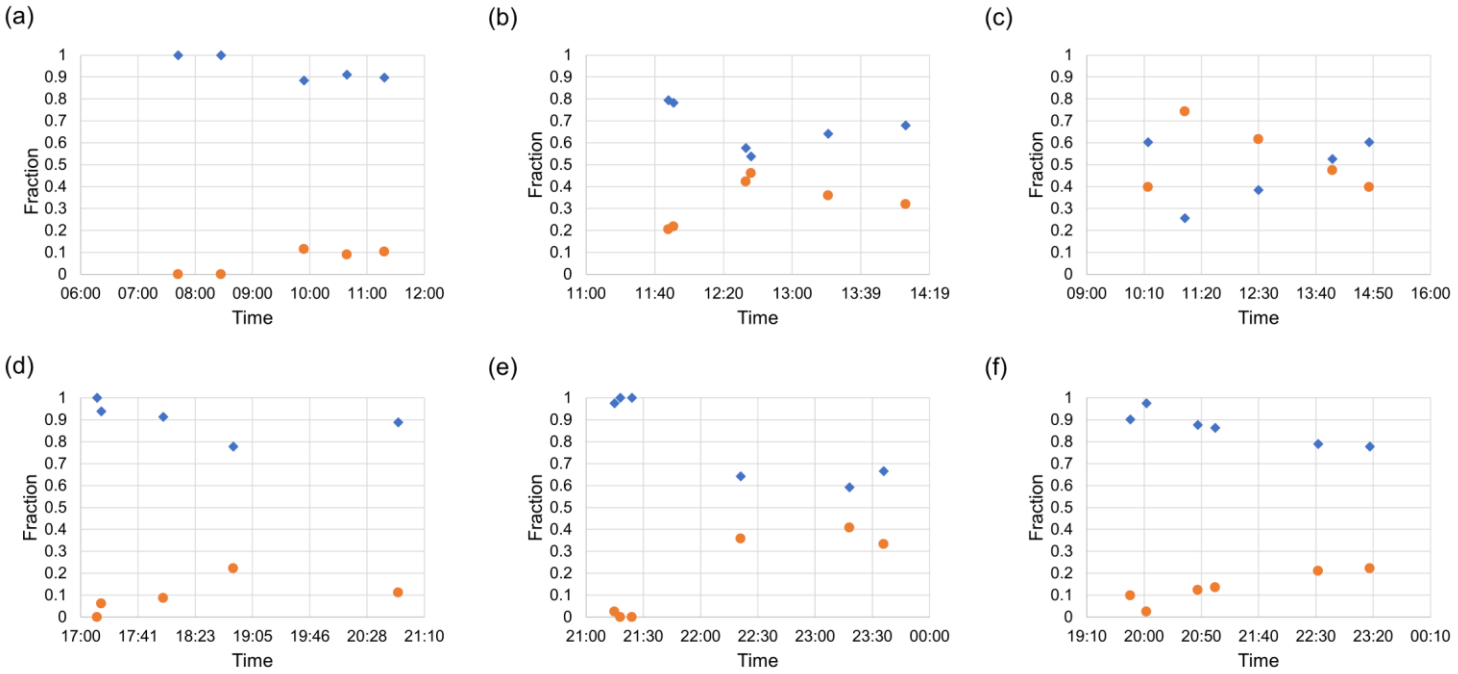

Figure 7-7: Ge/Si based hydrograph separation, plotted as fractions of soil water (●) and groundwater (♦) for (a) FPU1, (b) FPU2, (c) FPU3 flood events at GS3, (d) FPS1, (e) FPS2, and (f) FPS3 flood events at GS5. The fractions are estimated based on a two components mixing model (see section 7.3.5).

7.5 Discussion

7.5.1 Variations in Ge/Si ratio in groundwater

The Ge/Si ratio of groundwater (ranging from 0.09 to 0.85 µmol mol^{-1}; Table 7-2, Figure 7-3) were in the same order of that reported in the literature (ranging from 0.24 to 0.74 µmol mol^{-1}; Ameijeiras-Mariño et al., 2018; Kurtz et al., 2011; Lugolobi et al., 2010). Ge/Si ratios reported in groundwater are typically lower than that reported for silicate rocks (ranging from 1 to 2.9 µmol mol^{-1}; Ameijeiras-Mariño et al., 2018; Derry et al., 2005; Kurtz et al., 2002; Lugolobi et al., 2010; Mortlock and Frohlich, 1987; Murnane and Stallard, 1990). The preferential incorporation of Ge into secondary clay minerals results in higher Ge/Si ratios in secondary silicates than in silicate rocks (ranging from 4.8 to 24.3 µmol mol^{-1}; Ameijeiras-Mariño et al., 2018; Bernstein, 1985; Froelich et al., 1992; Lugolobi et al., 2010; Murnane and Stallard, 1990).

Residence times of groundwater sampled in this study amount to ~15, 33, 30, and 20 years for W1, W2, W3, and W4 respectively (Charlier et al., 2015), allowing chemical equilibrium of minerals in solution (Maher, 2011). In the groundwater investigated, Ge/Si ratio would therefore result from the concomitant dissolution of primary silicates and the neoformation of secondary silicates. The values of Ge/Si ratio of W1, W2, and W4 were in the same range (0.29-0.30 µmol mol^{-1}) while W3 was characterized by a slightly higher Ge/Si ratio (0.85 µmol mol^{-1}). This suggests that dissolution of primary silicate minerals and neoformation of secondary silicate minerals were likely the main processes controlling Ge and Si concentrations in W1, W2, and W4 whereas in W3, an additional contribution from secondary silicates dissolution may have contributed to increase the Ge/Si ratio.

W1 and W3 both reach groundwater coming from fractured andesitic lava. Chemical composition of these two wells was comparable for Na, K, Mg, Ca, and Si, but differed for Ge. Groundwater sampled from these two wells was therefore characterized by different values of the Ge/Si ratio, suggesting that different processes controlled their composition. W1 has a depth of 15 m, and the collected groundwater has a mean residence time of 15 years (Charlier et al., 2015). W3 has a depth of 80 m. The geological section of the well W3 consists from top to bottom of 30 m of pyroclastic deposits, followed

by 13 m of breccia deposits (avalanche flow), then by 29 m of fractured lava and 8 m of clay breccias at the bottom of the section (Charlier et al., 2015). This groundwater was sampled from 42.5 to 80 m depth in fractured andesitic lava and clay breccias, and had a mean residence time of 33 years. Two reasons could explain the higher Ge/Si ratio in groundwater from W3 than in groundwater from W1. Firstly, the longer mean residence time of groundwater in W3 than in W1 could have led to concentrations closer to equilibrium in groundwater of W3 than in groundwater of W1. However, mean residence time to reach chemical equilibrium is typically of a year or less (depending on water temperature) for a system of K-feldspar, plagioclase, and halloysite (Maher, 2011), and chemical equilibrium would therefore have been reached in both groundwater of W1 and W3. Secondly, the weathering of clay breccias present in the bottom of the section of W3 (with clay being characterized by higher Ge/Si ratio as reported in the literature; Ameijeiras-Mariño et al. (2018); Bernstein (1985); Froelich et al. (1992); Kurtz et al. (2002); Lugolobi et al. (2010); Murnane and Stallard (1990)) could have led to higher Ge/Si in groundwater of W3 than in W1.

7.5.2 Variations in Ge/Si ratio in soil solution and runoff water

The Ge/Si ratio of soil solutions SS-BA-173, SS-SC-180, and SS-FO-396 in our volcanic soils (from 0.71 to 1.64 µmol mol^{-1}) were within the same range of values obtained in soil solution from Acrisols from a volcanic province in Brazil (0.20 to 1.07 µmol mol^{-1}; Ameijeiras-Mariño et al. 2018), but four-fold lower than in soil solution of Ultisols on the volcanic tropical island of Puerto Rico (2.0 to 4.1 µmol mol^{-1}; Kurtz et al., 2011; Lugolobi et al., 2010) or ten-fold lower than horizons of highly desilicated volcanic soils in Hawaii (2 to 14 µmol mol^{-1}; Derry et al., 2005).

The values of Ge/Si ratio of soil solutions did not significantly differ between the forested (SS-FO-396) and cultivated sites (SS-BA-173, SS-SC-180) (Figure 7-3), whereas elemental concentrations in soil solutions (except for Na and Al) were significantly lower in the forested site SS-FO-396 than in the cultivated ones SS-BA-173 and SS-SC-180 (Table 7-2). The larger K, Mg, and Ca concentrations in SS-BA-173 and SS-SC-180 waters could be the result of fertilizer inputs. Indeed, the use of fertilizer and amendments in these plots involved potassium fertilizers as well as dolomite amendment (Henriet et al., 2008a; *Chapter 5*). This hypothesis is supported by two facts: (1) the reserve

of weatherable primary minerals did not significantly differ between the cultivated and forest plots (*Chapter 6*); (2) the Na concentration in soil solutions from cultivated and forest plots were similar. The larger Al concentration in the soil solution of the forest plot is not surprising considering the increase of the content of Al-humus complexes and gibbsite with the altitude in soils from the Pères River watershed (*Chapter* 2). Finally, Si concentration in the soil solution of cultivated plots was significantly larger than in the soil solution of the forest plot. Liming could have impacted the DSi release in the soil solution of the cultivated plots. However, Ge/Si ratio and the results of the two component mixing model indicate that phytolith dissolution was the main process controlling DSi concentration regardless of land use (Figure 7-6). In the studied soils, liming should have a minor impact on soil pH because of the very high soil buffering capacity (Figure 7-S2). Resulting impact of liming on phytoliths and minerals dissolution is therefore likely negligible. Since Si is highly mobile as uncharged aqueous $H_4SiO_4^0$ (Nguyen et al., 2016), rainfall strongly affected DSi concentration in soil solution without impacting the process controlling DSi itself. This is in perfect line with results obtained in *Chapter 2* that demonstrate that rainfall strongly controls the bio-available Si pool in soil of the studied watersheds. However, it is surprising that the Ge/Si ratio in soil solution under croplands did not differ from that under the forest (Figure 7-3), given the strong differences in Si soil to plant cycle in these plots (*Chapter 5* and *Chapter 6*). Banana and sugarcane are Si-accumulating plants that take up 171 and 457 kg Si ha^{-1} yr^{-1} respectively from the soil solution in the studied plots (BA-173 and SC-180 *Chapter 5*), while Si plant uptake amount to 43 kg ha^{-1} yr^{-1} under forest (FO-396 *Chapter 6*). Unlike other crops, where almost all plant parts are removed from the field (T. Klotzbücher et al., 2018; Vandevenne et al., 2011), "Si-rich" plant parts (mainly leaves) of sugarcane and banana plants are returned to soil, even in intensive cropping systems. This leads to very important returns of readily dissolving PhSi (Fraysse et al., 2010, 2009, 2006) into the topsoil in these cropping systems. Considering these points, it is not surprising that phytolith dissolution controls DSi concentration in soil solutions of the three plots. Moreover, these results are in perfect agreement with the evolution of DSi concentration in soil pedons from the BA-173 and SC-180 plots (*Chapter 5*). Indeed, in *Chapter 5* it has been observed that in surface soil horizons (00-25 cm), PhSi dissolution controls DSi concentration in soil

solution while in B horizons beneath, the dissolution of LSi minerals controls DSi concentration in soil solution.

Two soil solution samples under forest exhibited higher values of Ge/Si ratio (1.58 and 1.64 µmol mol^{-1}, Figure 7-3 and Table 7-S1) relatively to the other samples under forest (0.79 to 1.06 µmol mol^{-1}). These higher Ge/Si ratios might result from plant uptake or colloidal contribution. Plants discriminate against Ge (Blecker et al., 2007; Delvigne et al., 2009; Derry et al., 2005), and higher Ge/Si ratios in soil solution may result from an important Si uptake by plant. However, if these higher Ge/Si ratios were driven by plant uptake, it would be constant throughout a sampling time series. This is not the case since we have measured a lower value of Ge/Si ratio (0.96 µmol mol^{-1}) in the same sampling point at another period. The higher values of Ge/Si are likely related to a punctual event, and possibly the presence of colloidal Si such as proto-imogolite sol, which occurs in Andosols and Podzols (Farmer, 1982; Farmer et al., 1978; Farmer and Lumsdon, 2001). These colloids typically have high Ge/Si ratios (10-15 µmol mol^{-1} for allophane (Kurtz et al., 2002)) which would increase the Ge/Si ratio of the soil solution . This hypothesis is also supported by the very high macroporosity of this soil (*Chapter 6*; Dorel et al., 2000) in which colloids may easily be transferred (McIntosh et al., 2017), e.g., upon a rain event.

Collected soil solutions were gravity waters with likely short mean residence time due to the high macroporosity and frequent rainfall. Microporal soil water with longer mean residence time was not collected with the settled no-suction lysimeters. We suspect that the relative contribution of PhSi, PSi, and LSi greatly depends on the soil solution mean residence time (Gérard et al., 2003, 2002). We think that the composition of soil solutions with larger mean residence time would be more affected by the dissolution of poorly crystalline aluminosilicates and primary minerals if present (Gérard et al., 2003, 2002). However, the microporal soil solution likely less contribute to Si exports towards the hydrosystem.

The values of Ge/Si ratio in runoff waters were within the range of values of soil solutions, and could result from the concomitant dissolution of PhSi, LSi, and PSi minerals. PhSi is likely the main contributor as it controls the DSi concentration in the topsoil solution (*Chapter 5*). Al concentration was

slightly larger in runoff waters than in soil solutions, reflecting a possible contribution from PSi dissolution to increase the Ge/Si ratio.

Groundwater, soil solution, and runoff at the plot scale contribute to stream water. Soil solution and runoff water had Ge/Si ratios distinct from that of groundwater (Figure 7-3). In following sections, we will discuss the contribution of each aqueous compartment to stream water during base flow and flood periods using Ge/Si ratio.

7.5.3 Ge/Si ratio, a natural tracer of stream water origin

7.5.3.1 Base flow periods

The Ge/Si ratios of stream water of Pérou and Pères rivers at base flow (ranging from 0.13 to 0.26 µmol mol^{-1}) were close to that of groundwater (ranging from 0.09 to 0.85; Table 7-2, Figure 7-3) and were significantly lower than those of soil solutions (Figure 7-3). A similar observation can be made for the tributaries of the Pérou River (which were sampled at base flow). This supports that groundwater controls the elemental composition of these rivers at base flow, as it is widely recognized (Bishop et al., 1990; Burns et al., 2001; Charlier et al., 2011, 2008; Kurtz et al., 2011; Peters and Ratcliffe, 1998; Robson et al., 1992). Accordingly, Ge/Si ratio in stream waters at base flow has been considered elsewhere as representative of groundwater composition (Lugolobi et al., 2010, Ameijeiras-Mariño et al. 2018, Kurtz et al. 2011).

Charlier et al. (2015), using radiogenic strontium (Sr) isotopes, were able to define the hydrological functioning of the Pérou and Pères rivers. The Pérou River, whose impluvium is mainly located in the upstream part of the cultivated area, does not show any evidence of significant lateral inputs on its intermediate part where it crosses the lava flows. The Pérou River is therefore mainly influenced by surface and subsurface flow that results from heavy rains on steep slopes at high altitude (Charlier et al., 2015; Crabit et al., 2016). As we do not have any data on Ge/Si ratios of surface and subsurface water in the upstream part of the Pérou River, we can consider that the mean values of Ge/Si ratio of 0.21±0.03 µmol mol^{-1}, and Si concentration of 471±46 µmol l^{-1} at the upper gauging station (GS1) at base flow represent that component. Mean Ge/Si ratios were 0.18±0.03 and 0.17±0.03 µmol mol^{-1}, and Si concentrations were 515±141 and 517±52 µmol

l^{-1} at downstream gauging stations GS2 and GS3, respectively, and did not significantly differ relatively to that at GS1. This confirms the data of Charlier et al. (2015) suggesting that the composition of the Pérou river at base flow is mainly controlled by surface and subsurface flow resulting from heavy rains on steep slopes at high altitude.

The Pères River does not have a head of basin at high altitude and its geochemical signature seems totally controlled by the drainage of the aquifer of pyroclastic deposits (W4) (Charlier et al., 2015). In the Pères River gauging station (GS5), mean Ge/Si ratio at base flow was 0.13±0.04 µmol mol^{-1}, which was slightly below the Ge/Si ratio of sampled springs of the Pères River (0.22-0.26 µmol mol^{-1}), and below the one of groundwater representing the pyroclastic component (W4: 0.29 µmol mol^{-1}). This indicates that another groundwater reservoir with a lower Ge/Si ratio could control the composition of the Pères River at base flow level.

7.5.3.2 Flood periods

Stream hydrographs of the studied floods (Figure 7-2) highlight that different flood categories have been sampled. This allowed us to investigate the processes controlling the composition of river water according to flood size. For the floods of the Pérou River sampled at GS3, FPU1 can be considered as a big flood, FPU2 as a middle flood, and FPU3 as a small flood. For the floods of the Pères River sampled at GS5, FPS1 and FPS3 can be considered as small floods, and FPS2 as a big flood.

Figure 7-4 illustrates the Si concentrations against water discharges for the six floods. For each flood, the concentration of dissolved Si in stream water was lower at the end of the flood even if the discharge had returned to its initial state. The data highlight that the decrease in Si concentration in the stream water during the floods FPU1, FPU2, FPS2, and FPS3 was more limited that what would be expected with simple dilution by rainwater.

In contrast, for FPU3 and FPS1, dilution by rainfall could explain the evolution of the Si concentrations in streams. However, for these two floods, a second peak water discharge occurred during the flood. This second peak was associated to an increase of the Si concentration in the stream for both FPU3 and FPS1, which cannot be explained by rainwater dilution. These results support a contribution from an additional source of Si fluxes to rivers during

floods (Bazemore et al., 1994; Dewalle et al., 1988; Klaus and McDonnell, 2013; Rice and Hornberger, 1998). The plots of the Ge/Si ratios against the water discharges are shown on Figure 7-5 for FPU1-2-3 and FPS1-2-3. During all floods, Ge/Si ratio in stream waters increased. This suggests an influence from the soil solution or runoff waters during the floods, as observed by Ameijeiras-Mariño et al. (2018) and Kurtz et al. (2011). The results of the two components mixing model (Figure 7-7) helped us to evaluate the relative contribution of soil solution and/or runoff waters during the floods.

It appears that, in Pérou River, the less intense was the flood, the larger was the contribution from the soil solution and/or runoff water at plot scale. This suggests that during intense flood events generated by heavy rainfall, water only partially originated from soil solution or runoff in croplands. For such floods, the most likely is that water mainly came from surface and subsurface flows generated on the steep slopes in altitude as it was observed at base flow. This would explain the relatively stable Ge/Si ratio during intense flood events (Figure 7-5). However, due to rainfall, a slight dilution of Si and other elements occurred (Figure 7-4; Table 7-S2). In contrast, during relatively smaller floods, the data suggest that the relative contribution of soil solution and/or runoff under croplands is more important (Figure 7-7). This may be due to a lower contribution of surface and subsurface flows generated on the steep slopes in altitude, and a resulting larger relative contribution of soil solution and/or runoff generated under croplands.

In the Pères River, the data point to a larger contribution from soil solution and/or runoff water at plot scale during the FPS2 big flood event (~41%) than during the FPS1 and FPS3 small flood events (~22% for both floods). This indicates that the functioning of this river differed from that of the Pérou River. This could be due to the absence of a head of basin at high altitude for the Pères River. We can speculate that during floods in the Pères River, the contribution of groundwater remained unchanged while the contribution of soil solution and/or runoff generated under croplands was proportional to the intensity of the flood.

7.5.4 Impact of land use on the Si fluxes in rivers

As Ge/Si ratios in soil solutions of banana (BA-173) and sugarcane (SC-180) plots were very close to the one of soil solution from the forest (FO-396) plot,

it is very difficult to identify a land use impact on the Si fluxes in rivers. Moreover, the Ge/Si data in soil solution indicated that land use does not impact the proportion of Si originating from the dissolution of PhSi in soil solution (see Section 5.2). This is mainly due to the fact that most of the Si absorbed by the studied Si-accumulating crops sugarcane and banana, is returned to soil with plant debris (*Chapter 5*). Therefore, instead of decreasing the topsoil PhSi pool, these crops contribute to slightly increase the PhSi pool in the topsoil (*Chapter 6*).

However, conversion from forest to cropland not only modifies the soil-to-plant Si cycle but also strongly impacts the soil bulk density (*Chapter 6*). As an implication from this study, this could impact the distribution of water that infiltrates or runoffs, which could affect the contribution of soil solution and/or runoff water at plot scale to Si fluxes toward river water during flood events. The data indicate that the impact of land use on Si fluxes in rivers would only be significant during floods. If floods only occur about 10% of the time (Lloret et al., 2011), they accounted for 31 and 16% of the total annual Si fluxes in Pérou River (at GS3) and Pères River (at GS4) respectively (as obtained from the ratio [Annual Si fluxes during flood]/[Total annual Si fluxes] (see Section 7.4.4 and Table 7-3); with annual Si flux during floods at GS4 being a minimal value (see Section 7.3.4). These values are in the same range as contributions from floods to the annual chemical weathering fluxes of 21 to 31% that were obtained for twelve rivers from this area (Dessert et al. 2015). As another comparison, more than 60% of the dissolved organic carbon export occurred during floods of eleven rivers on the Basse-Terre Island in Guadeloupe (Lloret et al., 2011), and the dissolved organic carbon fluxes were the highest for the Capesterre River that is located very close to the Pérou and Pères rivers. This has been attributed to the fact that the Capesterre River basin is highly exposed to rainfalls, and that therefore its soils are prone to the erosive power of extreme meteorological events (Lloret et al., 2011).

Impact of land use on Si fluxes in the Pérou and Pères rivers could therefore be significant. In the Pères River, the Ge/Si ratio of the the stream water during floods allowed us to determine that the relative contribution of soil solution and/or runoff waters generated under croplands increases with increasing flood intensity. As this watershed is mainly covered by croplands

(~57%), we can tentatively explain that the impact of cropland on the Pères River composition increases with increasing flood intensity. For the Pérou River, the contribution of surface and subsurface flows generated in the head of the basin at high altitude could dilute the contribution from croplands during big flood events.

The use of the Ge/Si ratio tracer in these two rivers and associated end-members allowed us to determine that the impact of agricultural land use on the stream water composition only occurs during flood events and that it is more pronounced in small rivers where the watershed is exclusively covered by crops. In larger rivers, the agricultural land use impact could be dilute by contributions from higher altitude where watershed is not cultivated.

7.6 Conclusion

Phytolith dissolution contributes to ~70-95% of the dissolved Si in soil solutions regardless of land use. This indicates that land use change does not influence the relative contribution of phytoliths to the dissolved Si of the soil solution. In stream water, the Si concentration and Ge/Si ratio during floods differing in intensity in the Pérou and Pères rivers show that the impact of soil solution on Si fluxes in rivers is only significant during floods. The contribution of the soil solution and/or runoff from croplands during major flood events can be significant in small watersheds that are exclusively cultivated, but remains low in larger watersheds with a head of basin at high altitude where forests dominate. The determination of the Ge/Si ratio and elemental composition of aqueous samples from soil solution to river allow to better understand the functioning of two cultivated volcanic watersheds in Guadeloupe. However, during flood events, this tracer does not distinguish the respective contributions of the soil solutions from croplands and from forest areas to river waters.

Conclusion and perspectives

General discussion

The PhD research aimed to study the impact of land use on the soil-plant cycle of Si and its outreach to watersheds in humid tropical conditions.

The Si cycle plays numerous ecological roles directly linked to global changes issues. Dissolved Si fluxes in rivers directly impact the capacity of oceans to store carbon as Si is an essential element for diatoms (Tréguer et al., 2018; Tréguer and Pondaven, 2000). Si absorption by plants alleviates biotic and abiotic stresses (Coskun et al., 2019; Epstein, 1999), and may therefore increase crop yields. The biological pumping of silicon directly impacts the Si fluxes to rivers (Derry et al., 2005) because Si plant uptake leads to the formation of phytoliths that return to soil where they readily dissolve. Therefore, understanding the factors governing the mobility of Si in the soil-plant system is essential to address global changes issues, and provide Si ecosystems services.

The Introduction exposed the four main questions addressed. The replies to these questions are summarized here below and on Figure CP-1.

Q1. **What is the impact of mean annual rainfall on plant available Si in perhydrated, gibbsitic Andosols?**

We studied the soil Si pools along a topo-climosequence ranging from 65 m above sea level (asl) to 375 m asl and with Mean Annual Rainfall (MAR) evolving from 2650 mm to 4400 mm in Andosols from Basse-Terre, Guadeloupe. We observed that increasing rainfall led to (i) the exhaustion of the soil buffering capacity, (ii) the decrease in plant available Si and soluble phytolith content, and (iii) the increase in gibbsite content. Increasing rainfall thus increases Si leaching, thereby decreasing plant available Si, and further leads to increasing dissolution of soil phytoliths. Al and organic matter further accumulate leading to increasing gibbsite content and Al-humus complexes. Rainfall therefore majorly controls the mobility of Si in the studied highly weathered Andosols and the nature of secondary products.

Q2. **What are the respective impacts of soil weathering stage and land use on the soil-plant Si cycle in the humid tropics?**

Literature data show that an increase in soil weathering led to a decrease in Si biocycling in wet tropical rice cropping systems. The opposite trend was observed in forest ecosystems. Converting forest area into cropland has thus a tremendous impact on the Si soil-plant cycle. This opposite picture is attributed to differences in rooting depth, litter, recycling or export of plant residues, density of Si-accumulating plant species, soil and soil fertility management. In particular, forest trees develop deep rooting while rice crop has a shallow root system. The forest litter is an environment densely explored by fine roots, in which limiting nutrients are concentrated, the turnover of C and nutrients is large, and phytolith dissolution is rapid. The deep rooting and litter environment of wet tropical forests minimize the loss of elements by leaching. Besides, crop harvesting exports Si out of cultivated ecosystems. Two Si sinks thus occur in natural forest ecosystems while they strongly decrease in croplands: the subsoil weatherable lithogenic Si pool that is exploited by deep roots of forest trees; the topsoil phytogenic Si pool that is directly exploited by a very dense root network.

Q3. How does the conversion from forest to cropland impact the soil-plant cycle of Si? How critical is the management of inedible plant parts?

We showed that the biological Si feedback loop was intense in the studied banana and sugarcane soil-plant systems, increasing the mobility of Si. Converting forest area into banana or sugarcane cropland strongly modified the soil-plant Si cycle. Namely, an ecosystem in which Si is largely stored in the standing biomass, and for which the biological Si feedback loop is rather low is replaced by an ecosystem in which the biological Si feedback loop becomes intense, strongly impacting the dissolution of lithogenic Si and pedogenic Si pools.

In the studied cultivated plots, we observed that DSi concentration in the soil solution of these croplands was large in upper soil horizons, then decreased in middle horizons, and finally increased in less weathered deep horizons in which weatherable lithogenic Si minerals are still present. Regarding the evolution of the soil weathering stage and considering the solubility of amorphous silica (0.002 mol l^{-1}), we interpreted the DSi concentration in soil solution of deep horizons as being controlled by the lithogenic Si pool, and the one of surface horizons as being controlled by the phytolithic Si pool. We further confirmed this by tracing the Si origin with the Ge/Si ratio. Indeed,

Ge/Si ratios, Si concentrations, and Al concentrations of soil solutions collected in the banana and sugarcane crops suggest that phytoliths and lithogenic silicates are the two main contributors of dissolved Si in soil solutions. The use of a two components mixing model suggests that phytolith dissolution contributes to 70-95% of Si collected in soil solutions of banana and sugarcane plots. We attributed this to two main facts. Firstly, the dominance of Si accumulating crops on the three last centuries on the studied plots. Secondly, the restitution of the inedible plant parts on soil. The management of the inedible plant parts at harvest is therefore a key factor to maintain large DSi concentrations in the top soil horizons, a high Si mobility in the soil-plant system, and soil fertility.

Q4. How does land use impact the dissolved Si fluxes to volcanic watersheds?

Analyses of the Ge/Si ratio and elemental composition of river waters at base flow, river waters during floods, groundwater, soil solutions, and runoff waters allowed us to better constrain the functioning of two cultivated volcanic watersheds in Guadeloupe. Pérou and Pères rivers located on the eastern flank of *La Soufrière* volcano in Guadeloupe were studied. In the Pérou River watershed, the head of the basin is covered by forests where rainfall is very important whereas a cultivated area dominates downstream. The Pères River has a small and mainly cultivated basin. The composition of the Pérou River at base flow is mainly controlled by surface and subsurface flow resulting from the heavy rains on the steep slopes at high altitude, while groundwater is the only end-member that can control the composition of the Pères River water at base flow level. Finally, the impact of soil solution on dissolved Si fluxes in rivers is only significant during floods. The contribution of the soil solution and/or runoff generated under croplands during major flood events can be significant in small watersheds that are exclusively cultivated, but remains low in larger watersheds with a head of basin dominated by forest at higher altitude.

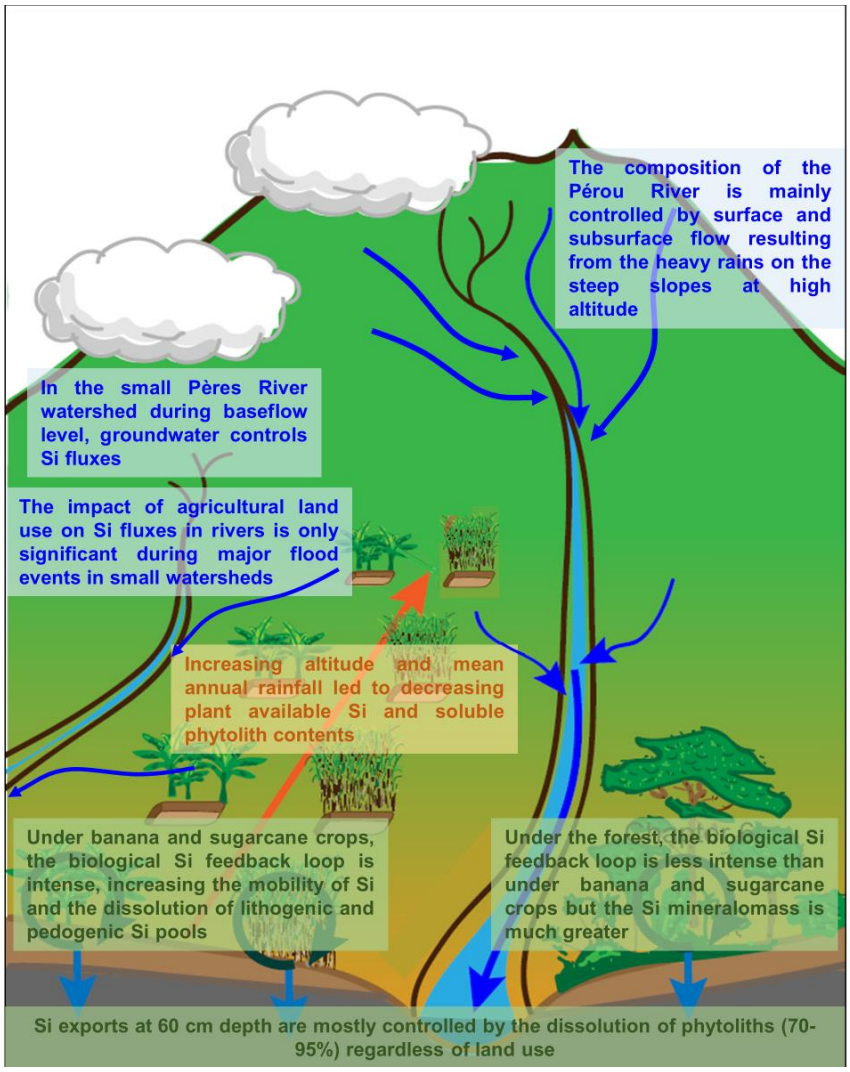

Figure CP-1: Scheme summarising the results of field experiments in Guadeloupe (Q1-3-4). Results relative to Q1 are written in orange, results relative to Q3 are written in green, and results relative to Q4 are written in blue.

Perspectives

Our results highlight important remaining gaps that open new perspectives (P). Figure CP-2 illustrates a schematic view of the proposed perspectives.

Perspective 1 (P1): How to quantify the soil phytolith pool?

Chapters 2 and 3 of this PhD thesis pointed to analytical difficulties in the methods quantifying phytoliths, notably in volcanic ash soils. So far, the quantification of soil phytoliths has relied on chemical and physical extractions. The chemical extraction has the advantage of being much less time consuming than the physical one that proceeds through heavy liquid separation. The advantage of the latter is that we can observe and control the extracted particles.

<u>The chemical extraction - discrimination of phytoliths is a complicated challenge</u>

The chemical extraction is based on the fact that amorphous silica, among which phytoliths, dissolve quickly in heated alkaline reagents while crystalline silicates dissolve slowly and linearly (DeMaster, 1981). It goes without saying that non-biogenic amorphous phases also dissolve quickly in such solutions (Huang et al., 2002; Kamatani and Oku, 2000; Wada, 1989). It includes short-range-ordered pedogenic aluminosilicates, volcanic glasses, pedogenic or lithogenic opals. Moreover, it has been observed that part of crystalline minerals may also dissolve quickly in such solutions (Li et al., 2019; *Chapter 3*). The use of Si/Al atomic ratio of alkaline extracts was proposed to discriminate PhSi from SRO minerals and volcanic glasses, attributing $Si/Al \geq 5$ to PhSi and $2 \geq Si/Al \geq 0.5$ to SRO and crystalline minerals in soil (Barão et al., 2014; Clymans et al., 2015a; Kamatani and Oku, 2000; Koning et al., 2002). However, this technic only works in soils devoid of amorphous silicate minerals and Al hydroxides (*Chapters 2 and 3*). The interpretation of Na_2CO_3 extracts to quantify the PhSi pool remains thus hazardous in a number of soils. Ash derived Andosols contain volcanic glass, SRO minerals, Al-humus, poorly crystalline Al oxide and gibbsite, which all dissolve quickly in alkaline solutions (Clymans et al., 2015a; Jackson, 1956; Kamatani and Oku, 2000; Pereira et al., 2009; Taboadela, 1953; Wada, 1977). The use of the Si/Al atomic ratio is thus not unequivocal because several soil components readily dissolve in alkaline solutions.

In *chapters 2 and 3* we proposed to pretreat soil samples with dark oxalate prior to alkaline extraction that removes amorphous PSi and, likely, poorly crystalline Al hydroxide (Huang et al., 2002). However, Na_2CO_3 may remove volcanic glass and gibbsite. The presence of both of these soil components would therefore make it difficult to quantify the proper PhSi pool.

Moreover, we proposed to dose not only Si and Al but also Mg and Fe in alkaline extracts to identify the presence of volcanic glass. However, in *Chapter 3* we observed that released Al, Mg and Fe can precipitate during alkaline extractions when alkaline extractable LSi are present.

W**e suggest to use germanium (Ge) to trace Si in alkaline extracts** (Delvigne et al., 2018). LSi, PSi, and PhSi have distinct Ge/Si ratios. PhSi have amongst the lowest Ge/Si ratios as plants discriminate against Ge (Blecker et al., 2007; Delvigne et al., 2009; Derry et al., 2005). During the neoformation of PSi, Ge substitutes for Si and the PSi is therefore enriched in Ge as compared to the parent material (Kurtz et al., 2002; Murnane and Stallard, 1990). This tool discriminates DSi from phytolith dissolution from DSi from LSi/PSi dissolution.

<u>The chemical extraction – only fresh phytoliths are dissolved</u>

Na_2CO_3 extractant mainly dissolves fresh and readily soluble phytoliths while it is less selective for aged phytoliths that are poorly dissolved in Na_2CO_3 (Meunier et al., 2014). Moreover, little is known about the entrapment of PhSi within soil microaggregates and the impact this could have on phytolith dissolution in soils and in alkaline reagents.

In *Chapter 3*, we tested if previous elimination of aggregative soil components (mainly SRO minerals, organic matter, Fe oxides) impact the size of the quantified PhSi pool with alkaline reagents. However, we did not measure any significant impact of these treatments.

<u>The heavy liquid separation – not only phytoliths are extracted</u>

The <u>heavy liquid method</u> proposed by Kelly (1990) relies on two hypotheses. Firstly, soil phytoliths are mainly present in the silt fraction of the soil. Secondly, PhSi has a density of ~2.3 g cm^{-3}. Following these hypotheses, the method consists in dividing the silt fraction into light (PhSi) and heavy

components (other minerals), through a series of heavy liquid separations, using a solution with a density of 2.3 g cm^{-3}. However, other soil components may have similar densities as PhSi. In the gibbsitic Andosols that we studied, the presence of cristobalite (2.32-2.36 g cm^{-3}), tridymite (2.25-2.28 g cm^{-3}), and gibbsite (2.34 g cm^{-3}) prevents an accurate assessment from being made for the PhSi content in soil.

The physical extraction – DCB treatment could dissolve phytoliths

The physical extraction method is commonly preceded by an elimination of Fe oxides to avoid soil aggregation. Fe oxides are typically removed with a Dithionite-Citrate-Bicarbonate (DCB) extraction at 75°C (pH~9). In *Chapter 3*, we observed that the chemically quantified PhSi pool was slightly lower after DCB pretreatment of the soil. We hypothesized that a part of the PhSi pool could dissolve in DCB because of the relatively high temperature (75°C) and alkalinity (pH~9) that enhance PhSi dissolution (Fraysse et al., 2009, 2006).

As a perspective, **we propose to test the UV-oxalate extraction to remove Fe oxides and SRO minerals**. As oxalate solution is buffered at pH3, this could avoid the dissolution of PhSi unlike the DCB extraction.

We further propose to **realize X-ray diffraction on the undissolved, solid fractions** to better constrain the extracted components.

Finally, **we propose to quantify the content of crystalline silicate minerals through XRD data** to evaluate the phytolith amount in soil. This method needs however further investigations to be well calibrated.

Perspective 2 (P2): Improve the understanding of the agricultural impact on the soil-plant Si cycle.

Agricultural land use impacts the Si cycle (a.o. Barão et al., 2014; Clymans et al., 2015, 2011; Klotzbücher et al., 2018; Struyf et al., 2010; Vandevenne et al., 2011, 2015). Impacts of Si exports through crop harvest (Struyf et al., 2010; Vandevenne et al., 2011) and erosion (Clymans et al., 2015b), Si inputs with fertilizers (a.o. Li et al., 2019, 2018; Savant et al., 1996; Seyfferth et al., 2013) and irrigation waters (Desplanques et al., 2006; Riotte et al., 2018b), or liming (Haynes and Zhou, 2018; Li et al., 2019) have been investigated.

However, little is known about the impact of the soil weathering stage (*Chapter 4*), the management of the inedible plant parts at harvest (*chapters 5 and 6*), agroforestry, plant species used during fallows, root systems of cultivated plants, cover crops, tillage, soil compaction, species involved in agricultural rotations, etc. A huge field of research is therefore open.

We observed in *Chapter 4* that an increase in *soil weathering stage* led to a decrease in Si biocycling under rice croplands. However, results are still lacking to extend these conclusions to other crops. Moreover, the soil weathering stage would also influence the impact that liming could have on the Si cycle (Haynes, 2019). Therefore, more studies are needed to shed light on the impact of the soil weathering stage on the soil-plant Si cycle in cultivated areas.

In *chapter 5 and 6*, we showed that the *restitution of inedible plant parts on the soil at harvest* could increase the mobility of the Si in banana and sugarcane soil-plant systems. However, to the best of our knowledge, the impact of long-term incorporation of inedible plant parts has never been studied for other crops. We therefore suggest to follow the path we traced concerning the impact of long-term inedible plant parts incorporation in soil to other crops and other soil types.

Agroforestry, which consists of planting trees and crops together, could also impact the soil-plant Si cycle. In particular, deep roots of trees could allow to take up Si in deep and less weathered soil horizons and to return it to soil through litter fall, making it available for crops. Agroforestry can also decrease soil erosion, which could limit physical PhSi exports.

The plant species used during fallows could greatly influence the Si sol-plant cycle. Indeed, the use of Si-accumulating plants could replenish the topsoil in PhSi at the end of the fallow period if the plants are crushed and returned to soil. If plant parts are exported for hay, this could be an additional important Si export.

Root systems of cultivated plants may greatly vary according to plant species and cultivars. This directly affects the volume explored by plants to take up Si. This could therefore strongly impact the Si uptake by crops and therefore the impact of croplands on the soil-plant Si cycle.

Cover crops are planted between cropping seasons. They play an important role in protecting soil against erosion and nutrient leaching. The use of cover crops could therefore impact Si leaching. The use of Si-accumulating species could greatly limit Si leaching.

Tillage plays different roles in cultivated soils, and results in a homogenized upper soil horizon. This could bring up PhSi particles from soil surface to deeper soil, which could impact PhSi particles dissolution (Li, 2019). Tillage also impacts the physical and hydrological properties of soils (Hill, 1990). It creates, among other things, a ploughing sole. This limits water infiltration and can increase soil erosion (Poulenard et al., 2001), which could impact Si leaching and Si losses due to erosion (Clymans et al., 2015b).

We think that *species involved in agricultural rotations* could impact the soil-plant Si cycle through differences in rooting systems, Si-accumulation, Si exports through harvests, etc. Further investigations are thus needed to fully understand the implications the rotation could have on the soil-plant Si cycle.

These are examples of possible agricultural practices that could impact the Si cycle. It shows how much the impact of agricultural on the Si cycle is full of mysteries!

Perspective 3 (P3): How to include Si fertilization in agricultural practices? How to determine the Si quantity and the Si form to apply?

Agricultural land use is often associated with a decrease in the bioavailability of Si (Barão et al., 2014; Struyf et al., 2010; Vandevenne et al., 2015). Moreover, Si fertilization increases crop yields, especially for Si-accumulating crops grown on highly weathered soils (A. Klotzbücher et al., 2018; Li et al., 2018). Furthermore, common agricultural practices still do not include Si fertilization.

One reason is that only few data are available about Si bioavailability in soils around the world. Meunier et al. (2018) proposed to use pH as a proxy to estimate the pool of bioavailable Si. This method is very promising as it would allow to easily deduce Si bioavailability from pH data that are widely available worldwide. However, the relations they found are only validated for the region they studied in India. **Thus a very important and exciting perspective**

would be to extent the relation between pH and Si bioavailability to other regions and soil types. We expect that this relation would greatly depend on soil type. For example, in Ferralsols, Fe oxides are major secondary minerals that may adsorb monosilicic acid. This sorption process can decrease Si bioavailability (Haynes, 2019; Haynes and Zhou, 2018; Tavakkoli et al., 2011). In other soils, high pH values could be associated with large Si bioavailability as PhSi readily dissolve in such conditions (Fraysse et al., 2009, 2006; Guntzer et al., 2012).

Another reason is that farmers are still poorly documented about the beneficial effects that Si can have on crops. The demand for silicate fertilizers therefore remains marginal, which limits the interests of the industry to develop a real offer. In addition, silicate fertilizers are available in many different forms (silicate slags, straw residues, biochar, ground basalt, silica gel, etc.) (Ayres, 1966; D'Hotman and Villiers, 1961; Li et al., 2019, 2018; Ma and Takahashi, 1989; Mantovani et al., 2016; Marxen et al., 2016; Wickramasinghe and Rowell, 2006), but we do not know which type of fertilizer is best suited; this could depend on the type of soil and climate conditions. **Studies testing different forms of Si fertilizers according to soil type would therefore be of a great interest to optimize fertilization technics and further develop an efficient market.**

Finally, $CaCl_2$-Si is generally used as the estimator of the bio-available Si pool (Sauer et al., 2006). However, the link between the $CaCl_2$-Si pool and the Si content in plants is not always obvious (*Chapter 2*) maybe because of the impact that soil properties could have on this link. This means that critical $CaCl_2$-Si values could depend on soil type. This opens up a field of research of major importance especially if critical $CaCl_2$-Si is linked to plant response. **Studies aimed at establishing critical $CaCl_2$-Si values according to soil type would be of great interest to improve Si fertilization need and management.** We are convinced that, when reliable tests will be available to assess the real bio-available Si pool and the associated critical values, Si fertilization would rapidly develop. **We preconize to start studies in soils for which Si bio-availability is low and crops sensibility to diseases is high**. In this respect, the southern part of the Basse-Terre Island, Guadeloupe, could be a perfect field of study. Indeed, in this region, the sensibility of banana crop to diseases is particularly high (Dorel and Perrier, 1990). Such

investigation is promising since the link between Si availability and banana plant resistance to diseases has been established (Kablan et al., 2011; Vermeire et al., 2011), and parameters impacting Si concentrations in banana leaves are known (Henriet et al., 2008a).

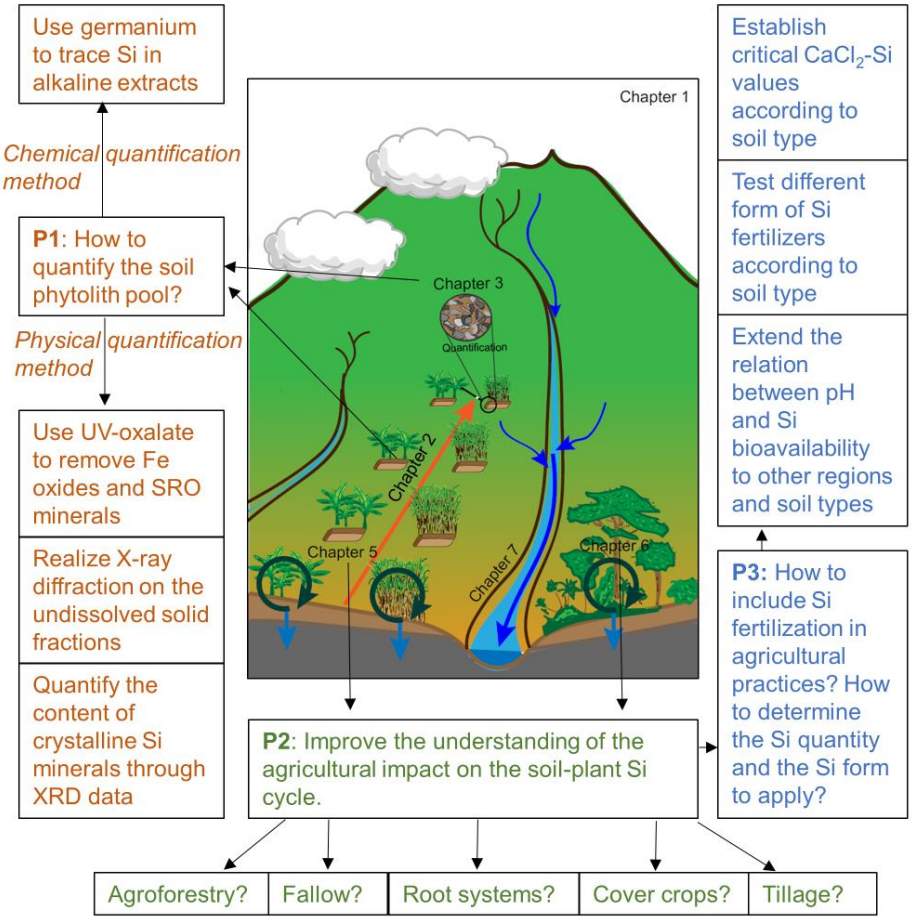

Figure CP-2: Scheme summarizing the perspectives of the PhD thesis Perspectives relative to P1 are in orange, perspectives relative to P2 are in green, and perspectives relative to P3 are in blue.

Appendixes

Appendixes relative to chapter 2

Evolution of the silicon bio-availability in volcanic soils along a climo-toposequence in Guadeloupe

Table 2-S1: Total Si, Al, and Fe contents, DCB extractable Al and Fe contents (d), dark acid oxalate extractable Si, Al and Fe contents (o), and pyrophosphate extractable Al and Fe contents (p) in soil samples. Average values are computed from the individual values measured on the three composite samples of each plot (BA: banana; SC: sugarcane).

Altitude (m)	**Land use**	**Total elemental content (g kg^{-1})**			**DCB extractable content (g kg^{-1})**		**Dark oxalate extractable content (g kg^{-1})**			**Pyrophosphate extractable content (g kg^{-1})**	
		Si_t	**Al_t**	**Fe_t**	**Al_d**	**Fe_d**	**Si_o**	**Al_o**	**Fe_o**	**Al_p**	**Fe_p**
65	BA	177.6	131.3	79.3	18.50	42.59	16.49	36.17	10.91	8.64	3.30
65	SC	181.1	128.4	87.9	17.95	44.96	11.96	27.01	12.54	9.19	5.30
100	BA	153.3	131.5	96.2	20.67	44.70	25.27	51.84	12.00	7.68	2.68
100	SC	171.3	127.1	84.3	18.41	43.90	20.25	42.91	11.46	7.33	3.24
150	BA	151.6	133.4	100.7	19.97	49.08	20.80	41.03	12.01	6.79	3.25
150	SC	144.4	131.4	91.1	22.93	45.94	16.81	36.85	13.87	14.55	8.71
200	BA	145.8	135.3	97.3	18.20	49.34	17.23	34.59	13.31	8.56	5.29
200	SC	148.5	130.4	89.7	17.78	46.24	14.16	32.36	14.36	9.64	6.81
250	BA	152.0	133.6	93.0	17.54	49.46	10.43	26.86	10.92	12.32	7.58
250	SC	145.2	136.8	99.3	18.90	53.15	11.78	30.35	12.88	11.16	8.49
300	BA	145.9	138.8	86.1	16.60	45.65	13.24	31.93	12.39	8.18	6.63
350	BA	145.6	121.1	82.0	16.78	39.74	12.70	32.86	16.62	13.01	13.42
375	BA	141.5	110.8	79.7	16.43	37.61	10.66	32.67	18.42	12.82	12.79

Table 2-S2: Particle size analysis, Total Reserve in Bases (TRB), Si/(Al+Fe), Fe_d/Fe_t and Fe_o/Fe_d atomic ratios, contents of organic C and allophane, $Si_o/(Al_o-Al_p)$ ratio (standard deviations in brackets). Average values computed from the individual values measured on three composite samples of each plot at each altitude. Differences between banana (BA) and sugarcane (SC) plots were tested at each altitude with an ANOVA statistical test with the aov function of the R programming language. Different lowercase letters express significant differences at $p<0.05$ level for TRB, Si/(Al+Fe), Fe_d/Fe_t, Fe_o/Fe_d, C and allophane content, and $Si_o/(Al_o-Al_p)$.

Alitude	**Land use**	**Particle size analysis (%)**			**Bulk density**	**TRB**	**Si/(Al+Fe)[a]**	**Fe_d/Fe_t**	**Fe_o/Fe_d**	**C**	**Allophane[b]**	**$Si_o/(Al_o-Al_p)$[c]**	**Gibbsite**
m		**Clay**	**Silt**	**Sand**	**g cm^{-3}**	**$cmol_c$ kg^{-1}**				**g kg^{-1}**	**g kg^{-1}**		**g kg^{-1}**
65	BA	41.4	46.6	12.0	0.83	110 a	1.01 a	0.54 a	0.24 a	43.3 a	113 a	0.54 a	37.4
65	SC	37.0	49.5	13.5	0.82	118 a	1.02 a	0.51 a	0.28 a	41.4 a	77 b	0.64 b	24.5
100	BA	45.7	34.9	19.4	0.81	136 a	0.83 a	0.46 a	0.27 a	49.8 a	179 a	0.55 a	73.0
100	SC	51.6	30.0	18.4	0.75	138 a	0.98 b	0.52 a	0.26 a	50.0 a	144 b	0.55 a	72.3
150	BA	40.1	34.3	25.6	0.76	134 a	0.80 a	0.49 a	0.24 a	45.9 a	142 a	0.58 a	84.9
150	SC	41.2	38.6	20.2	0.73	102 a	0.79 a	0.51 a	0.30 b	64.2 b	103 b	0.72 b	117.3
200	BA	24.2	50.7	25.1	0.74	98 a	0.77 a	0.51 a	0.27 a	47.6 a	112 a	0.64 a	113.1
200	SC	36.2	42.2	21.6	0.73	85 a	0.82 b	0.52 a	0.31 b	61.6 b	95 b	0.60 a	112.6
250	BA	37.0	47.3	15.7	0.70	86 a	0.82 a	0.53 a	0.22 a	50.1 a	65 a	0.72 a	101.0
250	SC	34.5	44.5	21.0	0.70	83 a	0.75 b	0.54 a	0.24 a	47.5 a	80 a	0.59 a	102.7
300	BA	37.1	41.0	21.9	0.73	71	0.78	0.53	0.27	51.6	95	0.54	112.7
350	BA	34.1	47.6	18.3	0.57	88	0.87	0.48	0.39	78.2	85	0.69	103.6
375	BA	35.5	38.2	26.3	0.51	93	0.91	0.47	0.49	97.0	80	0.52	101.9

Table 2-S3: Average concentrations in soil of total Si (Si_t), bioavailable Si ($CaCl_2$-Si), Na_2CO_3-Si, Na_2CO_3-Al, ox-Na_2CO_3-Si, ox-Na_2CO_3-Al, and phytolith content as extracted by heavy liquid separation (hlPhSi), and Si concentrations in banana leaf at each altitude. Differences between banana (BA) and sugarcane (SC) plots were tested at each altitude with an ANOVA statistical test with the aov function of the R programming language. Different lowercase letters express significant differences at $p<0.05$ level for Si_t, $CaCl_2$-Si, Na_2CO_3-Si, ox-Na_2CO_3-Si and ox-Na_2CO_3-Al.

Altitude	**Land use**	**Si_t**	**$CaCl_2$-Si**	**Na_2CO_3-Si**	**ox-Na_2CO_3-Si**	**ox-Na_2CO_3-Al**	**XRD-*hl*PhSi**	**Leaf Si concentration (banana)**
m		**g kg^{-1}**	**mg kg^{-1}**	**mg kg^{-1}**	**mg kg^{-1}**	**mg kg^{-1}**	**g kg^{-1}**	**g kg^{-1}**
65	BA	177.6 a	62.2 a	14191 a	7277 a	7873.2 a	6.04	4.49
65	SC	181.1 a	65.5 a	11221 a	7946 a	7157.4 a	6.06	nd
100	BA	153.3 a	53.9 a	12494 a	5434 a	8500.5 a	25.64	5.30
100	SC	171.3 b	73.9 b	12620 a	6277 a	6826.6 a	16.93	nd
150	BA	151.6 a	31.9 a	11315 a	4630 a	8051 a	15.24	4.77
150	SC	144.4 a	31.3 a	11662 a	4045 a	7483 a	17.63	nd
200	BA	145.9 a	46.1 a	11233 a	4356 a	9183 a	22.39	4.03
200	SC	148.5 a	30.8 b	11006 a	3778 a	8087 a	35.52	nd
250	BA	152.0 a	44.9 a	10764 a	4143 a	9194 a	26.29	3.81
250	SC	145.2 a	31.1 b	11548a	4460 a	9889 a	18.40	nd
300	BA	145.9	24.4	10380	3373	8487	27.09	4.31
350	BA	145.6	21.1	10070	2636	6792	47.06	4.44
375	BA	141.5	14.0	11408	2040	5223	53.45	nd

Table 2-S4: p-value determining the significance of each parameter (MAR, TRB, pH) involved in the linear model of each Si pool (see Equation 2-1). The linear models were realized with the lm function of the R programing language. A parameter significantly explains the results when the p-value < 0.05.

	MAR	**TRB**	**pH**
$CaCl_2$-Si	**p-value < 0.001**	p-value = 0.72	p-value = 0.34
Total Si	**p-value < 0.001**	p-value = 0.79	p-value = 0.11
Na_2CO_3-Si	**p-value = 0.03**	p-value = 0.62	p-value = 0.60
ox-Na_2CO_3-Si	**p-value < 0.001**	p-value = 0.70	p-value = 0.88
XRD-*hl*PhSi	**p-value = 0.03**	p-value = 0.11	p-value = 0.90
Leaf Si	p-value = 0.37	p-value = 0.09	p-value = 0.78

Table 2-S5: Selected soil chemical properties: pH H_2O, pH KCl, C and C contents, exchangeable bases, sum of exchangeable bases (SEB), cation exchange capacity (CEC), and base saturation (BS).

Altitude	**Land use**	**pH**		**C**	**N**	**Exchangeable bases ($cmol_c\ kg^{-1}$)**				**SEB**	**CEC**	**BS**
m		**H_2O**	**KCl**	**%**	**%**	**Ca**	**Mg**	**K**	**Na**	**$cmol_c\ kg^{-1}$**	**$cmol_c\ kg^{-1}$**	**%**
65	BA	5.9	4.9	4.3	0.4	7.0	2.6	0.1	2.8	12.6	53.0	23.9
65	SC	6.0	4.8	4.1	0.4	5.6	3.3	0.2	3.0	12.1	46.6	26.0
100	BA	5.8	5.0	5.0	0.5	5.7	3.7	0.1	2.3	11.7	51.5	22.6
100	SC	6.3	5.2	5.0	0.5	10.6	3.2	0.2	2.7	16.8	53.8	31.2
150	BA	6.5	5.7	4.6	0.5	10.5	3.8	0.1	2.4	16.9	46.7	35.9
150	SC	5.8	4.8	6.4	0.6	2.1	2.1	0.2	1.3	5.7	47.6	12.1
200	BA	6.2	5.4	4.8	0.5	9.5	2.6	0.1	2.5	14.7	46.0	32.0
200	SC	6.0	5.1	6.2	0.6	7.3	1.7	0.2	0.8	9.9	44.4	22.3
250	BA	5.5	4.7	5.0	0.5	4.0	1.2	0.1	2.3	7.6	39.7	19.2
250	SC	5.9	5.0	4.7	0.5	3.8	1.5	0.1	1.4	6.8	43.6	15.6
300	BA	5.8	5.1	5.2	0.5	5.9	1.4	0.1	1.3	8.6	37.6	22.8
350	BA	5.3	4.7	7.8	0.8	4.0	1.1	0.1	0.6	5.7	44.6	12.8
375	BA	5.2	4.5	9.7	0.8	2.9	0.6	0.1	0.3	3.8	48.3	7.7

Table 2-S6: Values of the mean H_4SiO_4 concentrations (mol l^{-1}) and pH in the $CaCl_2$ extracts at the different extraction times: 6 hours, 12 hours and 24 hours (1day), 2, 4, 8, 16, 32, and 64 days (B: banana; SC: sugarcane).

Extraction time (days)	**Altitude (m) Land use (BA, SC)**												
	65		**100**		**150**		**200**		**250**		**300**	**350**	**375**
	BA	SC	BA	SC	BA	SC	BA	SC	BA	SC	BA	BA	BA
	$log_{10}(H_4SiO_4)$ (mol l^{-1})												
0.25	-3.62	-3.63	-3.72	-3.58	-3.94	-3.95	-3.78	-3.96	-3.80	-3.96	-4.06	-4.12	-4.30
0.5	-3.65	-3.62	-3.70	-3.56	-3.94	-3.90	-3.74	-3.91	-3.71	-3.94	-4.04	-4.06	-4.24
1	-3.66	-3.60	-3.69	-3.55	-3.93	-3.86	-3.70	-3.85	-3.64	-3.90	-3.98	-3.99	-4.16
2	-3.63	-3.57	-3.66	-3.54	-3.94	-3.82	-3.68	-3.83	-3.60	-3.86	-3.93	-3.91	-4.09
4	-3.73	-3.59	-3.66	-3.52	-3.88	-3.78	-3.64	-3.77	-3.56	-3.85	-3.90	-3.86	-4.06
8	-3.56	-3.52	-3.63	-3.49	-3.85	-3.74	-3.53	-3.67	-3.49	-3.77	-3.83	-3.82	-4.00
16	-3.64	-3.57	-3.66	-3.53	-3.92	-3.73	-3.61	-3.70	-3.49	-3.80	-3.82	-3.78	-3.97
32	-3.65	-3.58	-3.65	-3.56	-3.89	-3.74	-3.63	-3.70	-3.48	-3.74	-3.77	-3.76	-3.96
64	-3.62	-3.55	-3.64	-3.53	-3.88	-3.68	-3.58	-3.64	-3.44	-3.75	-3.73	-3.65	-3.82
pH 64 days	5.4	5.1	5.2	5.4	6.4	4.9	5.6	5.3	4.8	5.0	5.2	4.7	4.6

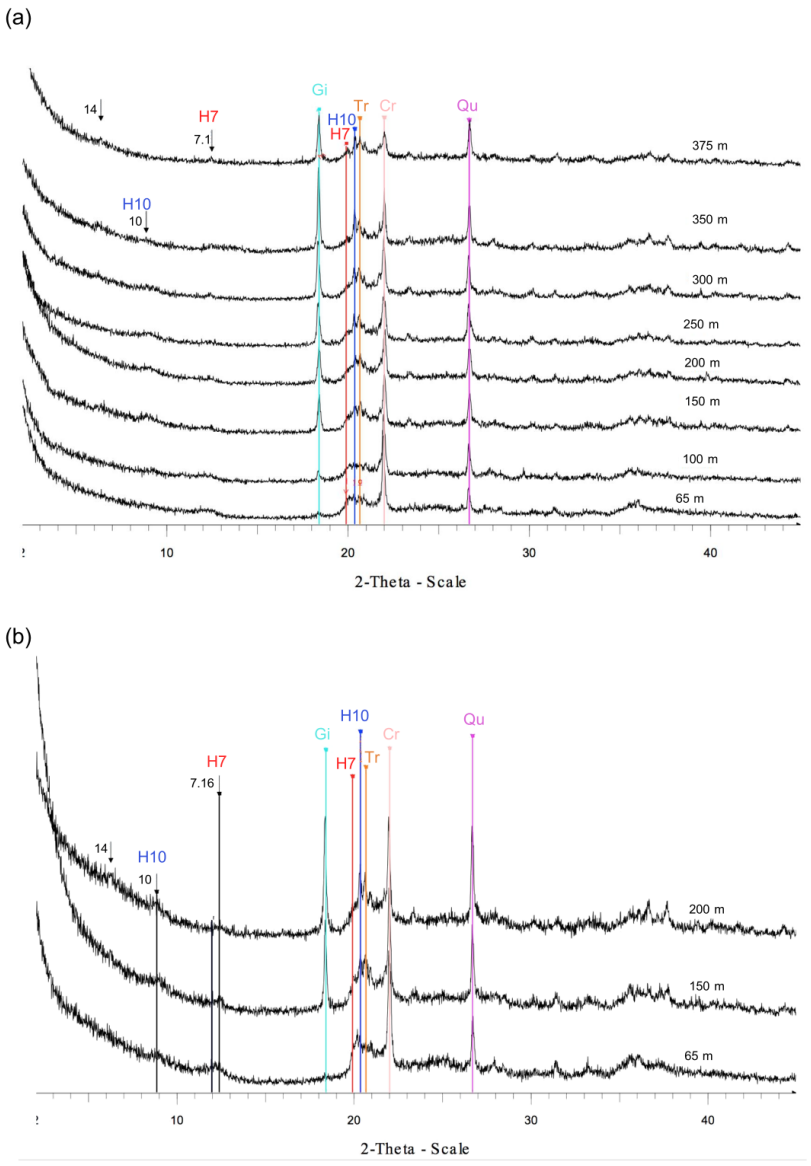

Figure 2-S1: X-ray diffraction (XRD) patterns performed on bulk soils (**a**) of banana plots at 65, 100, 150, 200, 250, 300, 350, and 375 m asl, and (**b**) sugarcane plots at 65, 150, and 200 m asl. Typical XRD peaks are identified with different colors : gibbsite (Gi) in light blue, halloysite-7Å (H7) in red, halloysite-10Å (H10) in dark blue, tridymite (Tr) in orange, cristobalite (Cr) in light pink, and quartz (Qu) in dark pink. Peaks at 7.1, 10, and 14 on the 2θ scale are pointed and are present when dehydrated halloysite, hydrated halloysite, and 2:1 minerals respectively occur.

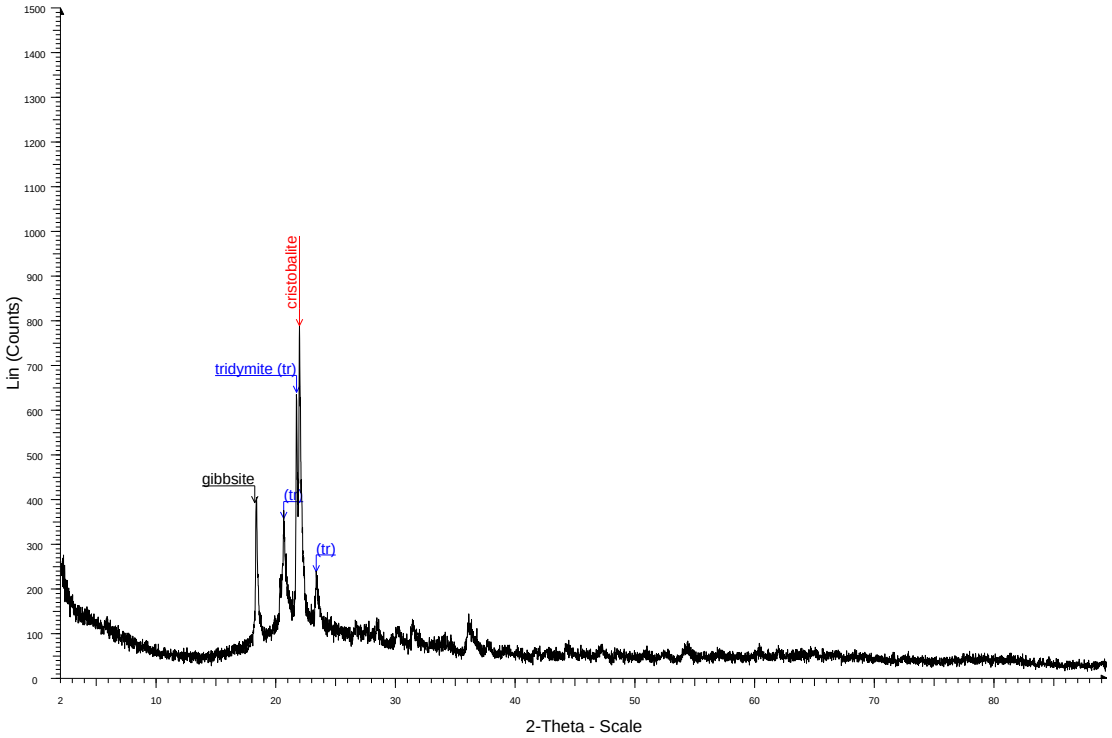

Figure 2-S2: X-ray diffraction (XRD) patterns performed on the phytoliths extracted by heavy liquid separation (sample tsBA350).

Appendixes relative to chapter 3

Phytolith quantification through alkaline extraction in gibbsitic Andosols

Table 3-S0-1: Total Si, Al, and Fe contents, DCB extractable Al and Fe contents (d), dark acid oxalate extractable Si, Al and Fe contents (o), and pyrophosphate extractable Al and Fe contents (p) in soil samples. ts samples were collected in banana plots (tsBA), sugarcane plots (tsSC), and forest plot (tsFO) at various altitude levels (from 65 to 390 m asl). pd samples were collected in soil horizons from the pedons pdBA, pdSC and pdFO, respectively at 173, 180 and 396 m asl.

	Total elemental content (g kg^{-1})			**DCB extractable content (g kg^{-1})**		**Dark oxalate extractable content (g kg^{-1})**			**Pyrophosphate extractable content (g kg^{-1})**	
	Si_t	**Al_t**	**Fe_t**	**Al_d**	**Fe_d**	**Si_o**	**Al_o**	**Fe_o**	**Al_p**	**Fe_p**
tsBA 65	177.6	131.3	79.3	18.50	42.59	16.49	36.17	10.91	8.64	3.30
tsSC 65	181.1	128.4	87.9	17.95	44.96	11.96	27.01	12.54	9.19	5.30
tsBA 100	153.3	131.5	96.2	20.67	44.70	25.27	51.84	12.00	7.68	2.68
tsSC 100	171.3	127.1	84.3	18.41	43.90	20.25	42.91	11.46	7.33	3.24
tsBA 150	151.6	133.4	100.7	19.97	49.08	20.80	41.03	12.01	6.79	3.25
tsSC 150	144.4	131.4	91.1	22.93	45.94	16.81	36.85	13.87	14.55	8.71
tsBA 200	145.8	135.3	97.3	18.20	49.34	17.23	34.59	13.31	8.56	5.29
tsSC 200	148.5	130.4	89.7	17.78	46.24	14.16	32.36	14.36	9.64	6.81
tsBA 250	152.0	133.6	93.0	17.54	49.46	10.43	26.86	10.92	12.32	7.58
tsSC 250	145.2	136.8	99.3	18.90	53.15	11.78	30.35	12.88	11.16	8.49
tsBA 300	145.9	138.8	86.1	16.60	45.65	13.24	31.93	12.39	8.18	6.63
tsBA 350	145.6	121.1	82.0	16.78	39.74	12.70	32.86	16.62	13.01	13.42
tsBA 375	141.5	110.8	79.7	16.43	37.61	10.66	32.67	18.42	12.82	12.79
tsFO 396	128.7	98.0	69.1	16.53	28.20	5.27	21.66	15.24	14.28	13.88
pdBA 173 Ap	148.4	129.0	86.6	17.10	43.22	21.24	43.74	17.21	10.74	7.04
pdBA 173 AB	146.8	137.9	94.1	17.80	46.79	24.04	48.64	18.49	10.14	6.63
pdBA 173 Bw	128.7	151.3	105.3	14.83	47.09	33.62	63.97	19.92	3.51	1.33
pdBA 173 BC	145.5	149.7	101.2	15.10	43.71	54.07	86.27	18.99	3.26	0.56
pdSC 180 Ap	145.3	122.1	77.9	20.38	45.40	17.21	36.67	15.53	13.09	8.51
pdSC 180 AB	154.6	135.3	84.3	18.48	44.02	20.04	41.67	16.90	13.44	8.68

pdSC 180 Bw1	160.0	135.4	88.3	18.59	44.25	23.27	45.84	16.08	11.18	6.88
pdSC 180 Bw2	162.4	139.1	96.0	17.51	45.30	32.28	55.70	14.25	6.30	3.26
pdSC 180 BC	166.8	136.1	104.0	14.79	41.33	42.04	66.83	12.39	3.27	0.75
pdFO 396 Ah1	108.0	101.8	62.5	20.46	37.61	1.90	23.87	19.72	18.97	19.53
pdFO 396 Ah2	144.6	110.4	73.8	22.72	44.10	3.46	27.55	21.80	20.72	22.45
pdFO 396 AB	146.0	137.2	92.0	20.75	48.10	5.72	31.95	27.12	18.75	22.52
pdFO 396 Bw1	171.3	128.1	89.3	18.60	54.52	7.39	45.81	31.91	8.09	8.21
pdFO 396 Bw2	162.8	127.9	88.0	16.35	48.83	16.64	66.12	25.18	5.12	2.52
pdFO 396 BC	108.0	204.4	132.9	10.97	31.79	21.32	53.11	9.64	2.89	0.18

Table 3-S0-2: DCB extractable Si, Al and Fe contents (d), and dark acid oxalate extractable Si, Al and Fe contents (o) obtained with pretreatments in methods 2 and 3.

Method	**Sample**	**Si_d $g.kg^{-1}$**	**Al_d $g.kg^{-1}$**	**Fe_d $g.kg^{-1}$**	**Si_o $g.kg^{-1}$**	**Al_o $g.kg^{-1}$**	**Fe_o $g.kg^{-1}$**
Method 2	tsBA 350	nd	nd	nd	19.2	40.3	25.8
	tsFO 396	nd	nd	nd	6.1	24.4	16.8
Method 3	tsB 350	2.1	16.5	37.8	15.5	25.1	8.2
	tsFO 396	2.0	16.7	26.4	4.3	9.7	5.4

nd means no data.

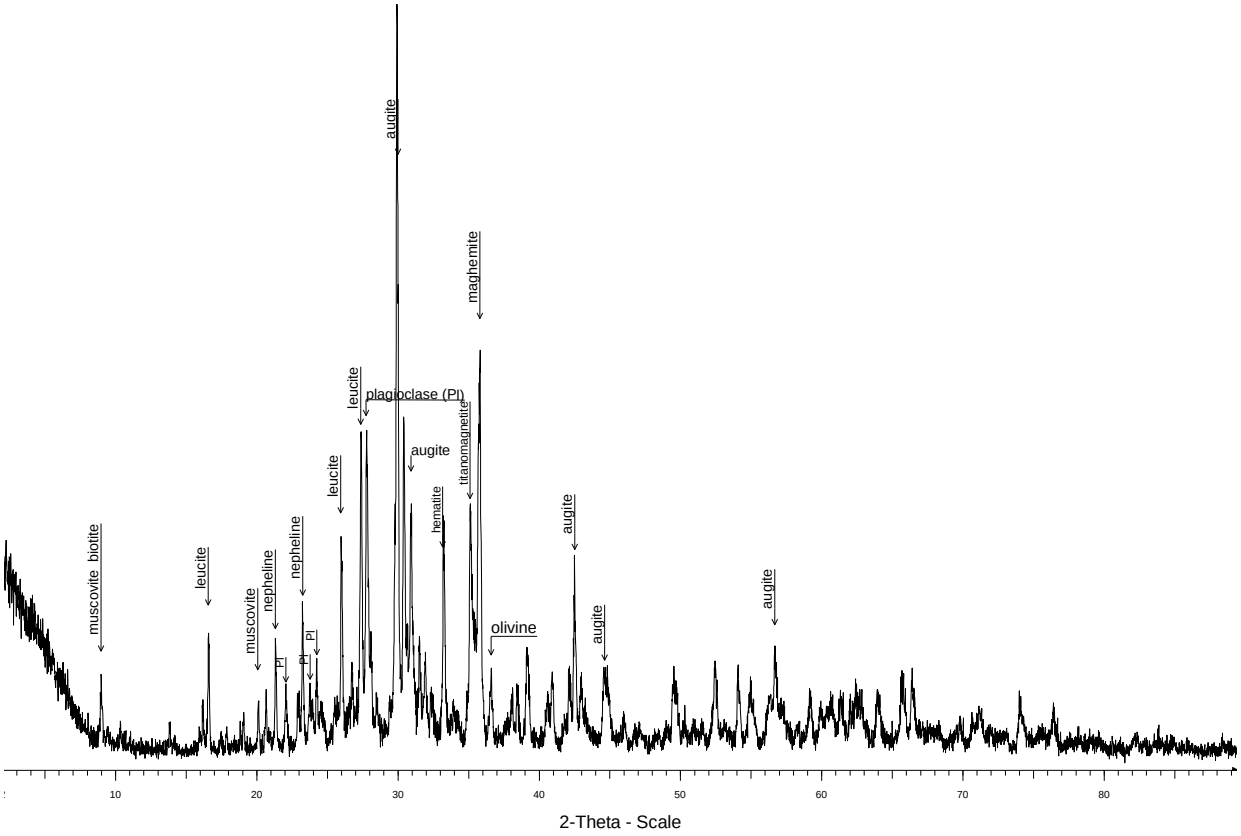

Figure 3-S1: XRD pattern performed on non-oriented powder sample from reference basalt. XRD data show the occurrence of olivine, augite, biotite, leucite, plagioclase, and nepheline.

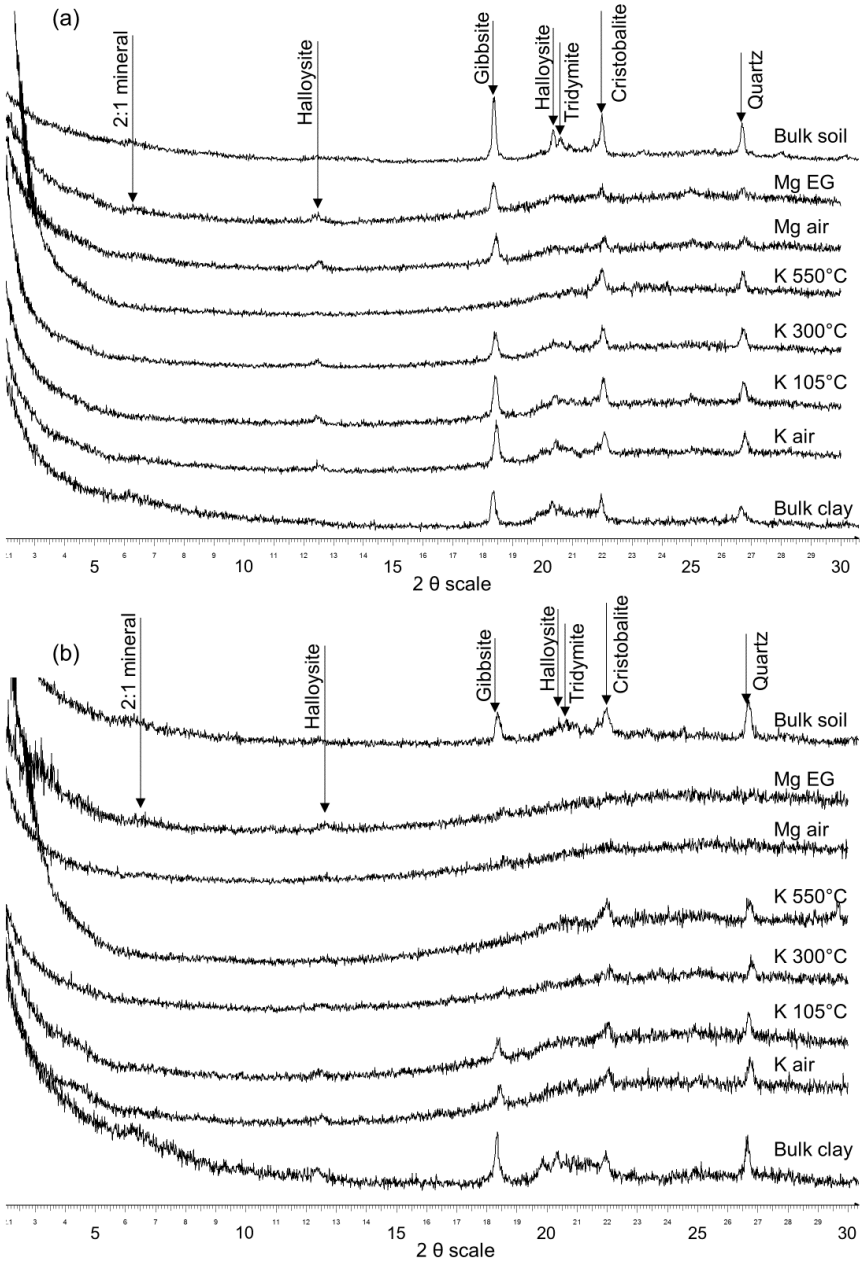

Figure 3-S2: X-ray diffraction (XRD) patterns on topsoil (ts) samples: (a) tsBA-350 and (b) tsFO-396. XRD were performed on bulk soils (non-oriented powder), oriented clays, bulk and saturated with either K^+ or Mg^{2+}, at room temperature (20 °C) after formamide intercalation, overnight ethylene–glycol saturation (EG), as well as after heating at 110, 300 and 550 °C (4 h).

Appendixes relative to chapter 5

Banana and sugarcane crops control the bio-availability of the silicon in a gibbsitic Andosol

Table 5-S0-1: Total Si, Al, Fe contents (t), DCB extractable Al and Fe contents (d), dark acid oxalate extractable Si, Al, and Fe contents (o), and pyrophosphate extractable Al and Fe contents (p) in soil horizons (f<2mm) of banana (BA-173) and sugarcane (SC-180) soil pedons.

Hor	**Depth**	**Total elemental content (g kg^{-1})**			**DCB extractable content (g kg^{-1})**		**Dark oxalate extractable content (g kg^{-1})**			**Pyrophosphate extractable content (g kg^{-1})**	
	cm	**Si_t**	**Al_t**	**Fe_t**	**Al_d**	**Fe_d**	**Si_o**	**Al_o**	**Fe_o**	**Al_p**	**Fe_p**
					BA-173 pedon						
Ap	0-12	148.4	129.0	86.6	17.1	43.2	21.2	43.7	17.2	10.74	7.04
AB	12-23	146.8	137.9	94.1	17.8	46.8	24.0	48.6	18.5	10.14	6.63
Bw	24-45	128.7	151.3	105.3	14.8	47.1	33.6	64.0	19.9	3.51	1.33
BC	46-62	145.5	149.7	101.2	15.1	43.7	54.1	86.3	19.0	3.26	0.56
2Bw1	63-80	179.5	140.9	93.9	12.8	45.8	29.8	49.0	13.7	3.36	1.08
2Bw2	81-95	172.1	139.1	100.4	13.6	44.1	44.2	68.2	17.2	3.14	0.57
2BC	96-128	182.1	135.1	98.6	10.9	36.2	45.5	69.8	14.2	2.78	0.34
					SC-180 pedon						
Ap	0-5	145.3	122.1	77.9	20.4	45.4	17.2	36.7	15.5	13.09	8.51
AB	6-24	154.6	135.3	84.3	18.5	44.0	20.0	41.7	16.9	13.44	8.68
Bw1	25-36	160.0	135.4	88.3	18.6	44.3	23.3	45.8	16.1	11.18	6.88
Bw2	37-63	162.4	139.1	96.0	17.5	45.3	32.3	55.7	14.2	6.30	3.26
BC	64-85	166.8	136.1	104.0	14.8	41.3	42.0	66.8	12.4	3.27	0.75
2Bw1	86-110	167.3	145.6	96.7	13.1	42.8	37.0	60.3	14.5	3.02	0.78

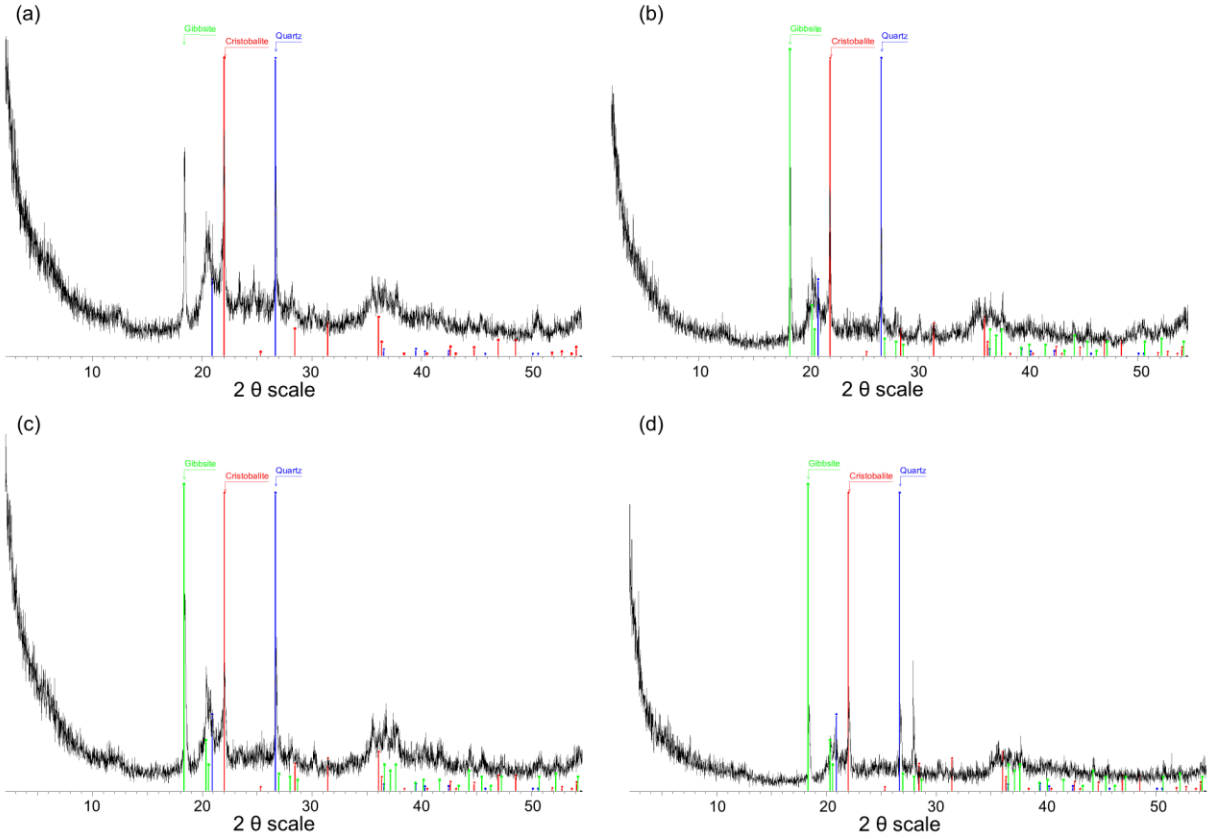

Figure 5-S1 : X-ray diffraction (XRD) patterns on horizon samples of the BA-173 profile: (a) Ap, (b) AB, (c) Bw, and (d) BC horizons. XRD were performed on bulk soils (non-oriented powder).

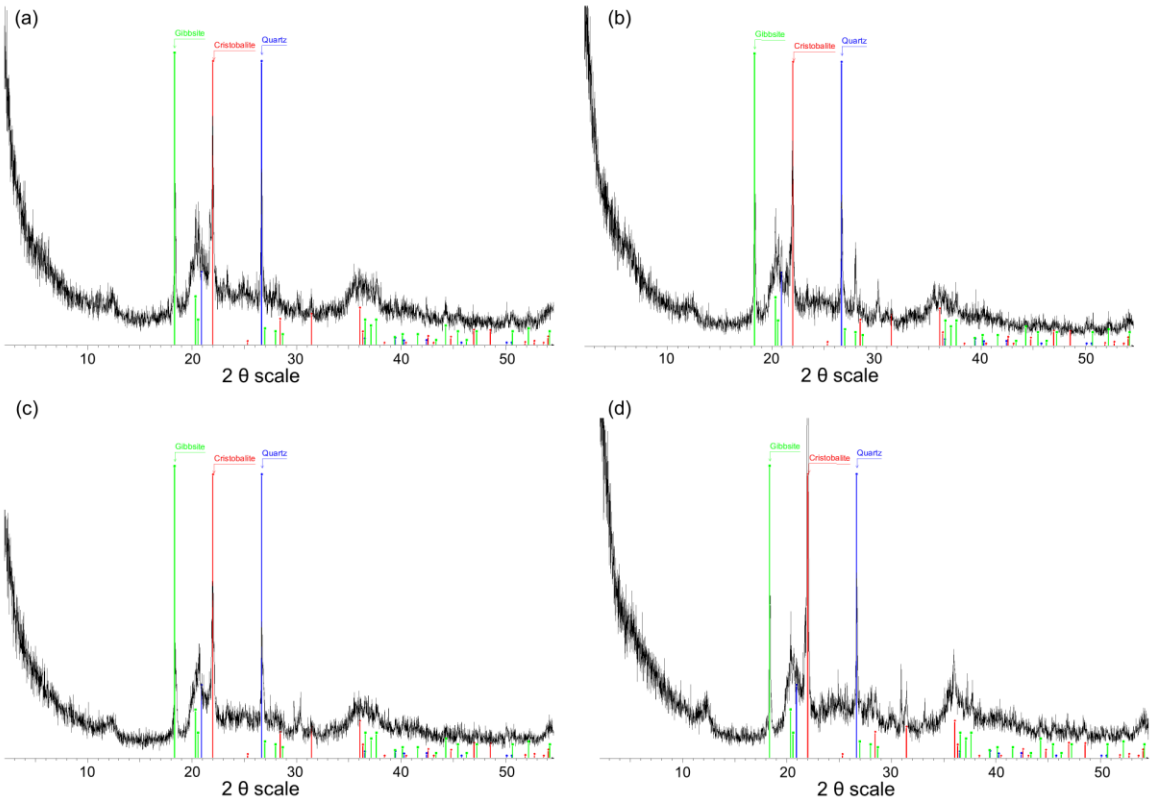

Figure 5-S2 : X-ray diffraction (XRD) patterns on horizon samples of the SC-180 profile: (a) Ap, (b) AB, (c) Bw1, and (d) BC horizons. XRD were performed on bulk soils (non-oriented powder).

Appendixes relative to chapter 6

The silicon soil-plant cycle in a tropical rainforest and a nearby banana field

Table 6-S0-1: DCB extractable Al and Fe contents (d), dark acid oxalate extractable Si, Al, and Fe contents (o), and pyrophosphate extractable Al and Fe contents (p) in soil horizons (f<2mm) of forest (FO-396) and banana (BA-343) soil pedons.

Hor	Depth	DCB extractable content (g kg^{-1})		Dark oxalate extractable content (g kg^{-1})			Pyrophosphate extractable content (g kg^{-1})	
	cm	Al_d	Fe_d	Si_o	Al_o	Fe_o	Al_p	Fe_p
FO-396 pedon								
Ah1	0-8	20.46	37.61	1.90	23.87	19.72	18.97	19.53
Ah2	8-16	22.72	44.10	3.46	27.55	21.80	20.72	22.45
AB	16-30	20.75	48.10	5.72	31.95	27.12	18.75	22.52
Bw1	30-55	18.60	54.52	7.39	45.81	31.91	8.09	8.21
Bw2	55-70	16.35	48.83	16.64	66.12	25.18	5.12	2.52
2BC	70-88	10.97	31.79	21.32	53.11	9.64	2.89	0.18
3A	88-90	12.84	48.11	5.61	18.50	8.27	3.29	1.07
3 Bw	90-120	13.75	41.22	28.00	65.87	5.38	4.47	0.88
BA-343 pedon								
AB	0-45	21.24	42.87	9.33	37.32	15.35	18.16	18.59
Bw	45-55	19.49	49.81	20.10	49.42	8.56	8.92	8.75
BC	55-70	12.87	39.88	39.69	93.02	15.77	4.03	1.43
2A	70-80	13.40	35.54	8.80	25.31	9.58	3.48	0.35

Table 6-S2: Total Si, Al, Fe, Ca, Mg, Na, K contents in soil horizons (f<2mm) of forest (FO-396) and banana (BA-343) soil pedons.

Hor	Depth	Total elemental contents						
	cm	Si	Al	Fe	Ca	Mg	Na	K
FO-396 pedon								
Ah1	0-8	107.98	101.81	62.52	8.92	14.19	1.87	1.08
Ah2	8-16	144.58	110.42	73.84	3.00	9.15	1.63	2.09
AB	16-30	146.04	137.19	91.98	3.39	11.14	1.21	1.82
Bw1	30-55	171.28	128.05	89.29	1.69	6.26	1.04	1.67
Bw2	55-70	162.81	127.94	88.01	2.67	8.88	1.52	2.35
2BC	70-88	107.99	204.41	132.87	2.34	11.91	0.85	0.87
3A	88-90	182.46	133.25	89.92	3.00	9.32	1.71	2.80
BA-343 pedon								
AB	0-45	160.44	118.91	81.63	3.86	11.15	1.45	2.37
Bw	45-55	182.85	131.58	97.74	5.47	15.18	1.51	2.38
BC	55-70	171.07	145.67	107.72	4.97	14.00	1.21	2.20
2A	70-80	195.87	130.61	96.23	3.12	12.55	1.72	2.46

Appendixes relative to chapter 7

Tracing silicon fluxes from forested and cultivated volcanic watersheds using Ge/Si ratio

Table 7-S0-1: Elemental concentrations, and Ge/Si ratios in Pérou River water (gauging stations GS1, GS2, GS3) and Pères River water (gauging stations GS5) at base flow, in soil solutions, and in runoff waters.

Sample	Date	Na	K	Mg	Ca	Al	Si	Ge	Ge/Si
		µmol l^{-1}						pmol l^{-1}	µmol mol^{-1}
		Base flow at gauging station 1 (GS1)							
GS1	25/07/2016	243	20	65	122	<dl[4]	460	97	0.21
GS1	02/08/2016	254	21	66	121	<dl	477	97	0.20
GS1	29/08/2016	277	24	76	147	<dl	529	97	0.18
GS1	12/09/2016	260	22	69	135	<dl	502	97	0.19
GS1	03/10/2016	226	20	59	115	<dl	426	111	0.26
GS1	07/11/2016	207	19	55	110	<dl	414	97	0.23
GS1	26/01/2017	244	21	66	127	<dl	512	nd[5]	nd
GS1	09/02/2017	252	22	69	133	<dl	502	nd	nd
GS1	13/03/2017	221	18	55	104	<dl	393	nd	nd
GS1	16/05/2017	255	22	68	153	<dl	507	nd	nd
GS1	12/06/2017	268	42	68	198	<dl	424	nd	nd
GS1	17/07/2017	255	24	68	127	<dl	508	nd	nd
		Base flow at gauging station 2 (GS2)							
GS2	25/07/2016	260	22	70	130	<dl	468	83	0.18
GS2	02/08/2016	272	23	72	134	<dl	489	83	0.17
GS2	29/08/2016	293	26	84	159	<dl	525	83	0.16
GS2	12/09/2016	275	24	75	144	<dl	483	83	0.17
GS2	03/10/2016	233	22	61	122	<dl	423	97	0.23
GS2	07/11/2016	209	22	56	111	<dl	402	83	0.21
GS2	26/01/2017	265	24	72	137	<dl	492	nd	nd
GS2	09/02/2017	272	25	75	145	<dl	511	nd	nd
GS2	13/03/2017	228	21	56	108	<dl	401	nd	nd
GS2	16/05/2017	266	25	73	148	<dl	513	nd	nd

GS2	12/06/2017	279	25	77	154	<dl	527	nd	nd
GS2	17/07/2017	464	79	175	451	<dl	939	125	0.13
		Base flow at gauging station 3 (GS3)							
GS3	25/07/2016	283	24	79	144	<dl	498	83	0.17
GS3	02/08/2016	301	30	81	148	<dl	520	83	0.16
GS3	29/08/2016	316	29	94	176	<dl	560	83	0.15
GS3	12/09/2016	304	27	86	164	<dl	545	97	0.18
GS3	03/10/2016	245	23	67	130	<dl	450	97	0.21
GS3	07/11/2016	231	27	65	133	<dl	428	nd	nd
GS3	26/01/2017	303	29	89	176	<dl	547	nd	nd
GS3	09/02/2017	323	29	97	187	<dl	584	nd	nd
GS3	13/03/2017	252	25	67	133	<dl	444	nd	nd
GS3	16/05/2017	293	29	84	173	<dl	541	nd	nd
GS3	12/06/2017	314	29	91	185	<dl	576	nd	nd
GS3	17/07/2017	265	24	73	136	<dl	506	nd	nd
		Base flow at gauging station 5 (GS5)							
GS5	25/07/2016	495	90	187	435	<dl	986	83	0.08
GS5	02/08/2016	514	74	194	439	<dl	989	125	0.13
GS5	29/08/2016	498	75	190	445	<dl	967	139	0.14
GS5	12/09/2016	459	73	179	425	<dl	947	139	0.15
GS5	03/10/2016	432	73	169	399	<dl	893	69	0.08
GS5	07/11/2016	423	98	165	427	<dl	833	153	0.18
GS5	26/01/2017	549	79	216	529	<dl	1039	nd	nd
GS5	09/02/2017	538	78	210	509	<dl	1025	nd	nd
GS5	13/03/2017	451	87	168	474	<dl	860	nd	nd
GS5	16/05/2017	446	79	165	466	<dl	885	nd	nd
GS5	12/06/2017	520	84	199	511	<dl	1021	nd	nd
GS5	17/07/2017	303	29	87	161	<dl	549	nd	nd

		Soil solution (SS)							
SS-BA-173[1]	20/09/2016	270	107	171	217	0.12	215	194	0.90
SS-BA-173	20/09/2016	193	57	125	120	0.03	195	167	0.85
SS-BA-173	20/09/2016	145	44	166	121	0.16	178	167	0.93
SS-BA-173	20/09/2016	299	51	230	140	<dl	156	111	0.71
SS-BA-173	20/09/2016	224	126	293	257	0.32	228	222	0.97
SS-BA-173	27/10/2016	199	76	99	124	0.12	197	167	0.84
SS-BA-173	27/10/2016	206	48	125	121	0.43	199	194	0.97
SS-BA-173	27/10/2016	207	54	313	195	0.55	182	194	1.06
SS-BA-173	27/10/2016	307	50	238	146	0.02	158	139	0.87
SS-BA-173	27/10/2016	258	200	375	384	3.35	193	208	1.07
SS-SC-180[2]	20/09/2016	188	69	145	295	0.24	175	167	0.94
SS-SC-180	20/09/2016	267	204	116	121	0.57	170	139	0.81
SS-SC-180	20/09/2016	271	1722	758	881	0.45	250	194	0.77
SS-SC-180	20/09/2016	186	46	206	143	<dl	160	181	1.12
SS-SC-180	20/09/2016	181	103	86	143	0.40	159	167	1.04
SS-SC-180	27/10/2016	145	277	121	201	0.89	183	167	0.90
SS-SC-180	27/10/2016	250	224	114	127	0.25	165	167	1.00
SS-SC-180	27/10/2016	113	912	266	351	1.53	258	194	0.75
SS-SC-180	27/10/2016	210	81	169	115	1.07	164	194	1.18
SS-SC-180	27/10/2016	140	24	143	100	<dl	144	139	0.96
SS-FO-396[3]	13/03/2017	197	2	59	40	0.81	86	83	0.96
SS-FO-396	13/03/2017	280	7	53	54	0.35	84	83	0.98
SS-FO-396	18/04/2017	172	18	26	31	3.13	78	83	1.06
SS-FO-396	18/04/2017	173	43	31	40	4.77	92	153	1.64
SS-FO-396	18/04/2017	259	6	67	55	1.20	123	97	0.79
SS-FO-396	11/05/2017	177	31	38	44	1.74	95	83	0.87
SS-FO-396	11/05/2017	137	12	22	40	1.80	78	83	1.05

SS-FO-396	08/06/2017	183	3	41	41	1.49	87	139	1.58
SS-FO-396	08/06/2017	217	4	47	39	1.14	103	97	0.94
		Runoff water (RW)							
RW-BA-173	12/10/2016	74	201	38	47	4.78	141	152	1.07
RW-BA-173	19/10/2016	87	299	51	58	4.51	139	165	1.19
RW-BA-173	27/10/2016	90	228	39	47	6.36	140	152	1.08

[1]SS-BA-173 = soil solution of banana plot (BA-173), [2]SS-SC-180 = soil solution of sugarcane plot (SC-180), [3]SS-FO-396 = soil solution of forest plot (FO-396), [4]<dl = beneath the detection limit, [5]nd = no data

Table 7-S0-2: Elemental concentrations, and Ge/Si ratios for (a) FPU1, (b) FPU2, (c) FPU3 flood events in the Pérou River (GS3), (d) FPS1, (e) FPS2, and (f) FPS3 flood events in the Pères River (GS5).

Time collected	Discharge	Na	K	Mg	Ca	Al	Si	Ge	Ge :Si
	$m^3 s^{-1}$				µmol l^{-1}			pmol l^{-1}	µmol mol^{-1}
(a) FPU1									
06:57	46.8	300.43	27.60	85.06	185.18	<dl[1]	513.35	nd[2]	nd
07:42	49.5	282.86	26.98	75.02	154.69	<dl	508.01	82.7	0.16
08:27	40.0	268.03	26.09	69.55	147.65	<dl	483.62	82.7	0.17
09:09	24.9	259.98	24.67	65.72	148.03	<dl	461.54	nd	nd
09:54	18.8	245.59	22.38	60.91	127.45	<dl	427.88	110.2	0.26
10:39	14.7	236.71	21.42	58.35	118.49	<dl	402.78	96.4	0.24
11:18	12.3	235.23	21.52	57.94	124.13	<dl	390.31	96.4	0.25
12:03	10.5	239.36	21.61	58.02	121.66	<dl	391.38	nd	nd
(b) FPU2									
10:27	6.91	324.31	29.82	95.88	186.13	<dl	562.50	nd	nd
11:03	32.5	298.56	28.85	80.86	167.02	<dl	536.50	nd	nd
11:48	21.3	212.22	22.37	47.28	102.30	1.07	288.14	96.4	0.33
11:51	20.8	192.00	20.78	40.24	85.95	1.43	242.98	82.7	0.34
12:33	15.0	175.82	18.03	36.29	78.97	1.67	192.72	96.4	0.50
12:36	14.8	171.47	17.61	34.55	74.38	1.72	181.70	96.4	0.53
13:21	11.7	178.99	16.88	35.30	76.97	1.56	183.71	82.7	0.45
14:06	9.60	179.99	17.28	36.87	94.14	1.55	197.77	82.7	0.42
(c) FPU3									
09:30	9.28	192.26	33.25	45.35	119.11	1.62	273.58	nd	nd
10:15	8.62	132.97	21.73	25.66	64.95	1.95	143.93	68.9	0.48
11:00	7.43	109.13	17.16	18.92	45.93	1.86	92.40	68.9	0.75

11:45	6.48	104.00	15.50	18.40	48.13	2.30	90.47	nd	nd
12:30	7.92	111.53	13.92	20.26	56.54	2.25	105.86	68.9	0.65
13:15	7.55	120.44	14.17	22.19	60.70	2.34	130.29	nd	nd
14:00	6.53	136.28	17.39	25.45	73.78	2.28	151.98	82.7	0.54
14:45	5.59	137.10	15.06	28.20	74.15	1.71	173.91	82.7	0.48
(d) FPS1									
17:12	0.64	494.56	73.35	182.51	458.33	<dl	893.34	96.4	0.11
17:15	1.08	302.48	96.88	113.58	422.90	1.03	573.01	110.2	0.19
18:00	0.64	235.36	77.26	80.82	290.17	1.06	391.20	82.7	0.21
18:45	0.382	232.54	85.47	76.24	264.27	1.78	354.10	nd	nd
18:51	0.97	218.57	72.92	72.76	244.69	1.63	349.27	110.2	0.32
19:36	0.32	225.62	74.12	80.25	261.98	2.05	393.87	nd	nd
20:21	0.28	254.98	76.60	88.02	285.93	1.87	449.79	nd	nd
20:51	0.26	262.81	76.52	90.66	289.17	1.52	474.72	110.2	0.23
(e) FPS2									
21:15	0.98	385.25	81.25	148.93	555.39	0.99	710.11	110.2	0.16
21:18	1.01	365.33	83.86	128.89	451.10	1.59	670.58	82.7	0.12
21:24	1.10	327.23	93.71	119.22	475.80	1.92	543.45	55.1	0.10
21:36	1.40	221.71	156.75	89.88	441.37	3.45	299.25	nd	nd
22:21	1.74	149.33	118.57	59.34	295.16	3.71	191.84	82.7	0.43
22:33	1.36	126.71	103.55	47.45	224.60	4.23	167.18	nd	nd
23:18	1.23	142.93	98.08	51.23	221.56	4.36	204.83	96.4	0.47
23:36	1.13	152.68	95.17	53.74	220.08	4.22	232.59	96.4	0.41
(f) FPS3									
19:48	0.51	466.29	115.83	162.84	543.66	1.23	758.01	165.3	0.22
19:51	0.52	506.31	108.31	160.53	481.29	1.46	856.30	nd	nd
20:02	0.78	499.35	104.12	166.54	496.01	1.13	883.19	137.8	0.16
20:47	0.47	410.70	168.49	130.62	436.63	2.92	701.03	165.3	0.24

21:02	0.42	381.47	164.81	117.86	397.70	2.73	659.19	165.3	0.25
21:47	0.36	348.11	156.11	117.00	399.45	3.37	573.72	nd	nd
22:32	0.32	345.15	149.90	118.60	397.95	2.85	576.92	179.1	0.31
23:17	0.37	279.47	153.58	104.16	401.95	3.83	426.99	137.8	0.32

[1]<dl = beneath the detection limit, [2]nd = no data.

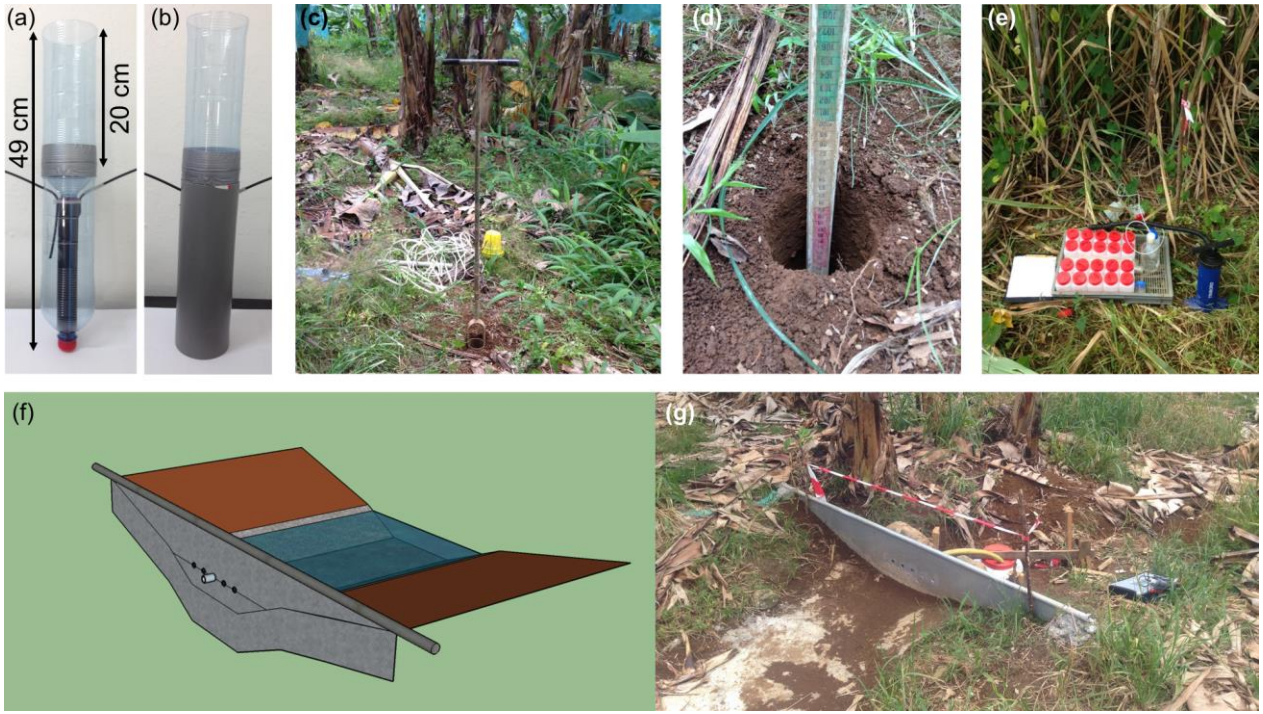

Figure 7-S1: Pictures of the lysimeter (a,b), lysimeter settlement (c,d), and lysimeter sampling (e). Schematic illustration of the device settled in the banana plot to collect runoff waters at the plot scale (f), and picture of this device in the banana field (g).

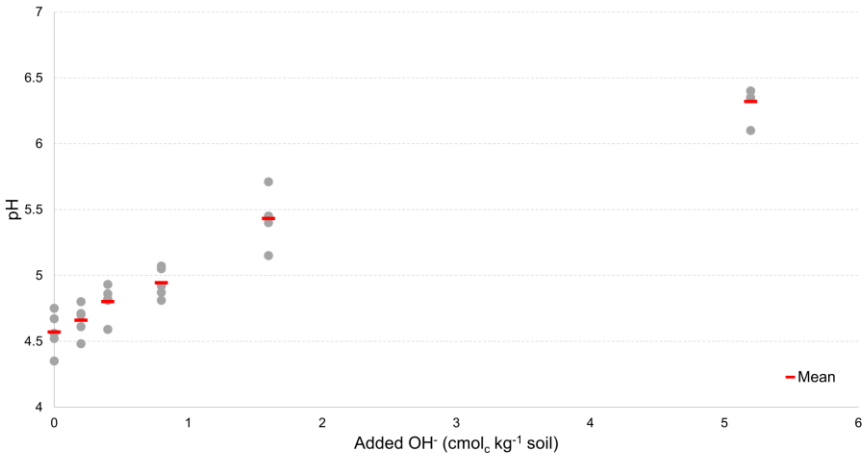

Figure 7-S2: pH buffer capacity of the topsoil of the BA-343 plot, as expressed by the plot of pH against OH^- addition. The buffering capacity of this soil is very high. Indeed, 6 tons of $CaCO_3$ per hectar would be necessary to increase soil pH to pH 7.

References

Adjadeh, T.A., Inoue, K., 1999. Andisols of the Kitakami mountain range, northeastern Japan: their characterization and classification. Soil Sci. Plant Nutr. 45, 115–130.

Aguirre, A.A., Derry, L.A., Mills, T.J., Anderson, S.P., 2017. Colloidal transport in the Gordon Gulch catchment of the Boulder Creek CZO and its effect on C-Q relationships for silicon. Water Resour. Res. 53, 2368–2383.

Alary, K., Babre, D., Caner, L., Feder, F., Szwarc, M., Naudan, M., Bourgeon, G., 2013. Pretreatment of soil samples rich in short-range-order minerals before particle-size analysis by the pipette method. Pedosphere 23, 20–28.

Alexandre, A., Bouvet, M., Abbadie, L., 2011. The role of savannas in the terrestrial Si cycle: a case-study from Lamto, Ivory Coast. Glob. Planet. Change 78, 162–169.

Alexandre, A., Meunier, J.-D., Colin, F., Koud, J.-M., 1997. Plant impact on the biogeochemical cycle of silicon and related weathering processes. Geochim. Cosmochim. Acta 61, 677–682.

Allorerung, D., 1989. Influence of steel slag application to red/yellow podzolic soils on soil chemical characteristics, nutrient content and uptake, and yield of sugarcane plantations (Saccharum officinarum L.). Bull Pus. Penelitan Perkeb. Gula Indones. 136, 14–42.

Ameijeiras-Mariño, Y., Opfergelt, S., Derry, L.A., Robinet, J., Govers, G., Minella, J.P., Delmelle, P., 2018. Ge/Si ratios point to increased contribution from deeper mineral weathering to streams after forest conversion to cropland. Appl. Geochem. 96, 24–34.

Anderson, D.L., 1991. Soil and leaf nutrient interactions following application of calcium silicate slag to sugarcane. Fertil. Res. 30, 9–18.

Ayres, A.S., 1966. Calcium silicate slag as a growth stimulant for sugarcane on low-silicon soils. Soil Sci. 101, 216–227.

Barão, L., Clymans, W., Vandevenne, F., Meire, P., Conley, D., Struyf, E., 2014. Pedogenic and biogenic alkaline-extracted silicon distributions along a temperate land-use gradient. Eur. J. Soil Sci. 65, 693–705.

Barboni, D., Bonnefille, R., Alexandre, A., Meunier, J.D., 1999. Phytoliths as paleoenvironmental indicators, West Side Middle Awash Valley, Ethiopia. Palaeogeogr. Palaeoclimatol. Palaeoecol. 152, 87–100. https://doi.org/10.1016/S0031-0182(99)00045-0

Bartoli, F., 1985. Crystallochemistry and surface properties of biogenic opal. J. Soil Sci. 36, 335–350.

Bartoli, F., 1983. The biogeochemical cycle of silicon in two temperate forest ecosystems. Ecol. Bull. 469–476.

Bazemore, D.E., Eshleman, K.N., Hollenbeck, K.J., 1994. The role of soil water in stormflow generation in a forested headwater catchment: synthesis of natural tracer and hydrometric evidence. J. Hydrol. 162, 47–75. https://doi.org/10.1016/0022-1694(94)90004-3

Beauducel, F., 2005. La Soufrière: un volcan actif.

Beckwith, R.S., Reeve, R., 1963. Studies on soluble silica in soils. I. The sorption of silicic acid by soils and minerals. Soil Res. 1, 157–168.

Beer, C., Reichstein, M., Tomelleri, E., Ciais, P., Jung, M., Carvalhais, N., Rodenbeck, C., Arain, M.A., Baldocchi, D., Bonan, G.B., Bondeau, A., Cescatti, A., Lasslop, G., Lindroth, A., Lomas, M., Luyssaert, S., Margolis, H., Oleson, K.W., Roupsard, O., Veenendaal, E., Viovy, N., Williams, C., Woodward, F.I., Papale, D., 2010. Terrestrial Gross Carbon Dioxide Uptake: Global Distribution and Covariation with Climate. Science 329, 834–838. https://doi.org/10.1126/science.1184984

Beerling, D.J., Leake, J.R., Long, S.P., Scholes, J.D., Ton, J., Nelson, P.N., Bird, M., Kantzas, E., Taylor, L.L., Sarkar, B., Kelland, M., DeLucia, E., Kantola, I., Müller, C., Rau, G., Hansen, J., 2018. Farming with crops and rocks to address global climate, food and soil security. Nat. Plants 4, 138–147. https://doi.org/10.1038/s41477-018-0108-y

Bernard, J., Gautheyrou, J., Colmet-Daage, F., 1980. Cartes des cultures et d'utilisation du sol de la Guadeloupe et de la Grande Terre à 1/20000è en Janvier 1980 établies à partir de photographies aériennes en couleur.

Bernhard Reversat, F., Huttel, C., Lemée, G., 1978. La forêt sempervirente de basse côte d'ivoire.

Bernstein, L.R., 1985. Germanium geochemistry and mineralogy. Geochim. Cosmochim. Acta 49, 2409–2422.

Berthelsen, S., Noble, A.D., Garside, A.L., 2001. Silicon research down under: past, present, and future, in: Studies in Plant Science. Elsevier, pp. 241–255.

Berthelsen, S., Noble, A.D., Kingston, G., Hurney, A., Rudd, A., Garside, A., 2003. Improving yield and ccs in sugarcane through the application of silicon based amendments. Final Rep. SRDC Proj. CLW009.

Bigham, J.M., Fitzpatrick, R.W., Schulze, D.G., 2002. Iron oxides. Soil Mineral. Environ. Appl. 323–366.

Bishop, K., Grip, H., O'neill, A., 1990. The origins of acid runoff in a hillslope during storm events. J. Hydrol. 116, 35–61.

Blakemore, L.C., 1983. Extractable iron, aluminium and silicon. Methods Chem. Anal. Soils 71–76.

Blakemore, L.C., 1981. Soil Bureau laboratory methods. A method for chemical analysis of soils. NZ Soil Bur Sci Pep 10, A5–9.

Blakemore, L.C., Searle, P.L., Daly, B.K., 1981. Methods for chemical analysis of soils. Dep. Sci. Ind. Res. https://doi.org/10.7931/dl1-sbsr-10a

Blecker, S.W., King, S.L., Derry, L.A., Chadwick, O.A., Ippolito, J.A., Kelly, E.F., 2007. The ratio of germanium to silicon in plant phytoliths: quantification of biological discrimination under controlled experimental conditions. Biogeochemistry 86, 189–199.

Blecker, S.W., McCulley, R.L., Chadwick, O.A., Kelly, E.F., 2006. Biologic cycling of silica across a grassland bioclimosequence. Glob. Biogeochem. Cycles 20.

Boudon, G., Dagain, J., Semet, M.P., Westercamp, D., 1987. Carte géologique 1: 20 000 du massif volcanique de la Soufrière (Département de la Guadeloupe, Petites Antilles). BRGM Paris.

Bouwer, H., 1986. Intake rate: cylinder infiltrometer. Methods Soil Anal. Part 1—Physical Mineral. Methods 825–844.

Bouysse, P., Westercamp, D., Andreieff, P., 1990. The Lesser Antilles Arc, Proceedings of the Ocean Drilling Program. Ocean Drilling Program. https://doi.org/10.2973/odp.proc.sr.110.1990

Brahy, V., Deckers, J., Delvaux, B., 2000. Estimation of soil weathering stage and acid neutralizing capacity in a toposequence Luvisol–Cambisol on loess under deciduous forest in Belgium. Eur. J. Soil Sci. 51, 1–13.

Bruijnzeel, L.A., Sampurno, S.P., 1990. Hydrology of moist tropical forests and effects of conversion: a state of knowledge review. Free University Amsterdam.

Burns, D.A., McDonnell, J.J., Hooper, R.P., Peters, N.E., Freer, J.E., Kendall, C., Beven, K., 2001. Quantifying contributions to storm runoff through end-member mixing analysis and hydrologic measurements at the Panola Mountain Research Watershed (Georgia, USA). Hydrol. Process. 15, 1903–1924.

Cabanes, D., Weiner, S., Shahack-Gross, R., 2011. Stability of phytoliths in the archaeological record: a dissolution study of modern and fossil phytoliths. J. Archaeol. Sci. 38, 2480–2490.

Camargo, M.S. de, Pereira, H.S., Korndörfer, G.H., Queiroz, A.A., Reis, C.B. dos, 2007. Soil reaction and absorption of silicon by rice. Sci. Agric. 64, 176–180.

Canadell, J., Jackson, R.B., Ehleringer, J.B., Mooney, H.A., Sala, O.E., Schulze, E.-D., 1996. Maximum rooting depth of vegetation types at the global scale. Oecologia 108, 583–595.

Carey, Joanna C, Fulweiler, R.W., 2012. The terrestrial silica pump. PLoS One 7, e52932.

Carey, J. C., Fulweiler, R.W., 2012. Human activities directly alter watershed dissolved silica fluxes. Biogeochemistry 111, 125–138.

Carlson, T.N., Traci Arthur, S., 2000. The impact of land use — land cover changes due to urbanization on surface microclimate and hydrology: a satellite perspective. Glob. Planet. Change 25, 49–65. https://doi.org/10.1016/S0921-8181(00)00021-7

Carlut, J., Quidelleur, X., Courtillot, V., Boudon, G., 2000. Paleomagnetic directions and K/Ar dating of 0 to 1 Ma lava flows from La Guadeloupe Island (French West Indies): Implications for time-averaged field models. J. Geophys. Res. Solid Earth 105, 835–849.

Cattan, P., Voltz, M., Cabidoche, Y.-M., Lacas, J.-G., Sansoulet, J., 2007. Spatial and temporal variations in percolation fluxes in a tropical Andosol influenced by banana cropping patterns. J. Hydrol. 335, 157–169.

Cerdan, O., Govers, G., Le Bissonnais, Y., Van Oost, K., Poesen, J., Saby, N., Gobin, A., Vacca, A., Quinton, J., Auerswald, K., 2010. Rates and spatial variations of soil erosion in Europe: a study based on erosion plot data. Geomorphology 122, 167–177.

Chadwick, O.A., Gavenda, R.T., Kelly, E.F., Ziegler, K., Olson, C.G., Elliott, W.C., Hendricks, D.M., 2003. The impact of climate on the biogeochemical functioning of volcanic soils. Chem. Geol. 202, 195–223.

Chao, T., Sanzolone, R., 1992. Decomposition techniques. J. Geochem. Explor. 44, 65–106.

Chaperon, P., L'Hote, Y., Vuillaume, G., 1985. Les ressources en eau de surface de la Guadeloupe. ORSTOM.

Charlier, J.-B., 2007. Fonctionnement et modélisation hydrologique d'un petit bassin versant cultivé en milieu volcanique tropical (PhD Thesis). UM2.

Charlier, J.-B., Arnaud, L., Ducreux, L., Ladouche, B., Dewandel, B., Plet, J., Lesueur-Jannoyer, M., Cattan, P., 2015. CHLOR-EAU-SOL Caractérisation de la contamination par la chlordécone des eaux et des sols des bassins versants pilotes guadeloupéen et martiniquais.

Charlier, J.-B., Cattan, P., Moussa, R., Voltz, M., 2008. Hydrological behaviour and modelling of a volcanic tropical cultivated catchment. Hydrol. Process. Int. J. 22, 4355–4370.

Charlier, J.-B., Lachassagne, P., Ladouche, B., Cattan, P., Moussa, R., Voltz, M., 2011. Structure and hydrogeological functioning of an insular tropical humid andesitic volcanic watershed: A multi-disciplinary experimental approach. J. Hydrol. 398, 155–170.

Churchman, G.J., Lowe, D.J., 2012. Alteration, formation, and occurrence of minerals in soils. CRC Press.

Clarke, J., 2003. The occurrence and significance of biogenic opal in the regolith. Earth-Sci. Rev. 60, 175–194.

Cloern, J.E., 2001. Our evolving conceptual model of the coastal eutrophication problem. Mar. Ecol. Prog. Ser. 210, 223–253.

Clymans, W., Barão, L., Van der Putten, N., Wasteg\a ard, S., Gísladóttir, G., Björck, S., Moine, B., Struyf, E., Conley, D.J., 2015a. The contribution of tephra constituents during biogenic silica determination: implications for soil and palaeoecological studies. Biogeosciences 12, 3789–3804.

Clymans, W., Struyf, E., Govers, G., Vandevenne, F., Conley, D., 2011. Anthropogenic impact on amorphous silica pools in temperate soils. Biogeosciences 8, 2281–2293.

Clymans, W., Struyf, E., Van den Putte, A., Langhans, C., Wang, Z., Govers, G., 2015b. Amorphous silica mobilization by inter-rill erosion: insights from rainfall experiments. Earth Surf. Process. Landf. 40, 1171–1181.

Colmet-Daage, F., 1977. Zonage cultural des régions bananières de Guadeloupe de 1976.

Colmet-Daage, F., Lagache, F., 1969. Carte des sols des Antilles (Guadeloupe—Martinique). ORSTOM Antill.

Colmet-Daage, F., Lagache, P., 1965. Caractéristiques de quelques groupes de sols dérivés de roches volcaniques aux Antilles françaises. Cah. L'ORSTOM Ser. Pédologie 8, 91–121.

Conley, D.J., 2002. Terrestrial ecosystems and the global biogeochemical silica cycle. Glob. Biogeochem. Cycles 16.

Conley, D.J., Likens, G.E., Buso, D.C., Saccone, L., Bailey, S.W., Johnson, C.E., 2008. Deforestation causes increased dissolved silicate losses in the Hubbard Brook Experimental Forest. Glob. Change Biol. 14, 2548–2554.

Cornelis, J.-T., Delvaux, B., 2016. Soil processes drive the biological silicon feedback loop. Funct. Ecol. 30, 1298–1310.

Cornelis, J-T, Delvaux, B., Georg, R., Lucas, Y., Ranger, J., Opfergelt, S., 2011. Tracing the origin of dissolved silicon transferred from various soil-plant systems towards rivers: a review. Biogeosciences 8, 89–112.

Cornelis, J.-T., Ranger, J., Iserentant, A., Delvaux, B., 2010. Tree species impact the terrestrial cycle of silicon through various uptakes. Biogeochemistry 97, 231–245.

Cornelis, Jean-Thomas, Titeux, H., Ranger, J., Delvaux, B., 2011. Identification and distribution of the readily soluble silicon pool in a temperate forest soil below three distinct tree species. Plant Soil 342, 369–378.

Cornu, S., 1995. Cycles biogéochimiques du silicium, du fer et de l'aluminium en forêt amazonienne (PhD Thesis). Aix-Marseille 3.

Cornu, S., Lucas, Y., Ambrosi, J.P., Desjardins, T., 1998. Transfer of dissolved Al, Fe and Si in two Amazonian forest environments in Brazil. Eur. J. Soil Sci. 49, 377–384.

Coskun, D., Deshmukh, R., Sonah, H., Menzies, J.G., Reynolds, O., Ma, J.F., Kronzucker, H.J., Bélanger, R.R., 2019. The controversies of silicon's role in plant biology. New Phytol. 221, 67–85. https://doi.org/10.1111/nph.15343

Crabit, A., Cattan, P., Colin, F., Voltz, M., 2016. Soil and river contamination patterns of chlordecone in a tropical volcanic catchment in the French West Indies (Guadeloupe). Environ. Pollut. 212, 615–626.

Crusciol, C.A.C., De Arruda, D.P., Fernandes, A.M., Antonangelo, J.A., Alleoni, L.R.F., do Nascimento, C.A.C., Rossato, O.B., McCray, J.M., 2018. Methods and extractants to evaluate silicon availability for sugarcane. Sci. Rep. 8, 916.

Dagain, J., 1981. La mise en place du massif volcanique Madeleine-Soufrière, Basse-Terre de Guadeloupe, Antilles.

Dahlgren, R.A., 1994. Quantification of allophane and imogolite. Quant. Methods Soil Mineral. 430–451.

Davidson, E.A., de Araújo, A.C., Artaxo, P., Balch, J.K., Brown, I.F., C. Bustamante, M.M., Coe, M.T., DeFries, R.S., Keller, M., Longo, M., Munger, J.W., Schroeder, W., Soares-Filho, B.S., Souza, C.M., Wofsy, S.C., 2012. The Amazon basin in transition. Nature 481, 321–328. https://doi.org/10.1038/nature10717

Delfosse, T., Delmelle, P., Iserentant, A., Delvaux, B., 2005. Contribution of SO3 to the acid neutralizing capacity of Andosols exposed to strong volcanogenic acid and SO2 deposition. Eur. J. Soil Sci. 56, 113–125. https://doi.org/10.1111/j.1365-2389.2004.00646.x

Delstanche, S., Opfergelt, S., Cardinal, D., Elsass, F., André, L., Delvaux, B., 2009. Silicon isotopic fractionation during adsorption of aqueous monosilicic acid onto iron oxide. Geochim. Cosmochim. Acta 73, 923–934.

Delvaux, B., Guyot, P., 1989. Caractérisation de l'enracinement du bananier au champ. Incidences sur les relations sol-plante dans les bananeraies intensives de la Martinique. Fruits 44, 633–647.

Delvaux, B., Herbillon, A.J., Vielvoye, L., 1989. Characterization of a weathering sequence of soils derived from volcanic ash in Cameroon. Taxonomic, mineralogical and agronomic implications. Geoderma 45, 375–388.

Delvigne, C., Guihou, A., Angeletti, B., BASILE-DOELSCH, I., Meunier, J.-D., 2018. Reliable Determination of Ge in Solid Environmental Samples Using a Chemical Preparation Procedure Developed for Si Isotopes and ICP-MS Analysis. Geostand. Geoanalytical Res. 42, 139–149. https://doi.org/10.1111/ggr.12197

Delvigne, C., Opfergelt, S., Cardinal, D., Delvaux, B., André, L., 2009. Distinct silicon and germanium pathways in the soil-plant system: Evidence from banana and horsetail. J. Geophys. Res. Biogeosciences 114.

DeMaster, D.J., 1981. The supply and accumulation of silica in the marine environment. Geochim. Cosmochim. Acta 45, 1715–1732. https://doi.org/10.1016/0016-7037(81)90006-5

Deng, Y., Dixon, J.B., 2002. Soil organic matter and organic-mineral interactions. Soil Mineral. Environ. Appl. 69–107.

Derry, L.A., Kurtz, A.C., Ziegler, K., Chadwick, O.A., 2005. Biological control of terrestrial silica cycling and export fluxes to watersheds. Nature 433, 728–731.

Desplanques, V., Cary, L., Mouret, J.-C., Trolard, F., Bourrié, G., Grauby, O., Meunier, J.-D., 2006. Silicon transfers in a rice field in Camargue (France). J. Geochem. Explor., Extended Abstracts presented at the 7th Symp. on the Geochemistry of the Earth's Surface (GES-7) 88, 190–193. https://doi.org/10.1016/j.gexplo.2005.08.036

Dessert, C., Lajeunesse, E., Lloret, E., Clergue, C., Crispi, O., Gorge, C., Quidelleur, X., 2015. Controls on chemical weathering on a mountainous volcanic tropical island: Guadeloupe (French West Indies). Geochim. Cosmochim. Acta 171, 216–237.

Dewalle, D.R., Swistock, B.R., Sharpe, W.E., 1988. Three-component tracer model for stormflow on a small Appalachian forested catchment. J. Hydrol. 104, 301–310. https://doi.org/10.1016/0022-1694(88)90171-0

D'Hotman, D., Villiers, O., 1961. Soil rejuvenation with crushed basalt in Mauritius. Int Sugar J 63, 363–364.

Dorel, M., Perrier, X., 1990. Influence du milieu et des techniques culturales sur la productivité des bananeraies de Guadeloupe. Enquête-diagnostic. Fruits.

Dorel, M., Roger-Estrade, J., Manichon, H., Delvaux, B., 2000. Porosity and soil water properties of Caribbean volcanic ash soils. Soil Use Manag. 16, 133–140.

Doumenge, F., 1985. Atlas des départements français d'Outre-Mer - 3 - la Guadeloupe, C.N.R.S.- O.R.S.T.O.M. Ann. Géographie 94, 492–493.

Drees, R., Wilding, L.P., Smeck, N.E., Senkayi, A.L., 1989. Silica in soils: quartz and disordered silica polymorphs. Miner. Soil Environ. 913–974.

Drever, J.I., 1994. The effect of land plants on weathering rates of silicate minerals. Geochim. Cosmochim. Acta 58, 2325–2332.

Dürr, H.H., Meybeck, M., Hartmann, J., Laruelle, G.G., Roubeix, V., 2011. Global spatial distribution of natural riverine silica inputs to the coastal zone. Biogeosciences 8, 597–620.

Epstein, E., 1999. Silicon. Annu. Rev. Plant Biol. 50, 641–664.

FAO, 2018. Food and Agriculture Organization of the United Nations (FAO). www.faostat.fao.org [WWW Document]. Food Agric. Organ. U. N. FAO Wwwfaostatfaoorg. URL http://www.fao.org/faostat/en/#data (accessed 1.18.19).

FAO, 2010. Évaluation des ressources forestières mondiales: Rapport national Guadeloupe (No. FRA2010/082). Food and Agriculture Organization of the United Nations.

Farmer, V., Delbos, E., Miller, J., 2005. The role of phytolith formation and dissolution in controlling concentrations of silica in soil solutions and streams. Geoderma 127, 71–79.

Farmer, V.C., 1982. Significance of the presence of allophane and imogolite in podzol Bs horizons for podzolization mechanisms: a review. Soil Sci. Plant Nutr. 28, 571–578.

Farmer, V.C., Fraser, A.R., Tait, J.M., Palmieri, F., Violante, P., Nakai, M., Yoshinaga, N., 1978. Imogolite and proto-imogolite in an Italian soil developed on volcanic ash. Clay Miner. 13, 271–274.

Farmer, V.C., Lumsdon, D.G., 2001. Interactions of fulvic acid with aluminium and a proto-imogolite sol: the contribution of E-horizon eluates to podzolization. Eur. J. Soil Sci. 52, 177–188.

Fieldes, M., Perrot, K.W., 1966. The nature of allophane in soils. I. Significance of randomness in pedogenesis. New Zeland J Sci 9, 622–632.

Foy, C.D., 1992. Soil chemical factors limiting plant root growth, in: Limitations to Plant Root Growth. Springer, pp. 97–149.

Fraysse, F., Pokrovsky, O., Meunier, J.-D., 2010. Experimental study of terrestrial plant litter interaction with aqueous solutions. Geochim. Cosmochim. Acta 74, 70–84.

Fraysse, F., Pokrovsky, O.S., Schott, J., Meunier, J.-D., 2009. Surface chemistry and reactivity of plant phytoliths in aqueous solutions. Chem. Geol. 258, 197–206.

Fraysse, F., Pokrovsky, O.S., Schott, J., Meunier, J.-D., 2006. Surface properties, solubility and dissolution kinetics of bamboo phytoliths. Geochim. Cosmochim. Acta 70, 1939–1951.

Froelich, P.N., Blanc, V., Mortlock, R.A., Chillrud, S.N., Dunstan, W., Udomkit, A., Peng, T.-H., 1992. River fluxes of dissolved silica to the ocean were higher during glacials: Ge/Si in diatoms, rivers, and oceans. Paleoceanogr. Paleoclimatology 7, 739–767.

Fulweiler, R.W., Nixon, S.W., 2005. Terrestrial vegetation and the seasonal cycle of dissolved silica in a southern New England coastal river. Biogeochemistry 74, 115–130.

Gaillardet, J., Louvat, P., Lajeunesse, E., 2011a. Rivers from volcanic island arcs: the subduction weathering factory. Appl. Geochem. 26, S350–S353.

Gaillardet, J., Rad, S., Rivé, K., Louvat, P., Gorge, C., Allègre, C.J., Lajeunesse, E., 2011b. Orography-driven chemical denudation in the Lesser Antilles: Evidence for a new feed-back mechanism stabilizing atmospheric CO2. Am. J. Sci. 311, 851–894. https://doi.org/10.2475/10.2011.02

Garrels, R.M., Christ, C.L., 1965. Solutions, minerals and equilibria. Miner. Harper Row N. Y.

Georg, R., Reynolds, B., Frank, M., Halliday, A., 2006. Mechanisms controlling the silicon isotopic compositions of river waters. Earth Planet. Sci. Lett. 249, 290–306.

Georgiadis, A., Sauer, D., Herrmann, L., Breuer, J., Zarei, M., Stahr, K., 2013. Development of a method for sequential Si extraction from soils. Geoderma 209, 251–261.

Gérard, F., François, M., Ranger, J., 2002. Processes controlling silica concentration in leaching and capillary soil solutions of an acidic brown forest soil (Rhône, France). Geoderma 107, 197–226.

Gérard, F., Mayer, K., Hodson, M., Ranger, J., 2008. Modelling the biogeochemical cycle of silicon in soils: application to a temperate forest ecosystem. Geochim. Cosmochim. Acta 72, 741–758.

Gérard, F., Ranger, J., Ménétrier, C., Bonnaud, P., 2003. Silicate weathering mechanisms determined using soil solutions held at high matric potential. Chem. Geol. 202, 443–460.

Godefroy, J., Dormoy, M., 1984. Un exemple d'utilisation du diagnostic sol à la programmation de la fertilisation en bananeraie. Fruits.

Goudie, A.S., Viles, H.A., 2012. Weathering and the global carbon cycle: Geomorphological perspectives. Earth-Sci. Rev. 113, 59–71.

Gousseland, J., 1983a. Etude de l'enracinement et de l'émission racinaire du bananier Giant Cavendish (Musa acuminata AAA, sous-groupe Cavendish) dans les andosols de la Guadeloupe. Fruits 38, 611–623.

Gousseland, J., 1983b. Etude de l'enracinement et de l'émission racinaire du bananier "Giant Cavendish" (Musa acuminata AAA, sous-groupe Cavendish) dans les andosols de Guadeloupe. Fruits 38, 611–628.

Greenland, D.J., Nye, P.H., 1959. Increases in the carbon and nitrogen contents of tropical soils under natural fallows. J. Soil Sci. 10, 284–299.

Guntzer, F., Keller, C., Poulton, P.R., McGrath, S.P., Meunier, J.-D., 2012. Long-term removal of wheat straw decreases soil amorphous silica at Broadbalk, Rothamsted. Plant Soil 352, 173–184.

Harsh, J., Chorover, J., Nizeyimana, E., 2002. Allophane and Imogolite. Soil Mineral. Environ. Appl. sssabookseries, 291–322. https://doi.org/10.2136/sssabookser7.c9

Hassuani, S.J., Leal, M., Macedo, I., 2005. Biomass power generation. Sugar Cane Bagasse Trash Publ. Programa Nacoes Unidas Para O Desenvolv. Cent. Technol. Canavieriva Peracicaba Braz.

Haynes, R.J., 2019. What effect does liming have on silicon availability in agricultural soils? Geoderma 337, 375–383.

Haynes, R.J., Zhou, Y.-F., 2018. Effect of pH and added slag on the extractability of Si in two Si-deficient sugarcane soils. Chemosphere 193, 431–437.

Haysom, M.B.C., Chapman, L.S., 1975. Some aspects of the calcium silicate trials at Mackay, in: Proceedings.

Henriet, C., Bodarwé, L., Dorel, M., Draye, X., Delvaux, B., 2008a. Leaf silicon content in banana (Musa spp.) reveals the weathering stage of volcanic ash soils in Guadeloupe. Plant Soil 313, 71–82.

Henriet, C., De Jaeger, N., Dorel, M., Opfergelt, S., Delvaux, B., 2008b. The reserve of weatherable primary silicates impacts the accumulation of biogenic silicon in volcanic ash soils. Biogeochemistry 90, 209–223.

Henriet, C., Draye, X., Oppitz, I., Swennen, R., Delvaux, B., 2006. Effects, distribution and uptake of silicon in banana (Musa spp.) under controlled conditions. Plant Soil 287, 359–374.

Herbillon, A., 1986. Chemical estimation of weatherable minerals present in the diagnostic horizons of low activity clay soils, in: Proceedings of the 8th International Clay Classification Workshop: Classification, Characterization and Utilization of Oxisols (Part 1)[Beinroth, FH, Camargo, MN and Eswaran (Ed.)][39–48](Rio de Janeiro, 1986).

Herbillon, A.J., Frankart, R., Vielvoye, L., 1981. An occurrence of interstratified kaolinite-smectite minerals in a red-black soil toposequence. Clay Miner. 16, 195–201.

Hill, R.L., 1990. Long-Term Conventional and No-Tillage Effects on Selected Soil Physical Properties. Soil Sci. Soc. Am. J. 54, 161–166. https://doi.org/10.2136/sssaj1990.03615995005400010025x

Hodson, M., White, P.J., Mead, A., Broadley, M., 2005. Phylogenetic variation in the silicon composition of plants. Ann. Bot. 96, 1027–1046.

Hood, J.L.A., Van Cappellen, P., 2014. Land-use drives seasonal riverine Si cycling at the landscape scale. Procedia Earth Planet. Sci. 10, 133–138.

Huang, P.M., Wang, M.K., Kämpf, N., Schulze, D.G., 2002. Aluminum Hydroxides. Soil Mineral. Environ. Appl. sssabookseries, 261–289. https://doi.org/10.2136/sssabookser7.c8

IUSS, W.G.W., 2014. World Reference Base for Soil Resources 2014. International soil classification system for naming soils and creating legends for soil maps. (No. 106), World Soil Resources Reports. FAO, Rome.

Jackson, M.L., 1956. Soil Chemical Analysis–Advanced Course: Published by the author, Dept. Soil Sci Univ Wis. Madison 907.

Jackson, P.C., Cavelier, J., Goldstein, G., Meinzer, F.C., Holbrook, N.M., 1995. Partitioning of water resources among plants of a lowland tropical forest. Oecologia 101, 197–203.

Jackson, R.B., Canadell, J., Ehleringer, J.R., Mooney, H.A., Sala, O.E., Schulze, E.D., 1996. A global analysis of root distributions for terrestrial biomes. Oecologia 108, 389–411.

Jennerjahn, T.C., Knoppers, B.A., Souza, W.F.L., Brunskill, G.J., Silva, E.I.L., Adi, S., 2006. Factors controlling dissolved silica in tropical rivers. Silicon Cycle Hum. Perturbations Impacts Aquat. Syst. Ed. Ittekkot V Unger Humborg C NT SCOPE 66, 29–51.

Jobbágy, E.G., Jackson, R.B., 2001. The distribution of soil nutrients with depth: global patterns and the imprint of plants. Biogeochemistry 53, 51–77.

Jones, L., Handreck, K., 1965. Studies of silica in the oat plant. Plant Soil 23, 79–96.

Jones, L.H.P., Handreck, K.A., 1963. Effects of Iron and Aluminium Oxides on Silica in Solution in Soils. Nature 198, 852–853. https://doi.org/10.1038/198852a0

Jongmans, A.G., Buurman, P., van Doesburg, J.D.J., van Oort, F., Jaunet, A.M., 1994. Morphology, Chemistry, and Mineralogy of Isotropic Aluminosilicate Coatings in a Guadeloupe Andisol. Soil Sci. Soc. Am. J. 58, 501. https://doi.org/10.2136/sssaj1994.03615995005800020036x

Jongmans, A.G., Van Oort, F., Denaix, L., Jaunet, A.M., 1999. Mineral micro-and nano-variability revealed by combined micromorphology and in situ submicroscopy. Catena 35, 259–279.

Kablan, L., Lagauche, A., Delvaux, B., Legr`ve, A., 2011. Silicon Reduces Black Sigatoka Development in Banana. Plant Dis. 96, 273–278. https://doi.org/10.1094/PDIS-04-11-0274

Kamatani, A., Oku, O., 2000. Measuring biogenic silica in marine sediments. Mar. Chem. 68, 219–229. https://doi.org/10.1016/S0304-4203(99)00079-1

Kawaguchi, K., 1966. Tropical paddy soils. Jpn. Agric. Res. Q. Ibaraki 1, 7–11.

Kealhofer, L., Penny, D., 1998. A combined pollen and phytolith record for fourteen thousand years of vegetation change in northeastern Thailand. Rev. Palaeobot. Palynol. 103, 83–93.

Keeping, M.G., 2017. Uptake of Silicon by Sugarcane from Applied Sources May Not Reflect Plant-Available Soil Silicon and Total Silicon Content of Sources. Front. Plant Sci. 8. https://doi.org/10.3389/fpls.2017.00760

Keller, C., Guntzer, F., Barboni, D., Labreuche, J., Meunier, J.-D., 2012. Impact of agriculture on the Si biogeochemical cycle: input from phytolith studies. Comptes Rendus Geosci. 344, 739–746.

Kelly, E.F., 1990. Methods for extracting opal phytoliths from soil and plant material: Workshop on biotic indicators of global change. Univ. Wash.

Kingston, G., 2008. Silicon fertilisers: requirements and field experiences, in: Proceedings of the 4th International Conference on Silicon in Agriculture, Port Edward, South Africa. p. 52.

Klaus, J., McDonnell, J.J., 2013. Hydrograph separation using stable isotopes: Review and evaluation. J. Hydrol. 505, 47–64. https://doi.org/10.1016/j.jhydrol.2013.09.006

Kleidon, A., Heimann, M., 1998. A method of determining rooting depth from a terrestrial biosphere model and its impacts on the global water and carbon cycle. Glob. Change Biol. 4, 275–286.

Klotzbücher, A., Klotzbücher, T., Jahn, R., Xuan, L.D., Cuong, L.Q., Van Chien, H., Hinrichs, M., Sann, C., Vetterlein, D., 2018. Effects of Si fertilization on Si in soil solution, Si uptake by rice, and resistance of rice to biotic stresses in Southern Vietnam. Paddy Water Environ. 16, 243–252. https://doi.org/10.1007/s10333-017-0610-2

Klotzbücher, T., Klotzbücher, A., Kaiser, K., Merbach, I., Mikutta, R., 2018. Impact of agricultural practices on plant-available silicon. Geoderma 331, 15–17. https://doi.org/10.1016/j.geoderma.2018.06.011

Klotzbücher, T., Klotzbücher, A., Vetterlein, D., Schneiker, J., Türke, M., van Sinh, N., Manh, N.H., van Chien, H., Marquez, L., Villareal, S., Bustamante, J.V., Jahn, R., 2015a. Plant-available silicon in paddy soils as a key factor for sustainable rice production in Southeast Asia. Basic Appl. Ecol. 16, 665–673. https://doi.org/10.1016/j.baae.2014.08.002

Klotzbücher, T., Leuther, F., Marxen, A., Vetterlein, D., Horgan, F.G., Jahn, R., 2015b. Forms and fluxes of potential plant-available silicon in irrigated lowland rice production (Laguna, the Philippines). Plant Soil 393, 177–191. https://doi.org/10.1007/s11104-015-2480-y

Klotzbücher, T., Marxen, A., Jahn, R., Vetterlein, D., 2016. Silicon cycle in rice paddy fields: insights provided by relations between silicon forms in topsoils and plant silicon uptake. Nutr. Cycl. Agroecosystems 105, 157–168.

Komorowski, J.-C., Boudon, G., Semet, M., Beauducel, F., Anténor-Habazac, C., Bazin, S., Hammouya, G., 2005. Guadeloupe, in: Volcanic Hazard Atlas of The Lesser Antilles. Seismic Research Unit, Univesrity of the West Indies, pp. 65–102.

Koning, E., Epping, E., Raaphorst, W.V., 2002. Determining Biogenic Silica in Marine Samples by Tracking Silicate and Aluminium Concentrations in Alkaline Leaching Solutions. Aquat. Geochem. 8, 37–67. https://doi.org/10.1023/A:1020318610178

Kosmas, C., Danalatos, N., Cammeraat, L.H., Chabart, M., Diamantopoulos, J., Farand, R., Gutierrez, L., Jacob, A., Marques, H., Martinez-Fernandez, J., Mizara, A., Moustakas, N., Nicolau, J.M., Oliveros, C., Pinna, G., Puddu, R., Puigdefabregas, J., Roxo, M., Simao, A., Stamou, G., Tomasi, N., Usai, D., Vacca, A., 1997. The effect of land use on runoff and soil erosion rates under Mediterranean conditions. CATENA 29, 45–59. https://doi.org/10.1016/S0341-8162(96)00062-8

Kurtz, A.C., Derry, L.A., Chadwick, O.A., 2002. Germanium-silicon fractionation in the weathering environment. Geochim. Cosmochim. Acta 66, 1525–1537.

Kurtz, A.C., Lugolobi, F., Salvucci, G., 2011. Germanium-silicon as a flow path tracer: Application to the Rio Icacos watershed. Water Resour. Res. 47.

Lacoeuilhe, J.-J., Godefroy, J., 1971. Un cas de carence en phosphore en bananeraie. Fruits 26, 659–662.

Laliberté, E., Grace, J.B., Huston, M.A., Lambers, H., Teste, F.P., Turner, B.L., Wardle, D.A., 2013. How does pedogenesis drive plant diversity? Trends Ecol. Evol. 28, 331–340.

Laruelle, G.G., Roubeix, V., Sferratore, A., Brodherr, B., Ciuffa, D., Conley, D., Dürr, H., Garnier, J., Lancelot, C., Le Thi Phuong, Q., others, 2009. Anthropogenic perturbations of the silicon cycle at the global scale: Key role of the land-ocean transition. Glob. Biogeochem. Cycles 23.

Li, Z., 2019. Impact of biochar on the biological silicon feedback loop in soil-plant systems. UCLouvain.

Li, Z., Delvaux, B., Yans, J., Dufour, N., Houben, D., Cornelis, J.-T., 2018. Phytolith-rich biochar increases cotton biomass and silicon-mineralomass in a highly weathered soil. J. Plant Nutr. Soil Sci. 181, 537–546. https://doi.org/10.1002/jpln.201800031

Li, Z., Lin, P., He, J., Yang, Z., Lin, Y., 2006. Silicon's organic pool and biological cycle in moso bamboo community of Wuyishan Biosphere Reserve. J. Zhejiang Univ. Sci. B 7, 849–857. https://doi.org/10.1631/jzus.2006.B0849

Li, Z., Song, Z., Cornelis, J.-T., 2014. Impact of rice cultivar and organ on elemental composition of phytoliths and the release of bio-available silicon. Front. Plant Sci. 5.

Li, Z., Unzué-Belmonte, D., Cornelis, J.-T., Vander Linden, C., Struyf, E., Ronsse, F., Delvaux, B., 2019. Effects of phytolithic rice-straw biochar, soil buffering capacity and pH on silicon bioavailability. Plant Soil 1–17.

Liang, Y., Nikolic, M., Bélanger, R., Gong, H., Song, A., 2015. Silicon Biogeochemistry and Bioavailability in Soil, in: Silicon in Agriculture. Springer, pp. 45–68.

Lloret, E., Dessert, C., Gaillardet, J., Albéric, P., Crispi, O., Chaduteau, C., Benedetti, M., 2011. Comparison of dissolved inorganic and organic carbon yields and fluxes in the watersheds of tropical volcanic islands, examples from Guadeloupe (French West Indies). Chem. Geol. 280, 65–78.

Lloret, E., Dessert, C., Pastor, L., Lajeunesse, E., Crispi, O., Gaillardet, J., Benedetti, M.F., 2013. Dynamic of particulate and dissolved organic carbon in small volcanic mountainous tropical watersheds. Chem. Geol. 351, 229–244.

Loucaides, S., Cappellen, P.V., Behrends, T., others, 2008. Dissolution of biogenic silica from land to ocean: role of salinity and pH. Limnol. Oceanogr. 53, 1614.

Lucas, Y., 2001. The role of plants in controlling rates and products of weathering: importance of biological pumping. Annu. Rev. Earth Planet. Sci. 29, 135–163.

Lucas, Y., Luizao, F., Chauvel, A., Rouiller, J., Nahon, D., 1993. The relation between biological activity of the rain forest and mineral composition of soils. Science 260, 521–523.

Lucas, Y., Nahon, D., Cornu, S., Eyrolle, F., 1996. Genèse et fonctionnement des sols en milieu équatorial. Comptes Rendus Académie Sci. Sér. 2a Sci. Terre 322, 1–16.

Lugolobi, F., Kurtz, A.C., Derry, L.A., 2010. Germanium–silicon fractionation in a tropical, granitic weathering environment. Geochim. Cosmochim. Acta 74, 1294–1308.

Ma, J., Miyake, Y., Takahashi, E., 2001. Silicon as a beneficial element for crop plants. Stud. Plant Sci. 8, 17–39.

Ma, J., Takahashi, E., 1989. Release of silicon from rice straw under flooded conditions. Soil Sci. Plant Nutr. 35, 663–667. https://doi.org/10.1080/00380768.1989.10434802

Ma, J.F., Takahashi, E., 2002. Soil, fertilizer, and plant silicon research in Japan. Elsevier.

Ma, J.F., Tamai, K., Yamaji, N., Mitani, N., Konishi, S., Katsuhara, M., Ishiguro, M., Murata, Y., Yano, M., 2006. A silicon transporter in rice. Nature 440, 688–691.

Madeira, M., Furtado, A., Jeanroy, E., Herbillon, A. dy1994, 1994. Andisols of Madeira island (Portugal). Characteristics and classification. Geoderma 62, 363–383.

Maher, K., 2011. The role of fluid residence time and topographic scales in determining chemical fluxes from landscapes. Earth Planet. Sci. Lett. 312, 48–58.

Makabe, S., KAKUDA, K., Sasaki, Y., Ando, T., Fujii, H., Ando, H., 2009. Relationship between mineral composition or soil texture and available silicon in alluvial paddy soils on the Shounai Plain, Japan. Soil Sci. Plant Nutr. 55, 300–308.

Mangalaa, K.R., Cardinal, D., Brajard, J., Rao, D.B., Sarma, N.S., Djouraev, I., Chiranjeevulu, G., Murty, K.N., Sarma, V.V.S.S., 2017. Silicon cycle in Indian estuaries and its control by biogeochemical and anthropogenic processes. Cont. Shelf Res. 148, 64–88. https://doi.org/10.1016/j.csr.2017.08.011

Mantovani, J.R., Campos, G.M., Silva, A.B., Marques, D.J., Putti, F.F., Landgraf, P.R.C., de Almeida, E.J., 2016. Steel slag to correct soil acidity and as silicon source in coffee plants. Afr. J. Agric. Res. 11, 543–550.

Markewitz, D., Richter, D.D., 1998. The bio in aluminum and silicon geochemistry, in: Plant-Induced Soil Changes: Processes and Feedbacks. Springer, pp. 235–252.

Martin-Prével, P., 1980. nutrition minérale du bananier dans le monde-Première partie. Fruits 35, 503–518.

Marxen, A., Klotzbücher, T., Jahn, R., Kaiser, K., Nguyen, V.S., Schmidt, A., Schädler, M., Vetterlein, D., 2016. Interaction between silicon cycling and straw decomposition in a silicon deficient rice production system. Plant Soil 398, 153–163. https://doi.org/10.1007/s11104-015-2645-8

Matichenkov, V.V., Calvert, D.V., 2002. Silicon as a beneficial element for sugarcane. J. Am. Soc. Sugarcane Technol. 22, 21–30.

Maury, R.C., Westbrook, G.K., Baker, P.E., Bouysse, P., Westercamp, D., 1990. Geology of the Lesser Antilles. Caribb. Reg. 141–166.

McIntosh, J.C., Schaumberg, C., Perdrial, J., Harpold, A., Vázquez-Ortega, A., Rasmussen, C., Vinson, D., Zapata-Rios, X., Brooks, P.D., Meixner, T., 2017. Geochemical evolution

of the C ritical Z one across variable time scales informs concentration-discharge relationships: J emez R iver B asin C ritical Z one O bservatory. Water Resour. Res. 53, 4169–4196.

McKeague, J., Cline, M., 1963. Silica in soil solutions: II. The adsorption of monosilicic acid by soil and by other substances. Can. J. Soil Sci. 43, 83–96.

McKeague, J.A., Day, Jh., 1966. Dithionite-and oxalate-extractable Fe and Al as aids in differentiating various classes of soils. Can. J. Soil Sci. 46, 13–22.

Meena, V.D., Dotaniya, M.L., Coumar, V., Rajendiran, S., Ajay, Kundu, S., Subba Rao, A., 2014. A Case for Silicon Fertilization to Improve Crop Yields in Tropical Soils. Proc. Natl. Acad. Sci. India Sect. B Biol. Sci. 84, 505–518. https://doi.org/10.1007/s40011-013-0270-y

Mehra, O.P., Jackson, M.L., 1960. Iron oxide removal from soils and clays by a dithionite–citrate system buffered with sodium bicarbonate, in: Clays and Clay Minerals: Proceedings of the Seventh National Conference. Elsevier, pp. 317–327.

Melzer, S.E., Knapp, A.K., Kirkman, K.P., Smith, M.D., Blair, J.M., Kelly, E.F., 2010. Fire and grazing impacts on silica production and storage in grass dominated ecosystems. Biogeochemistry 97, 263–278. https://doi.org/10.1007/s10533-009-9371-3

Meunier, J., Kirman, S., Strasberg, D., Nicolini, E., Delcher, E., Keller, C., 2010. The output and bio-cycling of Si in a tropical rain forest developed on young basalt flows (La Reunion Island). Geoderma 159, 431–439.

Meunier, J.D., Colin, F., Alarcon, C., 1999. Biogenic silica storage in soils. Geology 27, 835–838.

Meunier, J.D., Keller, C., Guntzer, F., Riotte, J., Braun, J.J., Anupama, K., 2014. Assessment of the 1% Na2CO3 technique to quantify the phytolith pool. Geoderma 216, 30–35. https://doi.org/10.1016/j.geoderma.2013.10.014

Meunier, J.-D., Sandhya, K., Prakash, N.B., Borschneck, D., Dussouillez, P., 2018. pH as a proxy for estimating plant-available Si? A case study in rice fields in Karnataka (South India). Plant Soil 432, 143–155. https://doi.org/10.1007/s11104-018-3758-7

Meyer, J., Keeping, M.G., 2005. The impact of nitrogen and silicon nutrition on the resistance of sugarcane varieties to Eldana saccharina (Lepidoptera: Pyralidae), in: Proc S Afr Sug Technol Ass. p. 363.

Miles, N., Manson, A.D., Rhodes, R., Antwerpen, R. van, Weigel, A., 2014. Extractable Silicon in Soils of the South African Sugar Industry and Relationships with Crop Uptake. Commun. Soil Sci. Plant Anal. 45, 2949–2958. https://doi.org/10.1080/00103624.2014.956881

Mitani, N., Ma, J.F., 2005. Uptake system of silicon in different plant species. J. Exp. Bot. 56, 1255–1261.

Mizota, C., Van Reeuwijk, L.P., 1989. Clay mineralogy and chemistry of soils formed in volcanic material in diverse climatic regions. Clay Mineral. Chem. Soils Form. Volcan. Mater. Diverse Clim. Reg.

Monger, H.C., Kelly, E.F., 2002. Silica Minerals. Soil Mineral. Environ. Appl. sssabookseries, 611–636. https://doi.org/10.2136/sssabookser7.c20

Montgomery, D.R., 2007. Soil erosion and agricultural sustainability. Proc. Natl. Acad. Sci. 104, 13268–13272.

Morell, M., Jérémie, J.-J., 1994. La Guadeloupe au fil de l'eau.

Mortlock, R.A., Frohlich, P.N., 1987. Continental weathering of germanium: GeSi in the global river discharge. Geochim. Cosmochim. Acta 51, 2075–2082.

Moulton, K.L., West, J., Berner, R.A., 2000. Solute flux and mineral mass balance approaches to the quantification of plant effects on silicate weathering. Am. J. Sci. 300, 539–570.

Murnane, R.J., Stallard, R.F., 1990. Germanium and silicon in rivers of the Orinoco drainage basin. Nature 344, 749.

Myers, N., 1988. Threatened biotas: "Hot spots" in tropical forests. The Environmentalist 8, 187–208. https://doi.org/10.1007/BF02240252

Ndayiragije, S., 1996. Caractérisation d'une séquence d'altération de sols dérivés de matériaux pyroclastiques sous climat tropical humide des Antilles (Guadeloupe). Ph. D. diss. Université Catholique de Louvain, Louvain, Belgium.

Ndayiragije, S., Delvaux, B., 2004. Selective sorption of potassium in a weathering sequence of volcanic ash soils from Guadeloupe, French West Indies. Catena 56, 185–198.

Ndayiragije, S., Delvaux, B., 2003. Coexistence of allophane, gibbsite, kaolinite and hydroxy-Al-interlayered 2: 1 clay minerals in a perudic Andosol. Geoderma 117, 203–214.

Nepstad, D., Lefebvre, P., Lopes da Silva, U., Tomasella, J., Schlesinger, P., Solórzano, L., Moutinho, P., Ray, D., Guerreira Benito, J., 2004. Amazon drought and its implications for forest flammability and tree growth: A basin-wide analysis. Glob. Change Biol. 10, 704–717.

Nepstad, D.C., de Carvalho, C.R., Davidson, E.A., Jipp, P.H., Lefebvre, P.A., Negreiros, G.H., da Silva, E.D., Stone, T.A., Trumbore, S.E., Vieira, S., 1994. The role of deep roots in the hydrological and carbon cycles of Amazonian forests and pastures. Nature 372, 666.

Neumann, K., Bostoen, K., Höhn, A., Kahlheber, S., Ngomanda, A., Tchiengué, B., 2012. First farmers in the Central African rainforest: A view from southern Cameroon. Quat. Int. 249, 53–62.

Nguyen, M.N., Dultz, S., Picardal, F., Bui, A.T., Pham, Q.V., Dam, T.T., Nguyen, C.X., Nguyen, N.T., Bui, H.T., 2016. Simulation of silicon leaching from flooded rice paddy soils in the Red River Delta, Vietnam. Chemosphere 145, 0e456.

Nieuwenhuyse, A., Van Breemen, N., 1997. Quantitative aspects of weathering and neoformation in selected Costa Rican volcanic soils. Soil Sci. Soc. Am. J. 61, 1450–1458.

Nizeyimana, E., Bicki, T.J., Agbu, P.A., 1997. An assessment of colloidal constituents and clay mineralogy of soils derived from volcanic materials along a toposequence in Rwanda. Soil Sci. 162, 361.

Norfleet, M.L., Karathanasis, A.D., Smith, B.R., 1993. Soil solution composition relative to mineral distribution in Blue Ridge Mountain soils. Soil Sci. Soc. Am. J. 57, 1375–1380.

Olsen, S.R., Sommers, L.E., Page, A.L., 1982. Methods of soil analysis. Part 2. Chem. Microbiol. Prop. Phosphorus ASA Monogr. 9, 403–430.

Opfergelt, S., Cardinal, D., André, L., Delvigne, C., Bremond, L., Delvaux, B., 2010. Variations of δ 30 Si and Ge/Si with weathering and biogenic input in tropical basaltic ash soils under monoculture. Geochim. Cosmochim. Acta 74, 225–240.

Opfergelt, S., Georg, R., Delvaux, B., Cabidoche, Y.-M., Burton, K., Halliday, A., 2012a. Silicon isotopes and the tracing of desilication in volcanic soil weathering sequences, Guadeloupe. Chem. Geol. 326, 113–122.

Opfergelt, S., Georg, R.B., Delvaux, B., Cabidoche, Y.-M., Burton, K.W., Halliday, A.N., 2012b. Mechanisms of magnesium isotope fractionation in volcanic soil weathering sequences, Guadeloupe. Earth Planet. Sci. Lett. 341, 176–185.

Parfitt, R.L., Childs, C.W., 1988. Estimation of forms of Fe and Al - a review, and analysis of contrasting soils by dissolution and Mossbauer methods. Soil Res. 26, 121–144. https://doi.org/10.1071/sr9880121

Parfitt, R.L., Henmi, T., 1982. Comparison of an oxalate-extraction methon and an infrared spectroscopic method for determining allophane in soll clays. Soil Sci. Plant Nutr. 28, 183–190. https://doi.org/10.1080/00380768.1982.10432435

Parfitt, R.L., Russell, M., Orbell, G.E., 1983. Weathering sequence of soils from volcanic ash involving allophane and halloysite, New Zealand. Geoderma 29, 41–57. https://doi.org/10.1016/0016-7061(83)90029-0

Parfitt, R.L., Wilson, A.D., 1985. Estimation of allophane and halloysite in three sequences of volcanic soils, New Zealand. Catena. Supplement 7:1 8.

Pépin, Y., Ponchant, L., Bajazet, T., Nannette, J.-B., Andrieux, P., 2017. Observatoire de la Pollution agricole aux AntilLEs (OPALE): Hydrologie de surface - Inventaire des données et Courbes d'étallonnage.

Pereira, J.A.M., Schwaab, M., Dell'Oro, E., Pinto, J.C., Monteiro, J.L.F., Henriques, C.A., 2009. The kinetics of gibbsite dissolution in NaOH. Hydrometallurgy 96, 6–13. https://doi.org/10.1016/j.hydromet.2008.07.009

Peters, N.E., Ratcliffe, E.B., 1998. Tracing hydrologic pathways using chloride at the Panola Mountain Research Watershed, Georgia, USA. Water. Air. Soil Pollut. 105, 263–275.

Piao, S., Friedlingstein, P., Ciais, P., Noblet-Ducoudré, N. de, Labat, D., Zaehle, S., 2007. Changes in climate and land use have a larger direct impact than rising CO2 on global river runoff trends. Proc. Natl. Acad. Sci. 104, 15242–15247. https://doi.org/10.1073/pnas.0707213104

Piperno, D.R., 1988. Phytolith analysis: an archaeological and geological perspective. Elsevier.

Plaisir, J., Démonio, W., Claudin, J., 2003. Atlas du Parc national de Guadeloupe. Ministère Ecol. Dév. Durable Guadeloupe.

Pokrovsky, O., Schott, J., Kudryavtzev, D., Dupré, B., 2005. Basalt weathering in Central Siberia under permafrost conditions. Geochim. Cosmochim. Acta 69, 5659–5680.

Ponnamperuma, F.N., 1972. The chemistry of submerged soils, in: Advances in Agronomy. Elsevier, pp. 29–96.

Poulenard, J., Podwojewski, P., Janeau, J.-L., Collinet, J., 2001. Runoff and soil erosion under rainfall simulation of Andisols from the Ecuadorian Páramo: effect of tillage and burning. CATENA 45, 185–207. https://doi.org/10.1016/S0341-8162(01)00148-5

Prakash, N.B., Chandrashekar, N., Mahendra, C., Patil, S.U., Thippeshappa, G.N., Laane, H.M., 2011. Effect of Foliar Spray of Soluble Silicic Acid on Growth and Yield Parameters of Wetland Rice in Hilly and Coastal Zone Soils of Karnataka, South India. J. Plant Nutr. 34, 1883–1893. https://doi.org/10.1080/01904167.2011.600414

Quigley, K.M., Donati, G.L., Anderson, T.M., 2017. Variation in the soil 'silicon landscape' explains plant silica accumulation across environmental gradients in Serengeti. Plant Soil 410, 217–229. https://doi.org/10.1007/s11104-016-3000-4

Rad, S., Cerdan, O., Rivé, K., Grandjean, G., 2011. Age of river basins in Guadeloupe impacting chemical weathering rates and land use. Appl. Geochem. 26, S123–S126.

Rad, S., Rivé, K., Vittecoq, B., Cerdan, O., Allègre, C.J., 2013. Chemical weathering and erosion rates in the Lesser Antilles: An overview in Guadeloupe, Martinique and Dominica. J. South Am. Earth Sci. 45, 331–344.

Ragueneau, O., Schultes, S., Bidle, K., Claquin, P., Moriceau, B., 2006. Si and C interactions in the world ocean: Importance of ecological processes and implications for the role of diatoms in the biological pump. Glob. Biogeochem. Cycles 20.

Rai, D., Kittrick, J.A., 1989. Mineral equilibria and the soil system. Miner. Soil Environ. 161–198.

Rashid, I., Mir, S.H., Zurro, D., Dar, R.A., Reshi, Z.A., 2019. Phytoliths as proxies of the past. Earth-Sci. Rev.

Raven, J., 2001. Silicon transport at the cell and tissue level. Stud. Plant Sci. 8, 41–55.

Raven, J.A., 1983. The transport and function of silicon in plants. Biol. Rev. 58, 179–207.

Reusser, L., Bierman, P., Rood, D., 2015. Quantifying human impacts on rates of erosion and sediment transport at a landscape scale. Geology 43, 171–174.

Rice, K.C., Hornberger, G.M., 1998. Comparison of hydrochemical tracers to estimate source contributions to peak flow in a small, forested, headwater catchment. Water Resour. Res. 34, 1755–1766. https://doi.org/10.1029/98WR00917

Riotte, J., Meunier, J.-D., Zambardi, T., Audry, S., Barboni, D., Anupama, K., Prasad, S., Chmeleff, J., Poitrasson, F., Sekhar, M., 2018a. Processes controlling silicon isotopic fractionation in a forested tropical watershed: Mule Hole Critical Zone Observatory (Southern India). Geochim. Cosmochim. Acta 228, 301–319.

Riotte, J., Sandhya, K., Prakash, N.B., Audry, S., Zambardi, T., Chmeleff, J., Buvaneshwari, S., Meunier, J.-D., 2018b. Origin of silica in rice plants and contribution of diatom Earth fertilization: insights from isotopic Si mass balance in a paddy field. Plant Soil 423, 481–501. https://doi.org/10.1007/s11104-017-3535-z

Robinet, J., Minella, J.P., de Barros, C.A., Schlesner, A., Lücke, A., Ameijeiras-Mariño, Y., Opfergelt, S., Vanderborght, J., Govers, G., 2018. Impacts of forest conversion and agriculture practices on water pathways in Southern Brazil. Hydrol. Process. 32, 2304–2317.

Robson, A., Beven, K., Neal, C., 1992. Towards identifying sources of subsurface flow: a comparison of components identified by a physically based runoff model and those determined by chemical mixing techniques. Hydrol. Process. 6, 199–214.

Rodrigues, G.P., 1997. Efeito do silicato de cálcio na cana-de-açúcar e sobre as características químicas do solo. Monogr. Curso Agron. Univ Fed Uberlândia Braz.

Ronsse, F., Van Hecke, S., Dickinson, D., Prins, W., 2013. Production and characterization of slow pyrolysis biochar: influence of feedstock type and pyrolysis conditions. Gcb Bioenergy 5, 104–115.

Ross, L., Nababsing, P., Cheong, Y.W.Y., 1974. Residual effect of calcium silicate applied to sugarcane soils. Int. Cong Soc Sugar Cane Technol 15, 539–542.

Rouiller, J., Burtin, G., Souchier, B., 1972. dispersion des sols dans l'analyse granulometrique, methode utilisant les resines echangeuses d'ions. Nancy Ecole Nat Super Agron Bull.

Rousteau, A., 1996. Structures, flores, dynamiques: réponses des forêts pluviales des Petites Antilles aux milieux montagnards. Phytogeogr. Trop. Realites Perspect. ORSTOM Ed. Paris 308–321.

Rousteau, A., Portecop, J., Rollet, B., 1994. Carte écologique de la Guadeloupe.

Saccone, L., Conley, D.J., Koning, E., Sauer, D., Sommer, M., Kaczorek, D., Blecker, S.W., Kelly, E.F., 2007. Assessing the extraction and quantification of amorphous silica in soils of forest and grassland ecosystems. Eur. J. Soil Sci. 58, 1446–1459. https://doi.org/10.1111/j.1365-2389.2007.00949.x

Samper, A., Quidelleur, X., Lahitte, P., Mollex, D., 2007. Timing of effusive volcanism and collapse events within an oceanic arc island: Basse-Terre, Guadeloupe archipelago (Lesser Antilles Arc). Earth Planet. Sci. Lett. 258, 175–191.

Samuels, G., 1969. Silicon and sugar. Sugar Azucar 66, 25–29.

Sanchez, P.A., 2019. Properties and Management of Soils in the Tropics, 2nd ed. Cambridge University Press. https://doi.org/10.1017/9781316809785

Sangster, A., Hodson, M., 1986. Silica in higher plants. Silicon Biochem. 90–107.

Sauer, D., Saccone, L., Conley, D.J., Herrmann, L., Sommer, M., 2006. Review of methodologies for extracting plant-available and amorphous Si from soils and aquatic sediments. Biogeochemistry 80, 89–108.

Savant, N.K., Korndörfer, G.H., Datnoff, L.E., Snyder, G.H., 1999. Silicon nutrition and sugarcane production: a review 1. J. Plant Nutr. 22, 1853–1903.

Savant, N.K., Snyder, G.H., Datnoff, L.E., 1996. Silicon management and sustainable rice production, in: Advances in Agronomy. Elsevier, pp. 151–199.

Schaller, J., Turner, B.L., Weissflog, A., Pino, D., Bielnicka, A.W., Engelbrecht, B.M.J., 2018. Silicon in tropical forests: large variation across soils and leaves suggests ecological significance. Biogeochemistry 140, 161–174. https://doi.org/10.1007/s10533-018-0483-5

Schelske, C.L., Stoermer, E.F., 1971. Eutrophication, silica depletion, and predicted changes in algal quality in Lake Michigan. Science 173, 423–424. https://doi.org/10.1126/science.173.3995.423

Schenk, H.J., Jackson, R.B., 2005. Mapping the global distribution of deep roots in relation to climate and soil characteristics. Geoderma 126, 129–140.

Schenk, H.J., Jackson, R.B., 2002. The global biogeography of roots. Ecol. Monogr. 72, 311–328.

Schwertmann, U., Taylor, R.M., 1989. Iron oxides. Miner. Soil Environ. 379–438.

Seyfferth, A.L., Kocar, B.D., Lee, J.A., Fendorf, S., 2013. Seasonal dynamics of dissolved silicon in a rice cropping system after straw incorporation. Geochim. Cosmochim. Acta 123, 120–133.

Shoji, S., Dahlgren, R., Nanzyo, M., 1993. Chapter 1 Terminology, Concepts and Geographic Distribution of Volcanic Ash Soils, in: Shoji, Sadao, Nanzyo, Masami, Dahlgren, Randy (Eds.), Developments in Soil Science, Volcanic Ash Soils. Elsevier, pp. 1–5. https://doi.org/10.1016/S0166-2481(08)70262-9

Smetacek, V., 1999. Diatoms and the ocean carbon cycle. Protist 150, 25–32.

Smith, D.M., Inman-Bamber, N.G., Thorburn, P.J., 2005. Growth and function of the sugarcane root system. Field Crops Res. 92, 169–183.

Smithson, F., 1956. Plant opal in soil. Nature 178, 107.

Sommer, Michael, Jochheim, H., Höhn, A., Breuer, J., Zagorski, Z., Busse, J., Barkusky, D., Meier, K., Puppe, D., Wanner, M., 2013. Si cycling in a forest biogeosystem–the importance of transient state biogenic Si pools. Biogeosciences 10, 4991–5007.

Sommer, M., Jochheim, H., Höhn, A., Breuer, J., Zagorski, Z., Busse, J., Barkusky, D., Meier, K., Puppe, D., Wanner, M., Kaczorek, D., 2013. Si cycling in a forest biogeosystem – the importance of transient state biogenic Si pools. Biogeosciences 10, 4991–5007. https://doi.org/10.5194/bg-10-4991-2013

Sommer, M., Kaczorek, D., Kuzyakov, Y., Breuer, J., 2006. Silicon pools and fluxes in soils and landscapes—a review. J. Plant Nutr. Soil Sci. 169, 310–329.

Street-Perrott, F.A., Barker, P.A., 2008. Biogenic silica: a neglected component of the coupled global continental biogeochemical cycles of carbon and silicon. Earth Surf. Process. Landf. 33, 1436–1457.

Struyf, E., Smis, A., Van Damme, S., Garnier, J., Govers, G., Van Wesemael, B., Conley, D.J., Batelaan, O., Frot, E., Clymans, W., others, 2010. Historical land use change has lowered terrestrial silica mobilization. Nat. Commun. 1, 129.

Taboadela, M.M., 1953. The clay mineralogy of some soils from Spain and from Rio Muni (West Africa). J. Soil Sci. 4, 48–55.

Takijima, Y., Gunawardena, S., 1969. Nutrient deficiency and physiological disease of lowland rice in Ceylon: I. Relationships between Nutritional Status of Soil and Rice Growth. Soil Sci. Plant Nutr. 15, 259–266.

Tavakkoli, E., Lyons, G., English, P., Guppy, C.N., 2011. Silicon nutrition of rice is affected by soil pH, weathering and silicon fertilisation. J. Plant Nutr. Soil Sci. 174, 437–446.

Totsche, K.U., Amelung, W., Gerzabek, M.H., Guggenberger, G., Klumpp, E., Knief, C., Lehndorff, E., Mikutta, R., Peth, S., Prechtel, A., 2018. Microaggregates in soils. J. Plant Nutr. Soil Sci. 181, 104–136.

Tréguer, P., Bowler, C., Moriceau, B., Dutkiewicz, S., Gehlen, M., Aumont, O., Bittner, L., Dugdale, R., Finkel, Z., Iudicone, D., Jahn, O., Guidi, L., Lasbleiz, M., Leblanc, K., Levy, M., Pondaven, P., 2018. Influence of diatom diversity on the ocean biological carbon pump. Nat. Geosci. 11, 27–37. https://doi.org/10.1038/s41561-017-0028-x

Treguer, P., Nelson, D.M., Van Bennekom, A.J., DeMaster, D.J., others, 1995. The silica balance in the world ocean: a reestimate. Science 268, 375.

Tréguer, P., Pondaven, P., 2000. Global change: silica control of carbon dioxide. Nature 406, 358–359.

Trostle, K.D., Ray Runyon, J., Pohlmann, M.A., Redfield, S.E., Pelletier, J., McIntosh, J., Chorover, J., 2016. Colloids and organic matter complexation control trace metal concentration-discharge relationships in Marshall Gulch stream waters:

Concentration-discharge relations for trace metals. Water Resour. Res. 52, 7931–7944. https://doi.org/10.1002/2016WR019072

Tubana, B.S., Babu, T., Datnoff, L.E., 2016. A review of silicon in soils and plants and its role in US agriculture: history and future perspectives. Soil Sci. 181, 393–411.

Umemura, M., Takenaka, C., 2014. Biological cycle of silicon in moso bamboo (Phyllostachys pubescens) forests in central Japan. Ecol. Res. 29, 501–510. https://doi.org/10.1007/s11284-014-1150-5

van Breemen, N., Mulder, J., Driscoll, C., 1983. Acidification and alkalinization of soils. Plant Soil 75, 283–308.

Vanacker, V., Ameijeiras-Mariño, Y., Schoonejans, J., Cornélis, J.-T., Minella, J.P.G., Lamouline, F., Vermeire, M.-L., Campforts, B., Robinet, J., Van de Broek, M., Delmelle, P., Opfergelt, S., 2019. Land use impacts on soil erosion and rejuvenation in Southern Brazil. Catena 178, 256–266. https://doi.org/10.1016/j.catena.2019.03.024

Vanacker, V., von Blanckenburg, F., Govers, G., Molina, A., Poesen, J., Deckers, J., Kubik, P.W., 2007. Restoring natural vegetation reverts mountain erosion to natural levels. Geology 35, 303.

Vandevenne, F., Struyf, E., Clymans, W., Meire, P., 2011. Agricultural silica harvest: have humans created a new loop in the global silica cycle? Front. Ecol. Environ. 10, 243–248.

Vandevenne, F.I., Barão, L., Ronchi, B., Govers, G., Meire, P., Kelly, E.F., Struyf, E., 2015. Silicon pools in human impacted soils of temperate zones. Glob. Biogeochem. Cycles 29, 2014GB005049. https://doi.org/10.1002/2014GB005049

Vermeire, M.-L., Kablan, L., Dorel, M., Delvaux, B., Risède, J.-M., Legrève, A., 2011. Protective role of silicon in the banana-Cylindrocladium spathiphylli pathosystem. Eur. J. Plant Pathol. 131, 621. https://doi.org/10.1007/s10658-011-9835-x

Vittecoq, B., Lachassagne, P., Lanini, S., Maréchal, J.C., 2010. Evaluation des ressources en eau de la Martinique: calcul spatialisé de la pluie efficace et validation à l'échelle du bassin versant. Rev. Sci. Eau 23, 325–429.

Wada, K., 1989. Minerals in Soil Environments. Soil Science Society of America.

Wada, K., 1977. Allophane and imogolite: in Minerals in the Soil Environments, JB Dixon and SD Weed, eds. Soil Sci. Soc. Am. Madison Wis.

Wada, K., Greenland, D.J., 1970. Selective dissolution and differential infrared spectroscopy for characterization of'amorphous' constituents in soil clays. Clay Miner. 8, 241–254.

Wadge, G., 1986. The dykes and structural setting of the volcanic front in the Lesser Antilles island arc. Bull. Volcanol. 48, 349–372.

Wedepohl, K.H., 1995. The composition of the continental crust. Geochim. Cosmochim. Acta 59, 1217–1232.

Westercamp, D., Tazieff, H., 1980. Martinique, Guadeloupe: Saint-Martin, La Désirade. Elsevier Masson.

White, A.F., Vivit, D.V., Schulz, M.S., Bullen, T.D., Evett, R.R., Aagarwal, J., 2012. Biogenic and pedogenic controls on Si distributions and cycling in grasslands of the Santa Cruz soil chronosequence, California. Geochim. Cosmochim. Acta 94, 72–94.

Wickramasinghe, D.B., Rowell, D.L., 2006. The release of silicon from amorphous silica and rice straw in Sri Lankan soils. Biol. Fertil. Soils 42, 231–240.

Wilding, L., Drees, L., 1974. Contributions of forest opal and associated crystalline phases to fine silt and clay fractions of soils. Clays Clay Miner. 22, 295–306.

Williams, E., Walter, L., Ku, T., Baptist, K., Budai, J., Kling, G., 2007. Silicate weathering in temperate forest soils: insights from a field experiment. Biogeochemistry 82, 111–126.

Yang, J.-L., Zhang, G.-L., 2018. Silicon cycling by plant and its effects on soil Si translocation in a typical subtropical area. Geoderma 310, 89–98.

Yoshida, S., 1981. Fundamentals of rice crop science. Int. Rice Res. Inst.

Yoshida, S., Hasegawa, S., 1982. The Rice Root System: its development and function, in: Drought Resistance in Crops with Emphasis on Rice. International Rice Research Institute, Los Baños, Laguna, Philippines, pp. 97–114.

List of publications

International peer-reviewed journals[6]

Vander Linden, C., Delvaux, B., 2019. The weathering stage of tropical soils affects the soil-plant cycle of silicon, but depending on land use. Geoderma 351, 209-220. DOI: 10.1016/j.geoderma.2019.05.033

Li, Z., Unzué-Belmonte, D., Cornelis, J. T., **Vander Linden, C.**, Struyf, E., Ronsse, F., & Delvaux, B. (2019). Effects of phytolithic rice-straw biochar, soil buffering capacity and pH on silicon bioavailability. Plant and Soil, 438(1-2), 187-203.

Conference proceedings

Vander Linden, C., Delvaux, B., In the humid tropics, soil weathering stage affects differently the soil-to-plant silicon cycle depending on land use. *EGU 2019* – Vienna, Austria.

De Tombeur, F., **Vander Linden, C.**, Durviaux; Delvaux, B., Godin, B., Compère, P., Cornélis, JT., Soil control on tradeoffs between silica and cellulose as structural component in sugarcane leaf (Saccharum officinarum). *EGU 2019* – Vienna, Austria.

Vander Linden, C., Iserentant, A., Delvaux, B., Quantification of distinct phytolith pools in a perhydrated Andosol. *Goldschmidt 2018* – Boston, USA.

Li, Z., Unzué-Belmonte, D., Cornélis, JT., **Vander Linden, C.**, Struyf, E., Ronsse, F., Delvaux, B., Soil weathering degree controls silicon bioavailability by increased pH after biochar application. *Goldschmidt 2018* – Boston, USA.

[6] Several additional chapters of this thesis should be published in a near future. Publications "in preparation" are indicated in footnotes at the start of each chapter.

Vander Linden, C., Iserentant, A., Delvaux, B., Quantification of the phytoliths pool in a tropical Andosol, A new method. *Day of young soil scientists 2018* – Brussels, Belgium.

Vander Linden, C., Durviaux, A., Opfergelt, S., Delvaux, B., Does soil weathering stage impact the effects of intensive banana and sugarcane cropping on the silicon cycle? *IV Simposio Internacional INIVIT'2017* — Cuba, 2017.

Vander Linden, C., Sosnowski, P., Opfergelt, S., Delvaux, B., The forest-to-banana transition impacts the soil-plant silicon cycle in the humid tropics (Guadeloupe). *IV Simposio Internacional INIVIT'2017* — Cuba, 2017.